AC&DC Power Network Security Management : Assessment and Enhancement

Gianni Bakhos

THÈSE

Pour obtenir le grade de

DOCTEUR DE L'UNIVERSITÉ GRENOBLE ALPES

École doctorale : EEATS - Electronique, Electrotechnique, Automatique, Traitement du Signal (EEATS)
Spécialité : Génie électrique
Unité de recherche : Laboratoire de Génie Electrique

Gestion de la sécurité du réseau électrique AC & DC: évaluation et amélioration

AC&DC Power Network Security Management: Assessment and Enhancement

Présentée par :

Gianni BAKHOS

Direction de thèse :

Seddik BACHA PROFESSEUR DES UNIVERSITES, Université Grenoble Alpes	Directeur de thèse
Abdelkrim BENCHAIB supergrid institute	Co-directeur de thèse
Luigi VANFRETTI Professeur, Rensselaer Polytechnic Institute	Co-directeur de thèse
Kosei SHINODA Ingénieur docteur, SuperGrid Institute	Co-encadrant de thèse

Rapporteurs :

Yassine AMIRAT
PROFESSEUR, ISEN Yncréa Ouest
Hadi KANAAN
FULL PROFESSOR, Université Saint-Joseph de Beyrouth

Thèse soutenue publiquement le **15 février 2024**, devant le jury composé de :

Xuefang LIN SHI, PROFESSEURE DES UNIVERSITES, INSA Lyon	Présidente
Seddik BACHA, PROFESSEUR DES UNIVERSITES, Université Grenoble Alpes	Directeur de thèse
Luigi VANFRETTI, FULL PROFESSOR, Rensselaer Polytechnic Institute	Co-directeur de thèse
Abdelkrim BENCHAIB, INGENIEUR HDR, SUPERGRID INSTITUTE	Co-directeur de thèse
Yassine AMIRAT, PROFESSEUR, ISEN Yncréa Ouest	Rapporteur
Hadi KANAAN, FULL PROFESSOR, Université Saint-Joseph de Beyrouth	Rapporteur
Georges KARINIOTAKIS, PROFESSEUR DES UNIVERSITES, MINES PARIS PSL	Examinateur
Raphaël CAIRE, MAITRE DE CONFERENCE HDR, Grenoble INP	Examinateur

Invités :

Juan-Carlos Gonzalez-Torres
INGENIEUR DOCTEUR, SUPERGRID INSTITUTE
Jing Dai
ASSISTANT PROFESSOR, Université Paris-Saclay, Ecole CentraleSupélec / Sorbonne Université / SuperGrid Institute

This work was supported by a grant overseen by the French National Research Agency (ANR) as part of the "Investissements d'Avenir" Program (ANE-ITE-002-01) of the French Government.

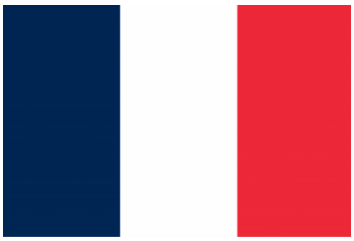

Dédicace

À mes parents, ma sœur et ma grande famille,

Pour la gloire de Dieu et le salut du monde,

À ma future famille,

Pour la paix dans le monde et dans le cœur des gens,

Je dédie ce modeste travail.

Acknowledgements

In this section, I would like to gratefully thank all the individuals who contributed to the success of this Ph.D. thesis work. Were these people directly involved in the work or not, I want to assure them of my deepest appreciation for all the effort they put to help me through the easiest and the toughest moments of my Ph.D. path.

First, I would like to thank Prof. Xuefang LIN-SHI for having presided over the Jury during my Ph.D. I would also like to thank Profs. Yassine AMIRAT and Hadi KANAAN for their time and efforts done to write their valuable report about my manuscript. Finally, I send my deepest thanks to Profs. Georges KARINIOTAKIS and Raphaël CAIRE, for examining my work and participating in my Jury as well.

I am more than grateful to you, Prof. Seddik BACHA, who accompanied me, challenged my work, suggested solutions to my problems, and, most importantly, have been present during and after my Ph.D. project was done. Your paternal presence recomforts me and it is the place where I felt and still feel protected. Your humility inspires me, and your assertiveness strengthens me. I am very honoured to having been your Ph.D. student and wish your guidance model was adopted by all thesis directors.

Prof. Luigi VANFRETTI, you were for me a rock on which my thesis work was based. Your responsiveness, your guidance and your availability still inspire me. Your positivity and the pragmatism you have stimulate me as well. Your confidence in my work and the efforts you put to accompany me and be present for the big moments and milestones will never be thanked for enough.

Dr. H.D.R. Abdelkrim BENCHAIB, God only knows what I would have been without your support. In my moments of doubts, you were here to assert me and draw for me paths to let me grow in wisdom and grace. Your professionalism and your managerial expertise helped me transform my mindset from that one of a Ph.D. student to the one of an R&D Engineer, Ph.D.. Kindly excuse my inability to thank you enough.

Dr. Kosei SHINODA, my supervisor, your constructive feedback was for me a necessity, to succeed in this Ph.D. thesis project. Thank you so much for all the time and efforts you put to help me grow in rigorousness and personality.

To you supervisor Dr. Juan-Carlos GONZALEZ-TORRES I send my deepest thanks for all the times you helped me, you supported me, and you gave me feedback, trust, and hope in my work. Your career path inspires me. Thank you.

In this part, I would like to extend my thanks to Dr. Jing DAI and Dr. H.D.R. Serge POULLAIN who were the members of my “Comité de Suivi Individuel” (CSI). Your feedback, remarks and encouragements were necessary for me to succeed in my work.

Eric COURBON, how could I finish my simulations on time without you helping me solve the accesses and the PC and software issues.

To all “Programme Architecture & Systèmes du SuperGrid” colleagues and management team, and specifically to Bruno LUSCAN (CTO of SuperGrid Institute and Head of Program), I send a sincere thank you. All your feedback, the participation to my follow-up meetings and the trust given to me were really appreciated.

I would also like to show my gratitude to Hubert DE LA GRANDIÈRE, CEO of SuperGrid Institute, for the trust you have put in our work and the stimulating working environment you have created for us in SuperGrid Institute. Your eyesight makes me feel more valuable and pushes me personally to give the best out of myself.

To Dr. Boussaad ISMAIL who helped me with the expertise in the optimization part, thank you also.

Furthermore, to all my colleagues in SuperGrid Institute who became my friends, my support, and the place where I feel professionally valued, I would like to express my sincere thanks.

To my colleagues in G2ELab, who were also interested in the work I made and with whom I built friendships, thank you very much.

To the members of GE Vernova/SuperGrid Institute chorus led by Gilles MAGNARD, thank you for the shared lunch breaks we spent together and the appreciated events where we sang.

To May RENAUDIN who helped me in the moments when I was injured, thank you so much.

Finally, I would like to thank my family, my friends, and all my life mentors and the people who helped me stand up when I was meant to fall. My deepest gratitude for your efforts and your presence.

Gianni BAKHOS

Abstract

As power transmission networks evolve, High-Voltage Direct Current (HVDC) links are and will be used to transfer power within the same synchronous network or between asynchronous networks (for example, between renewable energy production zones and an existing synchronous network). This exchange of power (~ MW to GW) via HVDC links is controlled by active and reactive power control mechanisms at the power converter level. This PhD thesis focuses mainly on the control of the active power exchanged between the Alternative Current (AC) and Direct Current (DC) networks. It is not the internal control of the converters but a higher-level control, that of the hybrid AC/DC power network.

At the power system level, control interactions may occur due to the existing coupling or simply because of addressing multiple stability problems simultaneously. The stability issues studied in this thesis include small-signal, rotor angle, frequency, and DC voltage. Multiple power system benchmarks are developed. Based on Modular Multilevel Converters (MMC), point-to-point or multi-terminal DC (MTDC) systems are modelled. They can be used to enhance the security of the considered benchmark power systems through supplementary power converter controllers.

These controllers are designed and implemented as ancillary HVDC services. The combination of these services may not always result in satisfactory dynamic performance. This is due to system constraints and the mentioned control interactions. Therefore, in this thesis, two coordinated active power control strategy are proposed and tested through comparative studies. The advantages of these approaches are mainly:

1) AC & DC stability phenomena – usually studied separately – are considered and enhanced in a wholistic approach, simultaneously,

2) the coordination strategy minimizes control interactions during operation without the need of modifying the tuning of the controller parameters.

Finally, an optimization approach is proposed to further enhance the stability of the studied hybrid AC/DC power system.

Résumé court en français

Avec l'évolution des réseaux de transport d'électricité, les liens à Courant Continu de Haute Tension (CCHT) sont et seront utilisés pour transférer de l'énergie au sein d'un même réseau synchrone ou entre des réseaux asynchrones (par exemple, entre des zones de production d'énergie renouvelable et un réseau synchrone existant). Ce transfert de puissance (~ MW à GW) via les liens CCHT est contrôlé par des mécanismes de contrôle de la puissance active et réactive au niveau du convertisseur de puissance. Cette thèse de doctorat se concentre principalement sur le contrôle de la puissance active échangée entre les réseaux à courants alternatif (CA) et à courants continus (CC). Il ne s'agit pas du contrôle interne des convertisseurs mais d'un contrôle de niveau supérieur, celui du réseau hybride CA/CC.

Au niveau du système électrique, des interactions de contrôle peuvent se produire en raison du couplage existant ou simplement en raison de simultanément traiter plusieurs problèmes de stabilité. Les problèmes de stabilité étudiés dans cette thèse comprennent les petits signaux, l'angle rotorique, la fréquence et la tension CC. Plusieurs systèmes de puissance de référence sont développés. Basés sur les convertisseurs multiniveaux modulaires (MMC), les systèmes CC point à point ou multi-terminaux (CCMT) sont modélisés. Ils peuvent être utilisés pour améliorer la sécurité des systèmes électriques de référence considérés grâce à des contrôleurs de convertisseurs de puissance supplémentaires.

Ces contrôleurs sont conçus et mis en œuvre en tant que services CCHT auxiliaires. La combinaison de ces services ne permet pas toujours d'obtenir des performances dynamiques satisfaisantes. Ceci est dû aux contraintes du système et aux interactions de contrôle mentionnées. Par conséquent, dans cette thèse, deux stratégies coordonnées de contrôle de la puissance active sont proposées et testées par le biais d'études comparatives. Les avantages de ces approches sont principalement les suivants :

1) Les phénomènes de stabilité CA et CC - habituellement étudiés séparément - sont pris en compte et améliorés dans une approche globale, simultanément,

2) la stratégie de coordination minimise les interactions de contrôle pendant le fonctionnement sans qu'il soit nécessaire de modifier le réglage des paramètres du contrôleur.

Enfin, une approche d'optimisation est proposée pour améliorer la stabilité du système hybride CA/CC étudié.

Résumé de la thèse en français

Chapitre 1 : Introduction générale

Les réseaux de transport d'électricité sont en train de subir des modifications significatives, engendrées par l'intégration des énergies renouvelables (ENRs) et le besoin de renforcement du réseau actuel (Figure n° *1*).

Pour cela, le système électrique du futur comporterait davantage d'électronique de puissance pour interfacer divers réseaux électriques. Ceci créera de nouveaux défis pour les gestionnaires de réseaux électriques.

Renforcer le réseau à courant alternatif (CA) avec des liens à courant continu (CC) peut se faire soit avec des liens CC de point à point ou multi-terminaux (CCMT).

Intégrer les ENRs dans le réseau actuel peut se traduire soit par un remplacement de générateurs synchrones soit par la connexion d'un moyen de production supplémentaire. Dans le premier cas, les réserves primaires du réseau CA sont réduites du fait de l'intermittence des ENRs. De plus, l'interface (convertisseur de puissance) qui permet l'injection de la production provenant des ENRs ne possède pas d'inertie naturelle comme c'est le cas pour les générateurs synchrones actuels.

Si les convertisseurs électriques permettent d'obtenir un contrôle plus rapide et plus flexible de la puissance, leur vulnérabilité face aux perturbations impacte la robustesse du système électrique en entier.

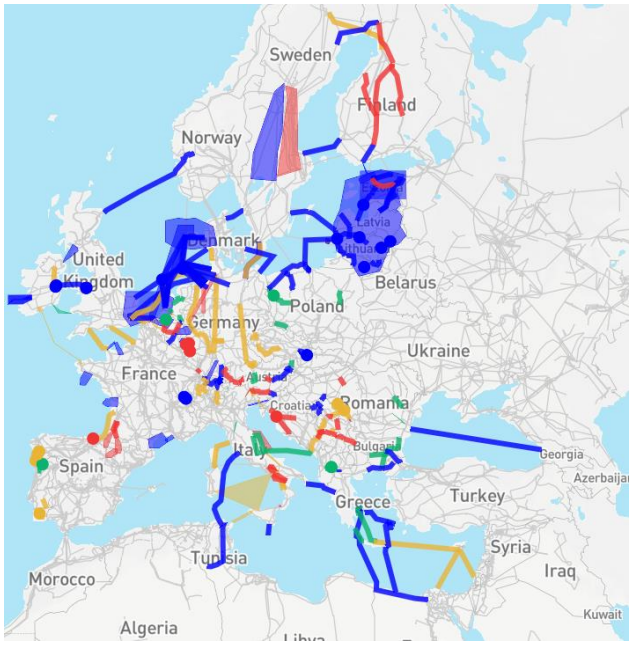

Figure n° 1 : Projets de développement du réseau actuel [5].

Les réseaux du futur seraient des réseaux hybrides CA/CC, et le contrôle des liens CC pourrait servir à les stabiliser. Néanmoins, le couplage entre les réseaux CA et CC impactera la stabilité des réseaux CA/CC.

Dans cette thèse de doctorat, nous cherchons donc à proposer une méthodologie d'évaluation et d'amélioration de la stabilité multicritère des réseaux CA/CC.

Cela est aligné avec les demandes de l'ENTSO-E disponibles dans la feuille de route de Recherche, Démonstration et Innovation pour 2020-2030. Plusieurs actions à court, moyen et long terme sont également proposées par l'ENTSO-E. Dans cette thèse, de nouveaux contrôles de puissance et des stratégies d'évaluation et d'amélioration sont proposées en utilisant les capacités techniques des liens CC. Tout cela fut testé sur des systèmes de puissance compréhensifs, développés durant la thèse. Une optimisation de la stratégie de contrôle proposée est également testée et validée dans cette thèse.

Le travail réalisé est basé sur deux approches : une analytique et une autre numérique.

La complexité des réseaux étudiés oblige de passer à l'approche numérique pour pouvoir étudier la stabilité multicritère des réseaux hybrides CA/CC. Cette approche est basée sur des simulations en domaine temporel et sur des analyses de modes.

Divers indicateurs de performance de stabilité (KPIs) ont été développés et utilisés pour étudier la stabilité des réseaux électriques. Ceux-ci doivent être préalablement initialisés afin de pouvoir conduire tout type de simulation numérique. Les systèmes initialisés ont été étudiés avec plusieurs types de perturbations plausibles :

- Défaut sur un lien CA conduisant à une perte de ligne,
- Perte de générateur synchrone,
- Variation de charge, etc.

Plusieurs contrôles ont été implémentés et deux stratégies de coordination de la puissance active furent proposées dans la thèse.

Dans ce qui suit, une synthèse individuelle des chapitres est présentée.

Chapitre 2 : Etat de l'art sur les liens CCHT et les défis rencontrés dans l'amélioration de la stabilité des réseaux CA

Dans ce chapitre, les avantages des liens CC haute tension (CCHT) sont présentés ainsi que les modèles de convertisseurs de puissance utilisés. Une définition et une classification de la stabilité des systèmes électriques haute puissance est également exposée. En outre, le couplage existant entre les différents réseaux CA et CC est étudié.

Les liens CCHT deviennent économiquement avantageux par rapport aux liens CAHT à partir d'une certaine longueur de liaison, dite seuil de rentabilité, bien que le coût initial de déploiement de liaison CC soit plus élevé que celui d'une liaison CA.

Diverses architectures de réseaux CC existent : CC de point à point ou CCMT. Dans le cas des CCMT, plusieurs configurations existent : série ou parallèle. Dans la catégorie des CCMT parallèle, des configurations complexes existent : CCMT radial ou maillé.

La complexité des liens CCMT dépasse celle des liens CCHT point à point, et elle est source de défis d'opération pour maintenir la stabilité du réseau CC (notamment, la tension CC) :

- Quelle configuration CCMT est la plus adéquate ? Quels codes et standards devront être respectés ? Quelle utilisation des liens CCMT : simple transmission de puissance ou proposition de services auxiliaires aussi ?
- Des problèmes d'interopérabilité des convertisseurs CA/CC peuvent apparaître, notamment dans le contexte d'utilisation de convertisseurs provenant de constructeurs différents.

Les convertisseurs mentionnés ci-dessus peuvent être de plusieurs types :

- Source de courant (LCC)
- Source de tension (VSC)
    - Deux niveaux
    - Multiniveaux

Les différences entre les technologies LCC et VSC sont présentées dans le tableau ci-dessous :

Tableau n° 1 : Différences entres les technologies LCC et VSC.

Composant	Avantages	Inconvénients
LCC	Plus faibles pertes au niveau de la station Plus faible coût initial Technologie mature (robuste, fiable) Puissances plus importantes	Beaucoup d'harmoniques Besoin d'importants compensateurs de puissance réactive Besoin d'être connecté à des réseaux CA opérationnels (pas de capacité d'auto-démarrage)

		Empreinte écologique plus importante Besoin d'inverser le signe de la tension pour inverser la direction de la puissance (non adapté pour les CCMT)
VSC	Opérable avec des réseaux CA de faible puissance (capacité d'auto-démarrage) Contrôlabilité de la puissance active et réactive Empreinte écologique réduite Harmoniques moins importants L'inversion de puissance est réalisable à travers l'inversion du courant (adapté pour les CCMT)	Plus grandes pertes de conversion Technologie moins mature (moins de retours d'expérience sur le terrain) Coûts plus élevés

Un couplage entre les réseaux CA et CC existe et a été démontré dans la literature puis dans la these.

Ce couplage peut avoir un impact considérable sur la sécurité du système électrique. Cette sécurité peut être déclinée en plusieurs éléments. Ceux en gras ci-dessous sont ceux considérés dans ce travail de thèse.

- Cybersécurité
- Sécurité face à des actes de terrorisme
- **Stabilité électrique**
    - **Stratégies de protection**
    - **Tensions**
        - **CA**
        - **CC**
    - **Angles rotoriques**
        - **Petits signaux**
        - **Grandes perturbations**
    - **Fréquence**
        - **Court-terme**
        - **Long-terme**
    - **Equipements**
- Sécurité de marché électrique
- Sécurité liée aux désastres naturels

Chapitre 3 : Cadre général de modélisation de systèmes de puissance CA/CC

Dans ce chapitre, les modèles des différents composants utilisés dans les simulations sont présentés avec leurs contrôleurs. De plus, les modèles de réseaux électriques développés et étudiés sont présentés. Ils visent à modéliser, de la manière la plus réaliste, le comportement du système hybride CA/CC durant des régimes d'opération normale ou perturbée.

Les différents composants utilisés sont :

- Pour le réseau CA :
    - Générateurs synchrones (machines électriques) comportant :
        - Alternateur
        - Gouverneurs de turbines pour la régulation mécanique de la puissance
        - Système d'excitation (AVR)
        - Système stabilisateur de puissance (PSS)
    - Charges (modèle de type ZIP)
    - Lignes (modèle de type π)
- Pour le réseau CC :
    - Câbles (modèle de type π)
    - Convertisseurs de type VSC et MMC : modèle de valeur moyenne

Différents réseaux de puissance ont été développés, en fonction du besoin d'étude à réaliser :

- Etude de l'effet de l'ajout de l'électronique de puissance
- Etude comparative sur les stabilités petits-signaux et grande perturbation des angles rotoriques
- Etude compréhensive de la stabilité de la fréquence et de la tension CC
- Etude complète avec tous les aspects de stabilité – mentionnés au Chapitre 2 – pris en compte.

Les diagrammes électriques systèmes développés sont visualisables au Chapitre 3, section III.

Il convient ici d'en présenter le dernier à la Figure n° *2* qui comporte le modèle utilisé pour l'étude de stabilité en tenant compte des angles rotoriques, de la fréquence et de la tension CC.

Les multiples cas d'étude de stabilité ont été détaillés dans ce chapitre.

Finalement, un flux de travail pour de telles études de stabilité est proposé dans la thèse. Le diagramme développé est disponible à la Figure n° *3*.

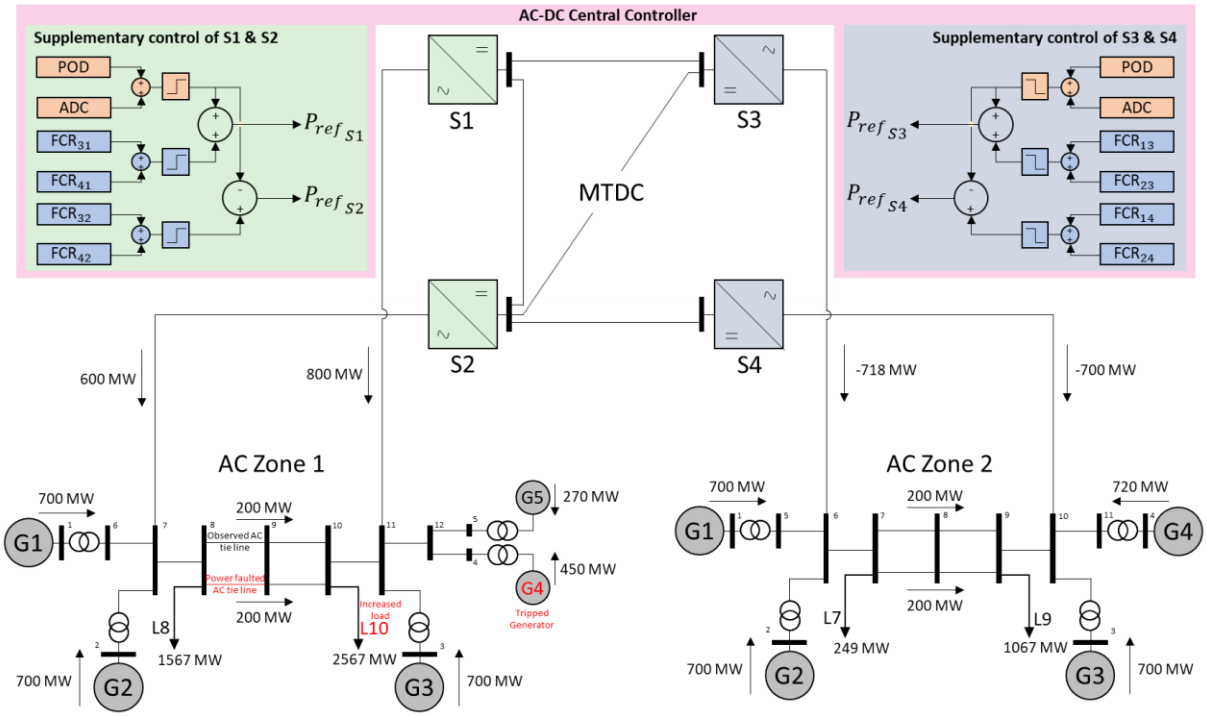

Figure n° 2 : Réseau de puissance CA/CC ainsi que son contrôleur central, développé pour l'étude de stabilité multicritère.

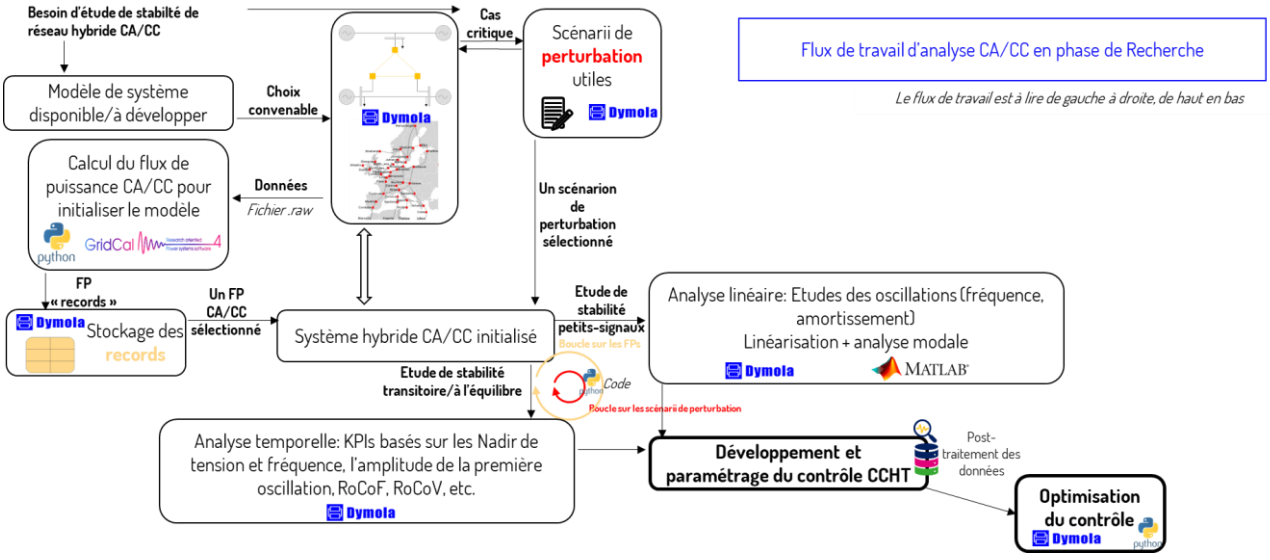

Figure n° 3 : Diagramme du flux de travail proposé pour l'étude de stabilité.

Chapitre 4 : Etude de la stabilité CA/CC : méthodes d'évaluation, indicateurs et contrôles

Dans ce chapitre, un modèle analytique du réseau de puissance est proposé pour en comprendre la dynamique. Celle-ci est ensuite étudiée à travers des simulations en domaines temporel et fréquentiel. Différents contrôles sont développés et implémentés pour améliorer les aspects de stabilité sélectionnés.

Deux contrôles visent à améliorer la stabilité des angles rotoriques :

- L'amortisseur d'oscillations de puissances (POD),
- Le contrôleur de différence d'angles (ADC) ou émulateur de ligne CA.

Un contrôle de tension est développé :

- Le contrôleur de statisme de tension CC.

Un contrôle de fréquence est développé :

- Le contrôleur de statisme de fréquence (type réponse rapide FFR en utilisant les réserves FCR de fréquence).

Tous ces contrôles supplémentaires sont implémentés et testés en utilisant les liens CC. Leur sortie est en effet une référence de puissance active envoyée aux convertisseurs autonomes pour contrôler les aspects de stabilité visés.

Dans un premier temps, des études de stabilité ont permis de montrer comment découpler mathématiquement le contrôle de fréquence de celui des angles rotoriques.

Dans un second temps, d'autres études ont permis de trouver un compromis entre deux aspects de stabilité en minimisant les interactions entre deux contrôleurs séparés. Il a été conclu que s'il n'est pas possible de découpler les contrôles mathématiquement, il reste possible d'optimiser la stabilité multicritère en adoptant tenant compte des indicateurs de chaque critère. Les contrôles étudiés ici sont le POD et l'ADC qui agissent ensemble sur la stabilité des angles rotoriques mais chacun à un moment différent théoriquement.

En somme, les études menées sont basées sur différents indicateurs de stabilité dits KPIs : le Nadir de tension CC, l'ISGA pour la stabilité des angles rotoriques et l'amortissement pour les oscillations interzones.

A la fin de ce chapitre, de multiples cadres de travail ont été proposés pour distinguer entre différents critères de contrôle et de mesure.

Les critères de cadre de travail adoptés sont d'une part le degré de coordination entre les contrôles implémentés et d'autre part le niveau de communication utilisé dans le contrôle.

Chaque cadre est distingué par une couleur et un numéro dans la Figure n° *4*.

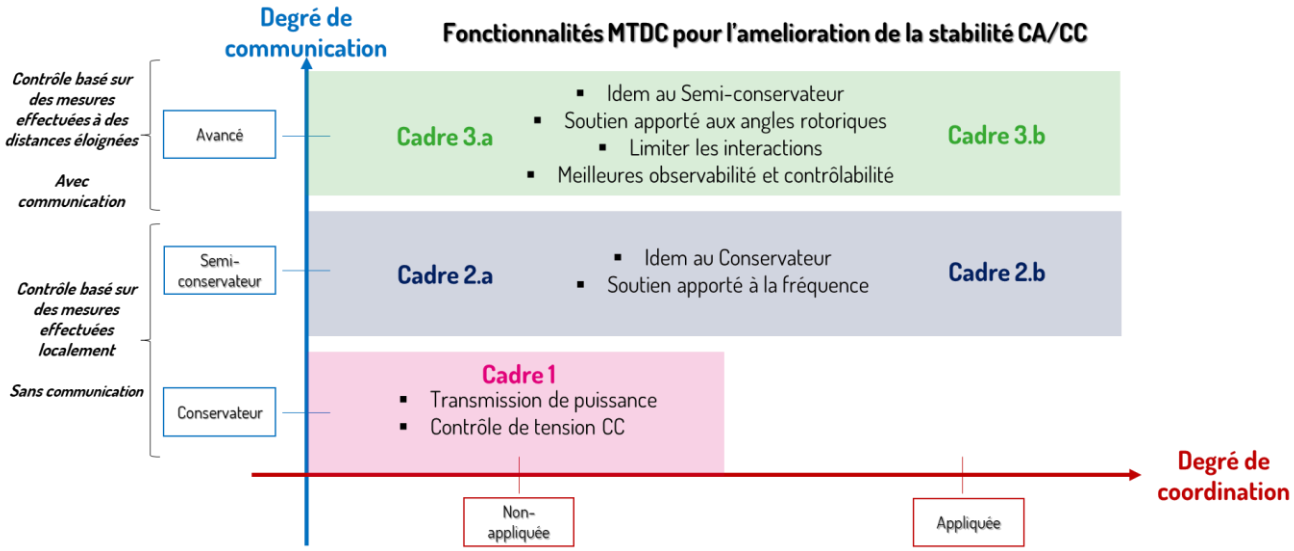

Figure n° 4 : Cadres de travail pour l'amélioration de stabilité à travers les différentes fonctionnalités proposables par les réseaux CCMT.

Chapitre 5 : Première approche globalisée, basée sur la réallocation de puissance active

Dans ce chapitre, une première approche globale d'étude de stabilité a été développé sur un système hybride CA/CC. L'étude est basée sur une analyse temporelle et modale des performances du réseau qui a subi une contingence : perte de générateur synchrone.

Dans l'approche adoptée, la déviation de la fréquence de chaque zone au sein d'un même réseau CA en fonction du temps, par rapport à la fréquence nominale, est, entre autres, observée (Figure n° 5). Cela permet d'identifier deux phénomènes de stabilité distincts au niveau du réseau CA, lorsqu'aucun service auxiliaire CC n'est proposé.

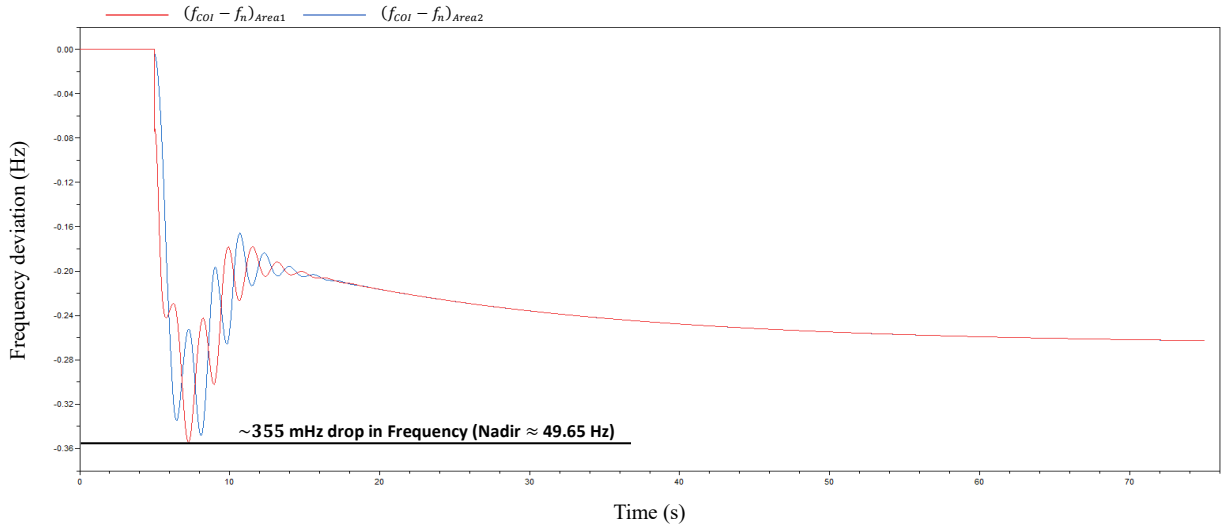

Figure n° 5 : Déviation de la fréquence du centre d'inertie des zones 1 et 2 (mesures prises au sein du réseau CA 1) de sa valeur nominale.

Une chute de la fréquence mesurée est observée ainsi que des oscillations apparaissant entre la fréquence de la zone 1 et la fréquence de la zone 2.

Pour comprendre le phénomène d'oscillations apparues, une analyse modale a été menée (Figure n° 6). Elle a permis de confirmer que le mode des oscillations correspond à un mode électromécanique

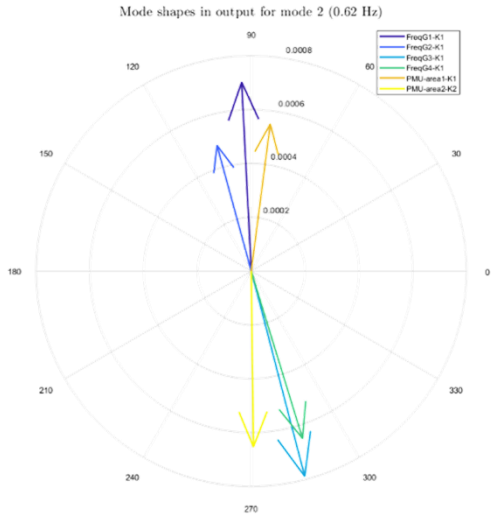

Figure n° 6 : Vecteurs correspondants au mode d'oscillation interzone au sein du

interzonal. Le mode identifié montre qu'un groupe de générateurs d'une zone oscille contre un autre groupe d'une autre zone au sein du même réseau CA.

Pour contribuer à stabiliser le système, les convertisseurs CA/CC ont été équipés de contrôleurs supplémentaires agissant sur les puissances actives de référence envoyées à chaque convertisseur en question. Le but est d'améliorer simultanément la chute de fréquence et d'amortir les oscillations interzones.

En implémentant ces contrôleurs dans le système CA/CC étudié par une simple somme, le résultat obtenu ne correspond pas à la somme des résultats obtenus si chaque contrôleur était implémenté tout seul. Cela est dû à la non-linéarité du système CA/CC complexe étudié. La sortie de chaque convertisseur est donnée en Figure n° 7. Le convertisseur 2 est saturé alors que le convertisseur 1 connecté au même réseau CA ne l'est pas.

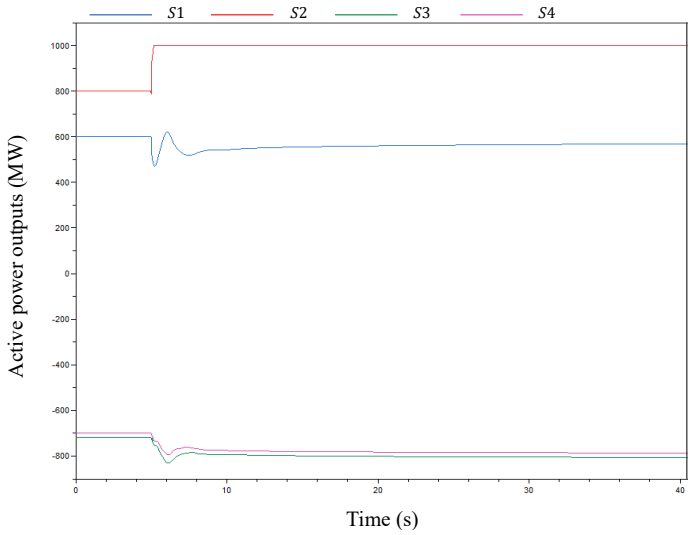

Figure n° 7 : Puissance active de sortie des convertisseurs.

Dans ce chapitre, une solution de coordination de contrôle a été testée et validée. Son principe est de réattribuer/réallouer une partie du contrôle de fréquence du convertisseur saturé à un autre convertisseur connecté au même réseau et qui n'est pas saturé.

Cela a permis d'obtenir le résultat suivant (Figure n° 8) :

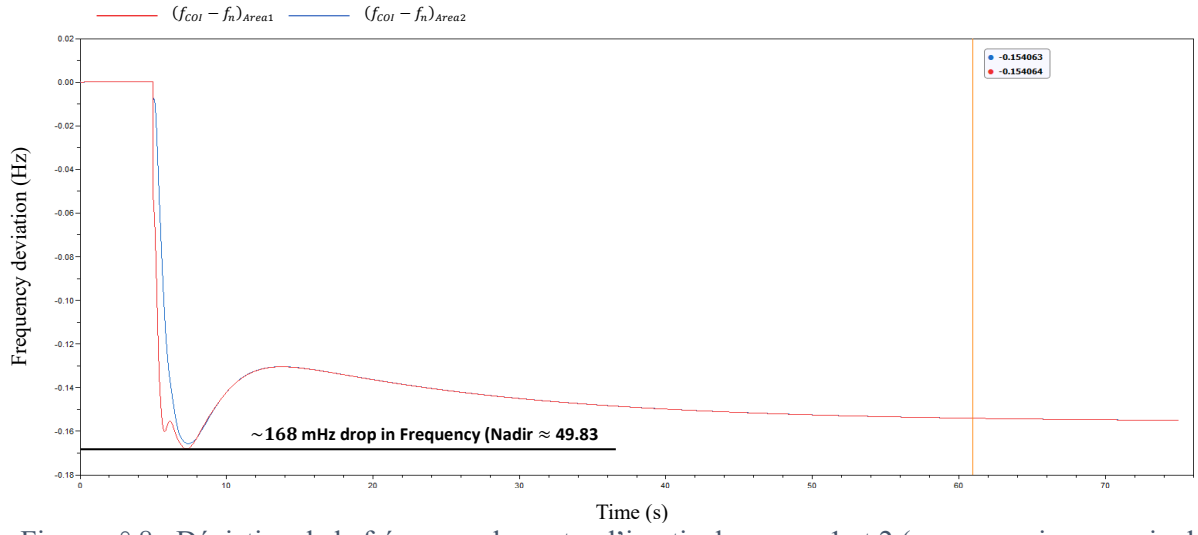

Figure n° 8 : Déviation de la fréquence du centre d'inertie des zones 1 et 2 (mesures prises au sein du réseau CA 1) de sa valeur nominale.

L’analyse modale (Figure n° 9) permet de confirmer l’amortissement accru du mode en question.

Finalement, le convertisseur problématique a été désaturé, comme le montre la Figure n° 10.

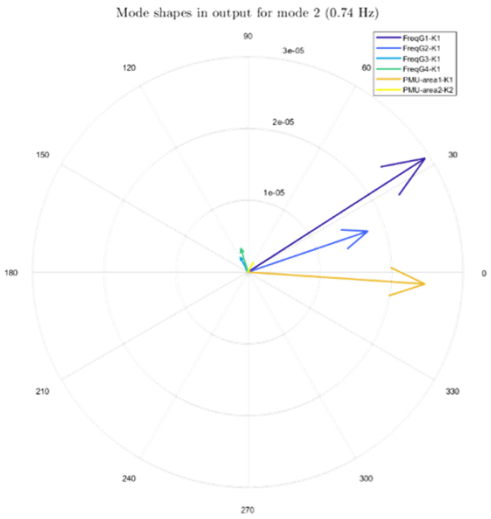

Figure n° 9 : Vecteurs correspondants au mode d’oscillation interzone au sein du réseau CA 1.

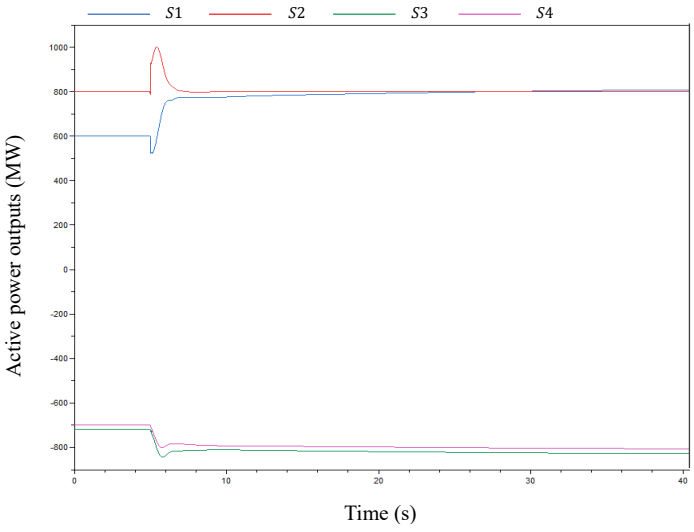

Figure n° 10 : Puissance active de sortie des convertisseurs.

Chapitre 6 : Amélioration de la stabilité globale CA/CC en se basant sur l'allocation de marges de puissance

Dans ce chapitre, un nouveau contrôle de fréquence distribué a été implémenté et testé sur le système CA/CC. Il vise à limiter les interactions entre la tension CC et la fréquence, tout en améliorant la performance en fréquence (Figure n° 11).

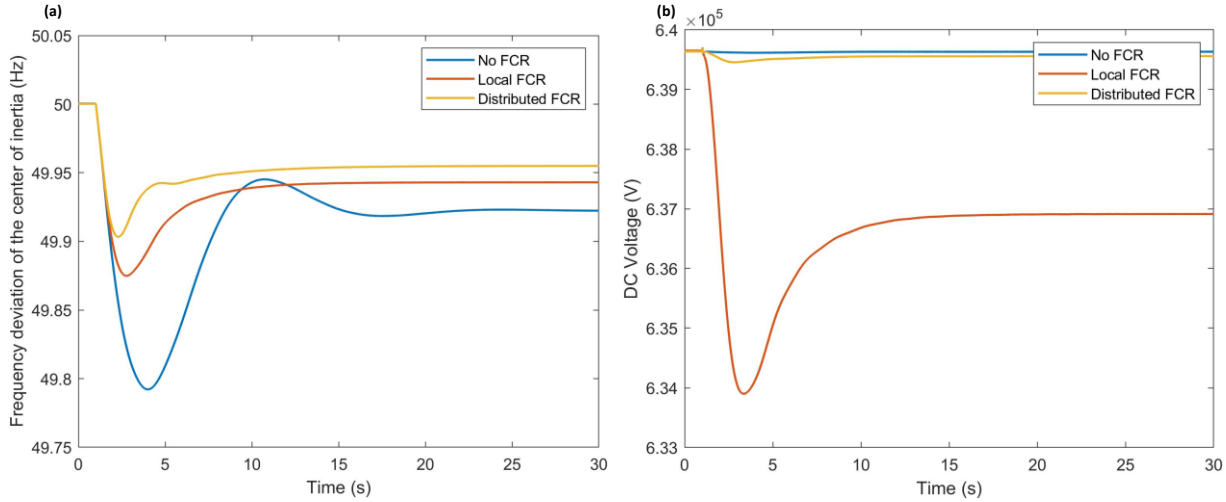

Figure n° 11 : Déviation de la fréquence du centre d'inertie du réseau perturbé CA 1 de sa valeur nominale (a) et variation de la tension CC (b) dans les cas sans FCR, avec contrôle lcoal et avec contrôle centralisé.

Dans ce chapitre, les contrôles suivants ont été combinés : POD, ADC et supports en fréquence et tension CC. Pour le faire, un nouveau contrôleur CA/CC central a été développé.

Le résultat de la simple combinaison de ces contrôles n'est pas satisfaisant car les oscillations persistent en dépit de la présence du contrôle POD (Figure n° 12). Ce n'est pas le cas si le même POD était implémenté tout seul.

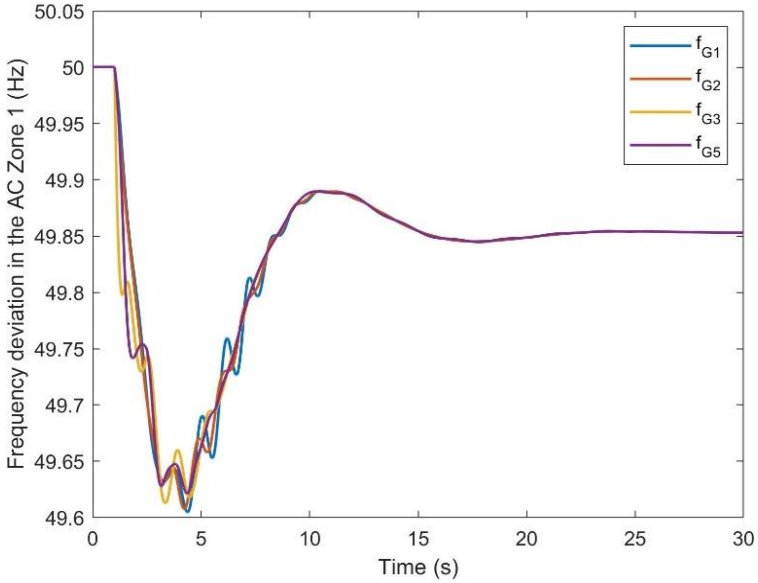

Figure n° 12 : Déviations de fréquence des générateurs restés connectés au réseau CA 1 de la valeur nominale après l'implémentation des contrôles POD, ADC et FCR au niveau du réseau CCMT.

Une stratégie de coordination des différents contrôles implémentés a été proposées en se basant sur l'allocation préalable de marges de puissance au niveau des convertisseurs. Le but de cette stratégie est de garantir à chaque contrôle une marge de référence de puissance avec laquelle il peut agir. Cela permet d'éviter la concurrence entre les sorties des contrôleurs, sorties résultant en des effets parfois antagonistes.

Le principe de la stratégie de coordination développée est de fragmenter la réserve de puissance active totale de chaque convertisseur et d'assurer la possibilité de canaliser la puissance active de référence à travers les liens CCHT. Ceci est possible en allouant, pour chaque contrôle, une marge de puissance active parmi la réserve de puissance totale au niveau des convertisseurs concernés par le contrôle en question.

La formulation mathématique de cette stratégie de contrôle a été développée en détail dans le chapitre. Elle peut se traduire par les marges présentées dans le diagramme suivant :

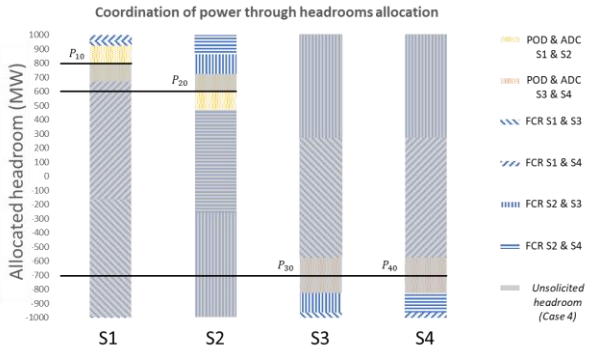

Figure n° 13 : Allocation de marge de puissance coordonnée entre toutes les stations et par lien virtuel.

Les courbes obtenues après implémentation de la stratégie de coordination implémentée montrent une amélioration des performances du système en termes de stabilité CA/CC.

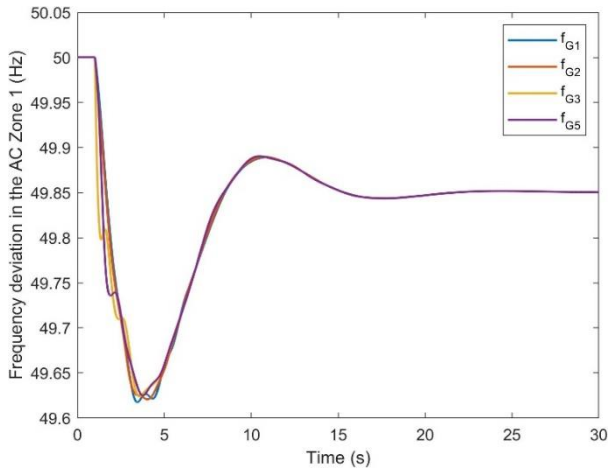

Figure n° 14 : Déviations de fréquence des générateurs restés connectés au réseau CA 1 de la valeur nominale après l'implémentation des contrôles POD, ADC et FCR au niveau du réseau CCMT, après implémentation de la stratégie de coordination du contrôle.

A ce stade, les gains des paramètres de contrôle ont été implémentés en adoptant une approche qui prend en compte plusieurs éléments à la fois dont :

- La valeur optimale des paramètres du contrôleur implémenté individuellement et en évaluant uniquement l'aspect de stabilité visé,
- Les constantes de temps de chaque contrôleur pour un éventuel découplage temporel,
- L'impact de la contingence sur la puissance de ligne CA et sur la fréquence,
- Les puissances nominales et disponibles au niveau des convertisseurs,
- L'essai-erreur lors de la combinaison de plusieurs contrôleurs.

Dans le chapitre suivant, une approche d'optimisation est adoptée.

Chapitre 7 : Optimisation du contrôle des liens CCHT pour l'amélioration de la stabilité CA/CC

Ce chapitre développe l'approche d'optimisation de contrôle afin d'améliorer davantage les performances du système CA/CC en termes de stabilité.

Le système à étudier dans le cadre de ce travail d'optimisation est de type boîte noire (Figure n° 15) parce que la relation entre un KPI donné et tous les paramètres de contrôle du système est quasiment impossible à déterminer. Ceci est dû aux non-linéarités dans le système et au couplage entre les contrôles, aux interactions entre un contrôle donné et un aspect de stabilité non visé, etc.

Une formulation du problème d'optimisation est réalisée à l'aide de la combinaison pondérée de KPIs normalisés et de dimension « par unité ». Certains KPIs ont été développés et d'autres utilisés directement à partir de la littérature dans cette thèse de doctorat.

La technique d'optimisation adaptée au problème formulé est de type métaheuristique car elle permet de converger rapidement et rigoureusement vers un optimum global sans connaître en détail le modèle mathématique régissant le système.

Une approche d'optimisation de type 'force brutale' (parcours de tout l'ensemble de valeurs possibles) a été implémentée pour des raisons d'illustration, en attendant la publication du travail sur l'approche de type métaheuristique qui a été développée sous Python.

Le gain des marges de puissance accordées aux contrôles de POD et ADC pour les convertisseurs $\{S1, S2\}$ et $\{S3, S4\}$ et FFR avec FCR pour le convertisseur $\{S1\}$.

Les résultats du parcours de domaine matriciel des valeurs de paramètres de contrôle donnent des combinaisons de gains qui mènent à une valeur de minimum global de la fonction coût calculée à partir des KPIs.

Les résultats d'optimisation se trouvent en Figure n° 16. Ils affichent deux combinaisons de gains distinctes qui permettent d'avoir un optimum global et un autre local mais très proche au niveau de la valeur de la fonction coût. Une analyse de ces deux optima a permis de comprendre lequel serait plus intéressant pour un opérateur gestionnaire de réseau électrique.

D'autres KPIs peuvent entrer en jeu tels que le coût de services auxiliaires par exemple. Leur inclusion pourrait encore changer les valeurs des marges de puissance optimales.

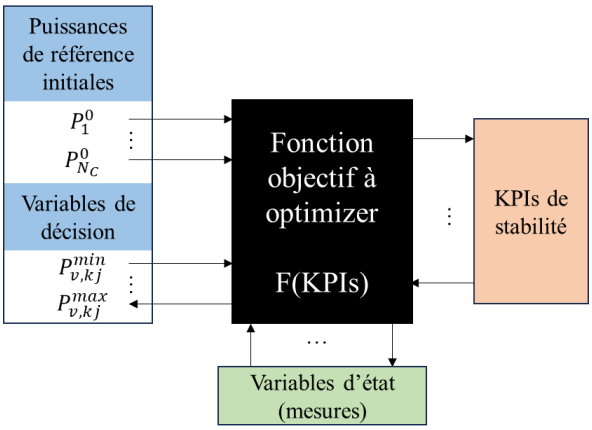

Figure n° 15 : Diagramme représentant le problème d'optimisation de type boîte noire.

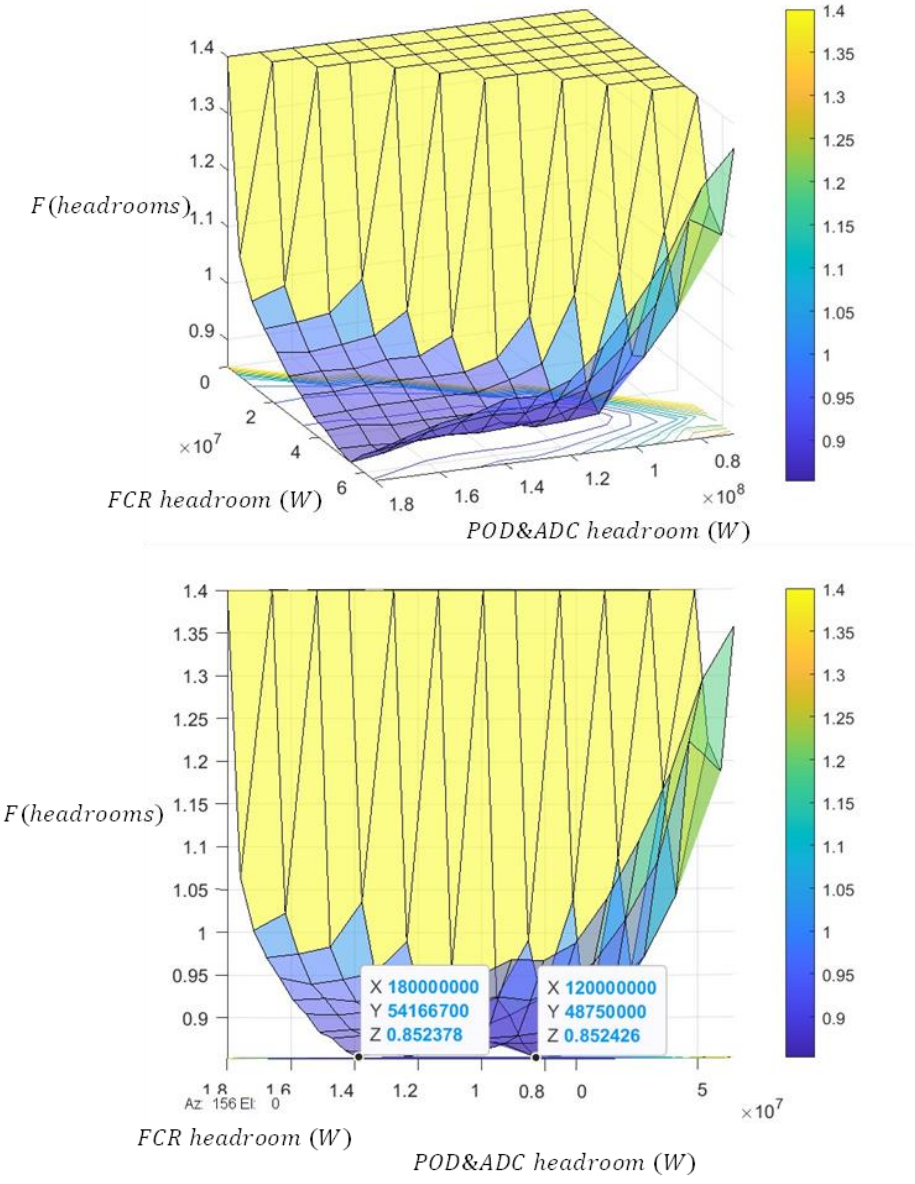

Figure n° 16 : Deux points de vue de la courbe 3D obtenue avec le parcours du domaine de possibilités pour les marges de puissance active pour les contrôles de {POD+ADC} et FCR.

Chapitre 8 : Conclusion et perspectives

Conclusion générale

Dans cette section, une conclusion par chapitre est réalisée ainsi qu'une conclusion générale. Ensuite, des perspectives de développement de la recherche sont proposées.

Dans le cadre de cette thèse de doctorat, différentes références de systèmes électriques ont été étudiées. Les études visaient à évaluer les critères de stabilité individuels et combinés d'un système électrique CA/CC. L'évaluation est basée sur des KPIs de stabilité qui utilisent les mesures du système électrique.

Les études ont montré le risque de développement d'interactions de contrôle conduisant à des impacts antagonistes sur les aspects de stabilité. Pour résoudre ce problème, des stratégies de découplage des commandes ont été proposées dans la thèse. Pour les systèmes électriques plus complexes, ces stratégies ne peuvent pas être utilisées directement. Par conséquent, des cadres de travail complets pour l'évaluation et l'amélioration de la stabilité ont été proposés.

Des contrôleurs distribués et centralisés ont été conçus pour améliorer la stabilité CA/CC. Des scénarios de perturbation spécifiques ont été développés et des conditions initiales spécifiques ont été testées. Les problèmes de stabilité réalistes résultant des perturbations ont d'abord été abordés individuellement, puis dans le cadre d'une approche globale.

Pour minimiser les interactions de contrôle mentionnées, deux approches de coordination du contrôle actif de la puissance sont explorées. La première proposée est basée sur la réaffectation de la puissance active entre les convertisseurs, tandis que la seconde est basée sur l'affectation de la marge de manœuvre sous contrainte.

Pour améliorer encore la stabilité, une couche d'optimisation est ajoutée au contrôle du système d'alimentation CA/CC.

Le problème à optimiser est formulé mathématiquement et un test est effectué. Les résultats valident l'intérêt de résoudre de tels problèmes d'optimisation, raison pour laquelle une approche d'optimisation métaheuristique a été développée et validée également. L'optimisation montre comment, pour améliorer la stabilité au mieux, on peut tirer le meilleur parti des degrés de liberté offerts par les systèmes CCHT en trouvant des compromis intéressants.

Perspectives

Pour aller plus loin dans la recherche, certaines perspectives de développement ont été identifiées. Bien que la combinaison d'autres aspects de stabilité soit intéressante, cette section se concentre sur différentes perspectives scientifiques. Elles sont décrites ci-dessous.

1. Pour l'optimisation

Quatre possibilités de développement principales existent pour la couche d'optimisation décrite dans la thèse.

- Optimisation de la première approche d'amélioration de la stabilité proposée :

Le problème d'optimisation a été formulé pour la deuxième approche de stabilité (allocation de la marge). Cependant, il est intéressant d'évaluer les résultats de l'optimisation des ratios de réallocation de la puissance active (dans la première approche) en termes d'amélioration de la stabilité multicritères.

- Optimisation des paramètres de contrôle :

Les paramètres de contrôle (ADC, POD, chute de tension CC, FCR) ont été définis en fonction de critères de stabilité physique (différence maximale d'angle de rotor, déviation maximale de la tension CC, etc.). Des essais par tâtonnement ont été effectués pour déterminer les meilleures valeurs pour ces paramètres. Cependant, une approche d'optimisation pourrait également aider à donner le meilleur ensemble de paramètres pour les contrôleurs mis en œuvre.

- Inclure le modèle de coût dans la fonction de coût :

Les KPIs actuels utilisés dans la fonction objective de l'optimisation n'incluent pas de modèle de coût pour l'application et la mise en œuvre des contrôles CCHT. L'impact de l'inclusion de ces coûts (OPEX et CAPEX) peut influencer la stratégie de déploiement des services auxiliaires CCHT d'un Gestionnaire de Réseau de Transport (GRT) et donc la stabilité des systèmes électriques.

- Utilisation de techniques d'optimisation avancées :

La technique utilisée dans le chapitre 7 est basée sur une sélection des paramètres de contrôle, mais d'autres techniques peuvent également être adaptées au problème exposé dans la thèse. C'est le cas des techniques basées sur une approche métaheuristique telles que PSO. Le travail sur cette approche est finalisé mais les résultats ne seront pas montrés dans ce manuscrit en l'attente de la publication préalable d'un article scientifique.

2. Pour la validation

Deux voies de développement principales ont été identifiées :

- De la simulation hors ligne à la simulation en temps réel :

Les études sont basées sur des approches de simulation hors ligne, adaptées à la phase de planification (par les GRTs). Il est scientifiquement intéressant de tester les stratégies de contrôle proposées sur un système électrique fonctionnant en temps réel.

- Hors ligne à en ligne :

Les stratégies de coordination proposées sont valables pour la simulation hors ligne. Elles peuvent être définitivement mises en œuvre par les GRTs selon le scénario le plus défavorable pour éviter l'instabilité. Par conséquent, les paramètres de contrôle sont définis en fonction du scénario le plus défavorable.

Toutefois, lorsque la perturbation n'aboutit pas au scénario le plus défavorable, l'ensemble de paramètres choisi peut ne pas correspondre aux meilleures performances de stabilité atteignables. L'ensemble des

paramètres peut devoir être modifié en ligne, en fonction de la perturbation détectée (déclenchement de générateur, déclenchement de ligne, etc.).

Bien entendu, les GRTs préfèrent que le comportement des réseaux électriques soit planifié. En outre, les GRTs ne modifient généralement pas leur ensemble de paramètres de contrôle en temps réel. En revanche, si les capacités de traitement informatique et l'acceptabilité du GRT le permettent, la situation peut évoluer. Il devient intéressant de tester des stratégies de coordination qui peuvent modifier les valeurs des paramètres de contrôle en fonction des indicateurs clés de performance du système mesurés en ligne.

3. Pour le contrôle

Deux avancées principales peuvent être intéressantes d'un point de vue scientifique :

- Utilisation de la commande prédictive par modèle (MPC) :

Pour le problème de stabilité du système électrique étudié dans la thèse, l'examen d'une stratégie d'amélioration basée sur le MPC peut être intéressant. Le MPC n'est pas vraiment développé dans la communauté des systèmes de puissance et les GRTs n'adhèrent pas complètement à de tels contrôleurs (puisqu'ils préfèrent les contrôleurs classiques). Néanmoins, le MPC est très adapté aux problèmes d'optimisation sous contrainte. Il les résout en prédisant l'état du système électrique dans les instants suivants, ce qui permet au MPC de trouver l'ensemble optimal de paramètres pendant l'exploitation d'un système électrique.

Le remplacement des contrôleurs classiques par des contrôleurs de type MPC constitue un changement de paradigme considérable pour les GRTs. L'examen de l'impact du contrôle MPC sur la recherche est toutefois réaliste.

- Utilisation de l'intelligence artificielle (IA) :

Dans cette thèse, des conceptions de contrôle classiques ont été mises en œuvre. L'objectif principal était de proposer une stratégie de coordination entre les contrôleurs de puissance active et, en outre, de formuler le problème d'optimisation à résoudre.

L'IA peut être mise en œuvre sous deux aspects différents :

- Évaluation : par exemple, classer les valeurs propres du système comme critiques ou non, etc.

- Amélioration : trouver le meilleur ensemble de paramètres basé sur l'apprentissage profond des performances du système électrique.

Cela mérite également un effort particulier, mais l'IA est sans aucun doute un domaine de recherche intéressant pour les systèmes électriques.

4. Pour les perturbations du réseau

L'étude des défauts de puissance du côté CC, du déclenchement des convertisseurs et de l'inversion du sens de la puissance échangée par les convertisseurs CA/CC nécessite des méthodes spécifiques de modélisation des défauts. Comme la version actuelle des bibliothèques utilisées ne permet pas de faire de telles études, il serait intéressant de s'attaquer à la modélisation de ces scénarii de perturbation (contingence).

Fin du résumé en français

List of Acronyms

- AC: Alternative Current
- ADC: Angle Difference Controller
- AI: Artificial Intelligence
- AVM: Average Value Model
- AVR: Automatic Voltage Regulators
- CAPEX: Capital Expenditure
- CNC: Connection Network Code
- COI: Center Of Inertia
- DC: Direct Current
- EAC: Equal Area Criterion
- EEAC: Extended Equal Area Criterion
- ENTSO-E: European Network of Transmission System operators for Electricity
- FACTS: Flexible AC Transmission Systems
- FCR: Frequency Containment Reserve
- FFR: Fast Frequency Response
- FSM: Frequency Sensitive Mode
- HIL: Hardware-In-the-Loop
- HV Gate: High-Value Gate
- HVAC: High-Voltage AC
- HVDC: High-Voltage DC
- IEV: International Electrotechnical Vocabulary
- IGBT: Insulated Gate Bipolar Transistor
- INELFE: Interconexión Eléctrica Francia-España (Electricity Interconnection France-Spain)

- iPOD: Intelligent POD
- ISGA: Integral Square Generator Angle
- KPI: Key Performance Indicator
- LCC: Line Commutated Converter
- LPF: Low-Pass Filter
- LV Gate: Low-Value Gate
- MiPOD: Multi-band iPOD
- MMC: Multi-Modular Converter
- MPC: Model Predictive Control
- MTDC: Multi-Terminal DC
- OPA: Operating Point Adjustment
- OPEX: Operational Expenditure
- P2P/PtP: Point-to-Point
- PCC: Point of Common Coupling
- PE: Power Electronic
- PF: PowerFlow
- PHIL: Power HIL
- PI: Proportional-Integral
- PLL: Phase-Locked Loop
- PMU: Phasor Measurement Unit
- POD: Power Oscillation Damper
- PSO: Particle Swarm Optimization
- PSS: Power System Stabilizers
- PWM: Pulse Width Modulation
- RC: Resistive-Capacitive

- RDIR: Research, Demonstration, and Innovation Roadmap
- RES: Renewable Energy Source
- RoCoF: Rate Of Change Of Frequency
- RoCoV: Rate Of Change Of Voltage
- SCL: Stator Current Limiter
- SG: Synchronous Generator
- SM: SubModule
- SMIB: Single-Machine Infinite Bus
- STATCOM: STATic synchronous COMpensator
- TSO: Transmission System Operator
- V2G: Vehicle-to-Grid
- VSC: Voltage Source Converter
- WAMS: Wide-Area MeasurementS
- WG: Working Group
- ZIP load: constant-impedance (« Z »), constant-current (« I »), and constant-power (« P ») load

Contents

List of Tables

List of Figures

Thesis Dissertation

Chapter 1 : General Introduction

I. Context

Power transmission system is undergoing structural changes mainly driven by the increase of share of renewable energies [1] implying more power electronic (PE) interfaced grids. These changes create challenges for the TSOs to operate the system. In this context, reinforcement and upgrading of the grid are necessary. Development and expansion of High-Voltage Direct Current (HVDC) point to point links [2] has proven to be the most mature solution in many situations. A more complex configuration of power transmission through DC lines is called MTDC implicating multiple terminals of conversion and therefore a more elaborated system compared to point-to-point HVDC. Since renewable power production devices are replacing conventional generators, their intermittence decreases availability of primary reserves of power system. Another problem emerges directly from the use of PEs: the inertia classically provided to the system by AC synchronous generators is not equivalently provided directly by power converters interfacing renewables [3]. While PE devices allow faster and more flexible power control for stability enhancement [4], their vulnerability against perturbations makes power system's robustness disputable.

The transmission projects in European continent are shown in this map (***Figure 1-1***) [5] where 58% (25'000 km of the 43'000 km) potential additional cables and lines are expected to be DC and 42% AC (18'000 km).

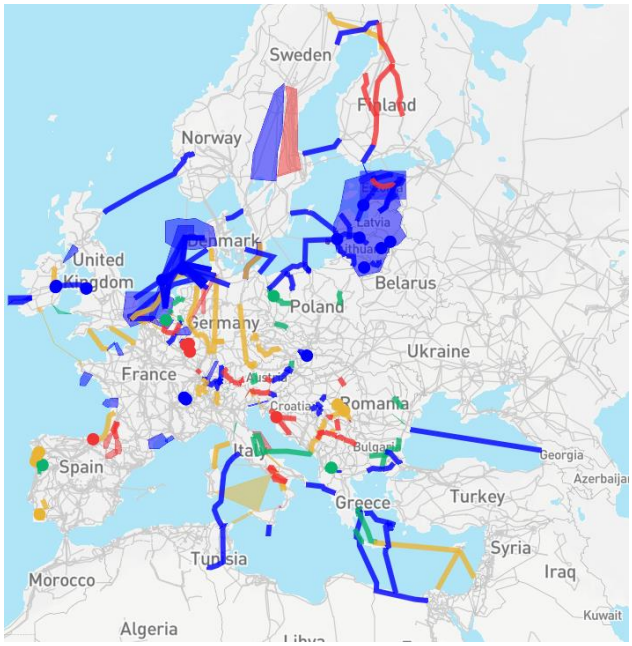

Figure 1-1: Map of power transmission projects in European continent [5].

The increasing integration of HVDC in the current grid, will lead to complex interconnected AC/DC grids. Controllability of HVDCs could serve in stabilizing the system [6] such as in power flow balancing and participation to frequency services to HVAC side [7]. MTDC grid can contribute as well to power balancing of connected AC grid. However, if no power storage or fast production systems are connected to the system, the DC power needed should come from/go to another AC system, creating

disturbances. The increasing amount of HVDC, associated with the use of supplementary controllers leads to interactions. These interactions address two initially decoupled AC systems, or an AC and DC interfaced grids. These couplings affect global AC/DC power system's stability [8]. For this reason, both architectures and operation of the MTDC grid must be adapted, even optimized. The main questions pointed on by the thesis are:

- What terminal to take the power from?
- What amount of power to take from each terminal?
- How are interoperability requirements addressed (feasibility, coordination, automation of actions, etc)?

In the ***Figure 1-2***, the related-to-this-topic ENTSO-E requirements for secure operation of widespread AC/DC grids are shown.

They are available under Flagship 5 of the ENTSO-E Research, Demonstration and Innovation Roadmap for 2020-2030 [9]. With the emergence of new hybrid AC/DC power systems, new assessment tools and controls are needed for stability enhancement.

In the ENTSO-E's position paper [10], short, medium, and long-term needed actions are developed. The interesting points are extracted and listed in the following.

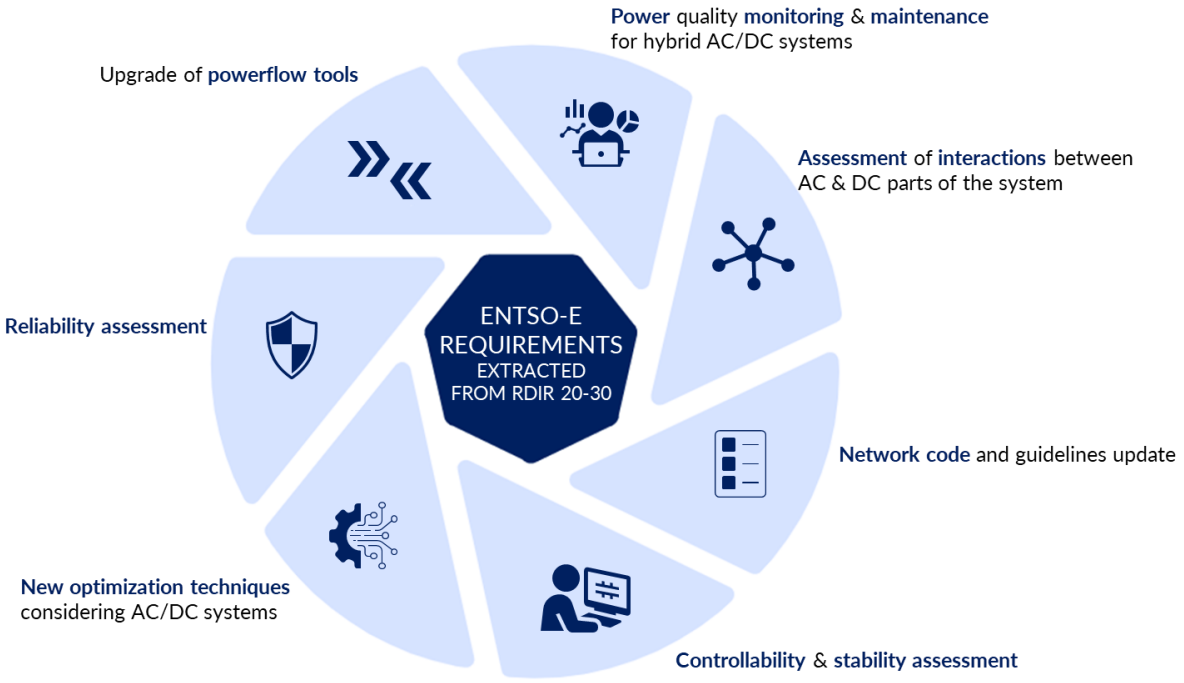

Figure 1-2: ENTSO-E requirements for the operation of AC/DC power systems (extracted from the Research, Demonstration, and Innovation Roadmap).

In cooperation with the policy makers and stakeholder, ENTSO-E and TSOs should:

- "In short term,
    - Create a common and comprehensive European roadmap for stability management based on a description of the necessary capabilities of the future power system and grid codes.
    - Identify areas for stability assessment and control where standardisation is necessary and/or beneficial.
    - Identify a range of new technical capabilities, system services and methodologies to handle the controllable resources and flexibility necessary to maintain system stability, system security and grid resilience.
- In mid-term,
    - Propose methods to predict and monitor system stability and handle controllable resources and flexibility, necessary to maintain system stability, system security and grid resilience.
    - Identify and specify the required technical capabilities of inverter-based assets such as grid forming and interoperability and propose grid code amendments for further harmonisation across Europe. The CNCs should evolve to ensure the equipment capabilities needed for a power system with a high penetration of RES. These new capabilities may be new fast frequency reserves or grid forming functionality. The timeframe for implementing network codes must considered as the challenges have to be faced in sufficient time. TSOs may need to acquire and operate some stabilising capabilities if the market is unable to provide them in time or if code amendments cannot be implemented sufficiently quickly.
    - Develop high-level specifications of power system models, asset models and simulation tools capable of analysing new and challenging European stability phenomena in PE-dominated systems with high penetration of RES. This also requires that the current issues regarding confidentiality and intellectual properties of manufacturers' models are solved.
    - Develop market mechanisms appropriate for ensuring the availability of necessary system services, the capabilities of controllable resources, and the flexibility to maintain system stability, system security and grid resilience.
    - Analyse roles and responsibilities with regards to the stability management of the pan-European grid, considering the cross-regional aspect of certain stability phenomena and the impact of cross-sector integration.

- In long term,
    - Deploy prediction, monitoring and communication systems for stability management on a pan-European level.
    - Ensure that stability issues are considered in the planning processes of network development.
    - Support vendors and manufacturers in the development and deployment of new capabilities in inverter-based assets through the testing and assessment of new technologies and to ensure interoperability.
    - Develop and verify power system models, asset models and simulation tools capable of analysing new and challenging European stability phenomena."

This PhD thesis is aligned with the cited targeted actions as it aims to propose a roadmap for stability assessment and enhancement, using new controls and assessment strategies using the technical capabilities of HVDC links. These control strategies are also tested in this PhD thesis on comprehensive power system models developed for this purpose.

II. Scope of work and objectives of the thesis

With the multiple opportunities that HVDC links offer for power transmission and control, the challenge of maintaining or even enhancing the power system stability remains relevant today. The considered time scales for the power system stability enhancement range from ~ 50 ms (DC voltage) to $\sim tens$ of seconds (AC frequency and AC rotor angle) [11].

The main objective of this thesis is to study the possibilities to enhance AC and DC stabilities through the exchanged active power via AC/DC conversion systems. A special focus is made on the ancillary services that a DC system can offer to an AC system by using power converters' additional functionalities. A methodology of tuning the controllers and two active power control coordination strategies are proposed to enhance the considered stability aspects. These aspects cover AC frequency, AC rotor angle and DC voltage. The combination of multiple controllers for the multi-stability aspects problem is not straightforward: enhancement of one stability criteria may deteriorate another one. Therefore, a trade-off should be found between the different control outputs to enhance the stability of the whole AC/DC power system in a global way.

The used AC/DC converters are VSC-based and MMC-based in grid-following mode [12]. Their active power is controlled from a hybrid AC/DC power system point of view. Therefore, the added control loops are external to the converter to which they send an active power reference. From the converter's internal control point of view, the necessary loops were already implemented in the existing libraries and were understood and used as they are.

This PhD thesis work tackles the issues related to the connection of HVDC links through different configurations: P2P embedded HVDC links, and non-embedded MTDC system (***Figure 1-3***). This contributes to the integration of HVDC links in the existing AC transmission system and deals with the

issues of power security degradation by using quantifiable stability key performance indicators (KPIs). Analytical approach was adopted in the beginning of the thesis for simple case studies, but numerical approach was necessary to understand the phenomena happening in larger power system benchmarks.

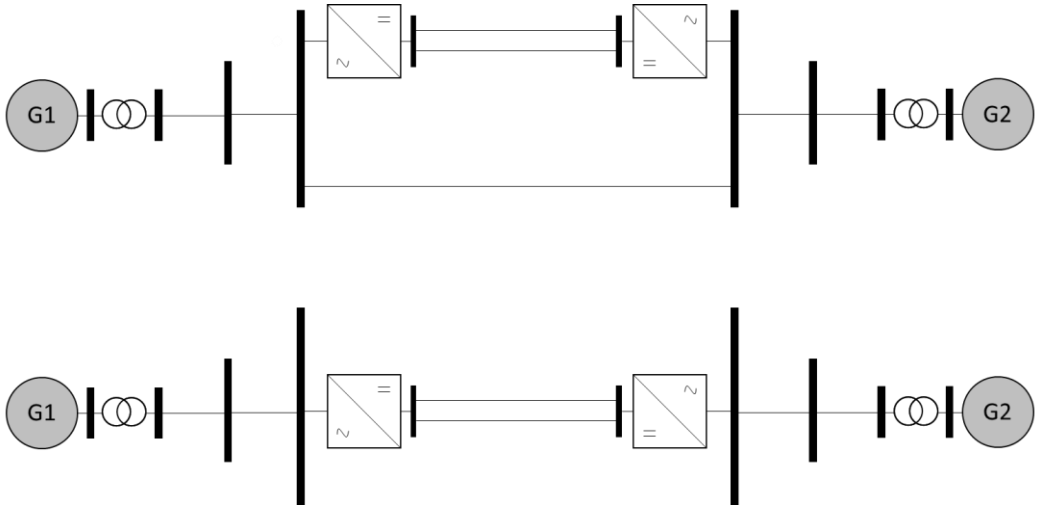

Figure 1-3: Example of embedded (top) vs non-embedded (bottom) P2P HVDC links in an AC/DC power system benchmark.

As simulation is a principal pillar of the thesis work, it necessitates significant development work effort to master and use multiple simulation environments, to understand different necessary simulation libraries, and to combine different components with their proper parameter tuning. The numerical approach also requires the development and testing of new power system benchmarks associated with relevant stability KPIs.

To capture these KPIs' sensitivity, time-domain and modal analyses were performed. This necessitates a plausible initial AC and DC power flow to initialize the simulation processes. It also requires the study and development of multiple perturbation scenarios:

- AC power fault followed by line tripping,
- Synchronous generator loss,
- Load variation, etc.

DC power faults were out of scope of this work although the case of power converter trip was tested briefly but necessitated further library models [13], [14]. Moreover, local, and central controllers are determined and tested for the deployment of HVDC ancillary services in order to mitigate the studied contingency scenarios.

Finally, in parallel to the tool development effort, analytical work is necessary to create interesting case studies, to properly design the controllers and to post-process the simulation results. Through the different case studies performed on various benchmarks, the aim was first to understand the ongoing stability issues and then capture the behaviour of the most significant physical variables. This allows to

propose controllers and design methodologies for their parameters. Accordingly, two coordination strategies are suggested to enhance the stability of the AC/DC system considering multiple controllers in the case of a non-embedded MTDC system.

III. Main contributions of the thesis

The main contributions of this thesis are summarized below:

- Examine the opportunities and challenges emerging from the usage of HVDC systems for power transmission,
- Investigate the different stability aspects to evaluate for planning and operation of a power system,
- Identify the potential control interactions emerging from:
  - The coupling of AC and DC power systems,
  - The simultaneous solicitation of different controllers leading to antagonist effects.
- Propose and develop different benchmarks to perform stability analysis: eigenvalue and time-domain approaches,
- Integrate decoupling strategies in power converter control to minimize control interactions,
- Propose different frameworks for stability assessment and enhancement,
- Establish two active power coordination methodologies and validate them through comparative studies,
- Propose new distributed and centralized controllers,
- Achieve the formulation of the objective function to be solved by an optimization layer of control. Test this optimization layer.

IV. List of publications

The publications resulting from this thesis are listed below:

Journal papers

- G. Bakhos, S. BACHA, J. C. Gonzalez-Torres, L. Vanfretti, A. Benchaib, K. Shinoda, et J. DAI, « Hybrid AC/DC Power System Stability: An Attempt of Global Approach » in EPSR Elsevier **(submitted)**.
- K. Shinoda, J. Dai, G. Bakhos, J. C. Gonzalez-Torres, A. Benchaib, et S. Bacha, « Design consideration for frequency containment reserve provisions by a multi-terminal HVDC system », IET Gener. Transm. Distrib., vol. 17, no 18, p. 4024-4037, 2023.

Conference paper

- G. Bakhos, K. Shinoda, J. C. Gonzalez-Torres, A. Benchaib, L. Vanfretti, et S. Bacha, « Aspects of stability issues of HVAC/HVDC coupled grids » in *2022 24th European Conference on Power Electronics and Applications* (EPE'22 ECCE Europe), Hanover, Germany, 2022, pp. 1-10.

Pre-print papers

- K. Shinoda, G. Bakhos, J. C. Gonzalez-Torres, J. Dai, et A. Benchaib, « FCR Provisions by Multi-Terminal HVDC System », doi: 10.36227/techrxiv.16644952.v1, TechRxiv, 2021.

- G. Bakhos, S. Bacha, J. C. Gonzalez-Torres, L. Vanfretti, A. Benchaib, J. Dai, K. Shinoda, « Hybrid AC/DC Power System Stability: An Attempt of Global Approach », doi: 10.2139/ssrn.4704802, SSRN Elsevier, 2024.

Webinar

- G. Bakhos, «Advantages and Challenges of HVDC links », CIGRE NGN France-Ireland, https://cnf-cigre.org/wp-content/uploads/2021/09/Collab-Interconnection-NGN-Posterfinal.pdf), 2021.

V. Organization of the manuscript

The manuscript is organized as follows:

- In Chapter 2, a general state of the art of the HVDC links' opportunities and challenges is presented. Then, the HVDC architectures (Point-to-Point, Multi-Terminal DC, radial, meshed, etc.) and types of AC/DC power converters were also discussed. From the various available converter technologies, VSC ones are the most adapted. Their advantages are also shown in the chapter. After this, the different existing stability aspects of a power system were illustrated. From these aspects, the rotor angle, frequency, and DC voltage were selected for the rest of the thesis. The chapter also clarifies the coupling issues between AC and DC power systems. These issues specifically emerge when perturbations occur in the power system.

- In Chapter 3, AC and DC power systems' components were presented. These components include:
    - The synchronous generators and their internal controllers (PSS, AVR, turbine governor),
    - The loads,
    - The AC and DC links,
    - The AC/DC power converters.

  Though this PhD thesis tackles power system control issues, power electronics' (MMCs) physical models are represented in the chapter. Their block diagram, and their outer and inner control loops are discussed as well.

  After this, power system benchmarks were built in an increasing complexity approach. These benchmarks are modelled in a MODELICA-based environment where two main types of stability assessments are lead. These types are eigenvalue analysis and time-domain analysis.

  In this chapter, simulations' methodology and workflow are developed.

- In Chapter 4, the different stability aspects are assessed on realistic benchmarks where HVDC ancillary services are implemented. The assessment approach is progressively built:

    - Study of impact of adding power converters on the stability of AC power systems.

    - Study of rotor angle stability aspect separately: transient, steady-state and small-signal

- Study of frequency, DC voltage and rotor angle stability aspects in a simultaneous approach.

The possible interactions between different controllers are studied. Afterwards, decoupling strategies are proposed in this chapter. Though these strategies work for simplistic benchmarks, frameworks for stability assessment and enhancement are proposed for more complex ones. Five frameworks were developed in this chapter They can be distinguished by their degree of communication and their degree of active power coordination.

- In Chapter 5, a power system benchmark composed of two Kundur-based systems connected through an MTDC meshed system is used. This allows to tackle multiple stability aspects simultaneously. In the studies, different stability controllers are combined at converter level. At this stage, they are local controllers that coexist together and propose supplementary functions by the power converters.

  Afterwards, a comparative case study is lead. The chapter shows how, when HVDC links propose multiple ancillary services simultaneously, control interactions emerge. These interactions may badly affect some stability aspects while enhancing others.

  To solve the issues raised by the antagonist interactions, a first stability enhancement strategy is proposed. The approach in this chapter relies on the concept of active power reallocation among the operating converters. After mathematically formulating the controller and testing it numerically, power system analysis is performed anew to validate the strategy.

- In Chapter 6, a different stability enhancement strategy is examined. Here, the approach is based on power converter headroom constrains. A centralized AC/DC controller is designed firstly. It contains a new frequency controller design to provide frequency containment reserve.

  Then, a power system stability analysis is made through comparative case studies. The active power headroom allocation strategy is mathematically formulated and then tested on the used power benchmark.

- In Chapter 7, an optimization approach is proposed and tested. After exploring the different types of optimization problems, the problem to optimize in this thesis is mathematically formulated. A proof-of-concept of the optimization approach is validated through a case study.

Chapter 2 : General state-of-the-art of HVDC links challenges to support hybrid AC/DC system stability

I. Introduction

1. Context

Electricity generation, transmission, and distribution is evolving at high stance nowadays thanks to technological developments and investments. Particularly, the use of renewable energy sources (RES) is expected to increase significantly in the coming years [1]. To accommodate this, many high-voltage direct current (HVDC) systems have been built to transfer efficiently the RES's energy to the consumers [15]. Practically, power electronics converters are being used to integrate these renewable energy sources such as photovoltaics and windfarms and new types of loads, such as electric vehicles.

In parallel, some specific changes are happening in power systems:

- The use of more renewable energy sources, such as solar and wind power, which are intermittent and sometimes unpredictable,
- The growth of distributed generation, which refers to the generation of electricity from small-scale sources, such as rooftop solar panels,
- The e-mobility policies (V2G issues),
- The development of smart grids, which use digital technologies to improve the efficiency and reliability of power systems,
- The development of interconnections between transmission grids in order to enhance stability and power exchange capabilities.

These changes are putting a strain on traditional power systems, which were designed to operate with a small number of large, centralized generators. Power electronics converters are being used to address these challenges by providing flexibility and controllability. They can be used to regulate voltage, balance power production and consumption, and integrate renewable energy sources. This will lead the power system operators to modify their power transmission strategies due to different dynamics brought by power electronics and due to the replacement of direct connected synchronous generators by power electronics-interfaced sources.

2. Organization of the chapter

In this chapter, information about HVDC links development is assembled and the used converter technologies to address this goal are discussed. With that, hybrid AC/DC power systems are created. In these systems, traditional inertial components (synchronous machines, etc.) coexist with new fast-reacting components.

The chapter is organized as follows: in section II, the advantages of the HVDC links are presented as well as the technologies that sustain their development. In section III, definition and classification of power system stability is presented under different stability criteria. Moreover, the coupling between

AC and DC power systems is discussed based on literature review. This coupling gives room to AC/DC interactions that may jeopardize the stability of the whole AC/DC power system.

II. Integration of the HVDC links in the existing power systems

1. Advantages of HVDC links over HVAC links

Currently, the HVAC transmission lines are the most used for power transfer. However, new developments in HVDC technology and the economic advantages of using DC links instead of AC links in some cases, suggest that HVDC transmission systems may become more developed in the future.

HVDC grid presents economic and stability advantages for the export of power compared to HVAC:

- Lower voltage drops therefore higher transmission distance capability due to the absence of reactive power flow in DC links.
- Higher transmission capacity with same quantity of copper, insulators materials, etc.
- Lower power transmission cost (after a breakeven distance, see ***Figure 2-1*** below). This is particularly useful for the connection of offshore windfarms.
- Ability to connect two AC zones operating in different frequencies (asynchronous zones). This is also useful for the integration of renewable energies to the existing AC power system.
- Higher controllability of power flow with the usage of power electronics. This allows for stability enhancement of AC systems using the DC power system.

The breakeven distance showing the economic advantage of using HVDC P2P links over HVAC is shown in the ***Figure 2-1*** below [16], [17].

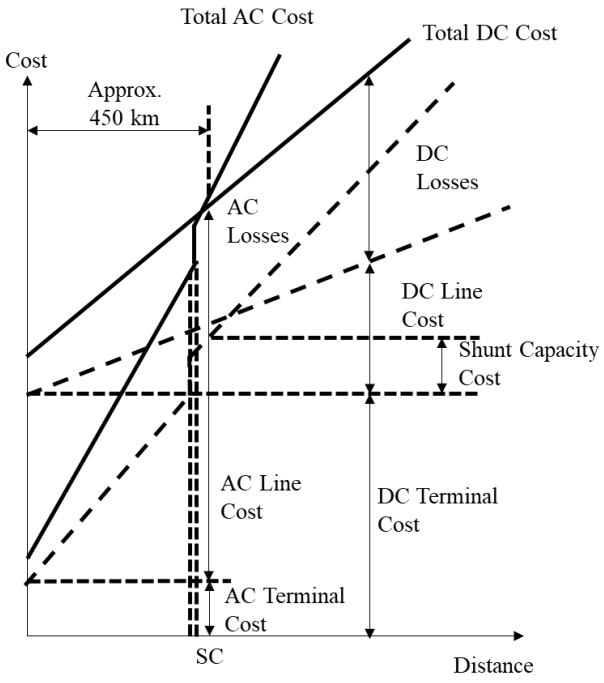

Figure 2-1: Evolution of AC and DC transmission costs per power transfer distance.

The initial cost of HVDC transmission system is higher than that of the HVAC due to expensive converting station cost. The DC line transmission cost is however lower than that of AC lines due to lower number of needed cables. The Shunt Capacitors (SCs) [18] are needed in AC transmission system to mitigate the AC voltage drops and rises, and to improve the Power Factor. They compensate the reactive power needed especially in the case of connection of inductive loads. The usage of AC lines instead of AC cables, requires installation of SCs every 100 to 200 km. To these costs in AC power transmission, the power losses are added and show great advantage of DC transmission instead of AC. This is particularly true after the breakeven distance of approximately 450 km.

2. HVDC architectures

The HVDC system can be composed of only two stations connected through a P2P link with specific configurations (monopolar, bipolar [19]) or of multiple stations that create a Multi-Terminal DC (MT-HVDC or MTDC) system. An MTDC system consists of one of the following configurations:

- Series MTDC: composed of multiple P2P DC links connected in series. The weakest link or converting station determines the power transfer capacity of the MTDC system.
- Parallel MTDC: composed of multiple P2P DC links connected in parallel. This allows for bidirectional power flows simultaneously and the power transfer capacity is equal to the sum of the capacities of the parallel links.

More complex configurations can be developed from the parallel MTDC structure (***Figure 2-2***):

- Radial: DC links emanate from a single point and connect the terminals together.
- Meshed: this configuration allows for more DC link redundancy than the radial one.

The paper [19] illustrates these configurations in the diagrams shown in the ***Figure 2-2*** below.

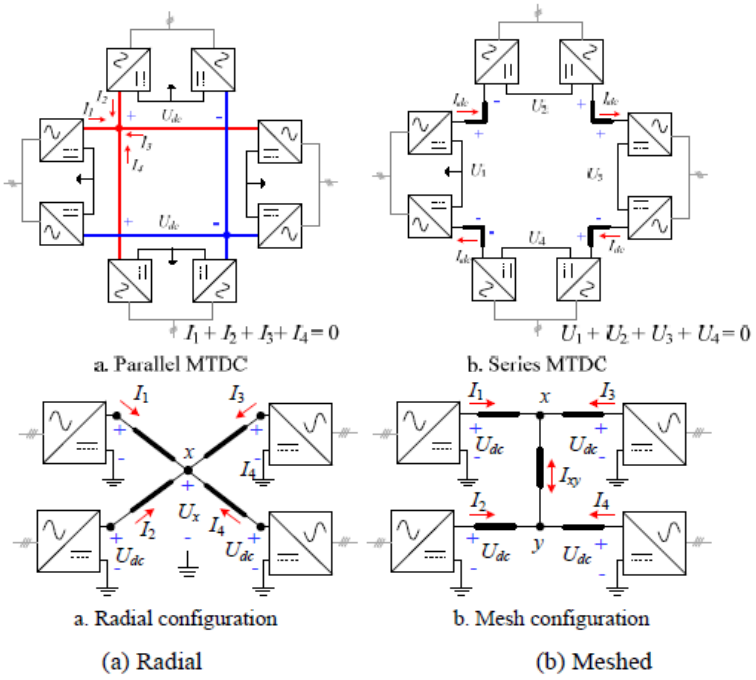

Figure 2-2: Various configurations of DC power systems [19].

The complexity in construction and operation of a P2P HVDC link is reduced compared to that of an MTDC. The stability of a P2P HVDC system may be guaranteed by one converter controlling the DC voltage (DC grid forming) while the other one extracts/injects the needed amount of power (DC grid following). However, in an MTDC system, the DC voltage-stable operation of power transfer must not be relying on only one station. This avoids total DC grid blackout if the station responsible of DC voltage control is lost. Therefore, some emerging challenges regarding the operation of an MTDC system [20] are explained here:

- MTDC system development and integration in the existing AC system are not straightforward. Which MTDC configuration should be installed? What are the DC grid code requirements to safely operate the MTDC grid? What objectives should be reached with the DC system: only power transfer or more services as well?

- MTDC system operation should comply with three main requirements: transfer of power (powerflow problematics), DC grid stability (relying only on DC voltage amplitude) and AC grid stability.

    - As explained before, the DC voltage control in an MTDC system is not as simple as in a P2P one. The DC voltage behaviour (dynamic and steady state) should also be compliant with the mentioned required grid codes and, consequently, the control of the MTDC terminals should be adequately designed.

    - Moreover, the powerflow through the DC links should be controlled only through DC voltage amplitude differences. Optimal DC powerflow solutions as well as flexibility of powerflow thanks the possible DC paths should be studied as well.

    - Provided that the integration of an MTDC system within an existing AC system is successfully accomplished (installation, connection, etc), the operation of the MTDC remains challenging when the AC/DC system stability is considered. In normal operation, the power exchange between each AC/DC converter and the connected AC system should be realized with respect to the stable operation of the AC grid. This means that the control of a converter should comply not only with its proper stability but also with the stability of a higher-level whole AC/DC system. The MTDC grid relies mainly on power converters which, if lost, could jeopardize the operation of the whole grid creating stability issues both at DC and AC sides of the converters.

    - Interoperability of AC/DC converter stations in the context of multiple vendors should also be tackled.

3. Types of AC/DC power converters

The AC/DC converters used can be either Line Commutated Converters (LCCs) or Voltage Source Converters (VSCs) or more hardly a combination of both [21], [22], [23]. The difference between them is developed in the following.

- **Line Commutated Converters (LCC)**

  Also known as Current Source Converters (CSCs) these converters use the thyristor valves for the commutation. As their LCC name suggests, these converters work based on the parameters of the AC line to which they are connected by changing the firing angle of the thyristors. Therefore, they require a strong synchronous voltage source to be connected to it at the receiving end to be able to commutate. In other words, an LCC alone cannot work in black-start mode and its AC fault ride-through capability is reduced.

  To evaluate the ability of an LCC to connect to an AC synchronous power system, the Short Circuit Ratio (SCR) indicator can be used as an indicator of the AC system's strength. As per [24], the SCR can be calculated as follows **(2.1)**:

$$SCR = \frac{S_{sc}}{P_d} \tag{2.1}$$

  where S_{sc} (in MVA) is the three-phase short-circuit capacity at the Point of Common Coupling (PCC) of the converter and P_d (in MW) is the active power rating of the DC power system.

  The parameter S_{sc} implicated the equivalent Thevenin impedance Z_{ac} as seen from the PCC and the Bus AC voltage U_{ac} in the equation **(2.2)** of the SCR:

$$S_{sc} = \frac{U_{ac}^2}{Z_{ac}} \tag{2.2}$$

  According to IEEE standard 1204–1997 [25], an AC system is considered weak or very weak if its SCR is respectively under 3 or under the Critical-SCR (CSCR) which is of 2 for a typical inverter design.

  The works [24], [26] reevaluate the usage of the SCR in the cases of power-electronics dominated system and multi-terminal or multi-fed DC systems.

  Added to the previous weak points of LCCs, this type of converters also requires reactive power for its proper operation which is an additional consumption necessary for active power transmission. Moreover, the LCC's current is unidirectional due to the usage of a thyristor. Consequently, DC power direction's inversion requires the inversion of DC voltage sign at both sending and receiving stations [27]. This makes the operation of LCCs unsuitable for the operation of DC meshed grids.

  From the other side, the main advantages of LCCs are the lower power losses, the degree of maturity of this technology and its minimal required maintenance.

- **Voltage Source Converters (VSC)** [28], [29], [30]

  The VSCs use Insulated Gate Bipolar Transistor (IGBT) technology controlled initially by Pulse Width Modulation (PWM). The voltage at the terminal of the converter is created independently of the state of the AC line to which it is connected, which allows for black start through VSCs. The PWM operates in frequency ranges of the order of kHz which reduces the size requirements of harmonic filters for a VSC compared to an LCC where the commutation frequency is in range [50-60] Hz.

  The VSC can operate in four quadrants meaning that the inversion of the power direction can be realized without the need for DC voltage sign inversion. This is particularly important for the usage of AC/DC converters in the context of an MTDC power system.

Additionally, the active and reactive power of a VSC can be controlled separately which offers the system operator the possibility to regulate the AC power as needed [27].
The first VSC project was realized by ABB in 1997 [31] for a 3 MW installation. The technology has evolved since then though the voltage and current ratings of IGBT-based converters are still inferior to those of thyristor-based ones [32]. A generic VSC station representation can be found in [32] as well.

Although the VSC technology allows for more flexible power flow and higher controllability of active and reactive powers at the converter, one drawback (other than that of the ratings of IGBTs) is that PWM control in a VSC station results in high switching losses due to high switching frequencies. This also reduces the maximum power that can be transferred by a classical VSC station.

A technology that addresses some of the drawbacks of the classical two-level VSCs is the **Modular Multilevel Converter (MMC)**. It can be described as an evolution of the VSC technology since it keeps the same characteristics (four quadrants operation without need to change voltage polarity, AC fault ride-through capability, etc) and addresses some of its drawbacks (higher power ratings, smoother outputs requiring smaller filters, lower power losses, etc).

The MMC technology was first used for Medium Voltage DC (MVDC) applications but is nowadays used for HVDC applications with the developments in the MMC's Sub-Modules (SMs). A state-of-the-art critical review of MMC configurations and submodule topologies is available in [33].

The main differences between LCC and VSC converters are synthesized in ***Table 2-1***. For the remainder of this work, and without contrary indication, the MMC-based VSC converter will be adopted for the studies.

Table 2-1: Comparison of LCCs and VSCs' advantages and drawbacks.

Component	Advantages	Disadvantages
LCC	Lower station losses Lower initial investment costs Mature technology (robust, reliable) High power capability	Huge harmonics contents Need for huge reactive power compensation Requires to be connected to high power AC system (no black-start capability) Larger footprint Reverse of power direction requires reverse of voltage polarity (not suitable for MTDC architectures)

VSC	Operable with weak AC grids (black-start capable) Active and reactive power controllability Reduced size so reduced footprint No need for large filters plant Reverse of power direction feasible through reverse of current direction (suitable for MTDC architecture)	Higher conversion losses Less mature technology (in development, weak experience feedback) Higher costs

III. Coupled AC/DC power systems: perturbations and interactions

1. Definition and classification of power system stability

Perturbations in a power grid affect its security (resilience) which is the main vigilance point in any power system.

In the ***Figure 2-3*** a distinction between the terms « reliability », « adequacy » and « security » for a power system [34], [35], [36] is made. There is no universal agreement on the definition of power system "resilience" but, in 2017, CIGRE Working Group (WG) SC C4.47 [37] has formulated a definition: **Power System Resilience** is the ability to limit the extent, severity, and duration of system degradation following an extreme event. According to this WG, to achieve or enhance power system resilience, key actionable measures should be deployed Before (B), During (D) and After (A) the occurrence of an event. These measures are listed below:

- "Anticipation" (B) refers to evaluating and monitoring the onset of potential disaster scenarios that can occur in the future.
- "Preparation" (B) is the process by which decision-makers move from resilience strategies to clear objectives that will guide the deployment of measures based on the knowledge gained during anticipation.
- "Absorption" (D): A system absorbs impacts of extreme events through the adequate process after which the event consequences are mitigated or avoided.
- "Maintaining" the operational capability of a power system that is impaired through sustaining critical system operations process (D, A).
- "Rapid recovering" (D, A) to contain or restrain the consequence of the perturbation on the operating power system.
- "Adaptation" (A) process after the event, changes the three levels of the power system's management, defence, and operational regimes.

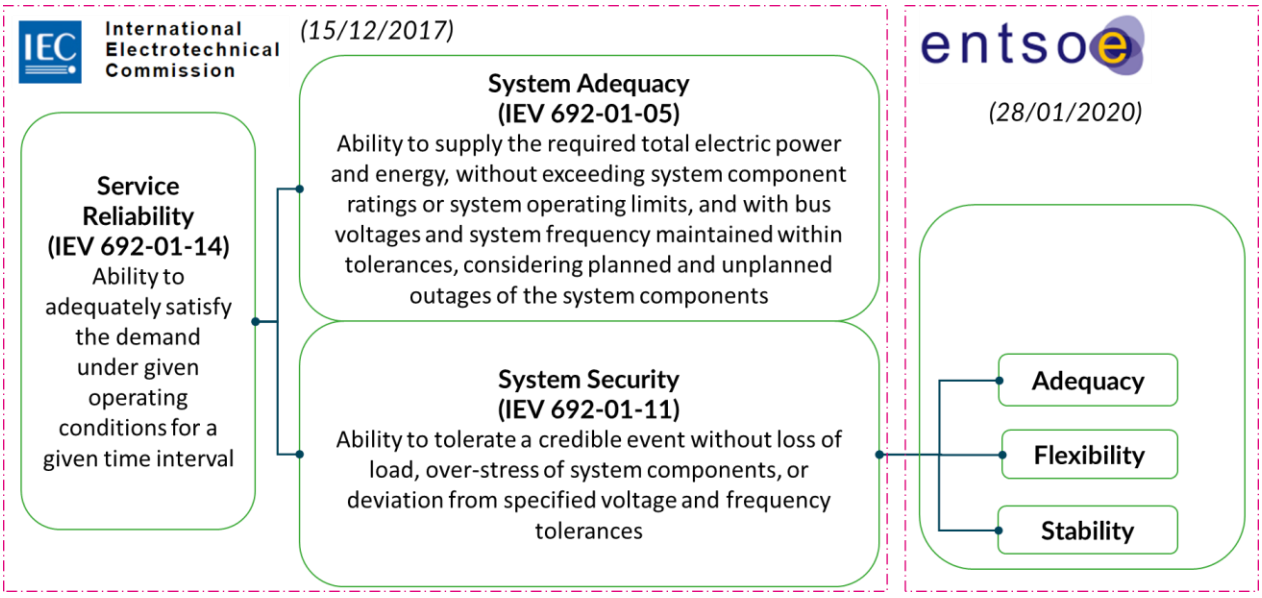

Figure 2-3: Distinction between reliability, adequacy and security related to power systems.

Some of the listed key measures are realizable through the control of the power system to keep it or move it to a secure operating zone. The term "security" can be projected to different domains such as cybersecurity, natural disasters etc. However, the considered security aspect in this thesis is related to the stability of the power system. In its turn, the stability can have multiple aspects [38], [39], [40], [41]. The considered ones are **shown** in the ***Figure 2-4*** below.

Based on literature review [39], [40], [42], the ANNEX 1 summarizes the stability physical aspects, their potential threats, and the encountered risks if a given stability is lost. Online measurable stability indicators are also mentioned in blue colour in the ANNEX 1.

Three main stability aspects are studied in the remainder of this work: AC frequency, AC rotor angle and DC voltage. They are related to active power variation in the AC and DC systems. The other stability aspects are not object of focus but could be developed elsewhere.

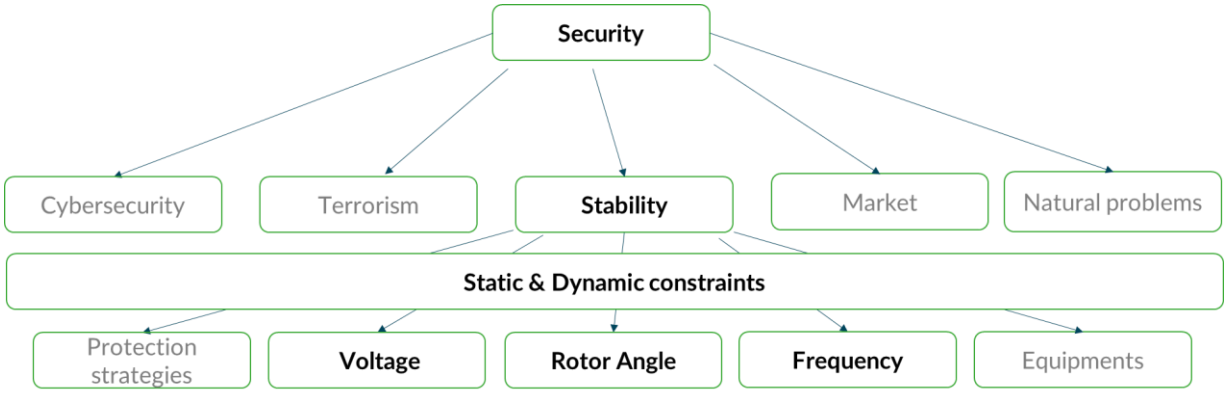

Figure 2-4: Considered power system security aspects.

2. Coupled perturbations and control interactions: requirement for controls' interoperability

With the development of hybrid AC/DC grids, new power stability issues are raised due to control interaction between AC and DC systems [43]. Moreover, during their operation, power systems are subject to disturbances which may jeopardize their stability if not efficiently mitigated. When considering hybrid grids, the coupling between AC and DC power systems makes room for coupled perturbations: if a contingency perturbates an AC system, the DC system may be disturbed as well and vice-versa.

In the following, a literature review on the existing perturbation coupling between AC and DC power systems and the interactions between their controls is made.

In [44], modal (small-signal) and time-domain analyses are performed on a hybrid AC/DC power system after studying the eigenvalues of AC system, a VSC alone and MTDC system separately. The provided tables in the paper show the eigenvalues corresponding to the main components of these power systems. First, the modes corresponding to each system alone are found again in the combined whole AC/DC system. Also, before implementing frequency support by the VSC converters, the modes corresponding to the PLLs are the only ones impacted (a little). However, when frequency support is added, the modes of the DC system are also modified since the active power control loop of the used frequency controller links the PLL measurements at the AC side of the system with the current control loop of the VSCs. This impacts the eigenvalues corresponding to the current control of the VSC. The time-domain analysis confirms that a perturbation of 80 MW on the AC side is coupled with a perturbation of the voltage on the DC side.

The coupling between AC and DC systems during perturbations is also proven in literature. It is partially due to the active power balance between AC and DC sides of a converter [45]. Perturbations can occur on AC side and/or DC side. The main types or perturbations are AC power fault leading to line outage, DC power fault leading to line trip, AC generator trip, converter outage, big load connection/disconnection, etc.

In [46], a three-phase AC fault is tested on VSC-based HVDC link in PSCAD/EMTDC. The AC fault impacts the DC voltage due to the active power controller of the converter. As a result, the DC voltage controller of another converter tries to bring the voltage values back to nominal, which may not always be possible if the controllers are not tuned to mitigate such contingency scenarios.

In [47], the impact of a converter outage on small-signal stability of electromechanical oscillations is analysed. The interactions between DC voltage droop control and electromechanical oscillations are investigated and a methodology to minimize these interactions is proposed.

In [48], [49], the effect of a DC fault is studied. As DC grid is of "low" inertia, a local fault can directly impact all the DC grid and impact the AC grid severely, which may lead to hybrid AC/DC system's instability. As DC voltage is directly impacted by DC faults, the frequency of the connected AC grid can be modified. This is due to the variation in power exchange between AC and DC grids after the DC voltage controller's output is changed when the fault occurs.

The interaction between supplementary frequency support by HVDC and Power System Stabilizers (PSS) and Automatic Voltage Regulators (AVR) in an AC system is investigated in [50]. The impact of the location of the point of injection of the AC/DC converter as well as the gain of the frequency controller are more specifically studied for the case of a Single-Machine Infinite Bus (SMIB) system. The analytically derived expression of the mentioned gain for optimal frequency support as well as the simulations show that the frequency controller may negatively impact AC rotor angle stability if it is tuned arbitrarily. Depending on the existing gains of the PSS and the AVR, and for a given location of the point of injection of HVDC system, the transient and small-signal stabilities of electromechanical oscillations are impacted. The analytical approach presented is valid for the simple case of a SMIB with one converter but is however questionable for AC/DC power systems with a higher number of synchronous machines and power converters. Nevertheless, the work shows clear interactions between existing AC and added HVDC controllers, which may put the stability of the hybrid power system at risk.

In [51], [52], [53], the impact of adding the converters to interface the AC system with DC system is studied. The studies show that the fast controllability of these converters results in new modes of high frequency range (kHz, compared to electromechanical oscillations of a frequency range less than nominal AC frequency) not initially existing in the AC systems. In the mentioned works, three types of control interactions have been identified [54], [55], [56]: AC voltage control (when LCC or VSC is used), electromechanical torsional and electromagnetic. Though important for the stability of the power system, these types of interactions are not investigated in this work.

IV. Conclusion

In this chapter, the following was discussed:

- An introduction to the advantages of using HVDC for power transmission instead of AC transmission grids. This was followed by a presentation on the HVDC potential configurations.
- A comparison between converter technologies (LCC and VSC, followed by MMC-based VSC). VSC converters are more adapted to weak grids and offer better controllability.
- An overview of the stability definitions followed by a discussion on the potential hybrid AC/DC power system's stability threats.
- A review of the coupled perturbation phenomena happening in such power systems as well as the control interactions between classical AC grids and newly developed DC grids according to recent literature.

The design and interoperability of different controls to enhance AC/DC stability is a topic of high interest today. The design of these controllers will be investigated in the next chapters. Before that, the simulation environment and the benchmark AC/DC power system propositions will be presented for control design and coordination.

Chapter 3 : AC/DC power system modelling – General Framework

I. Introduction

1. Context

In previous chapter, the importance of HVDC links in the future transmission projects was pointed out. This leads to the creation of hybrid AC/DC power systems composed of synchronous generators and/or loads forming synchronous AC grids, AC/DC converters connected to one or more DC grids. These grids can be, in turn, interfaced with asynchronous power sources such as wind farms or with other synchronous AC systems.

Particularly, the studied AC/DC converters in this work are VSC-based. This allows for better control and fault ride-through capabilities of the used converters during contingencies. Chapter 2 points on the fact that perturbations from one side of a converter may have repercussions on the other side. The VSC converters used in HVDC links are expected to help mitigating these perturbations with adapted control layers.

Therefore, a modelling of AC and DC components of the AC/DC power system is needed. As per the complexity of the models, numerical simulations are also needed to study the stability of AC/DC systems. The development of new simulation tools for such purpose is also a requirement in the Research and Development Innovation Roadmap (RDIR 2030) of ENTSO-E [10].

2. Organization of the chapter

In this chapter, model the AC and DC components and corresponding controls are modelled. The interface between these components is also explained in the current chapter. These components are then integrated in various power system benchmarks that are specifically created to host AC/DC stability studies via simulations. These models integrate the most realistic behaviour of the whole system (AC & DC) during normal and abnormal operation regimes.

Before doing any stability evaluation, the power benchmarks were initialized and tested first by simply connecting the DC grids through AC/DC converters to the AC systems. A special attention has been paid for initializing the DC grid, which is not natively embedded in the used Dymola software.®

The chapter is structured as follows: in section II, the models of AC and DC components are presented in addition to the power converters' models. In section III, the proposed power benchmarks are illustrated. Moreover, the computer-aided stability assessment and enhancement approach is discussed in section IV. A generic methodology is finally presented with a workflow diagram that explains the proposed stability study approach.

II. System modelling and control

In this part, the models of the considered AC and DC components are exposed. Generic AC and DC power system components are described first: synchronous machines (with their turbine governor, excitation system and power system stabilizer (PSS)), loads, lines, and cables. The machines are modelled using dq transformation to obtain direct d −axis and q −axis currents instead of three-phase

currents as a function of the varying rotor angle. Then, two types of AC/DC converters are described: MMCs and two-level VSCs in dq frame as well.

All these models are realized in Dymola which allows for object-oriented modelling environment. The models will later be used to design adequate controllers, to study transitory phenomena, and to analyse power system's stability.

1. AC components

i. Synchronous machines

The synchronous generators (SGs) (***Figure 3-4***) are the source of power in the used benchmarks. The dynamics of the modelled SGs in OpenIPSL library are given by the following equations using Park's transformation [57]:

$$\dot{\psi_d} = (R_s \cdot I_d + V_d) \cdot \omega_s + \psi_q \cdot \omega \tag{3.1}$$

$$\dot{\psi_q} = (R_s \cdot I_q + V_q) \cdot \omega_s - \psi_q \cdot \omega \tag{3.2}$$

$$\dot{E'_d} = \frac{1}{T'_{qo}} \cdot \left[-E'_d + (X_q - X'_q) \cdot \left[I_q - \frac{X'_q - X''_q}{(X'_q - X_{ls})^2} \cdot (\psi_{rq} + (X'_q - X_{ls}) \cdot I_q + E'_d) \right] \right] \tag{3.3}$$

$$\dot{E'_q} = \frac{1}{T'_{do}} \cdot \left[-E'_q - (X_d - X'_d) \cdot \left[I_d - \frac{X'_d - X''_d}{(X'_d - X_{ls})^2} \cdot (\psi_{rd} + (X'_d - X_{ls}) \cdot I_d - E'_q) \right] + E_{fd} \right] \tag{3.4}$$

$$\dot{\psi_{rd}} = \frac{1}{T''_{do}} \cdot [E'_q - (X'_d - X_{ls}) \cdot I_d - \psi_{rd}] \tag{3.5}$$

$$\dot{\psi_{rq}} = \frac{1}{T''_{qo}} \cdot [-E'_d - (X'_q - X_{ls}) \cdot I_q - \psi_{rq}] \tag{3.6}$$

$$\psi_d = \frac{X'_d - X''_d}{X'_d - X_{ls}} \cdot \psi_{1d} + \frac{X''_d - X_{ls}}{X'_d - X_{ls}} \cdot E'_q - X''_d \cdot I_d \tag{3.7}$$

$$\psi_q = \frac{X'_q - X''_q}{X'_q - X_{ls}} \cdot \psi_{2q} + \frac{X''_q - X_{ls}}{X'_q - X_{ls}} \cdot E'_d - X''_q \cdot I_q \tag{3.8}$$

These electrical equations are linked to the mechanical equations of the SG through the swing equations:

$$\dot{\delta} = \omega_g - \omega_s \tag{3.9}$$

$$\dot{\omega} = \frac{\omega_s}{2 \cdot H} \cdot \left[\frac{P_{mech} - D \cdot \omega}{\omega + 1} - T_{elec} \right] \tag{3.10}$$

With

$$T_{elec} = \psi_d \cdot I_q - \psi_q \cdot I_d \tag{3.11}$$

The variables used in equations **(3.1)** – **(3.11)** are defined as:

- V_d, V_q, I_d, I_q, ψ_d, ψ_q are respectively the dq rotor-equivalents of the stator voltages, currents, and flux linkages (pu) (V_{abc}, I_{abc} and ψ_{abc}) given by Park's transformation,
- R_s, X_{ls} are respectively armature resistance and leakage reactance (pu),
- ω_s, ω_g, ω are respectively the synchronous speed, the rotor speed and the speed deviation from synchronous speed (pu),
- E'_d, E'_q are respectively the d- and q- axis voltages behind the transient reactances (pu),
- T'_{do}, T'_{qo}, T''_{do}, T''_{qo} are respectively the d- and q- axis transient and sub-transient open-circuit time constants (s),
- X_d, X'_d, X''_d, X_q, X'_q, X''_q are respectively the d- and q- axis reactances, transient reactances and sub-transient reactances (pu),
- E_{fd} is the machine's field voltage (pu),
- ψ_{rd}, ψ_{rq} are the rotor flux linkages (pu),
- δ is the rotor angle (deg),
- H is the inertia constant (s),
- P_{mech} is the mechanical input power given by the turbine (pu),
- T_{elec} is the electrical torque (pu),
- D is the electromechanical damping of the machine (pu).

The mechanical power of the machine is regulated by the turbine governor which is represented in the following block diagram ***Figure 3-1***.

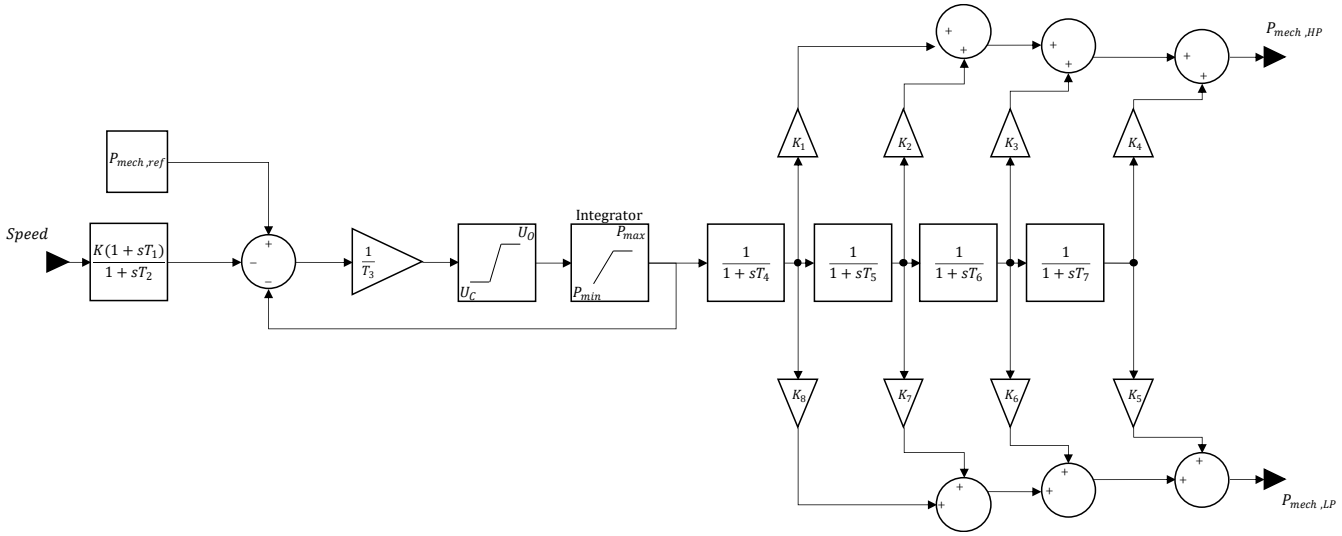

Figure 3-1: Block-diagram representation of the used turbine governor regulating the mechanical power of the machines.

In the ***Figure 3-1***, the parameters are defined as the following:

- K: Governor's gain (reciprocal of droop) (pu),
- T_1: Governor's lead time constant (s),
- T_2: Governor's lag time constant (s),
- T_3: Valve positioner time constant (s),
- U_O: Maximum valve opening velocity (pu/s),
- U_C: Maximum valve closing velocity (pu/s),
- P_{max}: Maximum valve opening (pu of MW),
- P_{min}: Minimum valve opening (pu of MW),
- T_4: High pressure turbine bowl time constant (s),
- K_1: Fraction of high-pressure shaft power after first boiler pass,
- K_5: Fraction of low-pressure shaft power after first boiler pass,
- T_5: Reheater time constant (s),
- K_2: Fraction of high-pressure shaft power after second boiler pass,
- K_6: Fraction of low-pressure shaft power after second boiler pass,
- T_6: Crossover time constant (s),
- K_3: Fraction of high-pressure shaft power after third boiler pass,
- K_7: Fraction of low-pressure shaft power after third boiler pass,
- T_7: Double reheat time constant (s),
- K_4: Fraction of high-pressure shaft power after fourth boiler pass,
- K_8: Fraction of low-pressure shaft power after fourth boiler pass.

Therefore, based on the measured rotor speed ω, the turbine governor adjusts its mechanical output to cope with the variations of the electrical torque T_{elec}. The time constants can be in the range [0.3; 10] seconds. The turbine governor has consequently the role of a mechanical regulator of the rotor speed and remains unable to cope with quick power transients.

The excitation system of the SG is a simplified version of the AC4C model in ***Figure 3-2*** extracted from [58]. From the original model, the stator current limiter (SCL subscript) and high-value (HV gate) and low-value (LV gate) logic gates were removed since the machine's capacities are not exceeded during simulations.

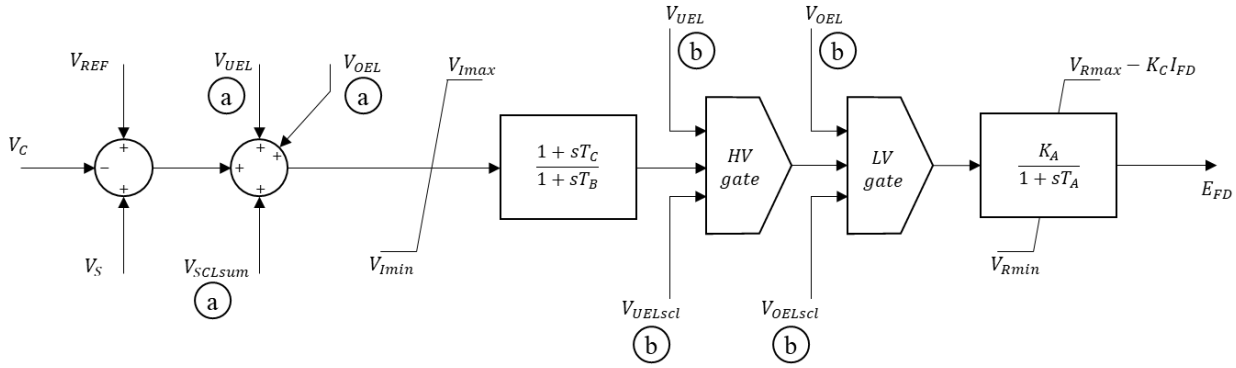

Figure 3-2: Block-diagram representation of the implemented excitation system of the synchronous generators.

Finally, the used SGs are equipped with PSSs that aim to damp local oscillating modes. The PSS measures local speed at the generator and sends a signal to the excitation system so that the excitation voltage E_{fd} takes into account the potential oscillations existing in the measured speed.

The used PSSs are a simplified version of PSS1A (***Figure 3-3***) also available in [58], in which the washout filter (block containing the time constant T_5) is removed and the parameters A_1 and A_2 in the second-order filter are set equal to zero.

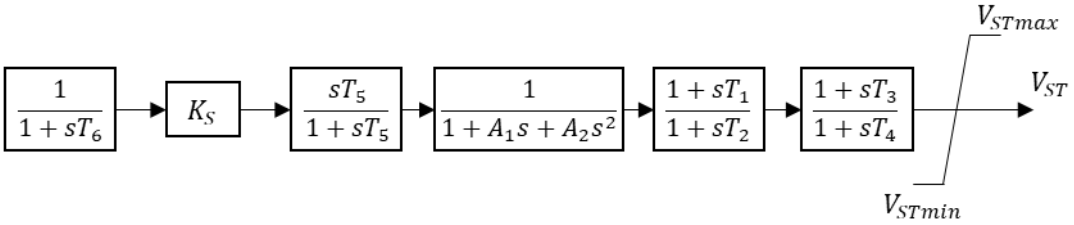

Figure 3-3: Block-diagram representation of the implemented power system stabilizer.

The final block diagram of a SG connected to an AC grid is illustrated in the following ***Figure 3-4***:

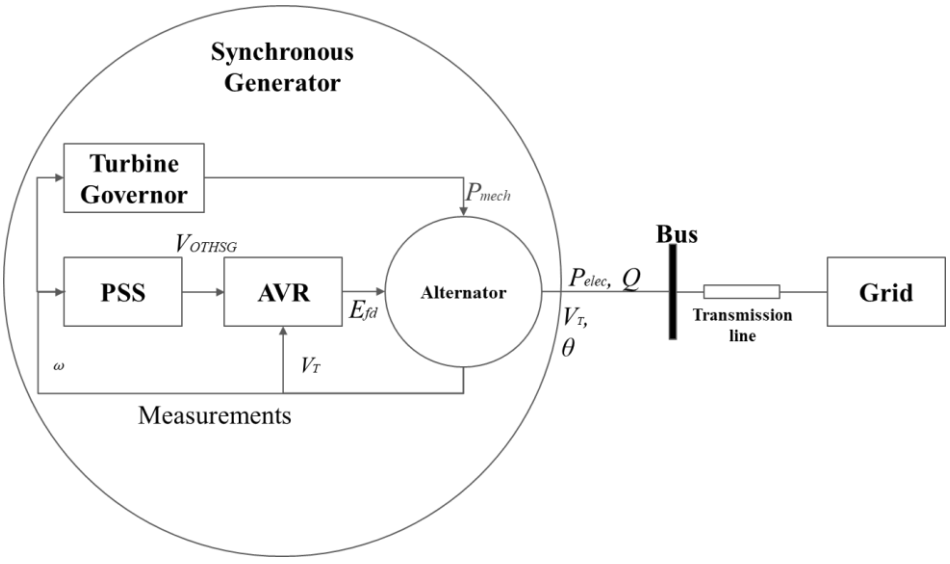

Figure 3-4: Block-diagram representation of the implemented synchronous generator.

ii. Loads

Load characteristics can directly impact power system's adequacy (its ability to continuously supply the needed power). Therefore, how the loads influence or are influenced by the variation of the power system's physical quantities is very important to determine whether a system can operate in a stable manner or not. In fact, the divergence between power production and consumption (loads) directly influences rotor angle differences and the frequency (at first, locally) within a synchronous zone.

For power transmission study purposes, the loads are **aggregated** for the sake of simplification. These aggregated models may vary slower than the SGs. In reality, hundreds of devices are connected to a same power transmission bus and the consumption of each one can vary with time, temperature, power cost, luminosity, etc. Since load representation is very important but detailed load modelling is not essential for proposed stability studies, these multiple devices were combined within single aggregated loads which can vary during the simulations. In this PhD thesis, focus was made on the loads of the AC power system which were designed and used in the simulation environment for stability studies.

Two load categories exist so far to represent a load for power transmission systems: static or dynamic models. The usage of static models is justified in the cases where the variation of voltage or frequency is of low amplitude. In this case, steady-state values of these physical quantities are reached quickly which justifies the absence of dynamic aspects (temperature variation, torque-speed characteristics, etc). For the current studies, usage of static loads did not hinder the study of dynamic stability aspects (interarea oscillations, transients, etc).

In the static load models used, active and reactive powers (P_{load} and Q_{load} respectively) have voltage (V) dependent characteristics in a polynomial model (ZIP model [59]):

$$P_{load} = P_0 \cdot \left[P_z \cdot \left[\left(\frac{V}{V_0} \right)^2 - 1 \right] + P_i \cdot \left[\left(\frac{V}{V_0} \right) - 1 \right] + 1 \right] \quad \textbf{(3.12)}$$

$$Q_{load} = Q_0 \cdot \left[Q_z \cdot \left[\left(\frac{V}{V_0} \right)^2 - 1 \right] + Q_i \cdot \left[\left(\frac{V}{V_0} \right) - 1 \right] + 1 \right] \quad \textbf{(3.13)}$$

where the subscripts z and i correspond to constant impedance and constant current components of the load power and the subscript 0 corresponds to the initial operating condition value of the voltage variable.

iii. Lines

The performances of AC lines can modify the power transmission capabilities and characteristics within a synchronous zone. Therefore, the AC lines' modelling is interesting from the stability study point of view. An AC transmission line can either be an overhead line or an underground cable. Both have the same characterizing parameters:

- **Series resistance** (considering the skin effect),
- **Shunt conductance** (neglected in current simulations and usually this parameter accounts for leakage current losses and corona effect),

- **Series inductance** (depending on the flux linkages between conductors and within a same conductor cross section, influenced by the spacing between conductors that affects the mutual flux linkage between them),
- **Shunt capacitance** (due to the potential difference between the conductors, a shunt capacitance is represented between them; the alternating voltage charges and discharges this capacitance).

The typical values of the mentioned parameters for overhead transmission lines and underground cables are available in [60].

The performances of AC transmission lines can be modelled in detail as was shown also in [60] or using an equivalent model. The purpose of using complete line model is to evaluate the performance of an AC link in terms of

- voltage and current amplitude at each point of the line,
- phase angle difference between sending voltage the voltage at a given point,
- lightning and switching surges by using the surge impedance loading in [60].

In this PhD thesis, for rotor angle stability studies, the only objects of interest are voltage amplitude at each end of an AC line and phase angle difference between two AC buses. Therefore, complete model of an AC line can be replaced by equivalent model to check the performances of the lines. Moreover, the interesting modes are between ~0.1 s to ~10 s. In consequence, a more detailed model is not required.

The used model is called the equivalent π circuit of a transmission line and is represented in the following diagram in ***Figure 3-5***. It is assumed that the three-phase AC lines are transposed, therefore, the per-phase representation is used in this diagram in ***Figure 3-5***.

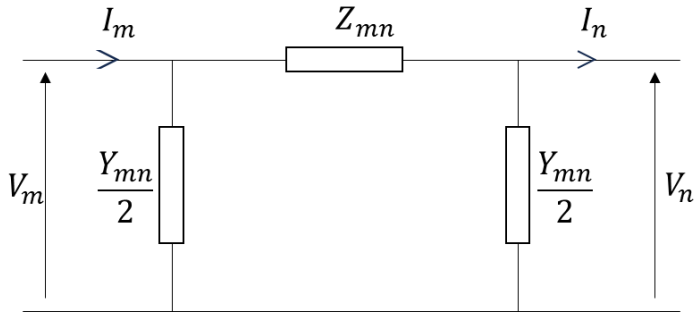

Figure 3-5: Equivalent π-model of an AC transmission line.

The subscripts m and n in the figure correspond to the buses m and n to which the line's terminals are connected. Z_{mn} corresponds to the total series impedance and Y_{mn} corresponds to the total shunt admittance between the buses m and n. With the condition $\omega\sqrt{L_{mn}C_{mn}} \ll 1$ respected, the values of Z_{mn} and Y_{mn} can be approximated as the following:

$$Z_{mn} = z_{mn} \cdot length_{mn} \approx (R_{mn} + j \cdot \omega L_{mn}) \cdot length_{mn} \quad \textbf{(3.14)}$$

$$Y_{mn} = y_{mn} \cdot length_{mn} \approx (G_{mn} + j \cdot \omega C_{mn}) \cdot length_{mn} \quad \textbf{(3.15)}$$

where R_{mn}, L_{mn}, G_{mn} and C_{mn} are respectively the per unit length series resistance (Ω/m), series inductance (H/m), shunt conductance (S/m) and shunt capacitance ($\mu F/m$); $\omega = 2\pi f$ is the pulsation of the system (rad/s) with f its frequency (Hz).

In the used modelling, the assumptions made for the power transmission lines are: $\forall m, n,\ G_{mn} \approx 0$ and $R_{mn} \ll \omega L_{mn}$.

2. DC component

i. Cables

DC cables have the same basic parameters as the AC transmission lines.

Several DC cable models exist:

- The simple RC model,
- The π model [61],
- The fitted π model: a cascading of multiple simple π models and usage of parallel RL branches in each π model itself. This considers better the frequency dependency of the DC cable parameters for a more realistic representation of the cable's behaviour [62],
- The adjusted π model for a pair of cables with opposite DC voltage polarities considering the coupling between them through a mutual inductance [63].

However, for the stability study, the small-signal stability of the DC voltage is not considered. Therefore, the classical π model is used for DC links (the same as the one used in [61]). The DC cables are RLC branches as represented in the ***Figure 3-6*** below.

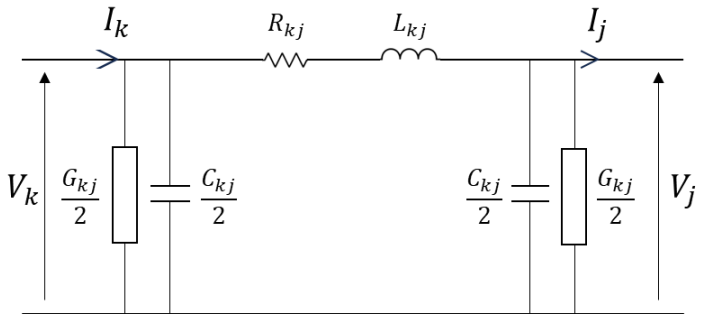

Figure 3-6: Equivalent π-model of a DC transmission cable.

The subscripts k and j correspond to the buses k and j to which the line's terminals are connected. R_{kj}, L_{kj}, G_{kj} and C_{kj} are respectively the per-length series resistance (Ω/m), series inductance (H/m), shunt conductance (S/m) and shunt capacitance ($\mu F/m$).

3. AC/DC converters

i. Context

The combination of power electronic devices with classical power systems components (synchronous generators, loads, etc) has allowed for more flexibility and efficiency in the electrical system.

Power electronic converters allow the creation of variable voltage, frequency, and rate of change of the physical variables involved in power injection/extraction. This diversity and flexibility in power control is utilized in different applications of power converters such as energy storage, renewable energy interfacing, power transmission over HVDC links, electrical mobility, Flexible AC Transmission Systems (FACTS) [64], and **ancillary services** proposition by HVDC.

For AC systems, FACTs were used in utilities around 1970 [65]. They provide reactive power support, improve stability (AC voltage, damping, etc) and increase power transfer capability of AC transmission systems. Power electronic based solutions (like STATCOM application) or other electromechanical based solutions may be applied.

The focus on this PhD thesis is put on the three stability aspects mentioned before: AC frequency, AC rotor angle, and DC voltage. Thus, FACTS solutions do not directly enter in the scope of this work. Besides, the models and the controls of the power converters are made through offline simulator.

ii. Model

Various types of modelling exist and the used one depends on the purpose of the study [66]. In ***Figure 3-7***, continuous and discrete-time modelling possibilities are exposed.

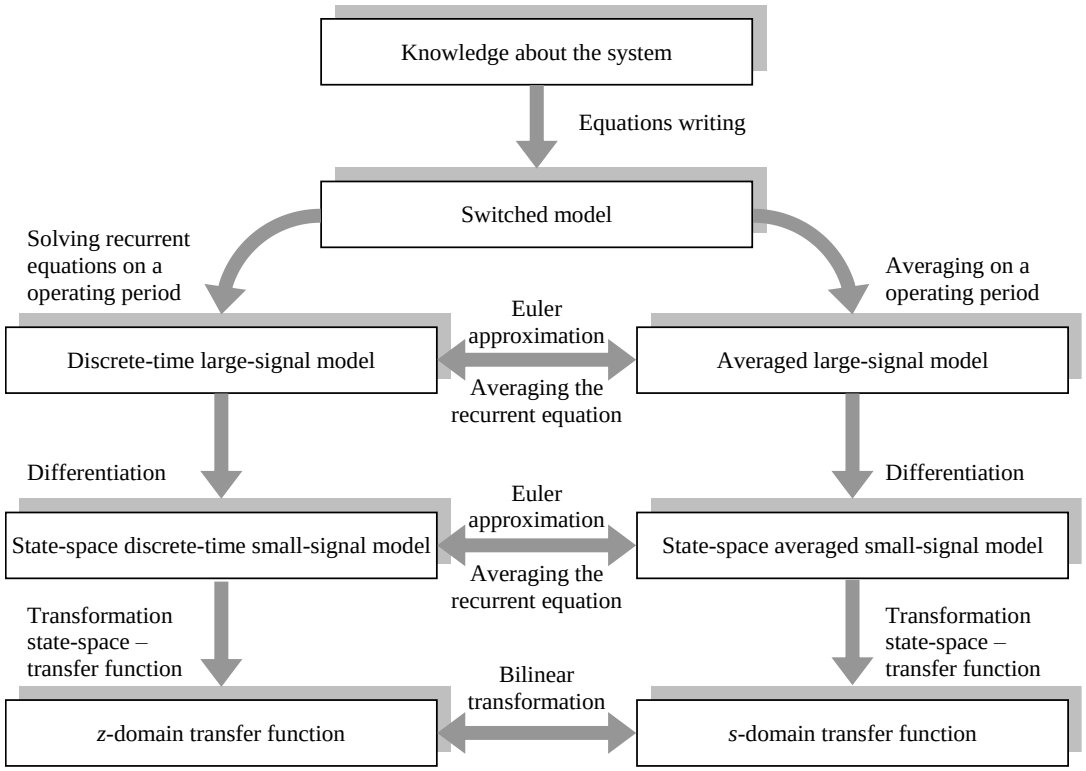

Figure 3-7: Relations between different types of models [66].

In power transmission over HVDC links, the role of the power converters' control is fundamental to ensure AC and DC stability. This role is studied through simulations in which a converter model is required. Two criteria are selected for the studies:

- Acceptable complexity of the models to represent their behaviour realistically,
- Acceptable simplicity of the model, to avoid non-ending simulations and/or non-useful degree of details.

The ***Table 3-1*** below classifies the modelling type according to the purpose of the simulations (phenomena and control to study).

Table 3-1: Modelling classes corresponding to study purposes.

Models	Simulation of dynamic phenomena	Simulation of transient phenomena
Static (knowledge-based or behavioural models)	Based on modal separation	N/A
Large-signal or small-signal average models, continuous behavioural models	**Depending on the dynamics to emphasize**	**Emphasizing the transients of fundamentals (magnitude and phase)**
Switched (topological) models	Too computational-time expensive	Emphasizing the harmonics phenomena

According to the scope of this PhD thesis, the characterization of high-frequency performance of the converters is not required. An **average value model** (AVM) (average of switched models during an appropriately small period) is sufficient to represent and analyse the AC/DC power systems' performance (***Table 3-1***). A complete description of switched and sliding average value models is available in Part I in [66].

1. MMC-based VSC converters

The used AC/DC converting stations are VSC-based MMC stations with $N = 200$ submodules (***Figure 3-8***) meaning that the line-to-neutral voltage waveform is of $N + 1 = 201$ levels. A typical topology of the three-phase converter is represented in the following ***Figure 3-8*** where N represents the total number of submodules per arm, the subscripts u and l refer to upper and lower arms respectively and L_{arm} represents the armature inductance (H).

The physical model of the MMC stations is based on the model presented in [67]. Four models are represented in [68], each one having a different degree of complexity. Model 1 ([68], p.26) gives full representation of IGBT/Diode component of the SM, including the existing non-linearity behaviour. This model is used for specific simulations that are interested in the blocking/opening behaviour of the converter's components, the faults inside the SMs, etc. Model 2 ([68], p.27) simplifies the IGBT/Diode models of each SM. Their semi-conductors are replaced by variable resistors and their capacitor is replaced by a current source in parallel of a resistor. The advantage of this model is to reduce the number of electrical nodes in the arms' grid, which significantly simplifies the calculation of voltage and current at the level of each SM's capacitor. Model 3 simplifies again the representation of an MMC by separating the ON state from the OFF state of each SM. Moreover, an average value model can be calculated from this model based on the assumption that all the SM are balanced. The switching state of each SM is no

longer available since the obtained AVM gives the voltage and current at the level of each arm only. Consequently, what remains in Model 3 is the macroscopic behaviour of each arm which is sufficient for the scope of this thesis.

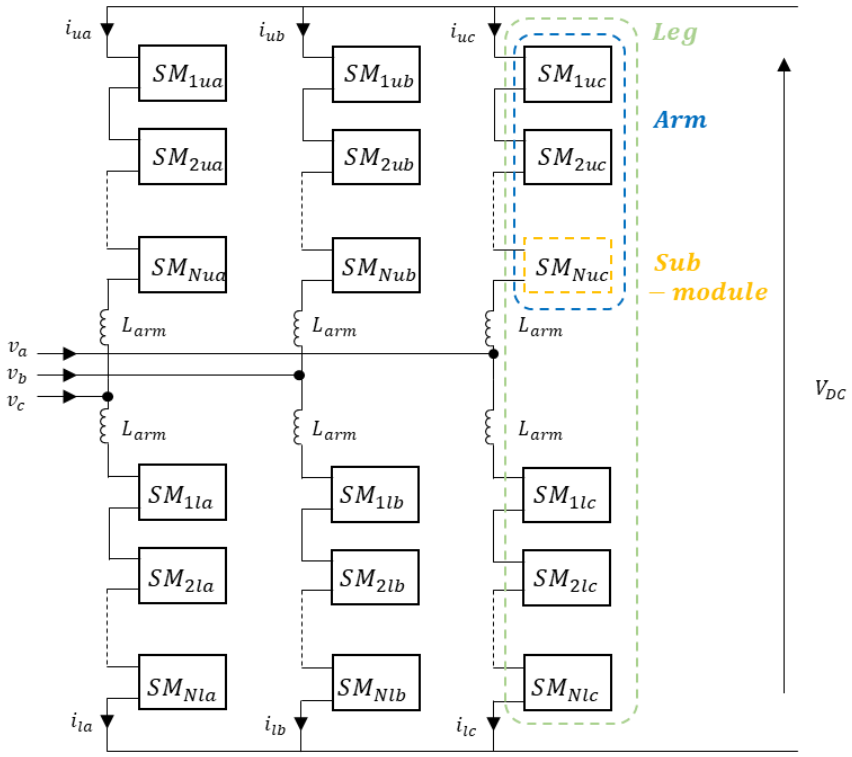

Figure 3-8: Modular multi-level converter three-phase topology.

The implemented circuit of the simplified MMC model is a deviation from Model 3 which simplifies it further without being too simplistic. The capacitor voltages at the level of each SM are considered to be all in the same range, so they can be replaced by an equivalent capacitor in the implemented model. Its representation in the *dq* reference frame is given in ***Figure 3-9*** from [69] where the d and q subscripts correspond respectively to the d- and q- axes of the variables in question, and:

- m_d, m_q are the control signals giving a ratio for the upper and lower right currents – i_{gd} and i_{gq} respectively – accordingly with the voltages v_{md} and v_{mq} compared to $\bar{v}_{Ctot}$,
- m_{dc} is the control signal given to each arm (all arms are balanced),
- L_{eq}^{dc}, R_{eq}^{dc}, L_{eq}^{ac}, R_{eq}^{ac}, C_{eq} are, for the first four parameters, the equivalent inductances and resistances characterizing the DC and AC sides respectively and, for the last parameter, the equivalent average capacitor,
- v_g, v_{dc} are respectively the voltage phase of the AC side of the converter and the DC voltage,
- i_g, i_{dc} are respectively the current at the AC and DC side of the converter,
- ω_g is the pulsation of the grid at the AC side of the converter.

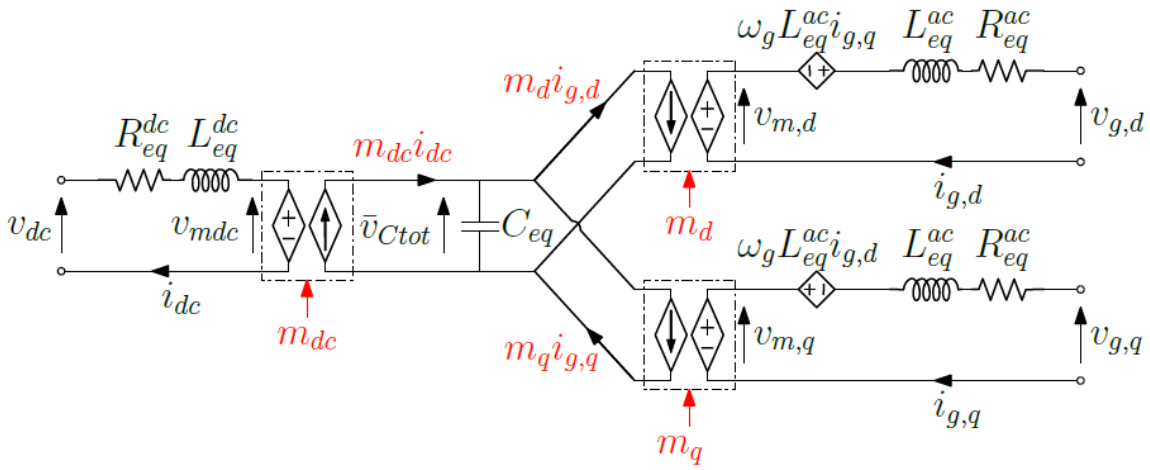

Figure 3-9: Circuit representation in dq frame of the physical layer implemented in the MMCs [70].

The block diagram representation of the AC and DC sides of the MMC in the dq reference frame is shown in ***Figure 3-10*** recalled from [70]. In the diagram, W_{tot} is the total energy in the MMC converter.

To control the physical layer represented in the block diagram in ***Figure 3-10***, a control structure composed of two cascaded control loops is implemented. An "inner" loop controls the AC and DC currents whose references are generated by an "outer" control loop. The outer loop's inputs are the active and reactive power references, as well as the DC voltage reference and stored energy reference.

In the inner loop (***Figure 3-11***) [69], three PI controllers are used to bring the current i_{gd}, i_{gq} and i_{dc} to their references as shown. In the AC side of the illustrated controller, two decoupling terms are used to independently regulate active and reactive powers in the MMC converter. The calculated voltage outputs v_{md}, v_{mq} and v_{mdc} are divided by the voltage at the equivalent capacitor $\bar{v}_{Ctot}$ and the outputs of the inner control loop are the control signals m_d, m_q and m_{dc} shown in ***Figure 3-9***. Once available, these signals can be remultiplied by $\bar{v}_{Ctot}$ to obtain the voltage references v_{md}^*, v_{mq}^* and v_{mdc}^* of the block diagram (***Figure 3-10***).

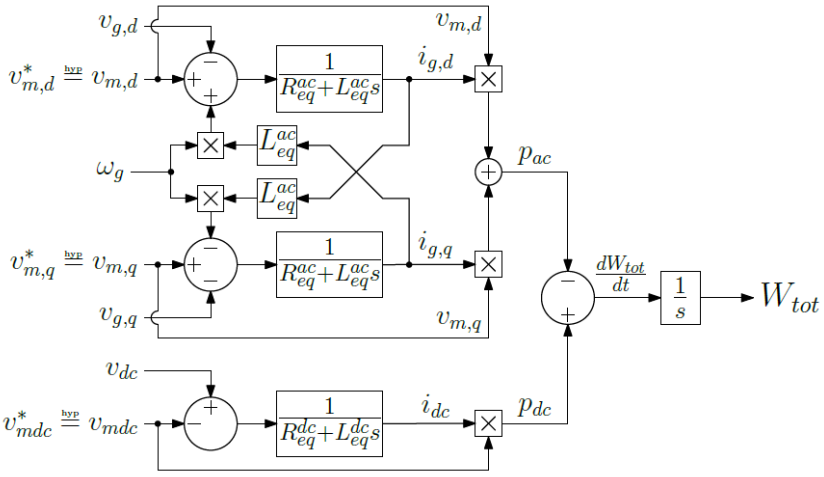

Figure 3-10: Block-diagram representation in dq frame of the physical layer implemented in the MMCs [70].

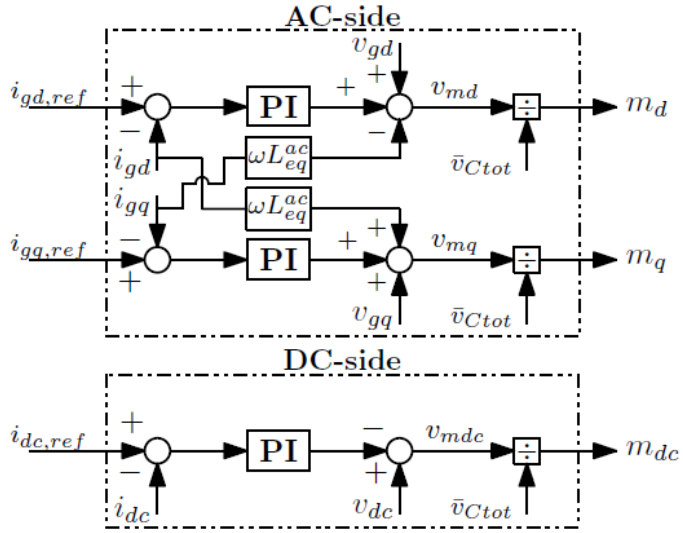

Figure 3-11: Inner current control loops implemented in the MMCs [70].

In the outer control loop (***Figure 3-12***) inspired from [69], the AC active and reactive power references set by the TSO are divided by the AC voltages v_{gd} and v_{gq} respectively to get the reference current $i_{gd}^{*} = i_{gd,ref}$ and $i_{gq}^{*} = i_{gq,ref}$. To get the direct current reference $i_{dc}^{*} = i_{dc,ref}$, the stored energy controller's output is added to the measured AC active power then divided by the DC voltage v_{dc}. The energy controller's objective is to regulate the energy exchange between the AC and the DC side of the converter to ensure the power balance at the AC/DC interface.

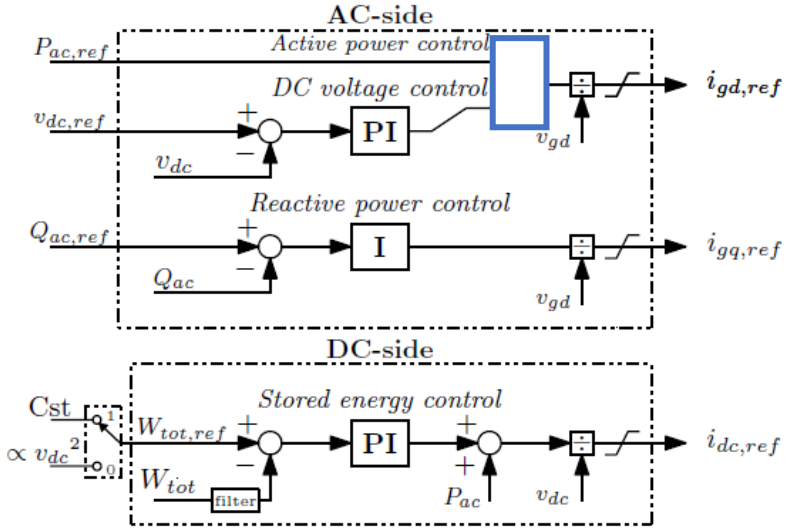

Figure 3-12: Outer control loops implemented in the MMCs [70].

In the ***Figure 3-12***, the blue-outlined block is determined by the TSO. Three cases are possible:

- The converter acts in power mode: 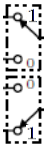
- The converter acts in Master mode: and the DC voltage control is replaced by another loop.
- The converter acts in DC voltage droop control mode:  and the corresponding PI is replaced by a simple P.

Also, in the ***Figure 3-12***, the TSO can decide to put the weighting factor for Energy control α equal to 1 or 0. In the first case, the energy is managed by the DC side, otherwise, energy reference is constant. In this latter case, the model's equivalent capacitor C_{eq} is fully decoupled from the performance of the DC grid.

The paper [71] shows two layers of MMC control:

- A high-level layer in which the outer and inner loops (mentioned above) send voltage references,
- A low-level layer in which the modulation technique and balancing algorithms send the corresponding switching signals to the MMC's electronic components.

These two levels are shown in the ***Figure 3-13*** below.

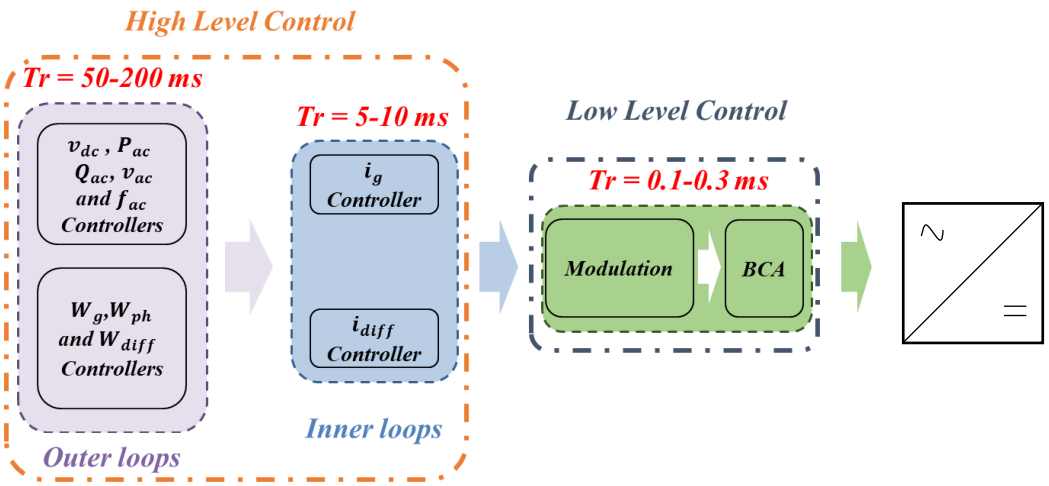

Figure 3-13: MMC control structure [71] sent to an MMC station.

In this PhD thesis, the focus is put on a power system level control and not that of the MMC converter control. However, more detailed explanation of the latter one can be found in [72], [73].

The AC and DC components are modelled with sufficiently realistic details for the studies. They now need to be combined to create a hybrid AC/DC power system. The power benchmarks chosen for the studies will be explained in the next section.

III. Choice of benchmarks

The working environment where the power system benchmarks were built and tested in Dymola based on MODELICA language (check section Chapter 3.IV).

1. Presentation of the benchmarks

For the sake of understanding the AC/DC power system stability concerns, three comprehensive benchmarks were constructed during the thesis, with increased complexity each time. In this section, the used power system benchmarks with initial power flow (initialization will be shown in the following sections) will be illustrated. In all the studies, power is considered positive when flowing from DC to AC.

The developed power benchmarks are used to test the developed command laws, check the parameter tuning and evaluate stability. The controllers are implemented on the power system benchmarks to enhance AC/DC stability.

i. Benchmark for study of effect of adding power electronics to AC system

The first benchmark (***Figure 3-14***) helped make a first analytical approach on a simple power system composed of two generators connected through an AC line and a power converter. The mathematical formulation of the dynamics of AC frequency and rotor angles depending on the exchanged power with the converter showed the complexity of such analytical approaches for higher-complexity power systems. A computer-assisted eigenvalue and time-domain analyses were then performed to evaluate the impact of adding the power converter on AC/DC stability.

The case studies performed on this benchmark will be explained in section Chapter 4.II.

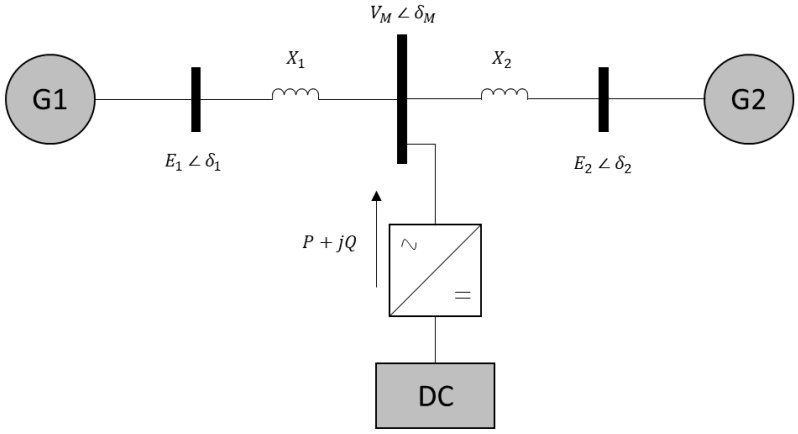

Figure 3-14: Power system benchmark No. 1.

ii. Benchmark for rotor angle stability study

This benchmark is inspired by the two-area Kundur system with a transformation. It included an embedded P2P HVDC link that was parallel to the AC line connecting the left and right areas of the synchronous system (***Figure 3-15***).

Since the AC/DC converters belong to the same synchronous zone, frequency support is not expected by the HVDC link. Nevertheless, DC voltage control was assured by one of the converters while both offered rotor angle support.

The main purpose of using this first benchmark is to illustrate the rotor angle stability issues that may arise in a synchronous zone. In fact, this power benchmark was created, initialized and perturbated in a way that emphasizes power oscillations between left and right sides of the synchronous zone, which may jeopardize the rotor angle stability aspect solely.

The HVDC link can provide synchronizing and damping power to the AC system subject to a contingency in order to support rotor angle stability. However, interactions may arise between the controllers implemented at the level of the HVDC – Power Oscillation Damper (POD) and Angle Difference Controller (ADC). This benchmark was also used for the study of these interactions.

The case studies performed on this benchmark will be explained in section Chapter 4.III.

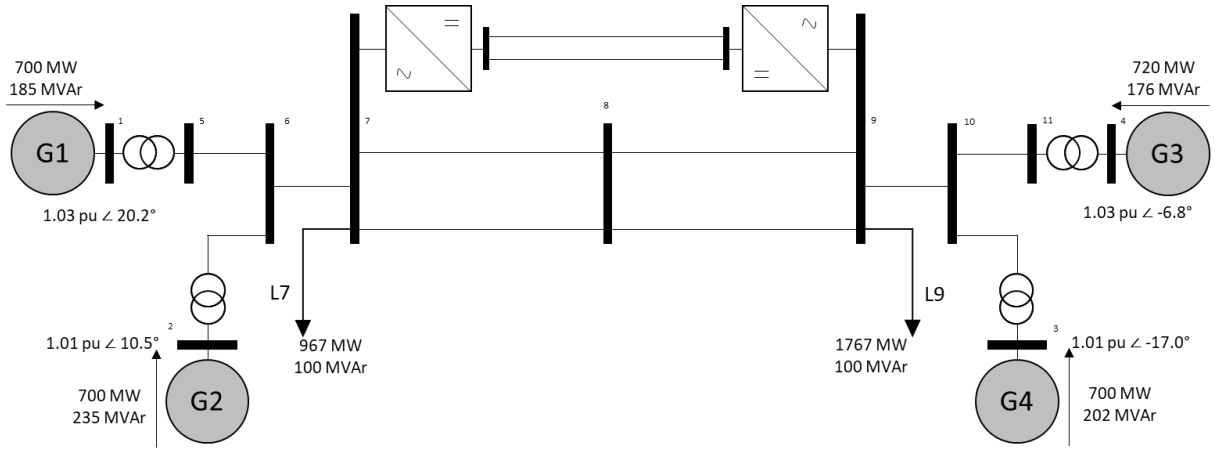

Figure 3-15: Power system benchmark No. 2.

iii. Benchmark for frequency and DC voltage stability study

The third power system benchmark was developed for the purpose of studying HVDC frequency support possibilities as well as the impact on DC voltage stability. From an embedded PtP HVDC link, the study transited to a semi-embedded three-terminals MTDC network. The AC/DC hybrid power system is illustrated in the ***Figure 3-16***. The initial powerflow is shown in the ***Table 3-2***.

In the case of this benchmark, frequency support can be expected from the HVDC links between the two AC zones denoted in the ***Figure 3-16*** since these are separate synchronous zones. The AC zone 2 is inspired by the previously used power systems (***Figure 3-14*** and ***Figure 3-15***).

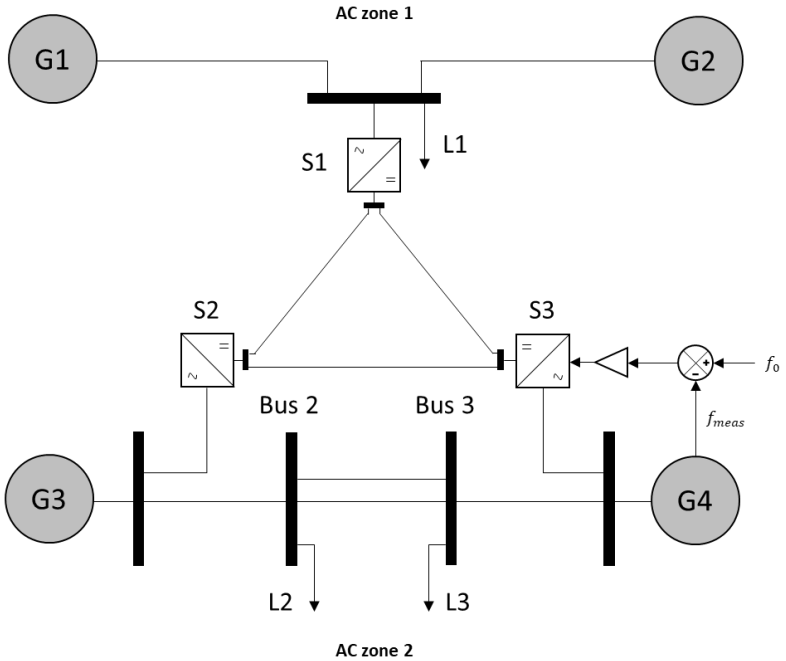

Figure 3-16: Power system benchmark No. 3.

Component	Initial Active Power Flow (MW)
Generator G1	500
Generator G2	527
Generator G3	500
Generator G4	500
Load L1	1027
Load L2	300
Load L3	700

Table 3-2: Initial powerflow used for the power benchmark No. 3 (Figure 3-16).

The converters 1 and 3 are in constant power control mode while converter 2 is in DC voltage droop control mode. The main purpose of this power benchmark is to evaluate the interaction between local frequency droop controller and DC voltage droop controller.

iv. Benchmark for combined rotor angle, frequency, and DC voltage stability study

The last benchmark constructed was intended to include multiple stability aspects simultaneously in the case study. Therefore, the AC/DC power system benchmark was built, initialized, and disturbed in a way to use the HVDC link for rotor angle support, frequency support and DC voltage control at the same time. Also, a new frequency control design was tested and implemented using this benchmark (distributed instead of local frequency support). This support is called Frequency Containment reserve (FCR). In addition, a new centralized control structure was developed for the stability study and implemented in the system benchmark.

The ***Figure 3-17*** illustrates the hybrid AC/DC power system including a four-terminal MTDC network as well as the initial AC/DC power flow. The system is composed of two AC zones connected through the MTDC. The difference with the previous benchmark is that rotor angle stability is also considered in this case. The type of the implements perturbations also differs in this power system and the used converters are MMC-based VSCs. The case studies will be provided in Chapter 5 and Chapter 6.

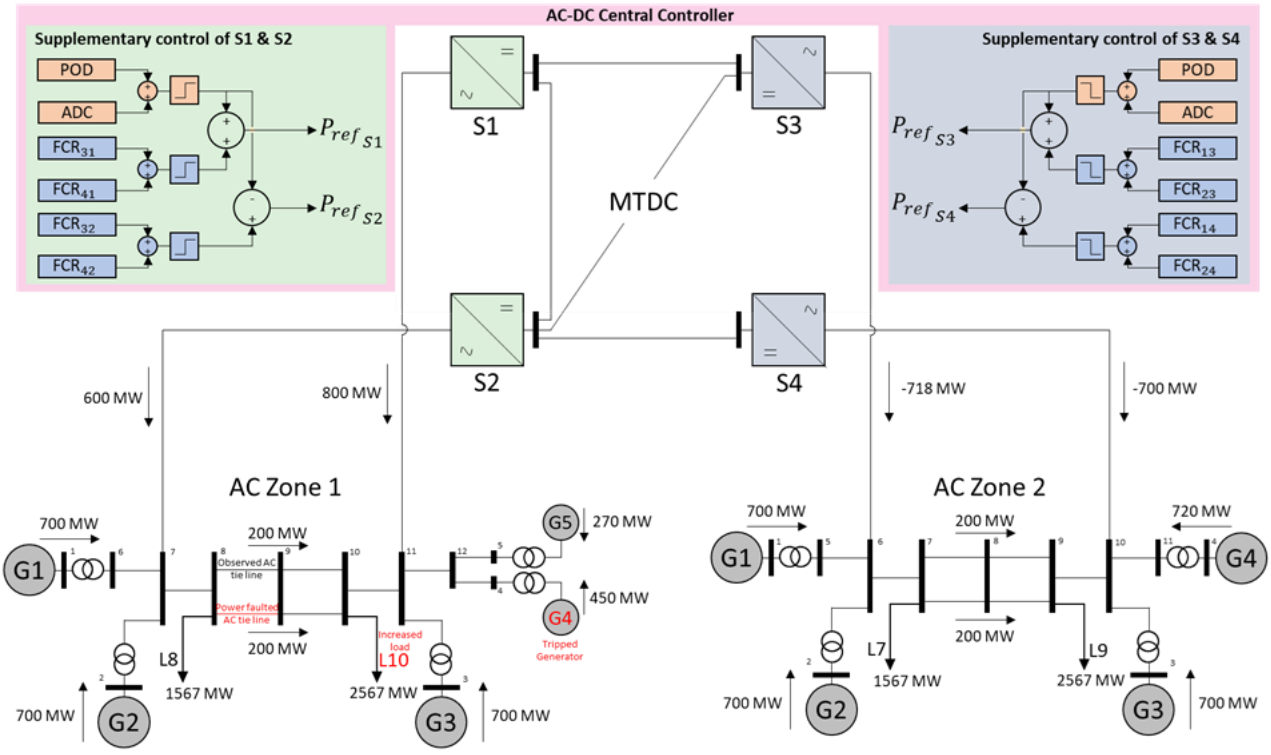

Figure 3-17: Power system benchmark No. 4.

2. Performed stability studies using the benchmarks

Stability issues can be divided in two categories of root causes for degradation of system stability:

- The issues that occur due to the physics of the power system under stress/disturbance (***physical*** stability issues),
- The issues that occur due to the interactions between the implemented controls (converter supplementary controls) of the power system (***interactional*** stability issues).

The ***Table 3-3*** below recalls the different DC and AC ***physical*** stability issues identified.

Table 3-3: Identified physical stability issues.

Physical quantity	**Stability aspect**	**Event likely to disturb stability**	**Incurred risk due to stability loss**
DC Voltage	Transient	▪ Large power injection (converter interfaced/generation) or extraction ▪ Converter trip	▪ Load shedding ▪ Trip of transmission lines and other network components due to protection systems ▪ Cascading outages ▪ Partial or total loss of DC network
	Small-signal (electromagnetic oscillations) – *not studied*	Badly damped DC modes	Trip of DC lines
AC Rotor Angle	Transient (electromechanical oscillations)	▪ Loss of transmission line leading to insufficient synchronizing power ▪ Generator loss leading to lower system inertia	▪ Large power oscillation swings ▪ Loss of synchronism leading to system split
	Small signal (electromechanical oscillations corresponding to local or interarea modes)	▪ High stress on/loss of transmission lines leading to mode excitation ▪ Loss of generation or the connection of load leading to power imbalance inside the synchronous zone ▪ Loss of PSSs	▪ Maintained power oscillations which may activate protection equipment
AC Frequency	Short-term/Long-term	▪ Loss of generation/connection of load leading to disequilibrium between electrical power production and consumption ▪ Imbalance between mechanical power (turbine) and electrical power due to turbine speed control ▪ Same elements leading to loss of inertia	▪ Frequency swings leading to the tripping of generation units ▪ Risky frequency performances due to loss of inertia ▪ System split into islanded areas prone to instability in case of large interconnected system ▪ Blackout

Two case studies concerning rotor angle ***physical*** stability issues were built where two HVDC supplementary controls (i.e., Power Oscillation Damper and Angle Difference Controller) were tested to help mitigate the issues.

The case studies are described in the following ***Table 3-4***.

Since model initialization is an important part to run simulations, it is also part of this ***Table 3-4***.

To go through with these case studies, the used controllers were combined in a single simulation where antagonist interactions were observed between them. This is the risk when multiple HVDC ancillary services are proposed by the same DC grid. Consequently, an analysis of the so-called ***interactional*** stability issues had to be performed on the selected ancillary services.

Different configurations of benchmarks and associated events were tested to highlight the considered phenomena.

Table 3-4: Description of principal case studies of physical stability issues.

Stability issues	**Stability assessment methods and tools**	**Used benchmark**	**Model initialization**	**Events**	**Implemented HVDC controls with parameter tuning**
Electrome chanical interarea oscillation	Model linearization Different values for control parameter (manual sweep due to the need of a linear model for each parameter) Calculation of the damping of the modes (corresponding to interarea oscillations)	Modified Kundur two areas with PtP HVDC link in parallel with AC line	Handmade: Make initial guess for balanced power flows. Replace some machines by an infinite bus and see the power flowing through them with the voltage and angle at steady-state and use these values for initialization. Then replace infinite bus by the machines	Loaded AC line tripping leading to interarea oscillation	Power Oscillation Damper (POD)
Transient stability	Different values for control parameter (automatic sweep via the user interface in Dymola) Time-domain analysis of first swing of rotor angle difference (maximum rotor deviation) with different values for control parameter	Idem	Idem	Loaded AC line tripping leading to transient angle difference at the boundaries of a loaded AC line.	Angle Difference Controller (ADC)

The ***Table 3-5*** below shows the case studies corresponding to the identified ***interactional*** stability issues.

Table 3-5: Description of principal case studies of interactional stability issues.

Difficulty	Stability issues	Stability assessment methods and tools	Used benchmark	Model initialization	Events	Implemented HVDC controls with parameter tuning
1	Interaction between POD and ADC	Different values for controls' parameters (automatic sweep via the user interface in Dymola) Time-domain analysis of the curves corresponding to interarea oscillations (first swing & oscillation damping)	Modified Kundur two areas with PtP HVDC link in parallel with AC line	Handmade: Make initial guess for balanced power flows. Replace some machines by an infinite bus and see the power flowing through them with the voltage and angle at steady-state and use these values for initialization. Then replace infinite bus by the machines	Loaded AC line trip leading to interarea oscillations and transient angle difference	POD ADC
2	Impact of frequency support on DC voltage stability	Different values for frequency control parameter (automatic sweep via the user interface in Dymola) Time-domain analysis of DC voltage curves by studying the DC Voltage drop.	Semi-embedded 3 MTDC terminals connecting two separate AC zones with 2 synchronous machines in each one	Idem	Increase in the load of one AC zone leading to frequency support by the other AC zone through the DC links.	Frequency droop control DC voltage droop control
3	Interaction between frequency support, DC voltage control and rotor angle control	Different values for control parameters (automatic sweep via the user interface in Dymola) Time-domain analysis of stability indicators: - Frequency RoCoF and Nadir - DC Voltage Nadir- - Rotor angle oscillations Manual setting of control parameters and power allocation	Two modified Kundur systems connected via a four-terminal meshed MTDC grid	For AC systems: machine initialization using PowerFlow generated by GridCal tool. For DC system: handmade initialization of converters and lines using infinite bus and DC voltage source.	Generator trip at one Kundur system leading to interarea oscillations inside this Kundur and frequency support by the other Kundur through the DC links.	Two studied frameworks: 1. Local and uncoordinated control of frequency (droop) and DC voltage (droop) 2. Control of frequency (local droop), DC voltage (local droop) and rotor angle (WAMS based POD) with manual active power coordination

IV. Tool for stability study: presentation and methodology

Due to the complexity of the power systems and their controllers, stability study approach is computer aided. Numerical tools were necessary to assess and enhance the AC/DC stability. Therefore, in this part, the used simulation tools and development of the workflow for AC/DC stability analysis will be described.

1. Simulation tools

To recall, the working environment where the power system benchmarks were built and tested is Dymola based on MODELICA language.

The simulations were developed in the static phasor Dymola tool in which one can directly:

- Build graphical or textual models, simulate them, and use plotting interface,
- Use parameter propagation for model components,
- Set experiments & analyse results using built-in tools,
- Configure objects for user interaction during simulation,
- Understand translation & simulation logs,
- Configure hierarchical models and use encapsulation and variable retrieval,
- Use built-in tool for pedantic coding, unit checking and system inversion,
- Use built-in tool for debugging and logging,
- Set graphical annotation and create object documentation,
- Use records for data management → Important for PowerFlow initialization,
- Interface Dymola with Python,
- Use Power analysis built-in tools.

By using Dymola, one can also benefit from the already existing libraries to perform stability studies on power systems: OpenIPSL as well as the library HVDC developed by SuperGrid Institute.

2. Simulation methodology

To perform the needed AC/DC stability studies, the following simulation ingredients coming from different sources were put together. A generic methodology was defined as well.

- Ingredients to develop and analyze hybrid AC/DC models:
    - Components

        - AC components: OpenIPSL library,
        - DC components: SuperGrid Institute HVDC Library,
            - DC lines and cables,
            - MMC Converters in different control modes,
            - Power sensors.
        - Hybrid AC/DC benchmarks
            - PtP HVDC links and MTDC grids (radial, meshed) with their control,
            - AC benchmarks (Kundur and Nordic 44 are available).
        - Other measurement components
            - PMUs (PLL-based): frequency and angle,
            - RoCoF and Nadir.
    - Calculation and analysis tools
        - AC/DC power flow initializer (GridCal + DC Power Flow),
        - Parameter sweeper,
        - Linearization tool to calculate damping of eigenvalues of interarea oscillations,
        - Mode shape analyzer to highlight the eigenvalues corresponding to interarea modes (in Matlab),
        - Plotters (2D, 3D) for post-processing,
        - Optimization toolbox for optimal tuning and coordination of active power control.

- Methodology
    - To run simulation
        - Define adequate disturbance scenarios (generator trip, line trip, converter trip, load variation),
        - Implement high-level control of active power,
        - Power flow initialization for AC and DC system,
        - Time-domain simulation.

- To highlight/mitigate stability issues (by linearization and time-domain analysis)
    - Post-processing analysis of stability indicators based on measurements to highlight the issues: calculation of eigenvalues, Integral Square Generator Angle, RoCoF, Nadir of frequency, RoCoV, Voltage dips,
    - Post-processing analysis of stability indicators based on measurements to mitigate single stability issues as well as interactions between controls: parameter tuning for each controller, active power coordination.

3. Simulation workflow

To apply the stability study methodology described in the previous section, a precise workflow has been developed using a combination of necessary tools.

- The interesting HVDC ancillary services and their potential interactions should be examined on a selected benchmark (either existent or to be specifically developed for this purpose). After choosing the appropriate benchmark, the model is developed in Dymola tool.
  A preliminary study of the pertinent contingency scenario is needed to highlight the stability phenomena on the chosen benchmark. This consolidates/makes modifications in the selected benchmark.
  At this stage, the final benchmark is developed in Dymola. The pre-established contingency scenarios are listed/developed also if no further study (related to Initial PowerFlow) is needed. More information is available in the Diagram 1 below.

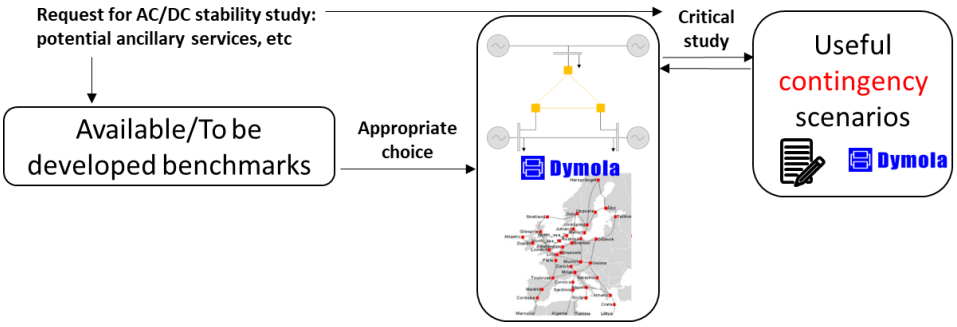

- At this stage, the benchmark should be initialized to run stability studies. Therefore, AC/DC PowerFlow (PF) is generated through GridCal tool which needs a '.raw' file to have a description of the buses, lines, generators, etc as input. This file can be generated through a PSSE tool library. A database of these '.raw' files of some known benchmarks (Kundur, etc) exists already and it can be directly used in GridCal tool without any PSSE tool needed.
  GridCal uses Python code to generate AC PFs and store them in the 'record' format for Dymola application.
  DC PFs still need to be handmade but some works on AC/DC automatic PFs have been initiated at SuperGrid and need further developments.

From the ‘records’ database of PFs, a single PF is used at a time to initialize AC/DC hybrid benchmark.

From the pre-established list of contingencies (previous part), a single or a group of disturbances are implemented in the initialized benchmark.
More information is available in the Diagram 2 below.

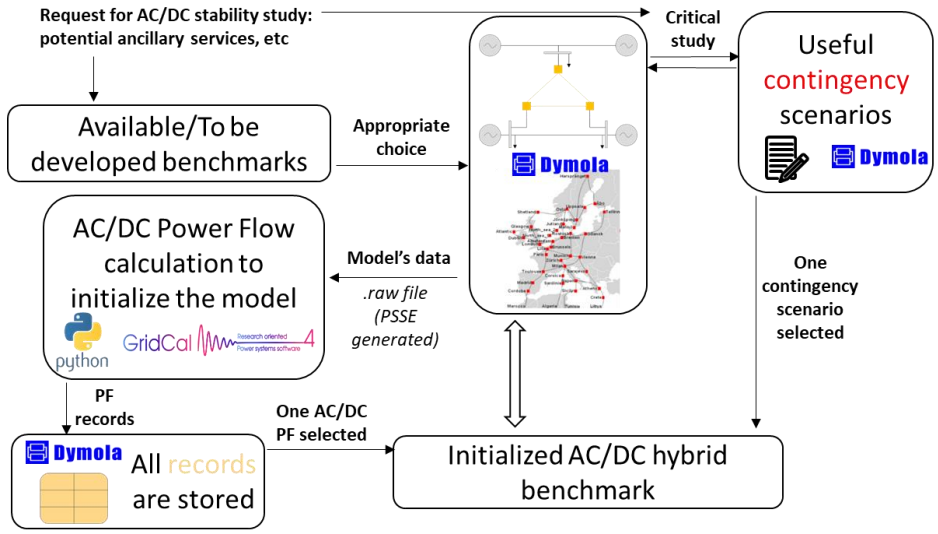

➢ The stability study can now start. Two complementary families of studies show the dynamic behaviour of the system: the small-signal behaviour from one side and the transient and steady-state behaviour from the other side.

First one is evaluated through eigenvalue analysis in which the badly damped – therefore risky – modes are extracted to develop the needed control.

Second category of studies corresponds to the time-domain simulations.
More information is available in the Diagram 3 below

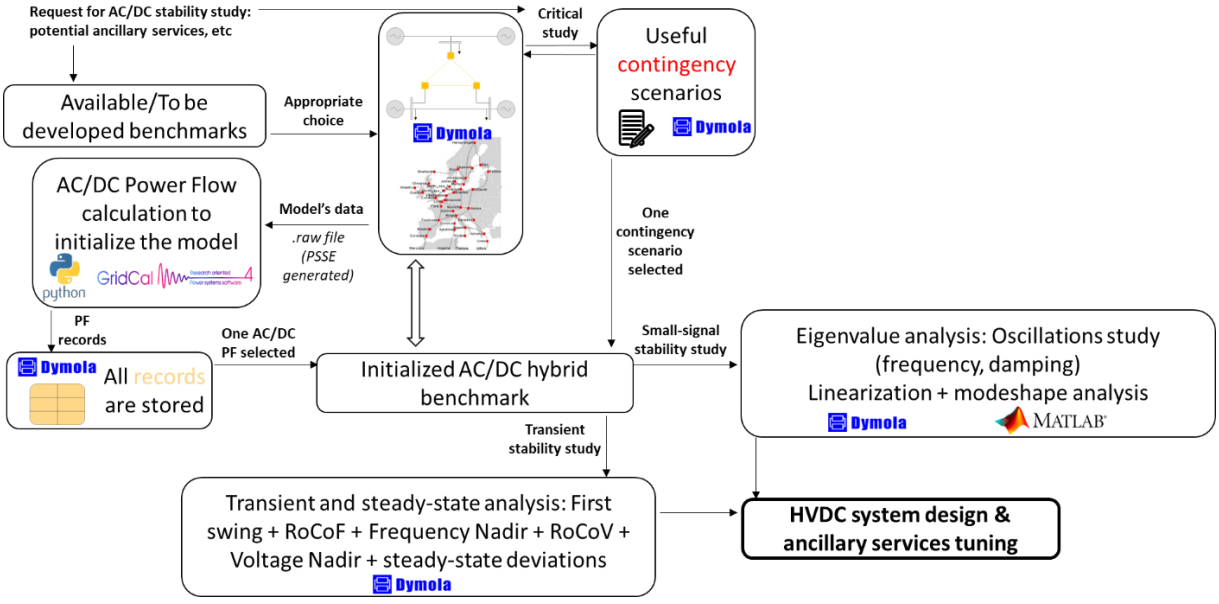

- To be able to design the final HVDC controls for the benchmark, this study should be reproduced for all the plausible contingency scenarios with all the 'relatively different' powerflows evaluated. Two loops of evaluation are therefore added in the workflow (Diagram 4 below).

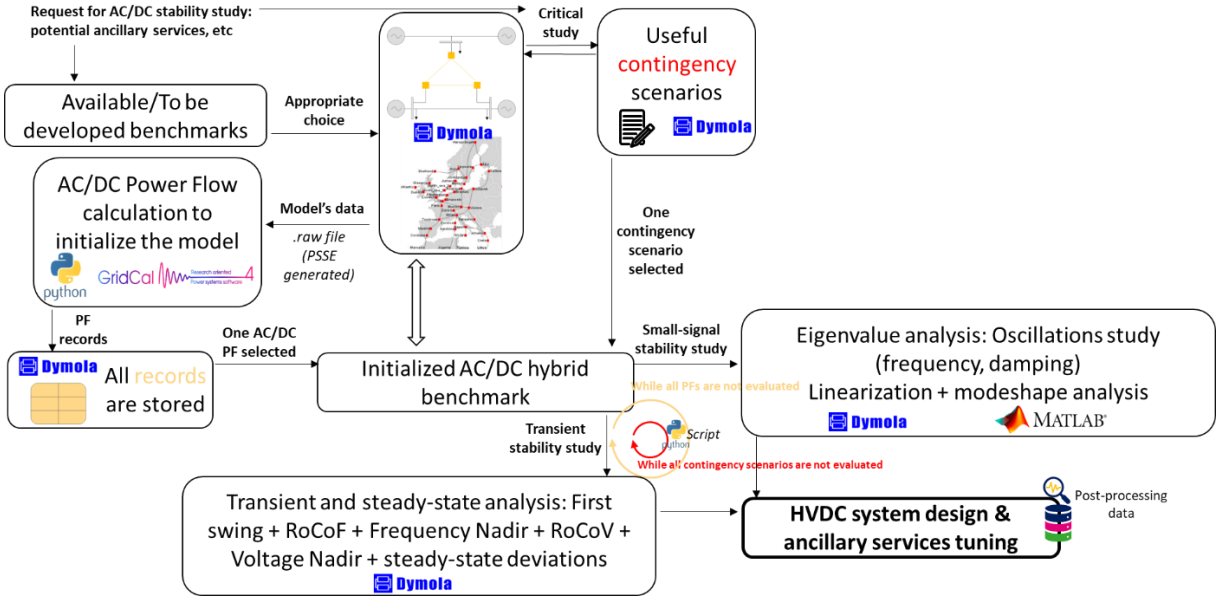

- The HVDC controls may require further optimization of their parameters to enhance the stability of the AC systems furthermore (in the context of combined controls, not of MPC control). Thus, the final workflow Diagram is the following (***Figure 3-18***).

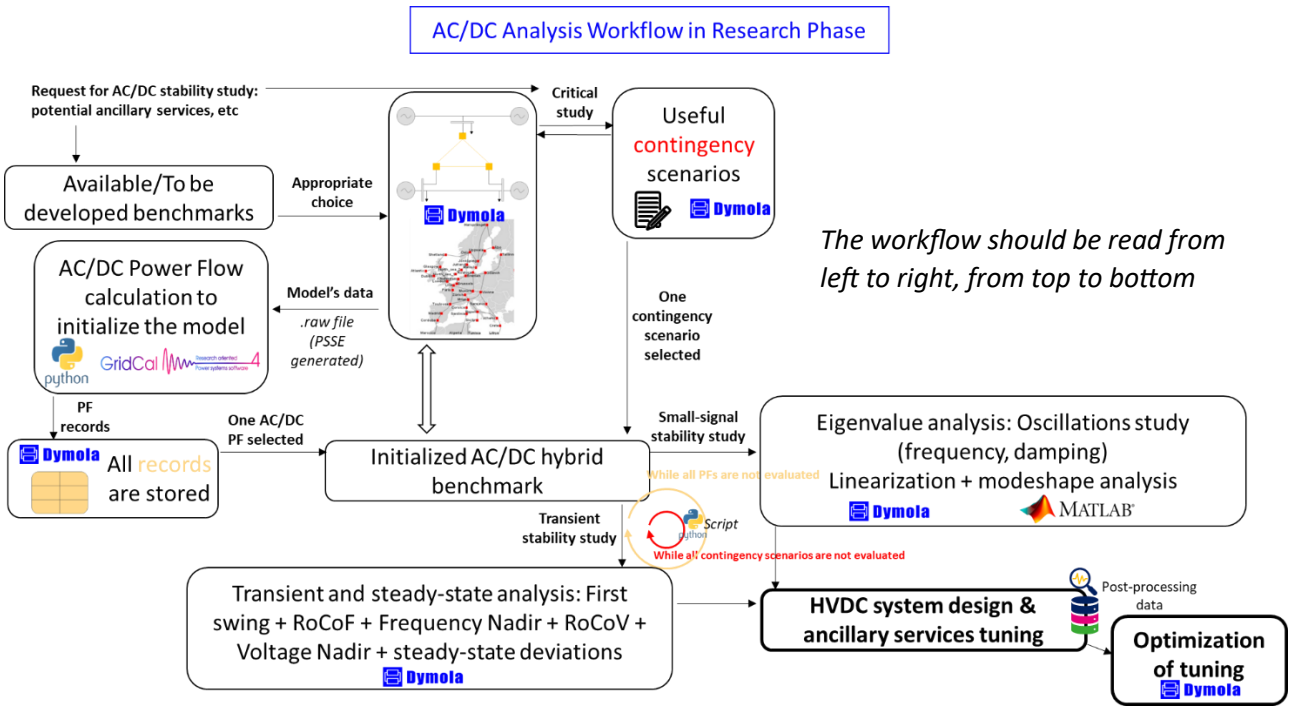

Figure 3-18: AC/DC analysis workflow diagram.

V. Conclusion

This chapter started by formulating the exact models of the components used in the hybrid AC/DC power systems. Three system components categories are defined: AC, DC, and AC/DC interface.

- For the AC part of the system, synchronous generator equations in *dq* reference frame were developed. Particularly, the swing equation is interesting for stability study since it includes the rotor angle and frequency variables. The implemented controllers of the generator were also illustrated since they contribute to stabilizing the system (turbine governor, PSS, AVR). The equations of the voltage-dependent loads and the AC links were shown as well.
- In the DC system, the only components of interest were the DC cables since no DC loads were considered in these studies.
- Concerning the AC/DC interface, the electric scheme of the used MMC-based VSCs was explained. This scheme contains the physical model of the MMC itself and the added inner and outer controls to adequately provide the requested power references sent by the TSO or a higher-level power system controller.

After modelling each component separately, a combination of these components was made to create the needed AC/DC power systems. The models of these systems are called power system benchmarks. Three elaborate benchmarks were developed during the thesis (as well as more simple benchmarks that are not shown in this chapter). The implemented power systems were progressively complicated and allowed leading AC/DC stability studies with increasing complexity during the thesis.

A summary of the stability studies performed on each benchmark was illustrated in this chapter. The defined and adopted computer-aided approach was explained. It is used to lead stability studies. The approach is based principally on a MODELICA-based simulating environment called Dymola. An interface between Dymola and other numerical software to initialize the complex benchmarks and perform stability analysis was created.

A workflow diagram (***Figure 3-18***) was finally developed to better understand the computer-aided AC/DC stability analysis methodology.

Having the models of the power system benchmarks explained, it is now possible to move to the stability studies. These will be explained in a progressive manner: from most simple to most complicated, which also corresponds to the pedagogy adopted during the thesis.

Chapter 4 : AC/DC stability studies: assessment methods, indicators, and controls.

I. Introduction

1. Context

In Chapter 3, AC and DC components with their internal controls were presented. These components were combined in multiple hybrid AC/DC power systems by interfacing them through power converters. The implemented controllers corresponding to each component were also shown.

For the synchronous generator, the PSS helps damp power oscillations principally belonging to the local system. The AVR regulates the machine's field voltage to ensure that local voltage is stable. Finally, the turbine governor ensures the mechanical-electrical power balance (frequency stability), beginning at the level of the machine (which may be electrically far from the other AC synchronous zone components). This distance may influence the ability of the AC system to maintain synchronism (rotor angle stability) if a perturbation occurs.

At the level of the converters, the shown controllers correspond to the proper control of the converters themselves (output voltage and current, inner control loops). This control can be described as "low-level" when seeing the converter from a power systems perspective.

Figure 4-1 shows the **layer of control** (power system level) at which this thesis aims to act to have an impact on the stability of the power system as a whole. One objective in the thesis is to provide support from the HVDC links by controlling the active power of the AC/DC converters in order to enhance the stability of the hybrid power system.

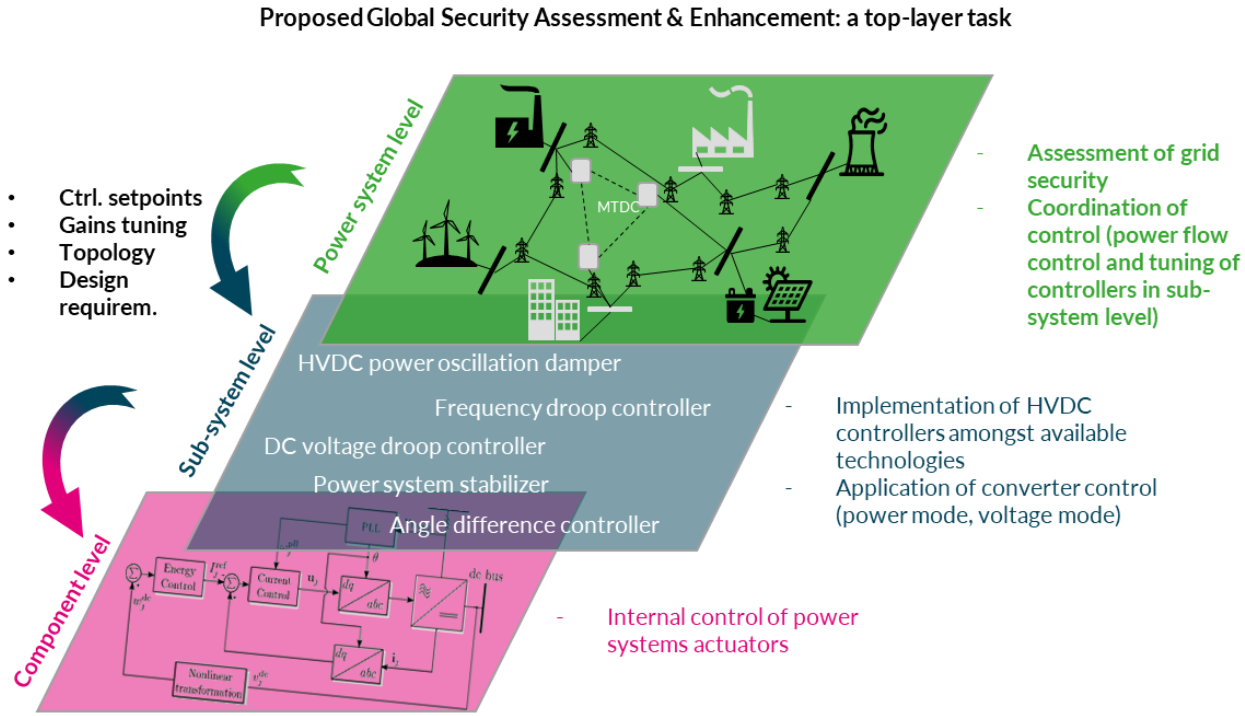

Figure 4-1: Three-layer control of active power.

This chapter discusses the preliminary stability analyses that helped design control for the various forementioned stability aspects. It also evaluates the possibility of minimizing the interactions between the different controllers. In this chapter too, a framework for AC and DC stability studies is proposed. It will help in designing a first active power control coordination strategy to enhance the global stability of the hybrid AC/DC system.

2. Organization of the chapter

The chapter is organized as follows. In a progressive way, multiple stability aspects were studied then tackled simultaneously. The first part focuses on the impact of adding DC components on a pre-existing AC system. Mathematical foundation of this impact was formulated before simulating the studied AC/DC power system. Time-domain and eigenvalue analyses were led to evaluate rotor angle, frequency and DC voltage stabilities as well as the potential interactions between different HVDC controllers. All these separate case studies helped establish several frameworks for stability enhancement approaches.

II. AC/DC power converter's impact on a power system

The impact of adding to a classical AC power system a power electronic-based interface and a DC grid is evaluated in this section under two angles: the impact of the location of the AC/DC interface from a time-domain approach and from a static eigenvalue analysis point of view.

1. Impact of choice of point of injection through a simple use case

Using the component models of the synchronous generators, AC lines and MMC converters shown in Chapter 3, a very simple power benchmark is built. It is composed of two synchronous generators connected through four purely inductive lines to which a power converter is connected through the bus M (***Figure 3-14***).

The dynamics of this system (***Figure 3-14***) will be recalled, inspired by [74] before introducing the MMC converter.

The swing equations shown in the section Chapter 3.II.1.i are recalled here using the angle and frequency differences:

$$\delta_{1-2} = \delta_1 - \delta_2 \tag{4.1}$$

$$\omega_{1-2} = \omega_1 - \omega_2 \tag{4.2}$$

The first part of the swing equations gives:

$$\frac{d\delta_{1-2}}{dt} = \omega_{1-2} \tag{4.3}$$

The second part of the swing equation, when applied to each SG separately then with frequencies deviation difference gives:

$$\frac{2H}{\omega_s} \cdot \frac{d\omega_1}{dt} = P_{mech_1} - P_{damp_1} - P_{elec_1} \quad \textbf{(4.4)}$$

$$\frac{2H}{\omega_s} \cdot \frac{d\omega_2}{dt} = P_{mech_2} - P_{damp_2} - P_{elec_2} \quad \textbf{(4.5)}$$

$$\frac{2H}{\omega_s} \cdot \frac{d\omega_{1-2}}{dt} = \left(P_{mech_1} - P_{damp_1}\right) - \left(P_{mech_2} - P_{damp_2}\right) - \left(P_{elec_1} - P_{elec_2}\right) \quad \textbf{(4.6)}$$

with the assumptions that the inertia constants are equal for the two generators $H_1 = H = H_2$ and with P_{mech} the mechanical power given by the prime movers of the considered generator, P_{damp} the power loss due to damping coefficient, P_{elec} the electrical power exchanged through the machine's connecting bus and ω_s the synchronous pulsation.

In this part, the dynamics of the VSC converter are introduced. For this, its AC terminal voltage and the power exchange with the AC system are considered.

The voltages at the generator terminals are considered to be regulated at $\tilde{E}_1 = E_1\angle\delta_1 = V\angle\delta_1$ and $\tilde{E}_2 = E_2\angle\delta_2 = V\angle\delta_2$ respectively (with V the regulated voltage amplitude at nominal value). The VSC's voltage is $\tilde{V}_M = V_M\angle\delta_M$ at the PCC at the bus M.

To simplify, the converter is assimilated to a load that may have positive or negative power inputs. Then, the currents flowing injected by generators G1 (at left) and G2 (at right) in ***Figure 3-14*** are given by:

$$\tilde{I}_1 = \frac{\tilde{E}_1 - \tilde{V}_M}{jX_1} = \frac{-j\tilde{E}_1 + j\tilde{V}_M}{X_1} \quad \textbf{(4.7)}$$

$$\tilde{I}_2 = \frac{\tilde{E}_2 - \tilde{V}_M}{jX_2} = \frac{-j\tilde{E}_2 + j\tilde{V}_M}{X_2} \quad \textbf{(4.8)}$$

where X_1 and X_2 are the impedances and $\tilde{V}_M = V_{Mreel} + j \cdot V_{Mimaginary}$.

The electrical powers in **(4.6)** can therefore be calculated:

$$P_{elec_1} = Re\left(\tilde{E}_1 \cdot \tilde{I}_1^*\right) = Re\left(\frac{j\tilde{E}_1\tilde{E}_1^* - j\tilde{E}_1\tilde{V}_M^*}{X_1}\right) \quad \textbf{(4.9)}$$

$$P_{elec_1} = Re\left(\frac{-j \cdot V(\cos\delta_1 + j \cdot \sin\delta_1)\left(V_{Mreel} - j \cdot V_{Mimaginary}\right)}{X_1}\right) \quad \textbf{(4.10)}$$

$$P_{elec_1} = Re\left(\frac{-jVV_{Mreel}\cos\delta_1 - VV_{Mimaginary}\cos\delta_1 + VV_{Mreel}\sin\delta_1 - jVV_{Mimaginary}\sin\delta_1}{X_1}\right) \quad \textbf{(4.11)}$$

$$P_{elec_1} = \frac{V\sin\delta_1}{X_1}\cdot V_{Mreel} - \frac{V\cos\delta_1}{X_1}\cdot V_{Mimaginary} \quad \textbf{(4.12)}$$

$$P_{elec_2} = \frac{V\sin\delta_2}{X_2}\cdot V_{Mreel} - \frac{V\cos\delta_2}{X_2}\cdot V_{Mimaginary} \quad \textbf{(4.13)}$$

The exchanged complex power at the AC terminal of the converter is given by:

$$-P - jQ = \tilde{V}_M \cdot (\tilde{I}_1^* + \tilde{I}_2^*) \quad \textbf{(4.14)}$$

To calculate the actual voltage $\tilde{V}_M$, the beginning is finding the complex conjugate of the power injected by the converter:

$$-P + jQ = \tilde{V}_M^* \cdot (\tilde{I}_1 + \tilde{I}_2) \quad \textbf{(4.15)}$$

$$-P + jQ = \tilde{V}_M^* \cdot \left[\frac{\tilde{E}_1 - \tilde{V}_M}{jX_1} + \frac{\tilde{E}_2 - \tilde{V}_M}{jX_2}\right] \quad \textbf{(4.16)}$$

$$jX_1 \cdot (-P + jQ) = \tilde{V}_M^* \cdot \left[\frac{\tilde{E}_1 - \tilde{V}_M}{jX_1} + \frac{\tilde{E}_2 - \tilde{V}_M}{jX_2}\right] \cdot jX_1 \quad \textbf{(4.17)}$$

$$jX_1 \cdot (-P + jQ) = \tilde{V}_M^* \cdot \left[\tilde{E}_1 - \tilde{V}_M + \frac{\tilde{E}_2 - \tilde{V}_M}{X_2}\cdot X_1\right] \quad \textbf{(4.18)}$$

$$jX_1 \cdot (-P + jQ) = \tilde{V}_M^* \cdot \left[\tilde{E}_1 + \tilde{E}_2 \cdot \frac{X_1}{X_2}\right] - V_M^2 \cdot \left[1 + \frac{X_1}{X_2}\right] \quad \textbf{(4.19)}$$

This gives:

$$\tilde{V}_M^* = \frac{jX_1 \cdot (-P + jQ) + \left(1 + \frac{X_1}{X_2}\right)\cdot V_M^2}{\tilde{E}_1 + \tilde{E}_2 \cdot \frac{X_1}{X_2}} = \frac{jX_1 \cdot (-P + jQ) + \left(1 + \frac{X_1}{X_2}\right)\cdot V_M^2}{\tilde{E}_1 + \tilde{E}_2 \cdot \frac{X_1}{X_2}} \quad \textbf{(4.20)}$$

$$\tilde{V}_M^* = \frac{\left(1 + \frac{X_1}{X_2}\right)\cdot V_M^2 - X_1 Q - jX_1 P}{\tilde{E}_1 + \tilde{E}_2 \cdot \frac{X_1}{X_2}} \quad \textbf{(4.21)}$$

To calculate V_M^2 in the expression of $\tilde{V}_M^*$, the product $\tilde{V}_M^* \cdot \tilde{V}_M$ gives:

$$V_M^2 = \frac{\left[\left(1 + \frac{X_1}{X_2}\right) \cdot V_M^2 - X_1 Q\right]^2 + [X_1 P]^2}{\left|\tilde{E}_1 + \tilde{E}_2 \cdot \frac{X_1}{X_2}\right|^2} \tag{4.22}$$

With

$$\begin{aligned}
\left|\tilde{E}_1 + \tilde{E}_2 \cdot \frac{X_1}{X_2}\right|^2 &= \left|V(\cos\delta_1 + \mathrm{j} \cdot \sin\delta_1) + \frac{X_1}{X_2} V(\cos\delta_2 + \mathrm{j} \cdot \sin\delta_2)\right|^2 \\
&= \left|V\left(\cos\delta_1 + \frac{X_1}{X_2}\cos\delta_2\right) + j \cdot V\left(\sin\delta_1 + \frac{X_1}{X_2}\sin\delta_2\right)\right|^2 \\
&= V^2\left(\cos\delta_1 + \frac{X_1}{X_2}\cos\delta_2\right)^2 + V^2\left(\sin\delta_1 + \frac{X_1}{X_2}\sin\delta_2\right)^2 \\
&= V^2\left(\cos^2\delta_1 + 2\frac{X_1}{X_2}\cos\delta_1\cos\delta_2 + \left(\frac{X_1}{X_2}\right)^2\cos^2\delta_2 + \sin^2\delta_1\right. \\
&\left. + 2\frac{X_1}{X_2}\sin\delta_1\sin\delta_2 + \left(\frac{X_1}{X_2}\right)^2\sin^2\delta_2\right) \\
&= V^2\left(1 + 2\frac{X_1}{X_2}(\cos\delta_1\cos\delta_2 + \sin\delta_1\sin\delta_2) + \left(\frac{X_1}{X_2}\right)^2\right) \\
&= V^2\left(2\frac{X_1}{X_2}\cos(\delta_1 - \delta_2) + 1 + \left(\frac{X_1}{X_2}\right)^2\right)
\end{aligned} \tag{4.23}$$

Replacing the equation **(4.23)** in equation **(4.22)** gives:

$$V^2\left(2\frac{X_1}{X_2}\cos(\delta_1 - \delta_2) + 1 + \left(\frac{X_1}{X_2}\right)^2\right) \cdot V_M^2 = \left[\left(1 + \frac{X_1}{X_2}\right) \cdot V_M^2 - X_1 Q\right]^2 + X_1^2 P^2 \tag{4.24}$$

$$\begin{aligned}
&\frac{(X_1 + X_2)^2}{X_2^2} \cdot V_M^4 - 2\frac{X_1 X_2}{X_2^2}(X_1 + X_2)Q \cdot V_M^2 + \frac{(X_1 X_2)^2}{X_2^2}(P^2 + Q^2) \\
&\qquad - \left[2\frac{X_1 X_2}{X_2^2}\cos(\delta_1 - \delta_2)\,V^2 + \frac{X_2^2 V^2}{X_2^2} + \left(\frac{X_1}{X_2}\right)^2 V^2\right] \cdot V_M^2 = 0
\end{aligned} \tag{4.25}$$

$$\begin{aligned}
&\frac{X_1 + X_2}{2X_1 X_2} \cdot V_M^4 + \left[-Q - \frac{\cos(\delta_1 - \delta_2)}{X_1 + X_2} \cdot V^2 - \frac{X_1^2 + X_2^2}{2X_1 X_2(X_1 + X_2)} \cdot V^2\right] \cdot V_M^2 \\
&\qquad + \frac{X_1 X_2}{2(X_1 + X_2)}(P^2 + Q^2) = 0
\end{aligned} \tag{4.26}$$

which can be solved as an equation of second degree:

$$a \cdot (V_M^2)^2 + b \cdot (V_M^2) + c = 0 \tag{4.27}$$

With

$$a = \frac{X_1 + X_2}{2X_1X_2} \tag{4.28}$$

$$\begin{aligned} b = & -Q - \frac{\cos(\delta_1 - \delta_2)}{X_1 + X_2} \cdot V^2 - \frac{X_1^2 + X_2^2}{2X_1X_2(X_1 + X_2)} \cdot V^2 \\ = & -Q - V^2 \frac{X_1^2 + 2X_1X_2\cos(\delta_1 - \delta_2) + X_2^2}{2X_1X_2(X_1 + X_2)} = -Q - S_{12} \end{aligned} \tag{4.29}$$

With

$$S_{12} = V^2 \frac{X_1^2 + 2X_1X_2\cos(\delta_1 - \delta_2) + X_2^2}{2X_1X_2(X_1 + X_2)} \tag{4.30}$$

$$c = \frac{X_1X_2}{2(X_1 + X_2)}(P^2 + Q^2) \tag{4.31}$$

The discriminant of the equation **(4.27)** is:

$$\Delta = b^2 - 4ac = Q^2 + 2QS_{12} + S_{12}^2 - P^2 - Q^2 = S_{12}^2 + 2QS_{12} - P^2 \tag{4.32}$$

The solution of this second-degree equation **(4.27)** is therefore (the positive solution):

$$V_M^2 = \frac{S_{12} + Q + \sqrt{S_{12}^2 + 2QS_{12} - P^2}}{\frac{X_1 + X_2}{X_1X_2}} \tag{4.33}$$

The complex voltage $\tilde{V}_M^*$ in equation **(4.21)** can be calculated to extract the reel and imaginary parts of V_M and use them to calculate P_{elec_1} and P_{elec_2}:

$$\tilde{V}_M^* = \frac{\left(1 + \frac{X_1}{X_2}\right) \cdot V_M^2 - X_1Q - jX_1P}{\left(\tilde{E}_1 + \tilde{E}_2 \cdot \frac{X_1}{X_2}\right)} \cdot \frac{\left(\tilde{E}_1 + \tilde{E}_2 \cdot \frac{X_1}{X_2}\right)^*}{\left(\tilde{E}_1 + \tilde{E}_2 \cdot \frac{X_1}{X_2}\right)^*} \tag{4.34}$$

$$\tilde{V}_M^* = \frac{\left(\left(1 + \frac{X_1}{X_2}\right) \cdot V_M^2 - X_1Q - jX_1P\right) \cdot \left(\tilde{E}_1 + \tilde{E}_2 \cdot \frac{X_1}{X_2}\right)^*}{\left|\tilde{E}_1 + \tilde{E}_2 \cdot \frac{X_1}{X_2}\right|^2} \tag{4.35}$$

$$\tilde{V}_M^* = \frac{\left(\left(1+\frac{X_1}{X_2}\right)\cdot V_M^2 - X_1 Q - jX_1 P\right)\cdot V\left(\left(\cos\delta_1 + \frac{X_1}{X_2}\cos\delta_2\right) - j\cdot\left(\sin\delta_1 + \frac{X_1}{X_2}\sin\delta_2\right)\right)}{V^2\left(2\frac{X_1}{X_2}\cos\left(\delta_1-\delta_2\right)+1+\left(\frac{X_1}{X_2}\right)^2\right)} \quad \textbf{(4.36)}$$

The denominator of $\tilde{V}_M^*$ in equation **(4.36)** can be rewritten:

$$V^2\left(2\frac{X_1}{X_2}\cos\left(\delta_1-\delta_2\right)+1+\left(\frac{X_1}{X_2}\right)^2\right) = V^2\left(\frac{X_1^2+2X_1X_2\cos\left(\delta_1-\delta_2\right)+X_2^2}{X_2^2}\right) = 2X_1\frac{(X_1+X_2)}{X_2}S_{12} \quad \textbf{(4.37)}$$

The numerator of $\tilde{V}_M^*$ in equation **(4.36)** can be rewritten:

$$\begin{aligned}
&\left(\left(1+\frac{X_1}{X_2}\right)\cdot V_M^2 - X_1 Q - jX_1 P\right)\cdot V\left(\left(\cos\delta_1 + \frac{X_1}{X_2}\cos\delta_2\right) - j\cdot\left(\sin\delta_1 + \frac{X_1}{X_2}\sin\delta_2\right)\right)\\
&= X_1 V\cdot\left(\left(\frac{X_1+X_2}{X_1X_2}\right)\cdot\frac{S_{12}+Q+\sqrt{S_{12}^2+2QS_{12}-P^2}}{\frac{X_1+X_2}{X_1X_2}} - Q - jP\right)\\
&\cdot\left(\left(\cos\delta_1 + \frac{X_1}{X_2}\cos\delta_2\right) - j\cdot\left(\sin\delta_1 + \frac{X_1}{X_2}\sin\delta_2\right)\right)\\
&= X_1 V S_{12}\cdot\left(1+\sqrt{1+2\frac{Q}{S_{12}}-\frac{P^2}{S_{12}^2}} - j\frac{P}{S_{12}}\right)\\
&\cdot\left(\left(\cos\delta_1 + \frac{X_1}{X_2}\cos\delta_2\right) - j\cdot\left(\sin\delta_1 + \frac{X_1}{X_2}\sin\delta_2\right)\right)\\
&= \frac{X_1}{X_2}VS_{12}\\
&\cdot\left[\left(X_2\cos\delta_1 + \mathrm{X}_1\cos\delta_2\right) + \left(X_2\cos\delta_1 + \mathrm{X}_1\cos\delta_2\right)\cdot\sqrt{1+2\frac{Q}{S_{12}}-\frac{P^2}{S_{12}^2}}\right.\\
&\left.+\left(X_2\sin\delta_1 + X_1\sin\delta_2\right)\cdot\frac{P}{S_{12}}\right] + j\\
&\cdot\frac{X_1}{X_2}VS_{12}\left[-\left(X_2\sin\delta_1 + X_1\sin\delta_2\right) - \left(X_2\sin\delta_1 + X_1\sin\delta_2\right)\right.\\
&\left.\cdot\sqrt{1+2\frac{Q}{S_{12}}-\frac{P^2}{S_{12}^2}} - \left(X_2\cos\delta_1 + \mathrm{X}_1\cos\delta_2\right)\cdot\frac{P}{S_{12}}\right]
\end{aligned} \quad \textbf{(4.38)}$$

The equation **(4.36)** becomes:

$$\begin{aligned}\tilde{V}_M^* &= \frac{V \cdot \left[(X_2 \cos\delta_1 + \mathrm{X}_1 \cos\delta_2) + (X_2 \cos\delta_1 + \mathrm{X}_1 \cos\delta_2) \cdot \sqrt{1 + 2\frac{Q}{S_{12}} - \frac{P^2}{S_{12}^2}} - (X_2 \sin\delta_1 + X_1 \sin\delta_2) \cdot \frac{P}{S_{12}}\right]}{2(X_1 + X_2)} \\ &- j \cdot \frac{V \cdot \left[(X_2 \sin\delta_1 + X_1 \sin\delta_2) + (X_2 \sin\delta_1 + X_1 \sin\delta_2) \cdot \sqrt{1 + 2\frac{Q}{S_{12}} - \frac{P^2}{S_{12}^2}} + (X_2 \cos\delta_1 + \mathrm{X}_1 \cos\delta_2) \cdot \frac{P}{S_{12}}\right]}{2(X_1 + X_2)}\end{aligned} \quad \textbf{(4.39)}$$

Which corresponds to the expression

$$\tilde{V}_M^* = V_{Mreel} - j \cdot V_{Mimaginary} \quad \textbf{(4.40)}$$

With equations **(4.39)** and **(4.40)**, the expressions of P_{elec_1} and P_{elec_2} can be calculated in equations **(4.12)** and **(4.13)** respectively:

$$\begin{aligned}P_{elec_1} = \frac{V \sin\delta_1}{X_1} \cdot V_{Mreel} - \frac{V \cos\delta_1}{X_1} \cdot V_{Mimaginary} \\ = \frac{V^2}{2(X_1 + X_2)} \\ \cdot \left[\left(\frac{X_2}{X_1}\cos\delta_1 \sin\delta_1 + \cos\delta_2 \sin\delta_1\right)\left(1 + \sqrt{1 + 2\frac{Q}{S_{12}} - \frac{P^2}{S_{12}^2}}\right)\right. \\ - \left(\frac{X_2}{X_1}\sin^2\delta_1 + \sin\delta_1 \sin\delta_2\right) \cdot \frac{P}{S_{12}} \\ - \left(\frac{X_2}{X_1}\cos\delta_1 \sin\delta_1 + \cos\delta_1 \sin\delta_2\right)\left(1 + \sqrt{1 + 2\frac{Q}{S_{12}} - \frac{P^2}{S_{12}^2}}\right) \\ \left. - \left(\frac{X_2}{X_1}\cos^2\delta_1 + \cos\delta_1 \cos\delta_2\right) \cdot \frac{P}{S_{12}}\right] \\ = \frac{V^2}{2(X_1 + X_2)} \\ \cdot \left[(\cos\delta_2 \sin\delta_1 - \cos\delta_1 \sin\delta_2)\left(1 + \sqrt{1 + 2\frac{Q}{S_{12}} - \frac{P^2}{S_{12}^2}}\right)\right. \\ \left. - \left(\frac{X_2}{X_1} + (\cos\delta_1 \cos\delta_2 + \sin\delta_1 \sin\delta_2)\right) \cdot \frac{P}{S_{12}}\right]\end{aligned} \quad \textbf{(4.41)}$$

$$P_{elec_1} = \frac{V^2}{2(X_1 + X_2)} \cdot \left[\sin(\delta_1 - \delta_2)\left(1 + \sqrt{1 + 2\frac{Q}{S_{12}} - \frac{P^2}{S_{12}^2}}\right) - \left(\frac{X_2}{X_1} + \cos(\delta_1 - \delta_2)\right) \cdot \frac{P}{S_{12}}\right] \quad \textbf{(4.42)}$$

$$P_{elec_2} = \frac{V^2}{2(X_1 + X_2)} \cdot \left[-\sin(\delta_1 - \delta_2) \left(1 + \sqrt{1 + 2\frac{Q}{S_{12}} - \frac{P^2}{S_{12}^2}} \right) - \left(\frac{X_1}{X_2} + \cos(\delta_1 - \delta_2) \right) \cdot \frac{P}{S_{12}} \right] \quad \textbf{(4.43)}$$

Therefore, the variation of the frequency difference between the two generators can be calculated using the swing equation **(4.6)**:

$$\frac{2H}{\omega_s} \cdot \frac{d\omega_{1-2}}{dt} = \left(P_{mech_1} - P_{damp_1}\right) - \left(P_{mech_2} - P_{damp_2}\right) - \left(P_{elec_1} - P_{elec_2}\right) \quad \textbf{(4.44)}$$

$$\frac{2H}{\omega_s} \cdot \frac{d\omega_{1-2}}{dt} = \left(P_{mech_1} - P_{damp_1}\right) - \left(P_{mech_2} - P_{damp_2}\right) - \frac{V^2}{2(X_1 + X_2)} \cdot \left[2\sin(\delta_1 - \delta_2) \left(1 + \sqrt{1 + 2\frac{Q}{S_{12}} - \frac{P^2}{S_{12}^2}} \right) - \left(\frac{X_2}{X_1} - \frac{X_1}{X_2} \right) \cdot \frac{P}{S_{12}} \right] \quad \textbf{(4.45)}$$

The equation **(4.45)** above shows, for a simplistic benchmark, the impact of injecting power through a converter in a synchronous AC system. Particularly, when the point of injection (PCC) is not electrically equidistant from the two machines in the benchmark ***Figure 3-14*** above, the active power injection can contribute to the variation of frequency difference between machine 1 and machine 2. This means that, when the term $\left(\frac{X_2}{X_1} - \frac{X_1}{X_2}\right)\frac{P}{S_{12}}$ is not null, frequency (therefore power) oscillations are created between the two machines.

To verify the impact of changing the location of the point of common coupling (PCC) of the converter, the simplistic benchmark ***Figure 3-14*** was modelled and simulated in Dymola with initial AC powerflow. To simplify, the reactive power injected by the converter is considered null: $Q = 0$.

In Dymola, the used benchmark is the following ***Figure 4-2***:

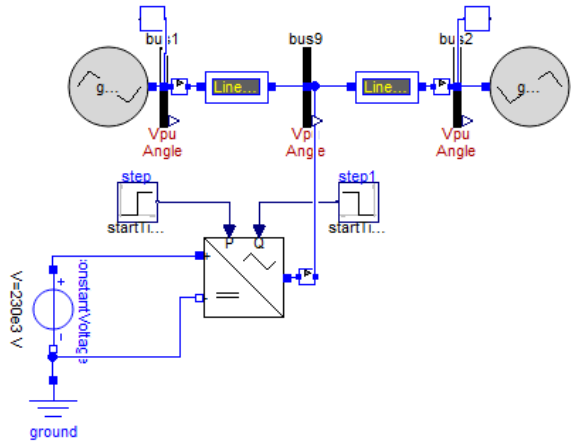

Figure 4-2: Dymola model of the power system benchmark shown in Figure 3-14.

The initial operating conditions that are interesting for the study correspond to the following ***Table 4-1***:

Table 4-1: Initial power flow used for the benchmark shown in Figure 3-14.

Component	Initial conditions
G1	P1 = 70 MW; Q1 = 88 MVAr; PSS gain = 0
G2	P2 = -69 MW; Q2 = -94 MVAr; PSS gain = 0
MMC converter	P = 0 MW; Q = 0 MW

The lines differ only by their length: the impedance in line 19 is called $X_1 = rX$ and the impedance in line 92 is called $X_2 = (2 - r)X$.

The contingency is an active power injection ($P = 100$ MW) by the converter at $t = 5$ s.

Two cases are simulated. In the first case (in blue), the converter is equidistant from the two synchronous machines (ratio of electrical distance is $r = 1$) while in the second case (in red), the converter is nearer to the left machine than the right one (ratio of electrical distance is $r = 0.1$). The simulation results are shown in the coming ***Figure 4-3***, ***Figure 4-4***, and ***Figure 4-5***:

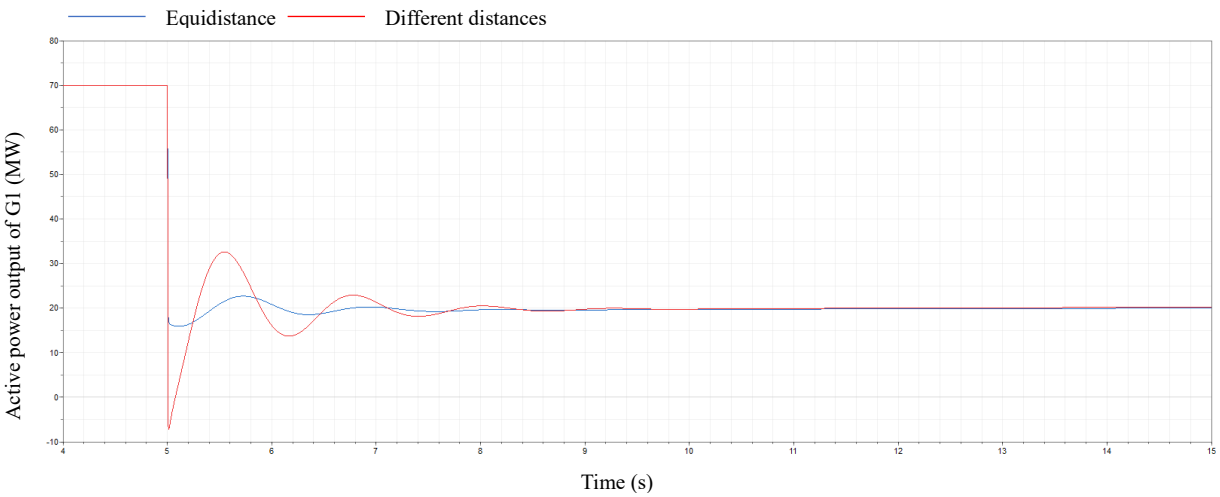

Figure 4-3: Active power outputs of generator G1.

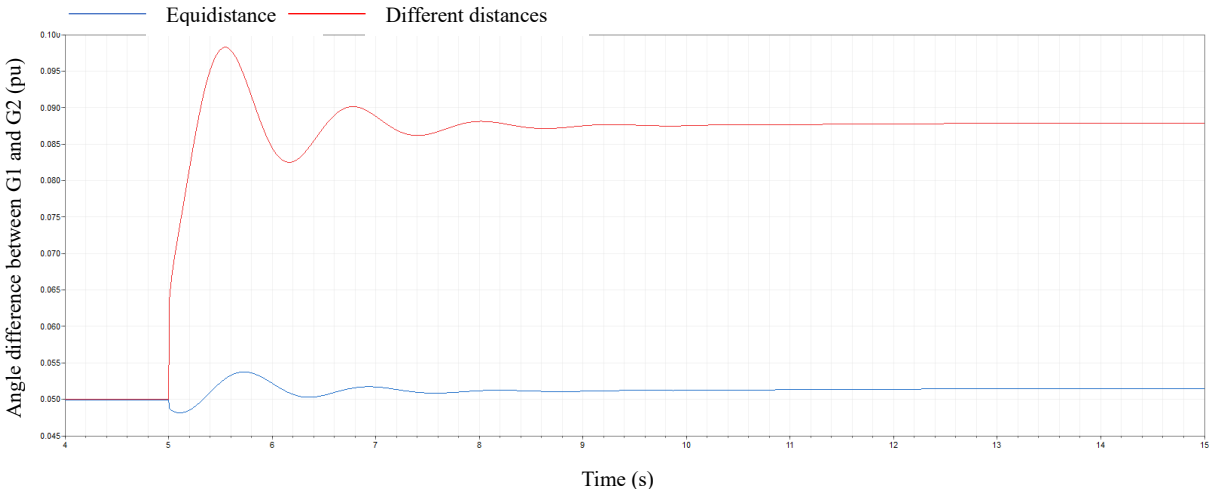

Figure 4-4: Rotor angle differences between generators G1 and G2.

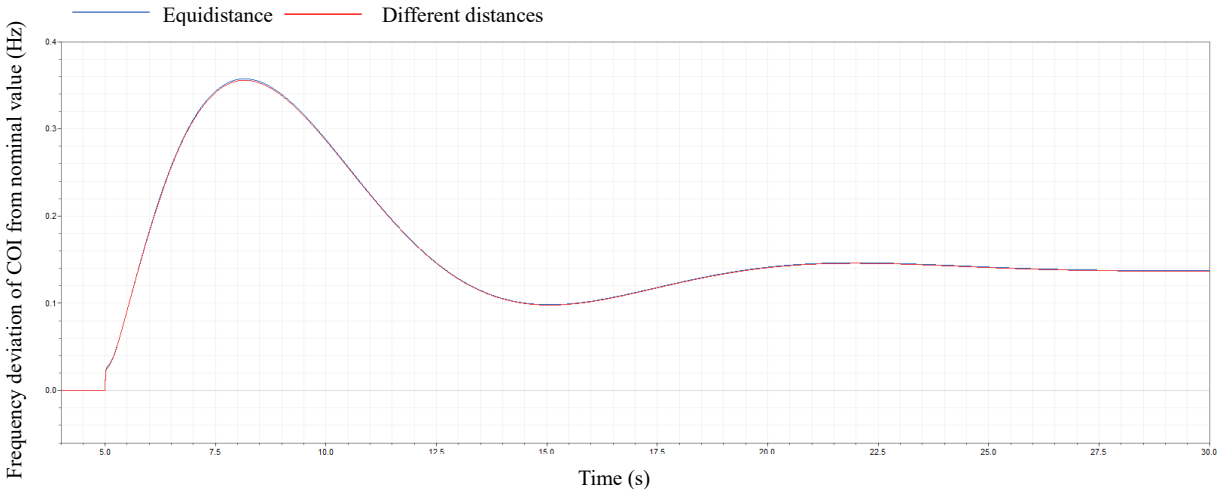

Figure 4-5: Frequency deviations – from the nominal value – of the centre of inertia of the synchronous AC zone.

The ***Figure 4-4*** shows that the angle difference deviation is higher and contains higher-amplitude oscillations than in the case when the converter is not equidistant from both machines. As the equation **(4.45)** suggests, by instantly injecting active power nearer to a machine than to the other, the frequency difference between machines 1 and 2 increases. This induces an increase in rotor angle deviation between machines 1 and 2 (positive derivative of rotor angle difference) (***Figure 4-4***). For small angle differences $\Delta = \delta_1 - \delta_2$, the equation **(4.45)** corresponds to a damped oscillator with the oscillating variable equal to Δ (shown by ***Figure 4-4***). These rotor angle oscillations also correspond to active power oscillations as shown in ***Figure 4-3*** since the term P_{elec} (in each machine's swing equation) contains a variating rotor angle due to the contingency.

From a power stability point of view, the location of the converter's PCC could cause power imbalance in such a two-area system which may lead to system split and loss of synchronism if the power oscillations are important. Therefore, during the design of a hybrid AC/DC system, the converters' PCCs should be considered to avoid destabilizing rotor angles of the system due to active power injection.

This preliminary study also shows the energizing effect of injecting active power through a converter: the frequency of the centre of inertia of the system increased (higher machine speed) (***Figure 4-5***). The localization of the PCC does not impact the final value of this physical parameter since the same energy is brought to the system in all cases (***Figure 4-5***).

2. Impact on system's eigenvalues

In the previous section, the theoretical and time-domain analyses showed the potential interactions between AC and DC systems due to the location of the PCC of the added converter.

Another type of study allows also to evaluate these interactions: modal analysis. In this section, the aim is to check what is the effect of purely adding an AC/DC converter to an existing AC synchronous system in terms of eigenvalues. At this stage of work progress, it was interesting to check whether the small-signal stability is impacted by adding an MMC converter to the system or not. This is a crucial step to

validate the integration of MMC converters in AC power systems to be able to assume that the small-signal stability is preserved and continue the studies.

To evaluate the impact of adding an MMC converter on the small-signal stability, a modal analysis was numerically performed on the simple benchmark ***Figure 4-2*** used in the previous section where three cases were studied. The worst-case scenario is adopted: the bus to which the converter will be connected is not equidistant to both machines.

- Case 1: pure AC system
- Case 2: pure DC system
- Case 3: hybrid AC/DC system

The complex eigenvalues plots corresponding to each case are superposed in this diagram (***Figure 4-6***):

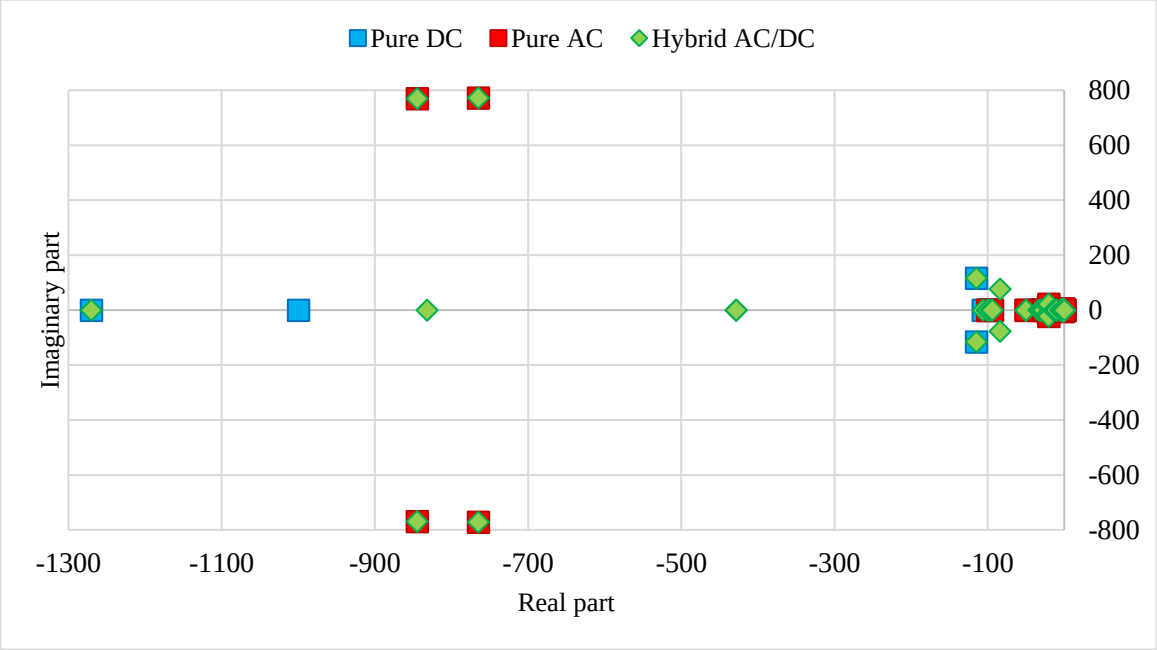

Figure 4-6: Complex eigenvalues calculated for the pure DC system, pure AC system and the hybrid AC/DC system.

According to the ***Figure 4-6***, when the separate AC and DC systems are combined in a single hybrid AC/DC system, the eigenvalues of each system are also combined without modification in the corresponding real and imaginary parts, except for some identified eigenvalues.

The modal analysis shows that some modes are modified, and others created due to the combination of AC and DC systems. The modes in question are shown in the ***Table 4-2*** below.

Table 4-2: Modified and created modes when AC and DC systems are combined.

Modified mode				Created modes		
Original mode in DC system		New mode in AC/DC system		New AC/DC modes		
Eigenvalue	Time constant (s)	Eigenvalue	Time constant (s)	Eigenvalue	Time constant (s) / Frequency (Hz)	Damping (%)
$\lambda_2 = -1000.00$	$T_2 = 0.0010$	$\lambda_6 = -832.0453$	$T_6 = 0.0012$	$\lambda_7 = -428{,}60873$	$T_7 = 0.0023$	-
				$\lambda_8 = -428{,}12772$	$T_8 = 0.0023$	-
				$\lambda_{21} = -13{,}20426$	$T_{21} = 0.0757$	-
				$\lambda_{22} = -13{,}189441$	$T_{22} = 0.0758$	-
				$\lambda_{52,53} = -83{,}97734 \pm 77{,}001076$	$f_{52,53} = 18.1334$	73.71

The modified mode λ_2 which became the mode λ_6 impacts the PLL used for the converter. The created modes λ_7, λ_8, λ_{21} and λ_{22} contribute to the converter's voltage and current respectively at C_{eq} and $L_{dc,eq}$ shown in ***Figure 3-9*** when the converter is connected to the AC system. Finally, the created complex modes λ_{52}, λ_{53} also impacts the PLL used for converter's control. The firstly mentioned modes are non-oscillatory while the last two modes are oscillatory but well-damped.

To conclude, the linear analysis shows an evolution of the modal characteristics related to the PLL component used in the AC/DC power benchmark. This evolution, however, does not jeopardize the power system's small-signal stability.

In contrast, when the converter's active power participates in the control of frequency or rotor angle stability, the PLL used for the converter, the internal current and voltage controllers will be not completely decorrelated the one from the other since the converter's measurements used for internal control come from the PLL. This is not the case when an external step of power reference is sent to the converter in an open loop (the previously shown simulation results). Therefore, in the case of added control (frequency, rotor angle), the DC modes (related to internal current and voltages of the converter) should evolute.

Four other case studies were elaborated and conducted on this simplistic benchmark to evaluate the modal behaviour of the AC/DC power system:

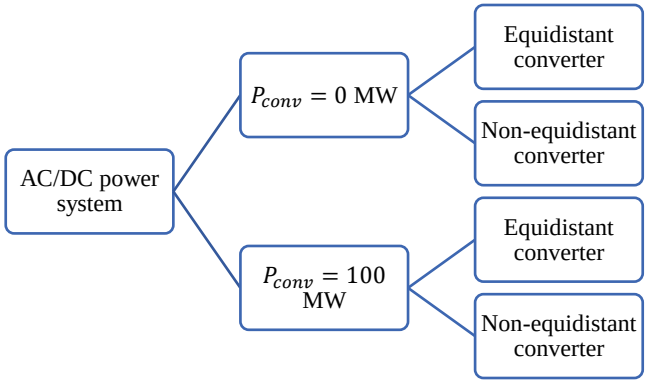

Figure 4-7: The four case studies made to evaluate the modal behaviour of the AC/DC system shown in Figure 3-14.

The in-depth analysis of the resulting eigenvalues shows no significant change in the values taken by the modes and the diagram (***Figure 4-6***) of the complex eigenvalues of the hybrid AC/DC system remains valid for all the four cases. Very slight changes were noticed on the real part of the mode λ_6 corresponding to the PLL but the small-signal oscillatory behaviour of the power system remains intact.

The main drawback of this preliminary study is the low degree of complexity of the used benchmark, but this was an intended to investigate the impact of adding an AC/DC converter (with constant active power control) in an AC system in terms of small-signal stability.

3. HVDC control to meet requirements of AC stability

Some functionalities are expected from HVDC links [6] during the operation of a power system:

- AC Voltage control
- Sub-synchronous damping
- Frequency control (Frequency Containment Reserve delivery)
- Emergency Power Control
- Power Oscillation Damping
- AC line emulation
- Synthetic inertia

In the next sections, a focus will be made on frequency control, power oscillation damping and AC line emulation.

III. Rotor angle stability

1. Context

In classical AC power systems, the rotor angle stability refers to the "ability of synchronous machines to remain in synchronism under N-situation and after being subject to a disturbance" [75]. No specific requirements are explicated for the range of rotor angles or that of rotor angle differences in the Network Codes established in [75], [76], [77].

Consequently, for the hybrid AC/DC systems used, the maximal rotor angle differences between two generators are constrained. Therefore, the active power value that their connecting AC line transfers remains constrained by the line's power transfer capacity. For a simple benchmark like in ***Figure 3-14***, if the power exchanged with the converter is null, this constraint can be written as

$$\left|P_{elec_1} - P_{elec_2}\right| \leq P_{line12,max} \tag{4.46}$$

with the first term of the inequality **(4.46)** expressed in equations **(4.44)** and **(4.45)**. For more complicated benchmarks, an analytical expression of the active power transferred through an AC line is harder to find. Therefore, for the case studies, it was verified through time-domain simulations that all the lines' power transfer capacities were not violated.

In this thesis, three rotor angle stability sub-aspects were dealt with:

- Transient (first swing),

- Small signal (electromechanical oscillations related to interarea modes),
- Steady state (rotor angle differences).

Rotor angle's transient stability can be analysed through several methods [78]:

- Equal Area Criterion (EAC)
- Extended Equal Area Criterion (EEAC)
- AC/DC Extended Equal Area Criterion (AC/DC EEAC)
- Lyapunov's direct method
- Time-domain assessment

Rotor angle's small-signal stability can be analysed through these methods:

- Lyapunov's indirect method (use of linearized system to evaluate the eigenvalues)
    - Linearization around equilibrium point
    - Exact linearization [79]
- Time-domain assessment

In this PhD thesis, the transient and steady-state aspects are assessed through time-domain analysis. The small-signal stability aspect is assessed through both modal (with numerical linearization around an equilibrium point) and time-domain analyses.

The following part will investigate the impact of adding dedicated rotor angle controllers on the mentioned stability sub-aspects.

2. Expected HVDC controls for rotor angle stability

In the following, a non-exhaustive list of potential controllers will be presented as they will be used in the thesis. For each controller, many technologies exist, each having its own advantages and drawbacks. A zoom is made on two controls applied on AC/DC converters' active power references for rotor angle stability enhancement.

i. Power oscillation damping

Power oscillation damping can be performed through multiple possibilities (***Table 4-3***).

Table 4-3: Power controllers helping in oscillation damping in a transmission power system.

Control strategy	Observability	Data acquisition	Actuators
•Power System Stabilizer •Power Oscillation Damper (local & remote inputs) •Load shedding (load side) & bang-bang type (converter side) controls •Operating Point Adjustment •Model Predictive Control	•Signals that contain most significant information	•Measurements •Transmission system •Time delays •Processing time	•Synchronous generators •HVDC interfaced converters

Before implementing Power Oscillation Damper (POD), the PSS was a decentralized method allowing for independent power oscillation damping action for each generator. New designs such as PSS4B and adaptive tuning of PSS can play a significant role in small-signal interarea mode damping [80], [81].

However, PSS requires tuning of 6 parameters (1 gain and 5 time constants) and a centralized POD can also play a supplementary role for a given power system's optimal operation.

POD controllers are widely studied today, and the emergence of machine learning and artificial intelligence allows for new ways of parameter tuning. Figures 6.12 to 6.18 in [82] compare different machine learning-based algorithms that predict eigenvalues and classify them to the true eigenvalues of the IEEE 14-bus power system. Promising results are shown but more investigation is needed for real-time real-life application of the deep-learning-based power oscillation damping. The 'intelligent POD' (iPOD) then 'multi-band iPOD' (MiPOD) shown in [83], [84] are one of the possible improvements proposed for intelligent tuning of POD but its comparison with conventional PSSs showed that, in certain circumstances, the latter can have better results. It is true that, compared to conventional PSS, the 'MiPOD' needs to tune only 1 parameter per oscillation band and assures selective and adaptive damping as well, but it assumes a control dependent on wide-area measurements (availability and reliability [85], transmission, processing [86]) and communication delays.

Finally, complementary actions to the supplementary POD control are bang-bang type control [87], Operating Point Adjustment (OPA) [88] and Model Predictive Control (MPC). This moves the system to a new condition to have better damping of critical modes. In case of OPA for instance, POD can be the first action implemented against disturbances, while OPA can be the longer-term action to improve system's small signal stability. Moreover, OPA can be applied before the occurrence of a disturbance, providing therefore additional stability margins. Coordination between POD and OPA may be needed, too.

Remote signal used to ensure power oscillation damping can outperform local signals [89] but delay margins limit their performance.

Two important points to evaluate when adding a POD are:

- The placement of the actuator
- Parameter tuning.

In the following, for a couple of converters k and j connected to the same synchronous area, the POD control sends the following power references to the converters (equation **(4.47)**):

$$\begin{aligned} P^*_{POD\,kj}(t) &= K_{POD,kj} \cdot \left(f_j(t) - f_k(t)\right) \\ P^*_{POD\,jk}(t) &= -P^*_{POD\,kj}(t) \end{aligned} \qquad \textbf{(4.47)}$$

where $K_{POD,kj} > 0$ is the gain of the POD between converters k and j, f_k and f_j are the measured frequencies at the PCCs, and $P^*_{POD\,kj}$ is the active power reference sent to converter k due to the POD control between it and converter j.

ii. AC line emulation

To enhance transient stability, one possibility is to emulate AC lines through VSC-HVDC control. Although this simple measure is normally done for better steady state of the AC system (powerflow concerns), it can also enhance dynamic behaviour of the power system.

The injection of synchronizing power (not only damping power) by POD through DC lines to support AC grid in case of three-phase fault was investigated [90] in addition to the main topic of transient stability enhancement.

Although ADC controller is a simple controller, particular attention is needed on filtering time constant of ADC which may impact transient stability negatively as was learnt in the case of INELFE DC interconnection [91], [92]. Extremely quick or slow time constants of ADC are considered to enhance transient stability while other values can jeopardize system stability. Since ADCs are mostly used for steady state concerns, choosing a slow time constant is the best option to avoid transient instability.

In the following, for a couple of converters k and j connected to the same synchronous area, ADC control sends the following power references (equation **(4.48)**) [93]:

$$\begin{aligned} P^*_{ADC\,kj}(t) &= K_{ADC,kj} \cdot \left(\theta_j(t) - \theta_k(t)\right) \\ P^*_{ADC\,jk}(t) &= -P^*_{ADC\,kj}(t) \end{aligned} \tag{4.48}$$

where $K_{ADC,kj} > 0$ is the gain of the ADC between converters k and j, θ_k and θ_j are the bus angles at the PCCs, and $P^*_{ADC\,kj}$ is the active power reference sent to converter k due to the existing ADC control between it and converter j.

A low-pass filter (equation **(4.49)**) can be added to the ADC to avoid unnecessary power compensations (oscillating power compensation, quickly disappearing events, etc.). Although the main purpose of ADC is steady-state enhancement, it may contribute to rotor angle stability during transients. The drawback with higher low-pass filter time constants is that AC line may be less emulated during quick transients since they are filtered. The s-domain transfer function of the implemented filter is shown in the equation **(4.49)** where the time constant $\tau_{ADC,kj}$ for the ADC implemented between converters k and j helps avoid emulating the power oscillations through the DC system.

$$LPF_{ADC,kj}(s) = \frac{\Delta\theta_{out}}{\Delta\theta_{in}} = \frac{1}{1 + \tau_{ADC,kj}s} \tag{4.49}$$

3. Preliminary rotor angle stability analysis

In this section, two approaches for rotor angle stability analysis are presented: modal (eigenvalue study) and time-domain. The studies will concentrate on the impact of adding supplementary HVDC controllers to enhance the rotor angle stability in a synchronous AC system.

The used power system benchmark for this purpose is a modified version of the one shown in figure E12.8 in [60]. The test benchmark is recalled (***Figure 4-8***). The initial powerflow is shown in the ***Figure 4-8*** as well. The used power electronic components are MMC converters.

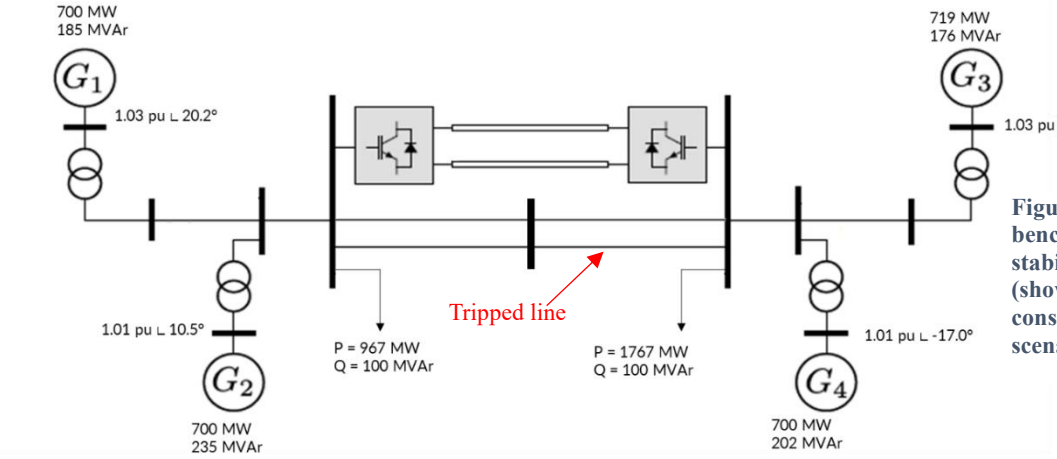

Figure 4-8: The benchmark used for stability study. A line trip (shown in red) is the considered perturbation scenario.

i. Eigenvalue analysis to evaluate the impact of adding a POD

The modes considered in this section are categorized as interarea modes. They are the modes that, when excited and when their damping value allows, cause power oscillations between two sub-zones within the same synchronous zone. Interarea modes are distinguished from local oscillating modes. In the latter case, a generator oscillates against another one within the same sub-zone, while, in the former case, one or a group of generators oscillates against an interconnected or a group of interconnected generators belonging to another sub-zone. The interconnection in question is generally characterized by relatively long-distance AC links with important power transfers.

To help in the damping of interarea oscillating modes, a Power Oscillation Damper can be added to the control of HVDC links. The impact of adding a POD is studied in this section through eigenvalue analysis. In [60], table E12.4 gives the eigenvalues of interarea modes when PSS is added to the synchronous generators: $\lambda_{interarea} = -0.501 \pm j \cdot 3.77$ which gives the frequency $f = 0.60$ Hz and the damping of $\xi = 13$ %. The evolution of these interarea modes was observed before and after adding a POD controller (**(4.47)**), and for different tuning of controller's gain as well. The modal analysis is also performed in Dymola tool which has a built-in toolbox for linearization. The modes are given in the ***Table 4-4***. The linearization is performed on the initial point of operation before the simulation runs and the system is disturbed by any contingency.

Table 4-4: Interarea modes eigenvalues for different case studies.

Case	Eigenvalues	Interarea frequency (Hz)	Damping
[60]– Thyristor with PSS excitation	$-0.50 \pm j3.77$	0.60	0.13
$k_{pod} = 0$	$-0.54058 \pm j3.9911$	0.6410	0.1342
$k_{pod} = 100e8$	$-0.56697 \pm j3.9864$	0.6408	0.1408
$k_{pod} = 100e9$	-0.80420 ± 3.9372	0.6396	0.2001

The complex eigenvalue plots for the three cases of POD gains given in the ***Table 4-4*** are superposed in the ***Figure 4-9***.

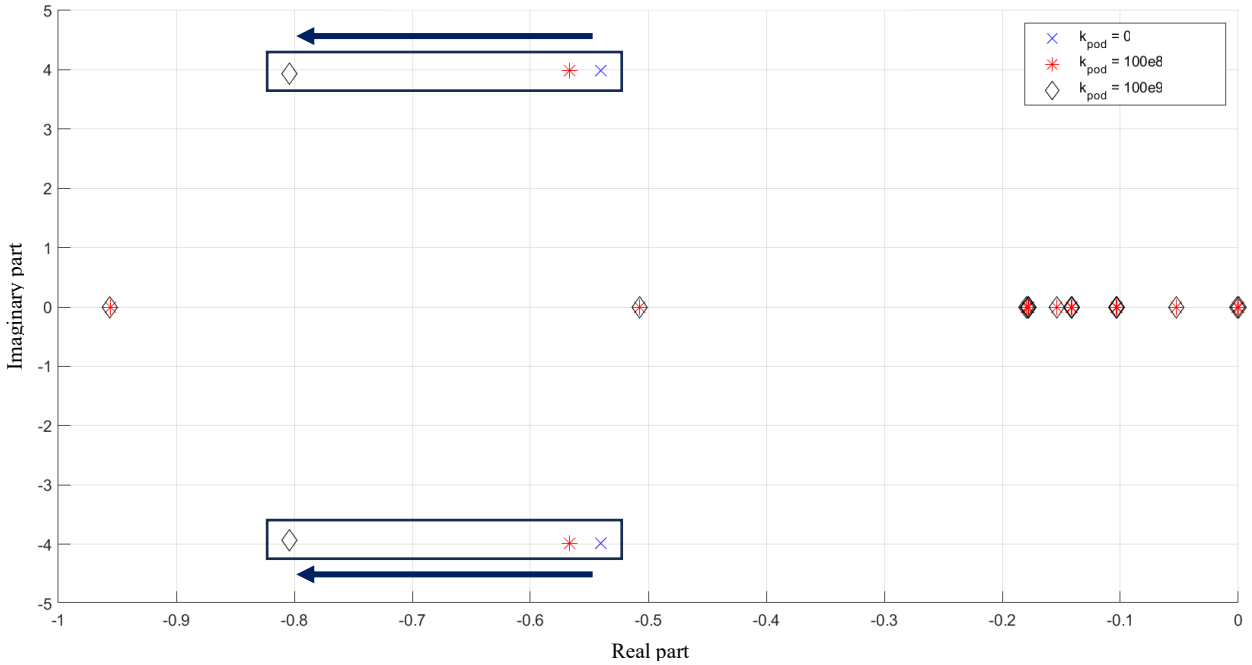

Figure 4-9: Complex eigenvalue evolution for three POD gain values.

The interarea modes move towards more negative real parts when the value of the POD gain increases. This means a better damping of the interarea power oscillations as the ***Table 4-4*** shows. The impact of POD control alone is enhancing the rotor angle small-signal stability of the AC/DC power system in terms of interarea oscillations. However, if the power oscillation damper is combined with the angle difference controller, what would be the impact of this combination on rotor angle stability?

ii. Time-domain analysis to tune POD and ADC parameters

In this section, a time-domain simulation is applied to analyse the impact of combining two dedicated rotor angle controllers (POD and ADC) on the rotor angle stability. To check this impact, a perturbation scenario is developed: a tripping of the line indicated in red the ***Figure 4-8*** at $t = 5$ s followed by line reconnection at $t = 5.5$ s.

Various values of control parameters were tested, and the results are shown in the following diagrams (***Figure 4-10***, ***Figure 4-11***, ***Figure 4-12***, and ***Figure 4-13***). The POD's output is zero when the frequencies measured at the PCCs of the converters are equal. The POD does not bring additional energy to the synchronous system. Therefore, the final frequency of the centre of inertia remains the same. The ADC's output is zero when the angle difference (given by the measures at the PCCs of the converters) is equal to the initial angle difference (before perturbation). Therefore, in the ADC's original power reference output given in equation **(4.48)**, the angle difference $\theta_j(t) - \theta_k(t)$ is replaced by $\theta_j(t) - \theta_k(t) - \Delta\theta_{jk_0}$. At this stage, no filter is added to the ADC's power output calculation.

To simplify the understanding of the results in ***Figure 4-10***, gain tuning variation of POD and ADC is evaluated separately. The results are shown in ***Figure 4-11*** and ***Figure 4-12***.

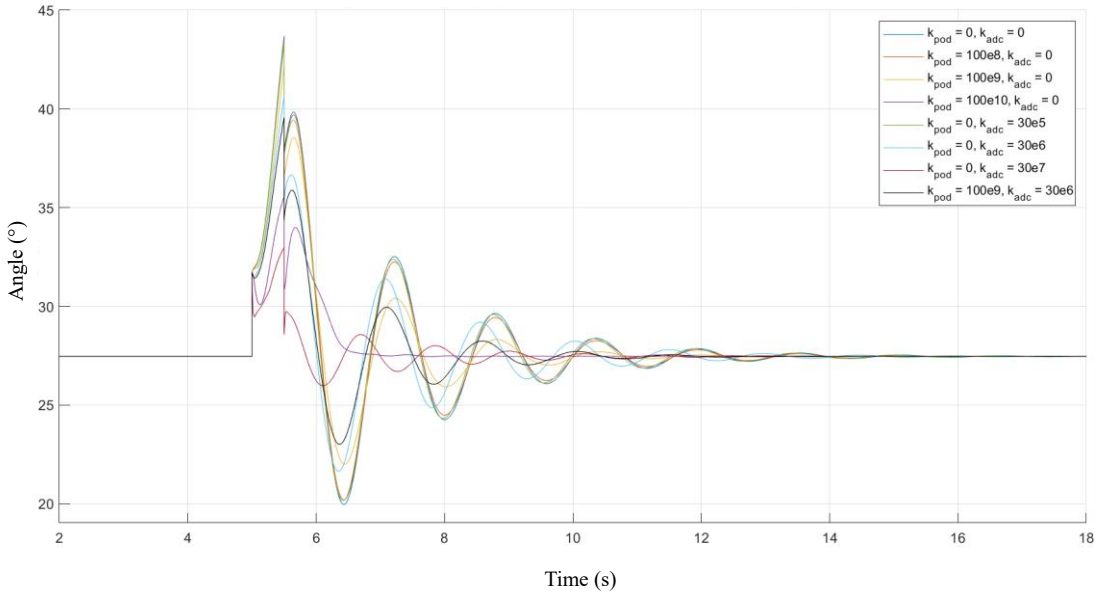

Figure 4-10: Rotor angle variation for different control parameters.

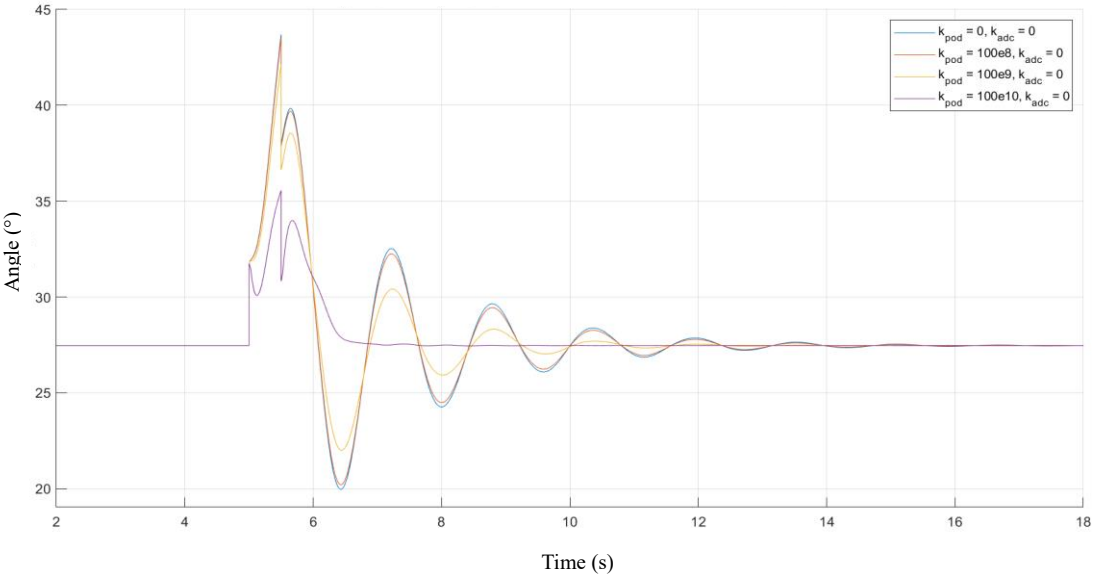

Figure 4-11: Rotor angle variation for different POD control parameters.

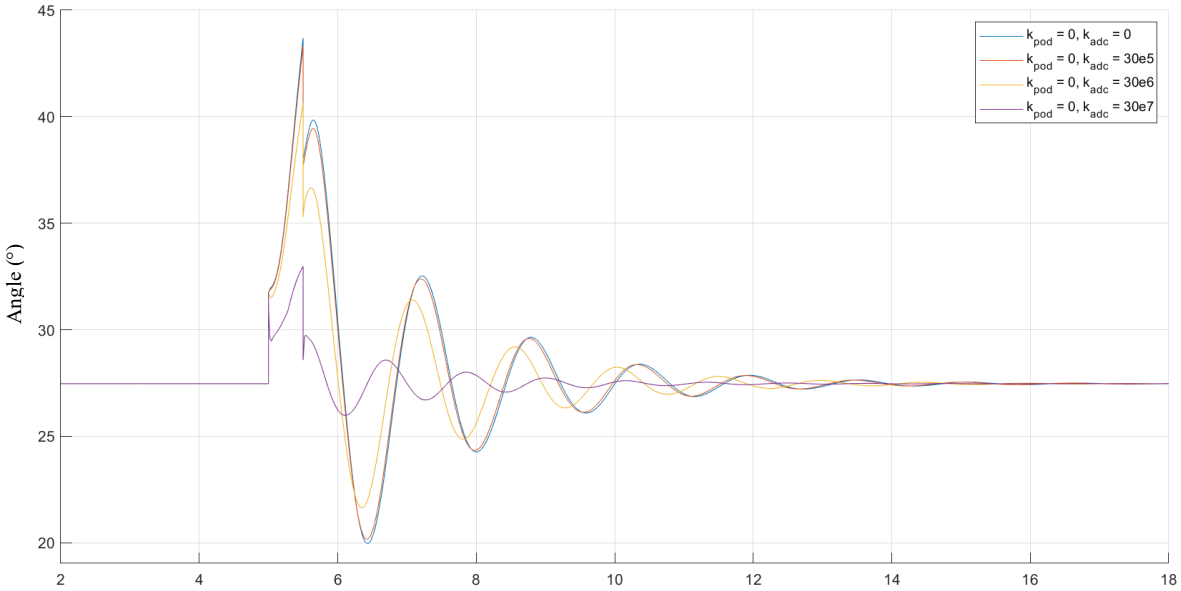

Figure 4-12: Rotor angle variation for different ADC control parameters.

Some interesting results of the previous time-domain analysis are given in the following ***Table 4-5***.

Table 4-5: Post-perturbation performance of the studied AC/DC power system.

POD gain	First swing amplitude (°)	Settling time (5%) (s)	Time to reach steady-state (s)
0	12.4	4.08	10.0
$100e9$ 100 MW/(rad/s)	11.1	2.65	6.8
ADC gain	**First swing amplitude (°)**	**Settling time (5%) (s)**	**Time to reach steady-state (s)**
0	12.4	4.08	10.0
$30e6$ 32.5 MW/°	9.19	3.22	10.0

The same conclusions given by the previous eigenvalue analysis (section Chapter 4.III.3.i) can be recalled: when the POD gain increases, the system is better damped (***Figure 4-11***, ***Table 4-5***). For the highest POD gain (purple curve in ***Figure 4-11***), the system is seemingly overdamped since the oscillations are almost inexistant.

For the ADC, based on the obtained results (***Figure 4-12***) and as shown in the ***Table 4-5***, the first swing amplitude is ameliorated when ADC gain increases.

To conclude this part, the effect of adding a POD is directly implicated with the small-signal stability characteristics (damping and duration to reach the steady-state). On the other hand, the effect of adding an ADC is directly implicated in transient swing value (since no filter is added to the ADC) and steady-state value (if the AC line was not reconnected, a different steady-state angle difference would have been reached) (***Figure 4-12***).

An overdamped system (purple case, ***Figure 4-11***) means high active power exchanged with the power converters (yellow case, ***Figure 4-13***).

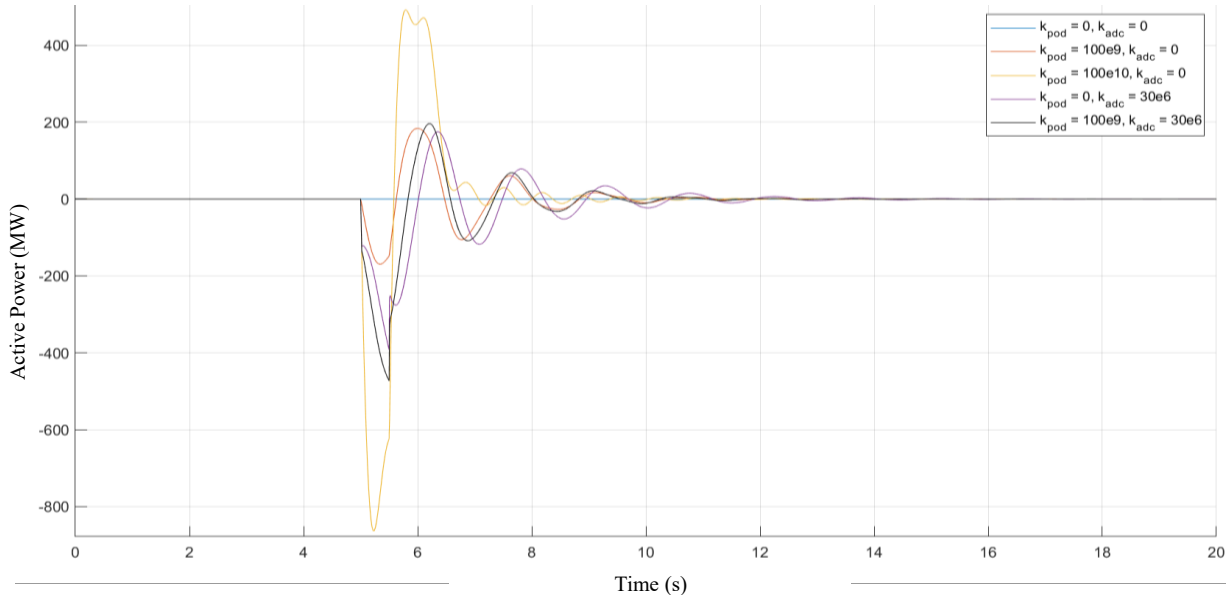

Figure 4-13: Active power output of left converter in the used benchmark.

In the end, the combination of POD ($k_{pod} = 100e9$) and ADC ($k_{adc} = 30e6$) (***Figure 4-10***, ***Figure 4-13***) was selected to enhance rotor angle stability of the studied power system. This tuning results in acceptable damping of power oscillations with minimal required power exchange through power converters. It also enhances the first swing angle difference during the transient.

IV. Frequency, DC voltage and rotor angle stability

1. Context: the minimum requirements (grid code)

i. Frequency stability

Frequency stability is the "the ability of the transmission system to maintain frequency stable in the N-situation and after being subjected to a disturbance" [75]. The 'N-situation' corresponds to the situation in which all its components of a power system are operational. An 'N-1 situation' corresponds to the situation in which one contingency occurred in the power system.

Although frequency stability is expected from the power system in the N-situation, according to the same regulation [75] (Article 35), the TSO is expected to activate a remedial action to restore a normal state of the N-1 situated transmission system. This new normal state is considered the new N-situation of the power system.

Specific frequency-related parameters (insensitivity of frequency response for Frequency Sensitive Mode (30 mHz in FSM), minimal droops for upward and downward regulations (0.1 %), capability of HVDC system to remain connected to AC system for a RoCoFs ($\pm$2.5 Hz/previous second), etc.) are observed during the operation of HVDC links and AC systems. The normal values assigned for these frequency-related parameters are extensively presented in [73], [74].

ii. DC voltage stability

In DC systems, the voltage should be monitored to avoid their stability loss. No specific regulations exist yet on the DC voltage values and variation, but a commonly adopted standard is to avoid DC voltage deviation by more than 5-10% of nominal value. The current regulations available in [77] are general requirements that need to be "specified" by TSOs at each time network codes need to be used for AC/DC interface.

In [94], DC power system stability was explored through multiple case studies at converter's level, and this affects stability of whole DC system – which affects AC & DC stability. A study of DC power system stability was done in [95] for *distribution* systems. If stability is only considered through checking the range of operation of DC components' variables at steady state in the article, it is however important to check the paths the DC voltage and powers follow to move from one operating point to the steady state equilibrium point. An HVDC power system cannot be considered stable if, at some point of the operation, the system's voltage deviates 'significantly' from nominal values before moving to acceptable equilibrium point at steady state.

Besides, stability margins for HVDC system are not the same for a DC power system where converters are saturated compared to a system operating at lower power stress. The problem of HVDC system stability is more eminent when converter ratings (voltage, power, etc) are violated.

To preserve DC voltage stability, some voltage profiles have been proposed as in figure 9 in [11], [96] to show to what extent DC voltage protections should stay untriggered but AC & DC interactions should be considered too to keep discrimination between AC & DC protections and avoid unvoluntary triggering of DC protections. Thus, conclusions for range of operation of DC voltage are not straightforward as coupling with AC side needs more examination and regulatory specifications are still missing.

Sudden loss of power converter is one of the main events that may jeopardize DC grid operation. This can be expressed as instant active power loss of injection or extraction, and EU legislation has already taken into consideration this case [77]. Nonetheless, network code does not express direct guidelines and methodologies for calculation of the maximum allowable active power loss, and it is left for TSOs to define and apply them. While the impact of a converter trip on the AC grid stability can be assimilated to a sudden load increase in simplistic studies, what about the impact on DC grid stability in case of MTDC system? Sudden loss of power converter can be much more impactful on DC side than on AC side, so what are the needed controls to preserve DC stability in such case?

Unfortunately, the simulation of converter trip was not evaluated in this thesis as specific fault modelling approaches need to be developed in MODELICA language and the currently existing libraries do not allow for the simulation of such type of faults.

2. Implemented HVDC controls for frequency and DC voltage stability

In this section, the used benchmark is the one shown previously in ***Figure 3-16***. Active power reference is considered positive when sent from DC to AC system.

Converter 2 is solely responsible of regulating the DC voltage of the HVDC system through droop control. The active power reference output of this control is expressed in equation **(4.50)**:

$$P^*_{V_{DC_{control}}} = k_{V_{DC_{droop}}} \cdot (V_{DC_{meas}} - V_{DC_{base}}) \quad \textbf{(4.50)}$$

where $k_{V_{DC_{droop}}} = 8$ MW/kV is the DC voltage droop controller gain, $V_{DC_{meas}}$ is the measured DC voltage at the DC terminal of converter 2, and $V_{DC_{base}}$ is the nominal voltage value.

Converter 3 is responsible of regulating the frequency in the AC zone 2 (***Figure 3-16***) through local frequency droop control. The active power reference output of this control is expressed in the equation **(4.51)**:

$$P^*_{f_{control}} = -k_{f_{droop}} \cdot (f_{meas} - f_n) \quad \textbf{(4.51)}$$

where $k_{f_{droop}} > 0$ is the frequency droop controller gain, f_{meas} is the measured frequency at the AC terminal of converter 3 at AC zone 2, and f_n is the nominal frequency of AC zone 2.

3. Interactions between frequency and DC voltage stability

The coupling between the DC voltage and AC frequency is reflected in the observed interactions between the controllers of each one of these physical parameters. These interactions are examined in this section.

The case study is based on a perturbation of AC zone 1: an increase of 100 MW at L1. This sends a step of 100 MW at $t = 10$ s in the power reference of converter 1. The converter 2 is equipped with DC voltage droop control (section Chapter 4.IV.2) and the converter 3 is equipped with frequency droop control (section Chapter 4.IV.2). The DC voltage profile of converter station 2 is observed for different values of frequency droop gains (***Figure 4-14***).

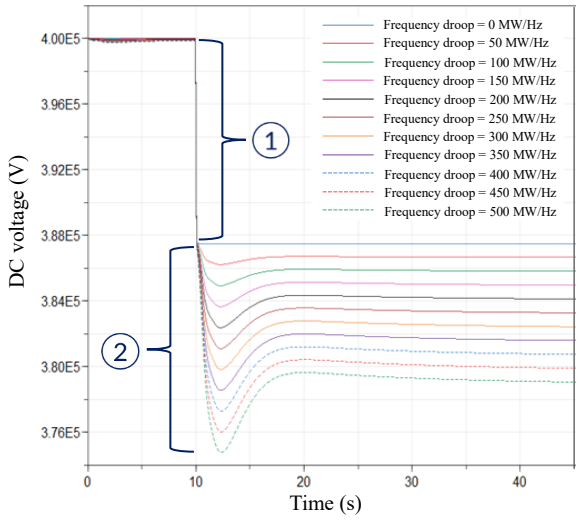

Figure 4-14: DC voltage performance at converter station 2.

As shown through the large vertical brace 1 ***Figure 4-14***, a common DC voltage drop exists due to the presence of DC voltage droop control.

For 100 MW step, final DC voltage value is calculated as the following equation **(4.52)**:

$$V_{DC_{final}} = V_{dc_{initial}} - \frac{P_{step}}{k_{V_{DC_{droop}}}} = 387500\,V = 0.96875\,p.u. \quad \textbf{(4.52)}$$

Then, as the large vertical brace 2 suggests in the same ***Figure 4-14***, a supplementary drop in DC voltage occurs. The amplitude of this DC voltage drop increases with the increase of the frequency droop gain. The growing drop can be observed both during transient and at steady state.

The following interaction model is built to describe the interactions between frequency and DC voltage controls (***Figure 4-15***).

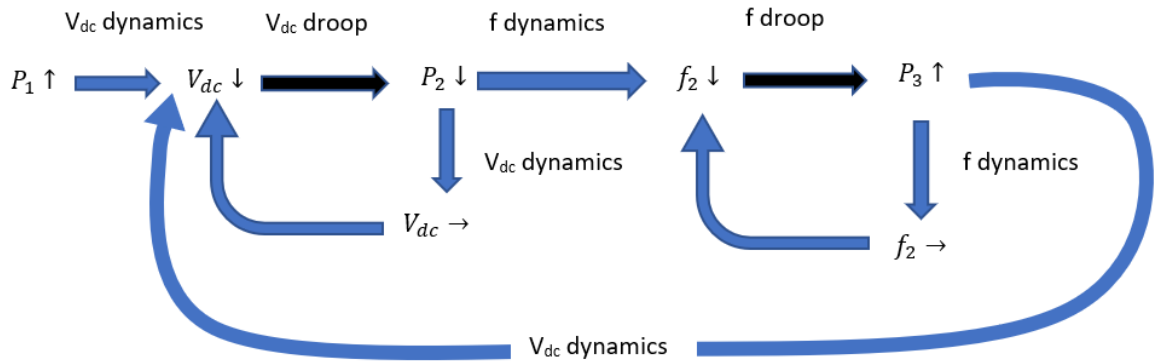

Figure 4-15: Diagram of interaction model between DC voltage and frequency controls.

After the power reference P_1 at converter 1 increases, the DC voltage starts to drop leading to a variation in the power reference P_2 of converter 2 due to DC voltage droop control. Therefore, the station 2 extracts from AC zone 2 the power needed to be transferred, through the MTDC system, to AC zone 1. This decreases the energy available in AC zone 2 which leads to a drop in its frequency. The variation of frequency is detected at converter station 3 where the frequency droop controller reacts and asks converter 3 to inject power in AC zone 2. In the end, an equilibrium is found between power injection and extraction from AC zone 2, which leads to an equilibrium of its frequency and of the DC voltage in the MTDC system.

4. Interactions between frequency and rotor angle stability

The rotor angle stability of the AC/DC system may be influenced by the control of frequency.

A simple case study was made to analyse the situation of small-signal stability when a disturbance occurs. The test system is the same as in ***Figure 3-16***. The perturbation is the same as the one in previous section Chapter 4.IV.3 but with an amplitude of 300 MW to emphasize the phenomena. Two frequency droop gains are evaluated: 0 MW/Hz and 300 MW/Hz. The results are compared in the following ***Figure 4-16***.

In both cases, interarea power oscillations appear between the generators belonging to AC zone 2. Nonetheless, in the case where frequency droop controller is implemented with a non-zero gain, the interarea modes are better damped as the ***Figure 4-16*** suggests. Two explanations exist for this phenomenon.

First, the exchange of power performed through converter 3 (in an opposite direction to the power reference sent by DC voltage droop at converter 2) reduces the stress put on the AC line connecting G_3 and G_4. Interarea modes were, in the case without frequency droop controller, excited by the sole extraction of power at converter 2 near to generator G_3 (check section Chapter 4.II.1). When frequency droop is implemented with a gain of 300 MW/Hz, the power injected by converter 3 near to generator G_4 limits the disturbance of frequency in AC zone 2 and the power balance (between the subzones (3 and 4) of AC zone 2) is restored quicker.

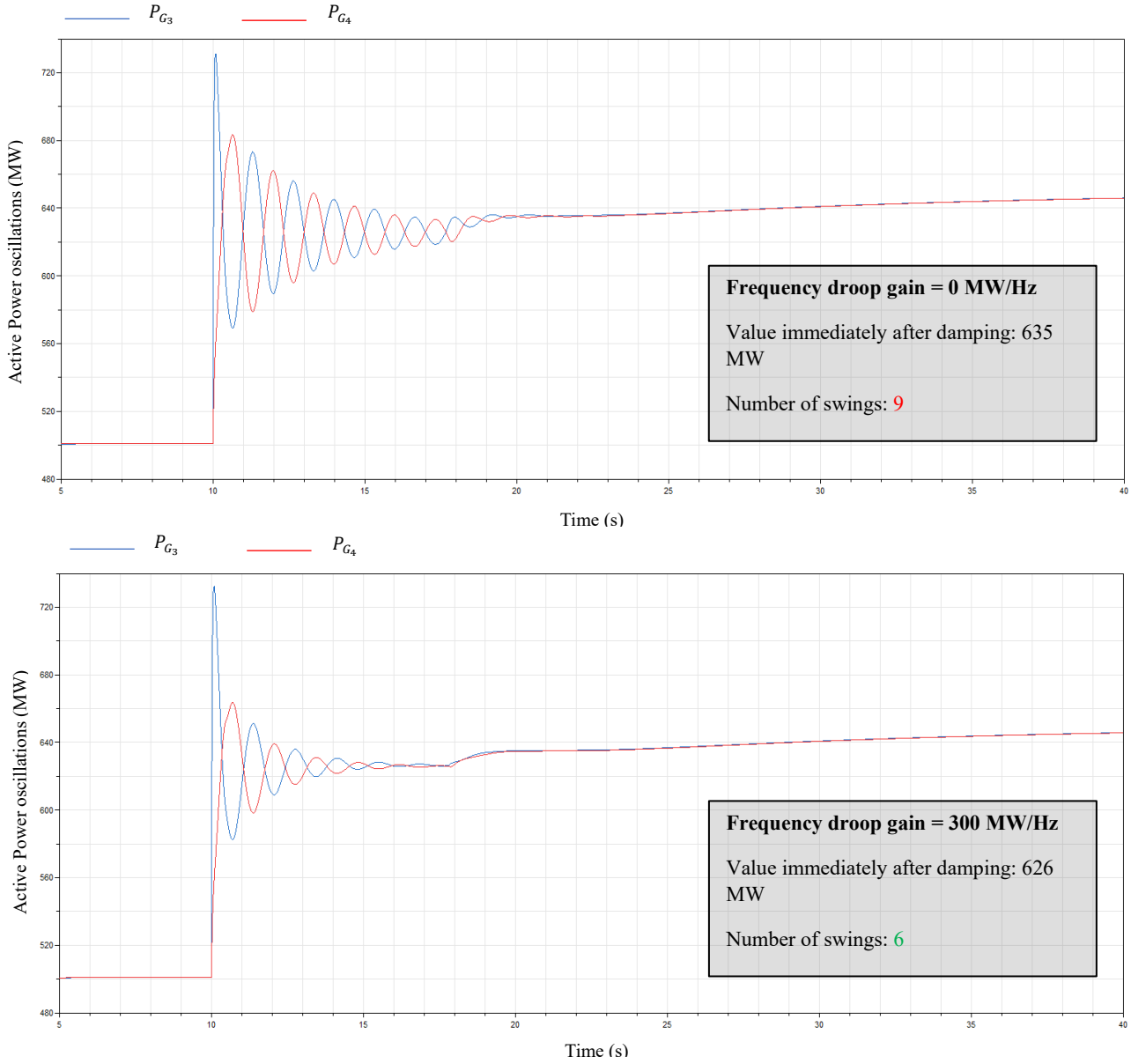

Figure 4-16: Profiles of active power oscillations for two frequency droop gains.

Second, the absence of a filter at the frequency droop controller also contributes to the damping of power oscillations. In fact, the measured frequency f_{meas}, which contains oscillations, is compared to a fixed

nominal frequency f_n and the output of the frequency droop controller aims to minimize the oscillating difference between f_{meas} and f_n. This means a contribution to minimizing the oscillating modes in f_{meas} which are principally composed of interarea modes.

Moreover, the power flowing through the AC line connecting G_3 and G_4 increases when frequency support is implemented since the converter 3 injects power to compensate for the power extracted by converter 2. This puts the rotor angle stability of AC zone 2 at risk since the angle difference between the buses connecting G_3 and G_4 increases.

To conclude this section Chapter 4.IV, the supplementary power converter controllers and their tunings play a major role in terms of power system stability. The potential interactions between different controllers were shown through two case studies that show the impact of the control actions on the frequency, DC voltage and rotor angle stabilities.

V. Decoupling or minimizing interactions between different controls

1. Potential interactions between different controls

The following diagram (***Figure 4-17***) clarifies the reasons that could lead to undesired interaction between a type of control and a given stability aspect. The full lines represent the desired interaction between a control and a corresponding stability aspect while, dashed lines represent the undesired interactions and potential reasons behind them.

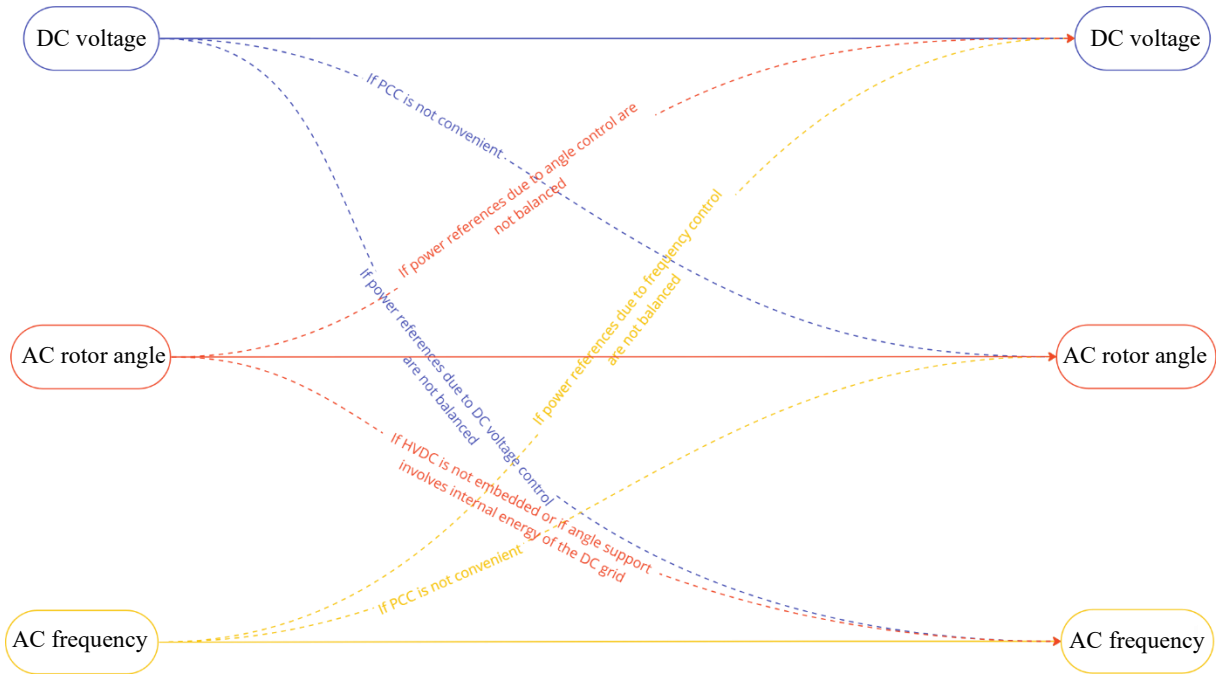

Figure 4-17: Diagram of potential effects of a given controller on a given stability aspect.

Some interactions are not represented in this diagram: the ones for the same aspect of stability when two dedicated controllers are used for different purposes. This is the case of POD and ADC interactions for the same rotor angle stability aspect.

The following sections will focus on minimizing the mentioned undesired interactions by control of active power and adequate tuning of controllers.

2. Indicator-based analysis for fine-tuning of rotor angle stability controllers

i. Context

In the unsaturated domain of operation of power converters, the linearization of AC/DC power system around an equilibrium point to perform eigenvalue analysis is valid. This stability assessment methodology is adopted in this section to evaluate the small-signal stability in terms of damping of interarea modes impacting rotor angle stability.

From rotor angles' transient stability point of view (angle difference during transient and in steady-state), a time-domain analysis is performed as well.

In this section, both eigenvalue and time-domain analyses are performed to simultaneously evaluate the impact of tuning the ADC's filter time constant both on rotor angle's transient and small-signal stability. The ADC is conventionally designed to improve the steady state of the rotor angles. However, in this section, the aim is to study the possibility of using the ADC for the improvement of transient stability of rotor angles as well. The aim is also to verify that the used ADC's impact on the original small-signal stability of the system is limited. The made assessment is based on the variation of the time filter of the ADC.

The used benchmark is in the following ***Figure 4-18***.

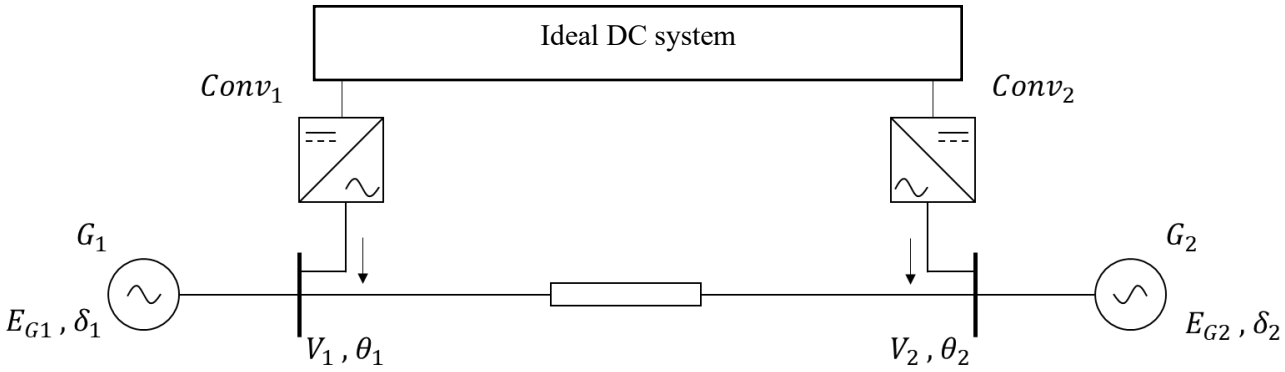

Figure 4-18: Used simple benchmark composed of two generators and two power converters connected to an ideal DC system.

In this benchmark, the DC dynamics are not considered, and DC system behaves like an ideal voltage source, and the converters, with initial zero power output, exchange active power with the AC system as required by power references.

The following simplifying hypotheses are made:

- $M_1 = M = M_2$ (moments of inertia of the machines),
- $D_1 = 0 = D_2$ (damping constants of the machines),
- $\boldsymbol{E_{G1} = V_1} = V = \boldsymbol{V_2 = E_{G2}}$ (machine's terminal and the connected bus voltage amplitudes are equal),

- $\boldsymbol{\theta_1 = \delta_1}$; $\boldsymbol{\theta_2 = \delta_2}$ (machine's rotor angle is equal to the connected bus phase),
- Generator's speed is measurable,
- Connecting branch is inductive.

The used stability indicators (KPIs) for this study, implemented with the progression of the thesis, are:

- ξ (damping in %) of the complex eigenvalues corresponding to the studied interarea mode $\lambda_{interarea} = a + j \cdot b \rightarrow \xi = -\frac{a_i}{\sqrt{a_i^2 + b_i^2}}$,
- $Integral\ Square\ Generator\ Angle$ for transient stability: $ISGA = \int_0^T f(t)dt$ where $f(t) = \sum_{i=1}^{N_g} \frac{M_i}{M_{tot}} \left(\delta_i(t) - \delta_{coi}(t)\right)^2$ with:
  - $\delta_{coi} = \sum_{i=1}^{N_g} \frac{M_i \delta_i(t)}{M_{tot}}$ the angle corresponding to a virtual center of inertia of the considered AC system with δ_i the rotor angle of the generator i,
  - $M_{tot} = \sum_{i=1}^{N_g} M_i$ the moment of inertia of the whole AC system with M_i the moment of inertia of the generator i of the N_g operating generators,
  - T the duration of simulation during which the $ISGA$ indicator is evaluated.

  The $ISGA$ indicator should be evaluated through its variation (there is no "good" $ISGA$ value).

The converters' active power reference is sent by an ADC with a low-pass filter. The controller sends the following active power reference **(4.53)** to the converters kj:

$$P^*_{ADC\,kj}(t) = K_{ADC,kj} \cdot \left(\theta_j(t) - \theta_k(t)\right) \cdot \frac{1}{1 + T_{filter} \cdot s}$$
$$P^*_{ADC\,jk}(t) = -P^*_{ADC\,kj}(t) \qquad \textbf{(4.53)}$$

The low-pass' filter parameter T_{filter} is varied during the study to perform stability assessment.

ii. Results

The main usage of ADC control is to emulate the AC line through DC links. In this section, the following study is performed on the benchmark in ***Figure 4-18***:

- Parameter to study: T_{filter}
- Perturbation: line disconnection (line impedance increase)

Two assessment approaches are used (***Figure 4-19***): one is for transient and the other for small-signal stability of rotor angles.

A system may be small-signal stable but not transient stable. But a small-signal unstable system will be necessarily transient unstable since the increasing amplitude of rotor angle oscillations will lead to transient instability.

The plots resulting from stability assessments (as indicated in the ***Figure 4-19***) are superposed in the ***Figure 4-20***.

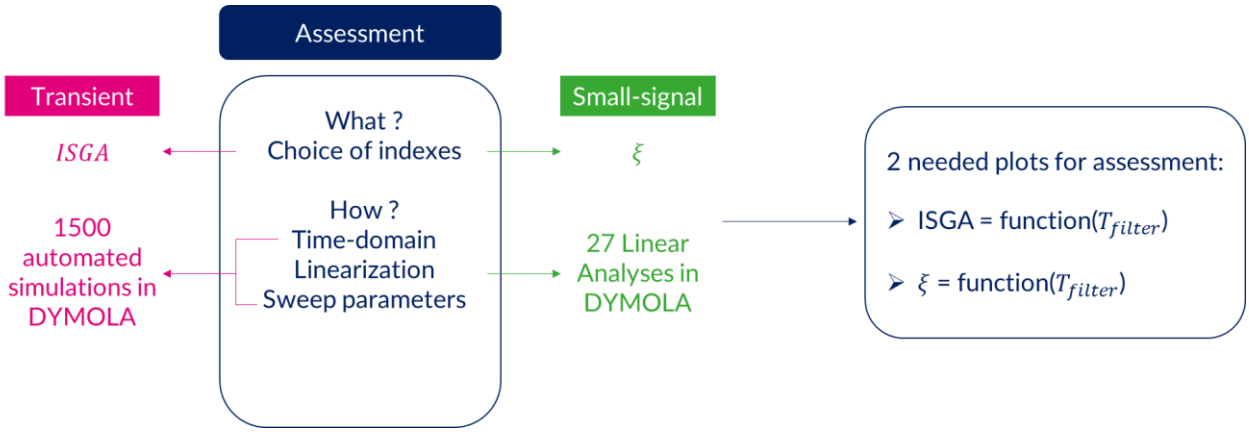

Figure 4-19: Used assessment approaches.

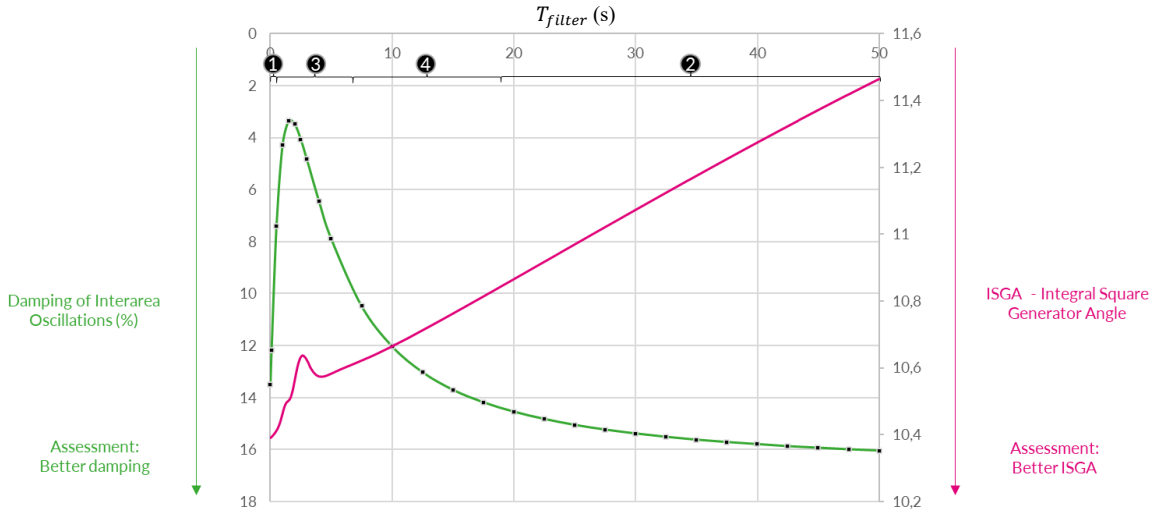

Figure 4-20: Evolution of small-signal and transient stability indicators for various filtering time values.

The curves varying with the filtering time constant of the ADC can be separated into four zones (these zones are directly indicated on the ***Figure 4-20***). The following ***Table 4-6*** qualitatively clarifies the reasons behind this zone separation per results in terms of filtering performance and damping and ISGA performances.

Table 4-6: Zone repartition according to the quality of the power system's performance.

Zone	Filtering	Damping	ISGA
①			
②			
③			
④			

In zone 1, the *ISGA* and damping indicators have good values, but the ADC's low pass filter is not as efficient as expected since its time constant is not high enough.

In zone 2, the ADC filters the unnecessary power oscillations leading to interactions with any other specific controller (POD), but the ADC's delay is relatively high. This prevents the HVDC system from quickly responding to transient rotor angle issues.

In zone 3, the small-signal stability indicator shows that the interarea modes are not damped enough.

Finally, zone 4 appears to be a zone of compromise between transient and small-signal performance of rotor angles in presence of the ADC controller.

The implemented T_{filter} is generally high ($T_{filter} = 50$ s in [92]), which affirms the usage of ADC for steady-state improvement of rotor angles. However, the study shows that it is possible to use the ADC to also improve the transient stability of rotor angles (for small values of T_{filter}). It is also possible to find a range (zone 4) for lower values of T_{filter} (7 to 19 s) that guarantees a damping value close to the one when T_{filter} is high (50 s). This leads to a better transient performance, without jeopardizing the small-signal stability of the AC/DC system, which also leads to the same steady state performance.

More generally, it was shown through this study that, using the mentioned stability assessment methods, the tuning of the parameters of the controllers of the converters can be optimized to enhance the stability of the AC/DC hybrid system. In this case, the enhanced parameter was the ADC's filter time constant for the individual rotor angle stability enhancement.

In the next section, the possibility of designing controllers will be shown in a way to decouple effects for multiple stability aspects simultaneously.

3. Decoupling frequency and rotor angle stability controls on a simple use case

i. Context

The frequency and rotor angle, as physical variables, are bounded through the swing equations **(3.9)** and **(3.10)**. A controller dedicated for frequency may impact rotor angle and therefore have an undesirable influence on rotor angle stability, and vice-versa.

For a simple case, decoupling the effect of frequency and rotor angle's dedicated power references sent to power converters was tested. For this, the same benchmark as in ***Figure 4-18*** is used. Decoupling by the design of the controls was tested.

ii. Results

The swing equations of each machine (benchmark in ***Figure 4-18***) are:

For G_1:
$$M_1.\frac{d^2\delta_1}{dt^2} = P_{m1} - P_{e12} + P_{conv1} - \frac{D_1 d\delta_1}{dt} \quad \textbf{(4.54)}$$

For G_2:
$$M_2.\frac{d^2\delta_2}{dt^2} = P_{m2} - P_{e21} + P_{conv2} - \frac{D_2 d\delta_2}{dt} \quad \textbf{(4.55)}$$

with the following hypotheses (same as in section Chapter 4.V.2.i):

- $M_1 = M = M_2$,
- $D_1 = 0 = D_2$,
- $\boldsymbol{E_{G1} = V_1 = V = V_2 = E_{G2}}$,
- $\boldsymbol{\theta_1 = \delta_1}$; $\boldsymbol{\theta_2 = \delta_2}$,
- Generator's speed is measured,
- Connecting branch is inductive.

By manipulating the above swing equations **(4.54)** and **(4.55)**, the following can be obtained:

$$M.(\dot{\omega}_1 + \dot{\omega}_2) = P_{m1} + P_{m2} + P_{conv1} + P_{conv2} \quad \textbf{(4.56)}$$

$$M.(\dot{\omega}_1 - \dot{\omega}_2) = P_{m1} - P_{m2} + P_{conv1} - P_{conv2} - 2.\frac{V^2}{X}\sin(\delta_1 - \delta_2) \quad \textbf{(4.57)}$$

The first equation **(4.56)** gives the frequency (of centre of inertia) dynamics while the second equation **(4.57)** gives the dynamics of rotor angles.

It is possible to decouple frequency and rotor angle dynamics, through the control of P_{conv1} and P_{conv2}, if the following control inputs are chosen:

$\begin{pmatrix} u_1 \\ u_2 \end{pmatrix} = \begin{pmatrix} 1 & 1 \\ 1 & -1 \end{pmatrix} \begin{pmatrix} P_{conv_1} \\ P_{conv_2} \end{pmatrix}$ which gives the individual converter power reference as shown in **(4.58)**.

$$\begin{pmatrix} P_{conv_1} \\ P_{conv_2} \end{pmatrix} = \begin{pmatrix} \frac{1}{2} & \frac{1}{2} \\ \frac{1}{2} & -\frac{1}{2} \end{pmatrix} \begin{pmatrix} u_1 \\ u_2 \end{pmatrix} \quad \textbf{(4.58)}$$

This decoupling between frequency and rotor angle stability, by control design, was validated through the time-domain simulations both on equation-based model (DAEs) (similar to Matlab/Simulink modelling) and physical component-based model (in Dymola).

The obtained results are illustrated in the ***Figure 4-21***.

The decoupling of the interactions between frequency and rotor angle difference was made possible through the used control structure. The tests were however validated on a simple benchmark where only two generators and two power converters were involved. It is not possible to conclude that, for an AC system where multiple generators exist, this kind of control design is replicable. It is also less applicable when the mentioned simplifying assumptions are not adopted.

Therefore, to minimize control interactions, other strategies will be adopted and explained in the remainder of this thesis. A framework for stability assessment and enhancement was developed during the thesis and the results were validated through simulation.

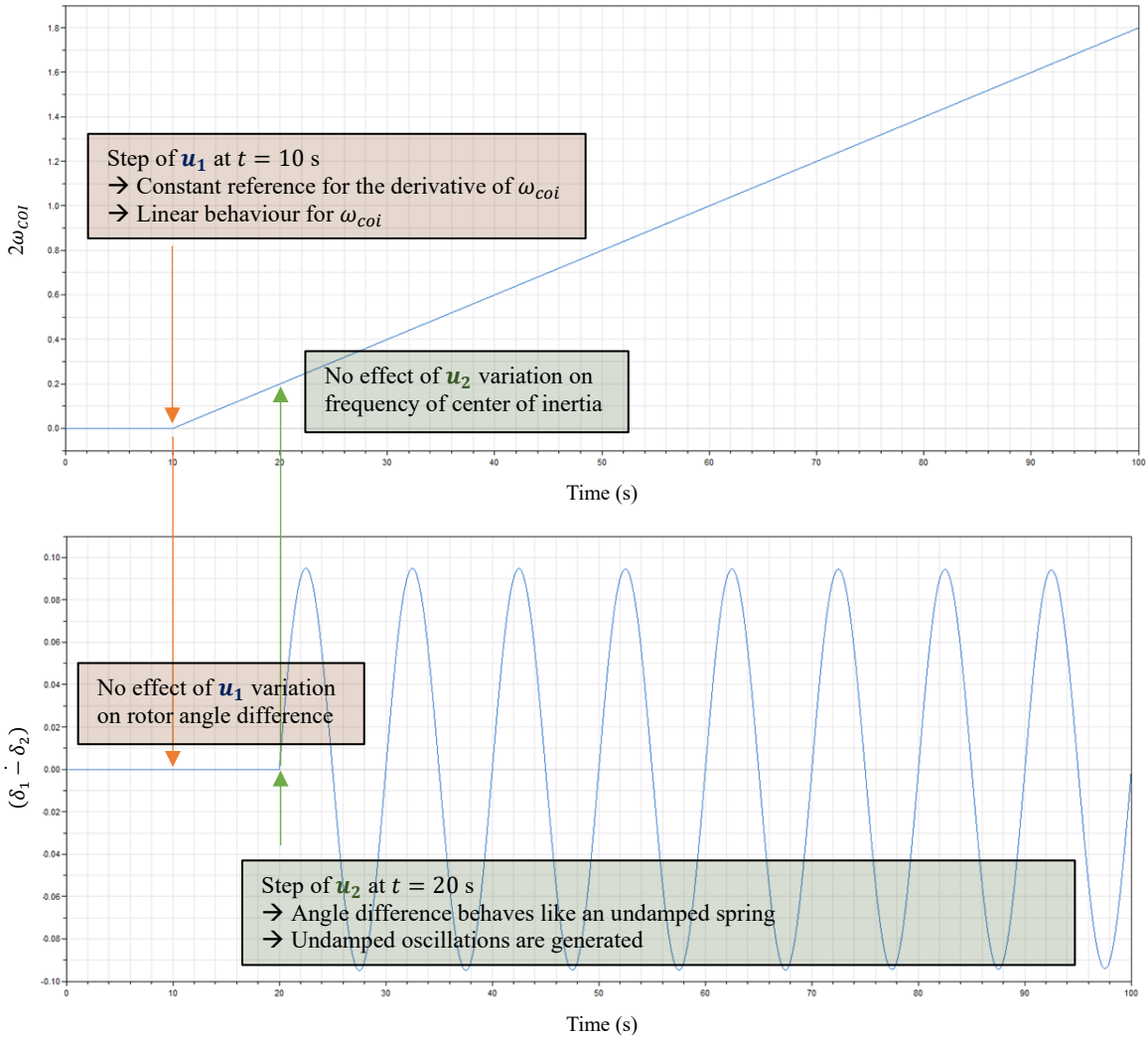

Figure 4-21: Decoupling of effects on frequency of centre of inertia and rotor angle difference's derivative.

VI. Need for a framework for AC/DC stability assessment

As previously seen, various supplementary control actions can be implemented in AC/DC systems to enhance their stability. The challenge is to enhance global power system's stability by simultaneously acting on individual stability aspects (frequency, rotor angle, DC voltage). Through active power coordination, one can avoid the antagonist interactions shown previously between the added control actions.

Hence, a framework for stability enhancement strategy is needed to define what services shall be added to a given power system and what are the expected outcomes of the strategy.

The frameworks are distinguished by two main parameters: the assumed level of communication within the hybrid AC/DC system and the degree of active power coordination.

The developed frameworks are classified as per these two mentioned parameters in the ***Figure 4-22***.

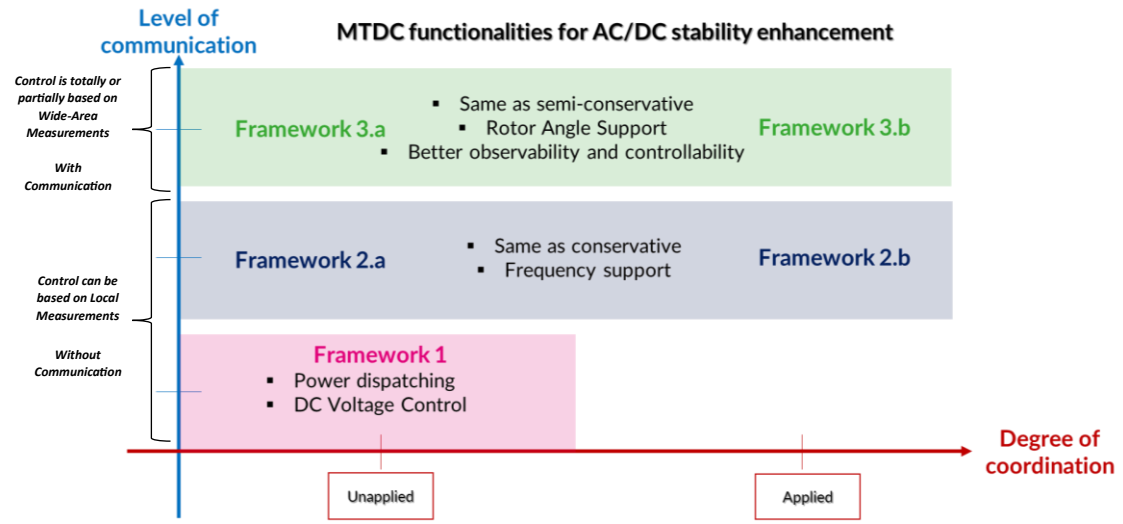

Figure 4-22: Frameworks of stability enhancement through various MTDC functionalities.

Framework 1 is conservative since the HVDC links offer only DC voltage support and allow for power dispatching. For this, no communication throughout the AC/DC system is necessary.

In Framework 2, frequency support is included. This support can be realized based on local measurements without communication. Framework 2 is semi-conservative since it aims to enhance AC power system's stability and not only securely operate power transfer as in Framework 1. The active power used for frequency support may be or not coordinated with DC voltage control's active power outputs depending on the choice of framework 2.b or 2.a respectively. Therefore, Framework 2 offers two possibilities of power control: without or with coordination as was studied in [8], [97], [98].

Framework 3 includes the rotor angle support feature. It relies on WAMS that require local measurements to be communicated to rotor angle controller. Since WAMS exist, higher observability and controllability of the stability aspects can be achieved ([99], [100]). Coordinated active power control strategy can be applied in Framework 3.

The stability enhancement strategies used in Frameworks 1, 2.a and 2.b were evaluated through literature or throughout case studies. However, the combination of all HVDC ancillary services in one power system study has not yet been covered. In the thesis, two control strategies to improve power system's stability while combining multiple control actions simultaneously were proposed. These strategies correspond to the suggestion in Framework 3.

A first stability enhancement strategy (in a use-case comparing several frameworks) will be proposed in the following Chapter 5.

Chapter 5 : First globalized approach based on active power reallocation

I. Introduction

1. Context

In this part, adding HVDC ancillary services will be made increasingly to enhance the stability of the AC/DC power system. In this part, the used power system benchmark is a version of the one shown in ***Figure 3-17*** but with the following main differences:

- Distributed controllers are progressively implemented during case studies instead of a central controller,
- The initial power flow (shown in ***Figure 5-1***),
- The perturbation: loss of a part of generator $G1$'s production (350 MW of 700 MW) at $t = 5$ s.

The used power benchmark is illustrated in the ***Figure 5-1***.

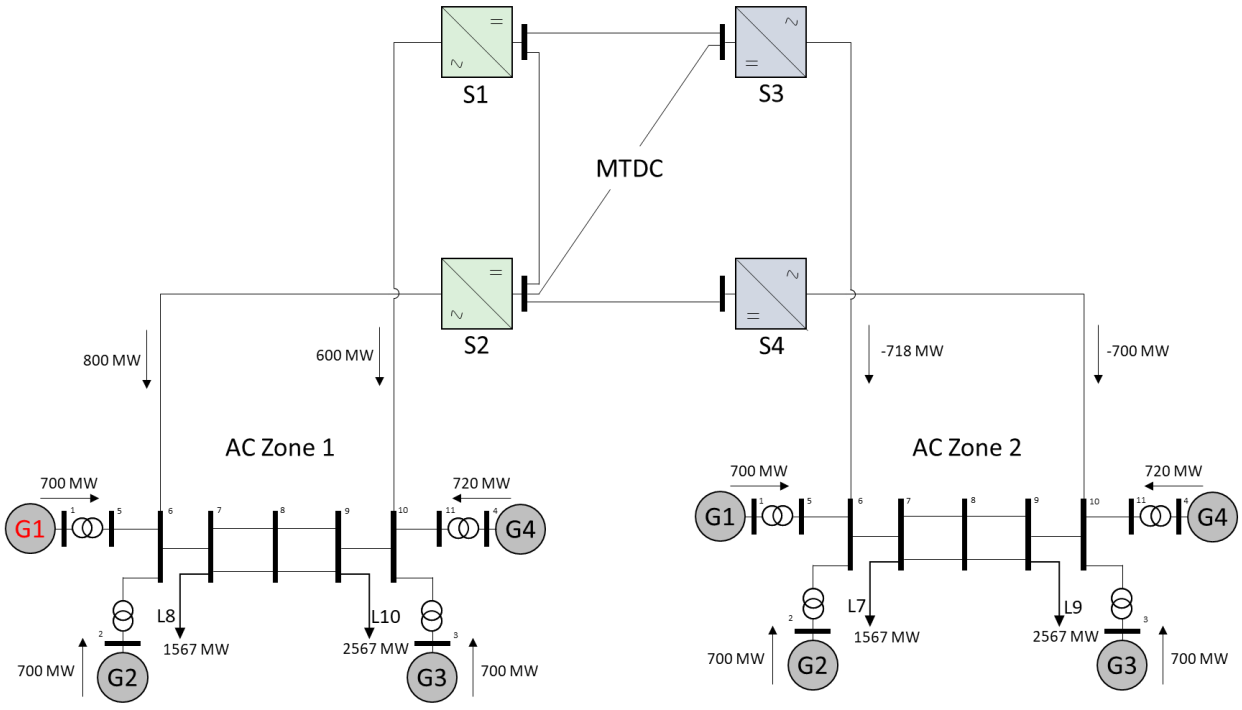

Figure 5-1: Power system benchmark No. 5.

Five case studies are made on this power system:

- **Case 0**: No HVDC supplementary service implemented **(Framework 1)**
- **Case 1**: Frequency support based on local measurements is added **(Framework 2.a)**
- **Case 2**: Power oscillation damping is added, based on WAMS **(Framework 3.a)**
- **Case 3**: Frequency support (FFR through deployment of FCR) and power oscillation damping, without active power coordination **(Framework 3.a)**
- **Case 4**: Same as Case 3 but with active power coordination **(Framework 3.b)**

2. Organization of the chapter

A comparative study is made between these frameworks going from framework 1 to 3.b. Finally, in the last case study, a first global stability enhancement approach based on active power reallocation strategy is proposed.

II. Comparative case studies

The results are given in the following subsections.

1. Case 0: No HVDC ancillary service implemented (Framework 1)

In this case, the HVDC links are used only for power transfer while regulating the DC voltage.

In AC zone 1 affected by the loss of power production at Generator $G1$, interarea power oscillations are observed between the cluster of generators $\{G1, G2\}$ (Area 1) and the cluster of generators $\{G3, G4\}$ (Area 2) (***Figure 5-2***).

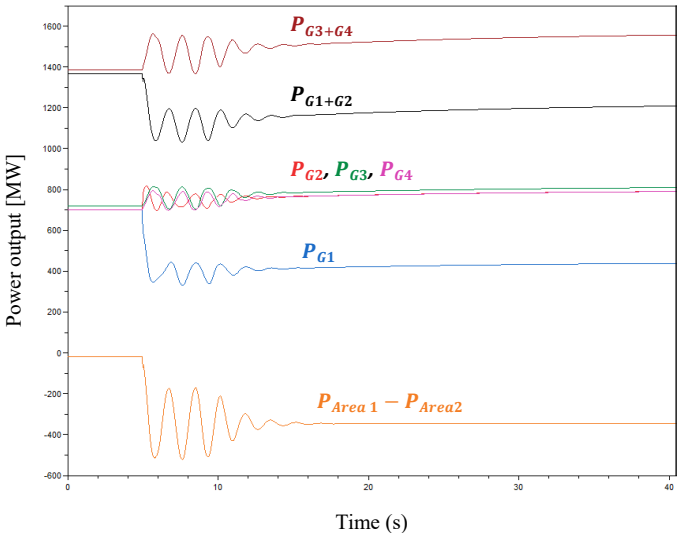

Figure 5-2: Active power outputs measured at AC zone 1.

At first seconds after perturbation, undamped oscillations appear. First swing amplitude of the physical quantity $P_{Area1} - P_{Area2} = P_{G1+G2} - P_{G3+G4}$ is ~520 MW. Then, around $t = 9.2$ s, the oscillations start to get damped until they totally disappear. In this case where no HVDC ancillary service is implemented to help in damping the power oscillations, the controller responsible of damping them is the PSS.

To check the performance of the PSSs during this perturbation, the input, and the output of the PSS of generator $G2$ are plotted in ***Figure 5-3***.

After the loss of 350 MW at $G1$, the PSSs implemented in the power system AC zone 1 are unable to directly deal with the huge oscillations appearing in ***Figure 5-2***. This is due to the large amplitude of frequency deviation at the input of the PSSs leading to the saturation of their output, resulting in undamped power oscillations at the first moments of the perturbation. A few seconds later, when the other generators' active power production is sufficiently increased by the mechanism regulating turbine

governors' output, the PSSs' input returns to values that desaturate their output. Power oscillation damping can be operated anew through the PSSs in question (around $t = 9.2$ s).

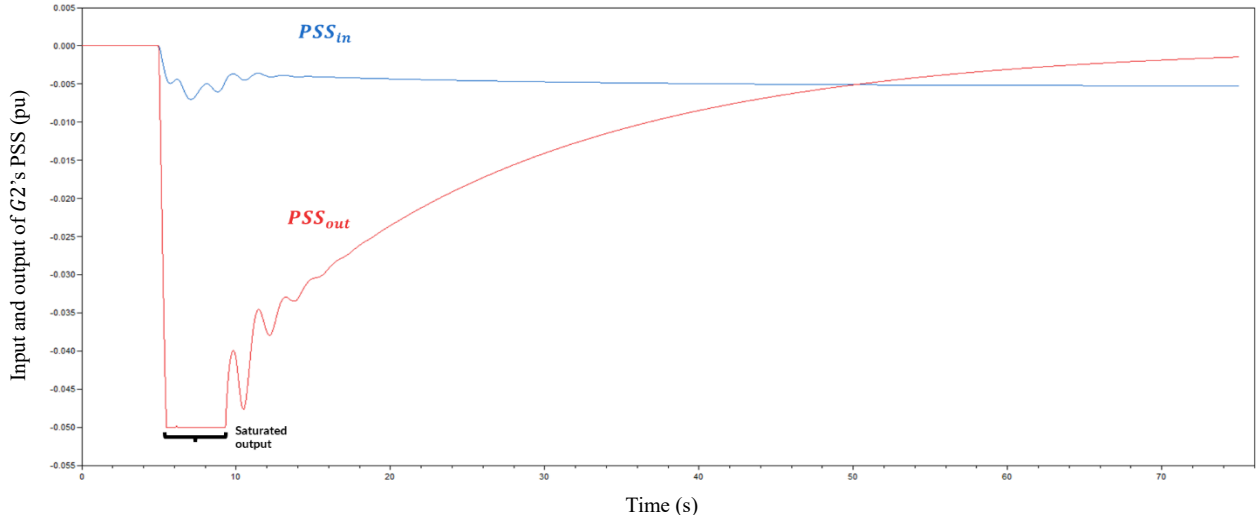

Figure 5-3: Power system stabilizer's input and output, as observed in generator $G2$.

To observe the frequency performance of the power system AC zone 1, the frequency deviation of the centre of inertia of each area of this AC synchronous zone 1 is plotted. The frequency behaviour of the two identified areas is plotted in ***Figure 5-4***.

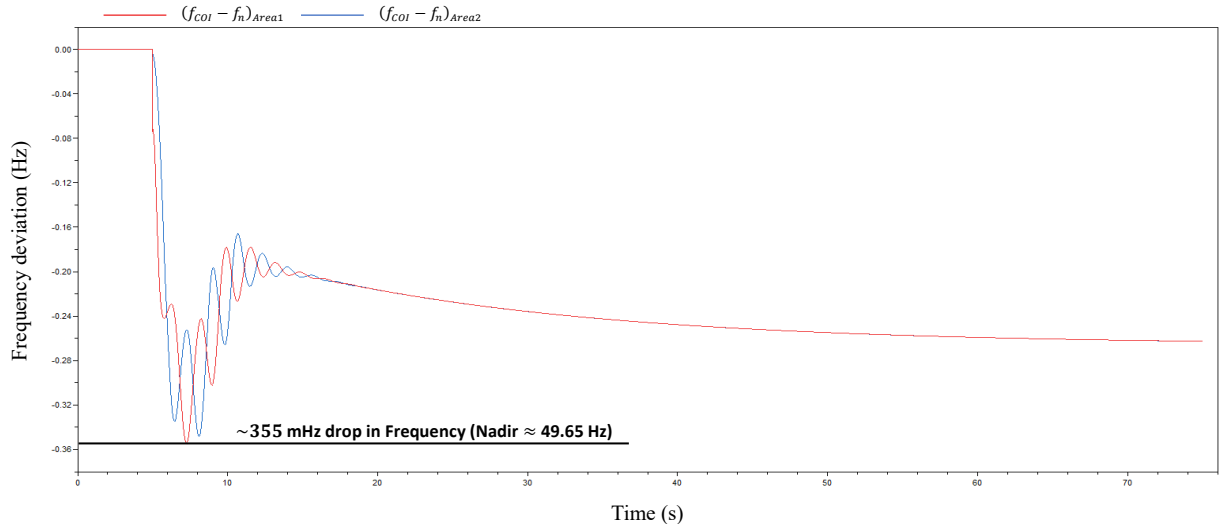

Figure 5-4: Frequency deviation from nominal value of the centre of inertia of areas 1 and 2 (measured in AC zone 1).

For this reference case, frequency Nadir reaches almost 49.65 Hz and frequency oscillations occur. To further analyse these oscillations, modal analysis was performed (***Figure 5-5***).

The analysis first identifies the mode whose frequency corresponds to the range of an interarea mode as well as the components oscillating against each other for this mode. The mode shapes corresponding to this mode are then plotted. The components of Area 1 and the components of Area 2 are respectively aggregated under golden and yellow arrows in the mode shapes. The result of the aggregation clearly illustrates opposite oscillating behaviours between Area 1 and Area 2 for the identified mode. This validates that the identified mode, with the convenient frequency, is effectively an interarea mode.

In this case, the identified mode that has a frequency of 0.62 Hz, shows clear opposite phase arrows for the mentioned areas. Therefore, this corresponds to the interarea mode visible in the frequency oscillations in ***Figure 5-4***. Moreover, the calculated damping of this mode is of 16.29 %.

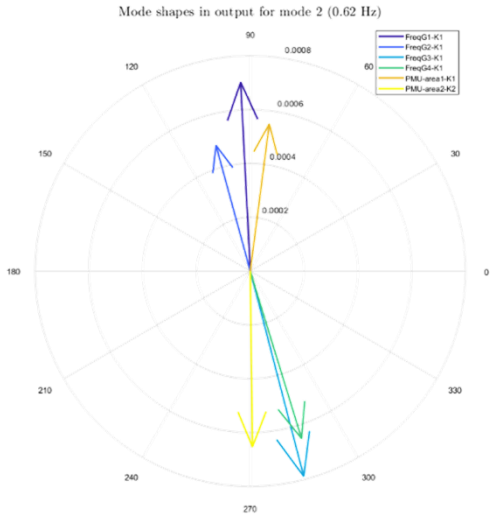

Figure 5-5: Mode shapes in output for interarea oscillation mode in AC zone 1.

The following points conclude this case where HVDC is only used for active power transfer without additional services:

- Frequency deviation is higher than 200 mHz in AC zone 1. Primary AC frequency response is activated to stop the frequency drop.
- The sole implementation of PSS is insufficient to damp interarea modes due to its saturation (in addition, a PSS is adapted for local modes damping rather than interarea mode damping).
- PSS' saturation disappears when Primary frequency response is sufficient

Therefore, as a first step to help desaturate the PSS and limit the frequency drop, frequency controllers based on local frequency measurements are added.

2. Case 1: Frequency support based on local measurements (Framework 2.a)

The implemented frequency support aims to share frequency regulation effort, after the active power loss at $G1$, between AC zone 1 and AC zone 2.

For each AC zone, two frequency droop controllers, each corresponding to a converter station connected to an area in the AC zone, are implemented based on equation **(4.51)**. Each controllers' input is the frequency measured at the PCC of the corresponding converter.

After implementing the controllers, the frequency performance of the centre of inertia of each area in AC zone 1 was plotted (***Figure 5-6***).

In this case, the frequency Nadir is higher than reference case by 180 mHz which preserves primary AC response from being activated.

The mode shapes corresponding to the identified interarea mode are illustrated in ***Figure 5-7***. The frequency of the oscillating interarea mode is 0.58 Hz in this case.

The curves in ***Figure 5-6*** and the modal analysis (amplitude of arrows) in ***Figure 5-7*** prove that the power oscillations are better damped (damping is 30.02 %) but still exist during the transient.

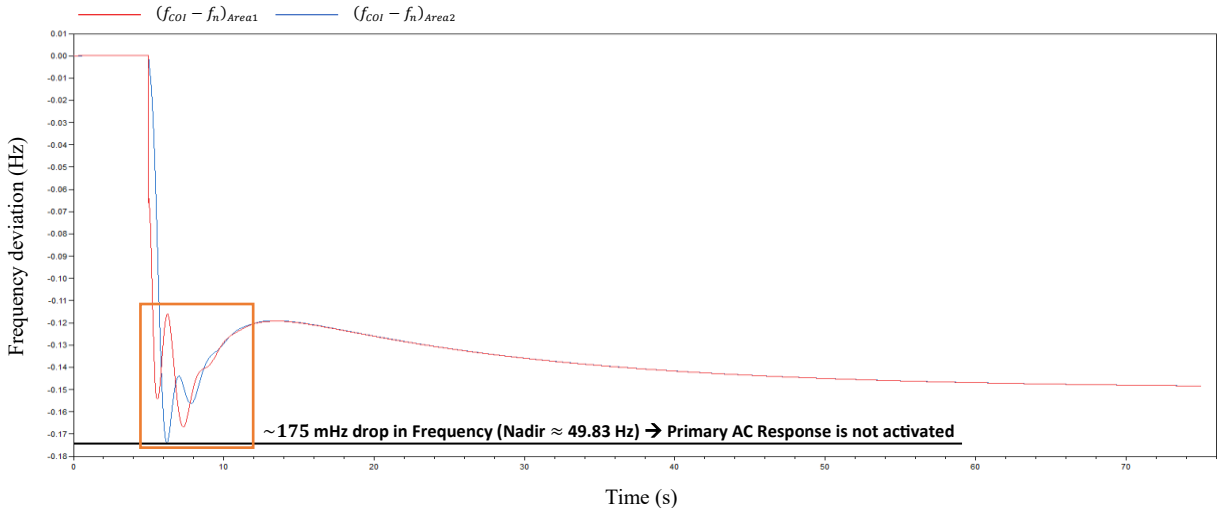

Figure 5-6: Frequency deviation from nominal value of the centre of inertia of areas 1 and 2 (measured in AC zone 1).

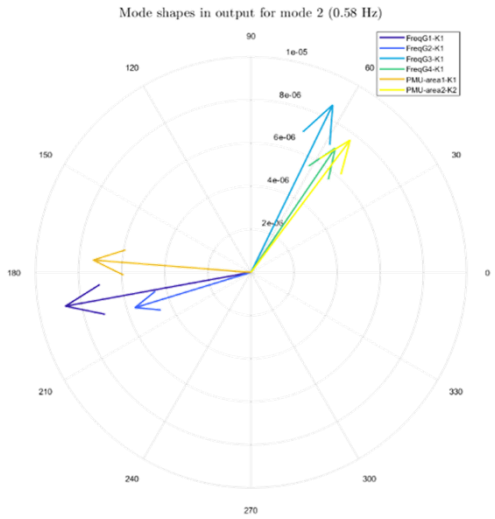

Figure 5-7: Mode shapes in output for interarea oscillation mode in AC zone 1.

Converters outputs or, in other words, the shared effort by which the converters contribute to cope with the generation loss, are plotted in the ***Figure 5-8***. The station $S2$ connected to the Area 1 where the power loss happens at $t = 5$ s shows a saturated active power output.

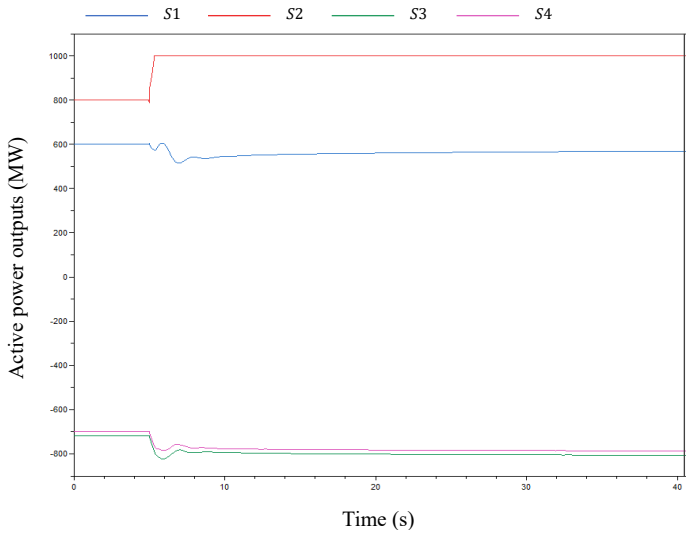

Figure 5-8: Active power outputs of the converter stations.

Local frequency droop controller implemented in $S2$ saturates its output (1 GW reached) but $S1$, also connected to Area 1 where active power injection is needed due to generation loss, still has 430 MW of available headroom which are not used.

Power sharing between AC zones 1 and 2 is realized through DC voltage droop control without coordination or communication between converters. The mechanism of power sharing used in this power system benchmark is explained in the following points:

1. Frequency droop controllers act on all converters. After the perturbation, $S1$ and $S2$ inject more power in AC zone 1. This leads to a voltage drop at the DC terminals of the power converters $S3$ and $S4$. Thus, they extract more power from AC zone 2 and inject it in MT-HVDC system to compensate for voltage drop.

2. DC Voltage droop control implemented in all converters is activated to stabilize DC voltage.

3. Stations $S3$ and $S4$ extract power from AC zone 2 to compensate DC voltage drop. Hence, AC zone 1 is fed by power coming from AC zone 2 without using communication means.

4. DC voltage drop is stopped (but DC voltage does not come back to initial value since no integrator exists in its control). Frequency support is provided to the needy AC synchronous zone which, in its turn, limits the frequency drop in it.

The DC voltage performance until reaching steady state described above is plotted in the ***Figure 5-9***.

The following points conclude this case where HVDC is used for active power transfer with frequency support based on local droop controller:

- The measured maximal frequency deviation is reduced by 50.7 % in AC zone 1. Primary AC frequency response is less solicited to stop the frequency drop because local frequency droop controller injects sufficient power in the perturbated zone.

- The sharing of effort between AC zone 1 and AC zone 2 is completed through DC voltage droop control in the MTDC system. This implies an interaction between the DC voltage in the MTDC and frequency of the AC system due to the implemented controllers.

- No communication was needed, though power sharing was possible between separate AC synchronous systems *via* the MTDC system.

- Power oscillations still exist during the transient: the main role of frequency controller is to support the AC system in terms of power balance between consumption and available power to consume in an AC system, and not to compensate the power imbalances between different areas within the same AC system. These power imbalances lead to power oscillations and need to be tackled to avoid system split.

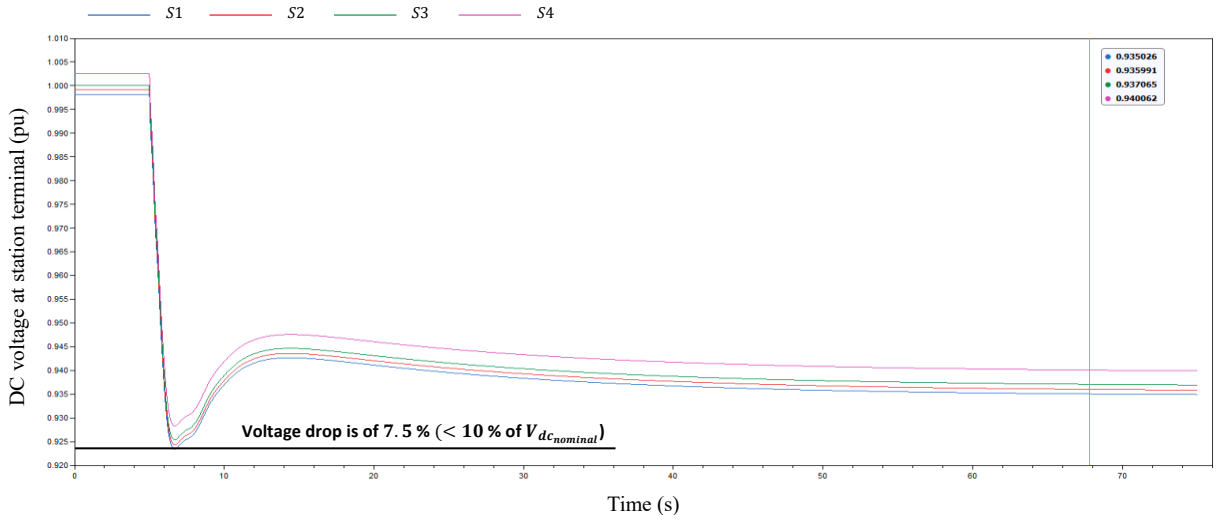

Figure 5-9: DC voltage measured at each converter station terminal.

Therefore, to help reduce the power imbalances appearing between the two areas of AC zone 1, a POD based on wide-area measurements (WAMS) was implemented as an additional power converter controller. Using WAMS means using communication means between different converters. However, active power coordination is still not implemented at this stage.

3. Case 2: Rotor angle support based on WAMS, without active power coordination (Framework 3.a)

In this section, no frequency support is implemented: rotor angle small-signal stability aspect is tackled separately.

For each AC zone, a frequency-based POD controller, acting on both converter stations connected to the same AC zone, is implemented based on equation **(4.47)**. However, in this case, each controllers' inputs are the frequency of centres of inertia of the areas to which the converters are connected within the same AC zone. The frequency of each area is calculated based on the measured frequencies at the generators contained in the area.

After implementing the controllers, the frequency performance of the centre of inertia of each area in AC zone 1 was plotted (***Figure 5-10***).

Frequency Nadir is not significantly improved by the action of the POD (compared to reference case in ***Figure 5-4***). The only small improvement in the current case (18 %) comes from the absence of oscillation peaks thanks to the enhanced damping. The curves presented in plot ***Figure 5-10*** correspond to the mean value of blue and red curves of the previous ***Figure 5-4*** of the reference case. The steady-state value of the frequencies obtained in both cases is almost the same as well. All this is explicable by the fact that the POD controller in AC zone 1 is conceived to transfer power within the same AC zone.

Thus, the POD controller does not bring additional energy from AC zone 2 to AC zone 1. This results in similar mean frequency performances in reference case (no POD) and in the current case (with POD only), in contrast with the previous case where frequency support was added.

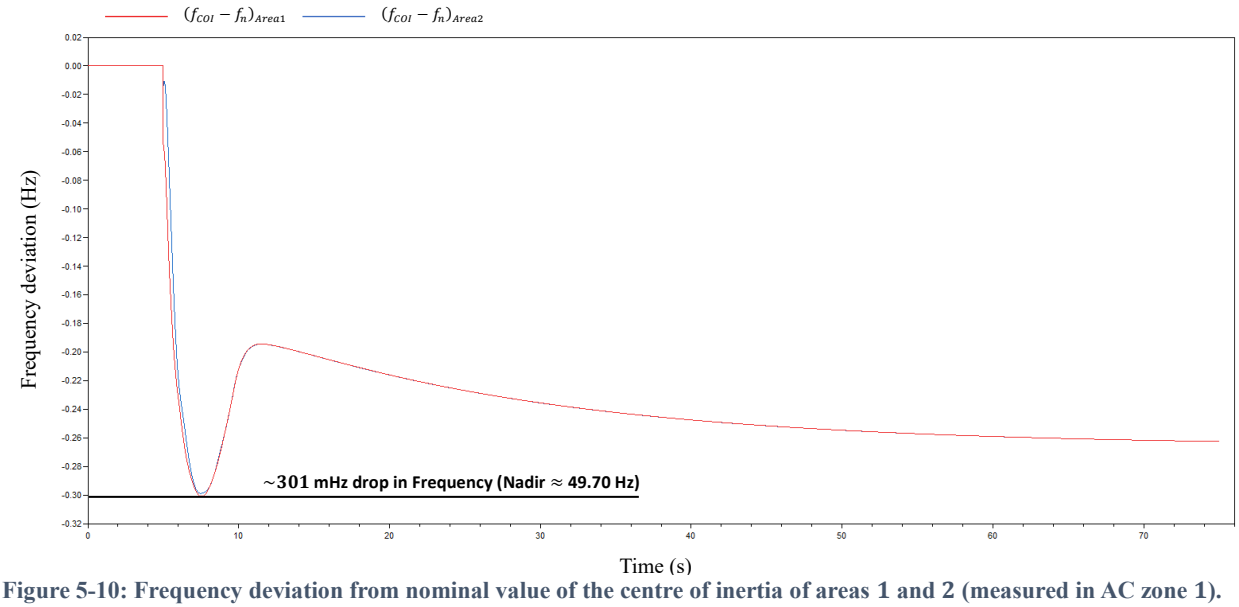

Figure 5-10: Frequency deviation from nominal value of the centre of inertia of areas 1 and 2 (measured in AC zone 1).

It can be clearly seen in ***Figure 5-10*** that the oscillations are very well damped. This causes the interarea mode to disappear from the top 20 (ranked by oscillations amplitude) modes in mode shape analysis. The interarea mode is not anymore detectable by the algorithm used for mode shape analysis.

Power oscillation damping is performed by opposite power transfers performed by converters $S1$ and $S2$ connected to the disturbed AC zone 1. These power transfers occur only during the transient (***Figure 5-11***), and when the two measured frequencies (of Area 1 and Area 2) become equal at steady-state, the POD controller's output is null.

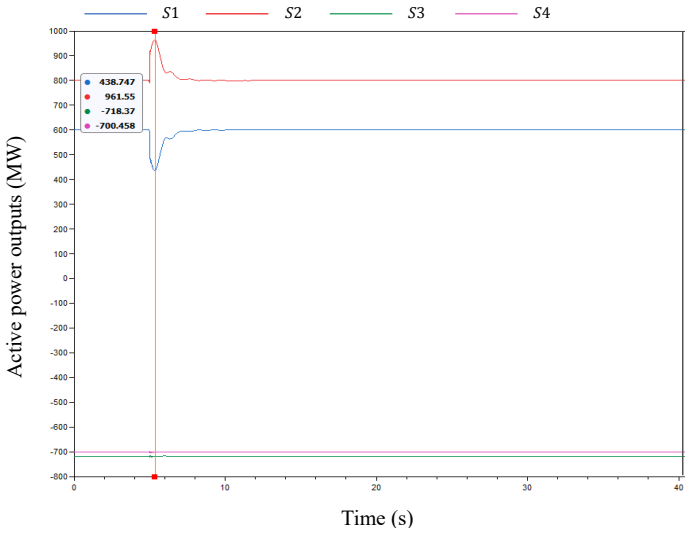

Figure 5-11: Active power outputs of the converter stations.

The steady state outputs of $S1$ and $S2$ are the same as the initial ones (given by power flow planning) since power oscillations disappear (***Figure 5-1***, ***Figure 5-11***).

The following points conclude this case where HVDC is used for active power transfer with power oscillation damping feature based on WAMS:

- The POD controller was able to damp the interarea oscillations appearing after a power imbalance between the areas to which two converters are connected within the same AC zone.
- The measured frequency deviation (during transient and steady state) is not significantly enhanced compared to reference case.
- Active power outputs of the converters show that rotor angle small-signal support is only needed during the transient while frequency support (Case 1) is needed all the time after the disturbance.
- Communication was needed to transfer measurement data and power reference output to/from the POD controller.

Therefore, to help reduce the frequency deviation, frequency support, previously studied individually, is re-added.

4. Case 3: Frequency support and power oscillation damping, without active power coordination (Framework 3.a)

In this section, frequency support is implemented along with rotor angle small-signal support. At this stage, the effect of simply combining different HVDC ancillary services is examined to prove the pertinence of active power coordination feature.

The frequency performance of the AC zone 1 resulting from the combination of the ancillary services is given in ***Figure 5-12***.

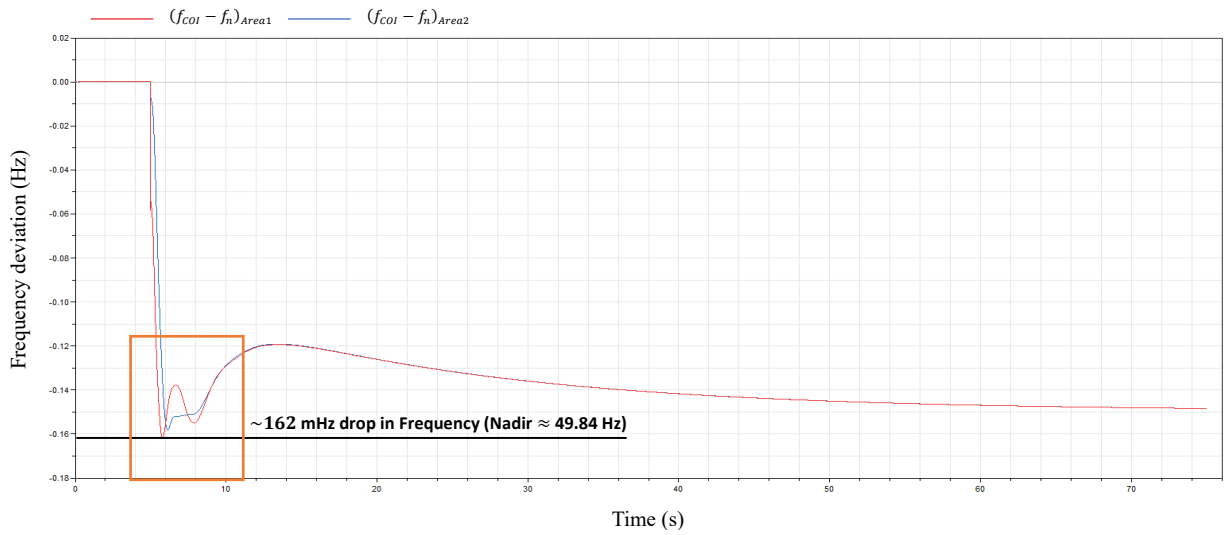

Figure 5-12: Frequency deviation from nominal value of the centre of inertia of areas 1 and 2 (measured in AC zone 1).

Though frequency deviation is enhanced, the frequency oscillations reappear (compared to Case 2 with only POD controller implemented). They particularly reemerge in the Area 1 connected to converter station $S2$.

The mode shape analysis, previously not detecting the interarea mode (Case 2), redetects it and gives the following plot in ***Figure 5-13***.

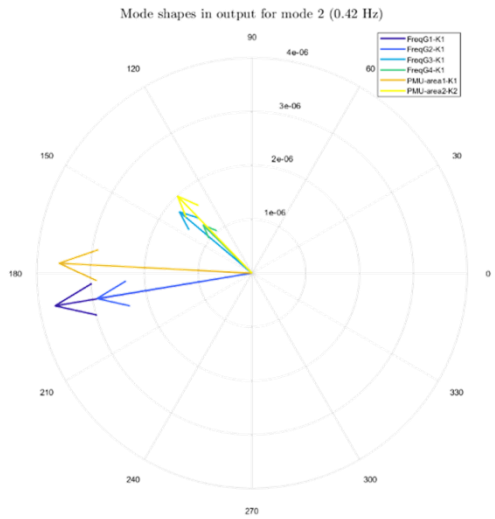

Figure 5-13: Mode shapes in output for interarea oscillation mode in AC zone 1.

The frequency of the interarea modes in AC zone 1 is 0.42 Hz and their damping is about 41 %. The amplitude of the arrows also shows an existence with higher amplitude of this mode in Area 1.

To understand what happened to let the modes reappear and be re-expressed in Area 1 outputs, the active power outputs of the converters is plotted in ***Figure 5-14***. As a reminder, these converters have in their active power reference a combination of the outputs of POD, FCR and DC voltage droop controllers.

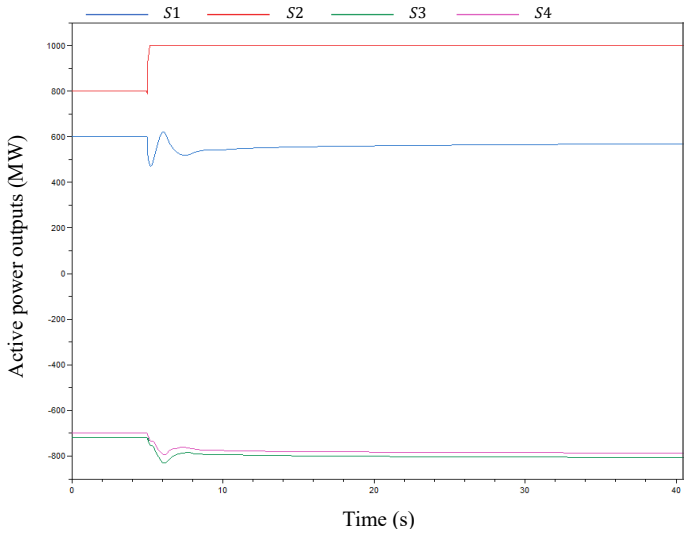

Figure 5-14: Active power outputs of the converter stations.

While $S1$, connected to Area 2 of AC zone 1, can fulfil the active power extraction request ordered by the POD controller, $S2$'s upper active power constraint hinders the station in question from fulfilling the active power injection request sent by the same POD controller. The station $S2$ is saturated due to the

combined active power references sent by POD and FCR simultaneously. Therefore, frequency oscillations reappear at the Area 1 – to which $S2$ is connected – due to the competition between POD controller and FCR controller at the level of the converter $S2$'s output.

The following points can be concluded for this case of multiple stability aspects controlled simultaneously without active power coordination:

- Station $S2$'s output is saturated (1 GW) and therefore $S2$ cannot fully satisfy the POD controller's power reference output and thereby fully contribute to the damping of interarea oscillations.
- Station $S1$ still has ~430 MW margin that should be used to enhance power oscillations damping while also satisfying the frequency controller's reference output.
- The active power constraints of the power converters may lead to converter saturation which forces it to operate in a non-linear zone. Thus, a main drawback of the Framework 3.a (where controllers are simply combined) appears. Due to non-linear operation of power electronic converters, the superposition of controllers' actions (where each action enhances an individual stability aspect) cannot be expected in the hybrid AC/DC power system.

A simple ancillary services combination can lead to headroom saturation of power converters, making services' fulfilment impossible in perturbation scenarios such as was proved in this case study. The competition between controllers' output may be avoided or reduced through active power coordination.

To further enhance power system stability, active power coordination is proposed in the following section.

5. Case 4: Same as Case 3 but with active power coordination (Framework 3.b)

As previous sections showed, stability may be degraded due to the interaction between different controllers. In the Case 3 explained previously, the interaction was due to reaching active power limit of power converter output. This limit led to competitiveness between frequency and rotor angle controllers.

To cope with this challenge, active power coordination is proposed in this section through converter active power reallocation during the operation of the power system (in offline simulation).

What are the control power references that can be reallocated between converters?

- POD controller reference: NO, concerned converters should act in equal but opposite directions to damp oscillations.
- FCR controller reference: YES, in the limit of available headroom in the other converters, and without exciting interarea modes by creating new power imbalance situations.
- DC voltage controller reference: YES, in the limit of available headroom in the other converters.

Discussion about DC voltage control reallocation: *DC voltage control reallocation should be evaluated carefully. The DC voltage control is not an ancillary, but a mandatory service provided by HVDC links. The active power reallocation of this control's power reference should be made knowing that the loss of the concerned converters to which active power is reallocated may jeopardize DC voltage stability. This may lead to full MTDC system blackout. The following reflection was made on the risk coming from MTDC system blackout. In contrast to HVAC systems, the MTDC system can quickly come back to operation after a blackout. However, when an MTDC system is lost after a given perturbation, the planned power transfer is stopped, and all the mentioned ancillary services are not provided anymore. This may lead to the loss of AC components in the AC power system. The loss of a converter in MTDC system may therefore lead to cascaded loss of other components, which violates the 'N-1' contingency rule. This risk study should be thoroughly made at the stage of planning of AC/DC hybrid power systems to avoid uncontrolled cascaded system blackouts.*

In the following, the study focuses on the benefits of reallocating the FCR controller's power reference (not DC voltage controller's power reference) among converters as an approach of active power control coordination for stability enhancement. The objective behind active power reallocation is to desaturate a converter that was hindered from fulfilling a given controller's request due to the active power limits of the converter. The concept is based on the following steps that constitute an algorithm for active power reallocation (ANNEX 2) and is thoroughly explored in the following study.

1. Detecting which converters are saturated and which are not,
2. Identifying which active power control reference can be reallocated and from which converter to which one,
3. Determining the ratio of active power reallocation (in a range of 0 to 100 % of the total of the active power control reference identified in the previous step 2),
4. Sending this active power reference from an original converter to an assigned one (identified in previous step 2).

For a converter k, the power reference sent to control multiple stability aspects as explained in this section and before applying power reallocation control was:

$$P_k^*(t) = P_k^{0^*}(t) + P_k^{POD^*}(t) + P_k^{FCR^*}(t) \quad \textbf{(5.1)}$$

where $P_k^{0^*}$ is the AC/DC's power flow reference initially before any perturbation, $P_k^{POD^*}$ is the POD controller's reference and $P_k^{FCR^*}$ is the FCR's reference, sent to converter k.

As discussed before, the FCR's power reference sent to a converter can be partially or totally reallocated to the other converters connected to the same AC zone. This is particularly interesting when such a converter is saturated, and the others still have remaining total headroom for active power.

In the case of two converters i (saturated) and j (unsaturated), such active power reallocation transforms the power references sent to the converters as expressed in the following equation **(5.2)**, with r_i the ratio of active power that converter i should be relieved from and r_{ij} the ratio of active power reallocation from converter i to converter j.

$$P_i^*(t) = P_i^{0^*}(t) + P_i^{POD^*}(t) + (1 - r_i) \cdot P_i^{FCR^*}(t)$$
$$P_j^*(t) = P_j^{0^*}(t) + P_j^{POD^*}(t) + P_j^{FCR^*}(t) + r_{ij} \cdot P_i^{FCR^*}(t) \quad \textbf{(5.2)}$$

For a saturated converter i, the ratio r_i, defined as the following, can be calculated based on the maximum obtained from equation **(5.1)**:

For a given time called t_{max}, the following happens:

$$P_i^{*max} := \max_{at\ t_{max}} (P_i^{0^*}(t) + P_i^{POD^*}(t) + (1 - r_i) \cdot P_i^{FCR^*}(t)) \quad \textbf{(5.3)}$$

This gives:

$$P_i^{*max} = P_i^{0^*}(t_{max}) + P_i^{POD^*}(t_{max}) + (1 - r_i) \cdot P_i^{FCR^*}(t_{max}) \quad \textbf{(5.4)}$$

Which leads to:

$$r_i = 1 - \frac{P_i^{*max} - P_i^{0^*}(t_{max}) - P_i^{POD^*}(t_{max})}{P_i^{FCR^*}(t_{max})} \quad \textbf{(5.5)}$$

The value r_{ij} expresses the ratio corresponding to converter j to desaturate the converter i.

For a set composed of N_{Conv_l} converters connected to the same AC zone l:

$$r_i \geq \sum_{\substack{j=1 \\ j \neq i}}^{N_{Conv_l}-1} r_{ij} \quad \textbf{(5.6)}$$

The equality is possible if the remaining $N_{Conv_l} - 1$ converters have enough headrooms to cover all the i-th converter's FCR controller's power reference that needs to be reallocated to them.

To calculate r_{ij} for the sake of getting the best multiple stability enhancement, an optimization approach could be adopted. In the next part, the values of r_i and r_{ij} are set to 1 and the simulation results applied on the benchmark in ***Figure 5-1*** are explained.

In this case study, converter $S2$ is saturated while the converter $S1$ connected to the same AC zone 1 is not. To compare, the power references (without DC voltage controller's reference) sent to station $S2$ are plotted in ***Figure 5-15*** for Case 3 (left) and Case 4 (right). The ***Figure 5-15*** shows that, during transient, the active power reallocated peak surpasses 300 MW. The whole FCR contribution, initially requested

from $S2$, is now requested from $S1$ ($r_i = r_{ij} = 1$ in **(5.2)**) without violating its power limits (see ***Figure 5-16***).

As a result of this power reallocation, the frequency performance of AC zone 1's both areas is plotted in ***Figure 5-17***. This plot as well as mode shape analysis (***Figure 5-18***) prove that the power oscillations were damped better thank to the strategy of reallocating active power between converters. The mode (0.74 Hz) appears to be approximatively vanished from generators $G3$ and $G4$ and its damping is of 58.23 %.

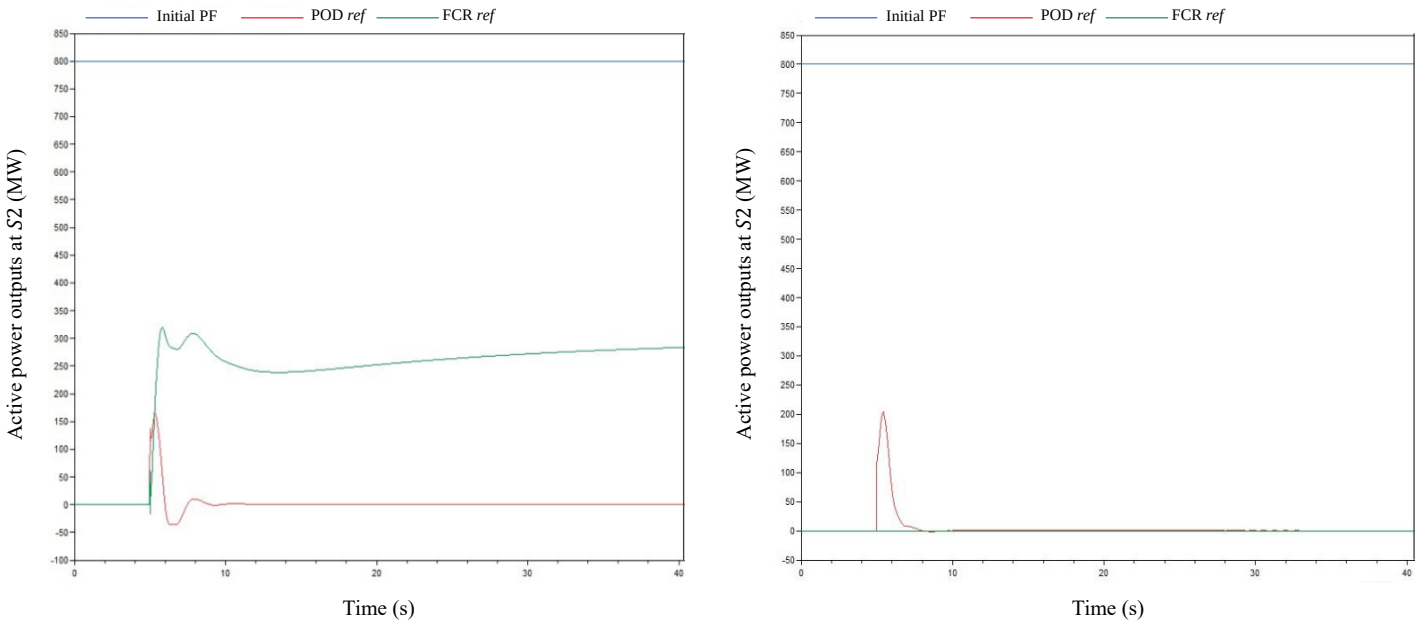

Figure 5-15: Active power references sent to the converter station $S2$ in Case 3 (left) and Case 4 (right).

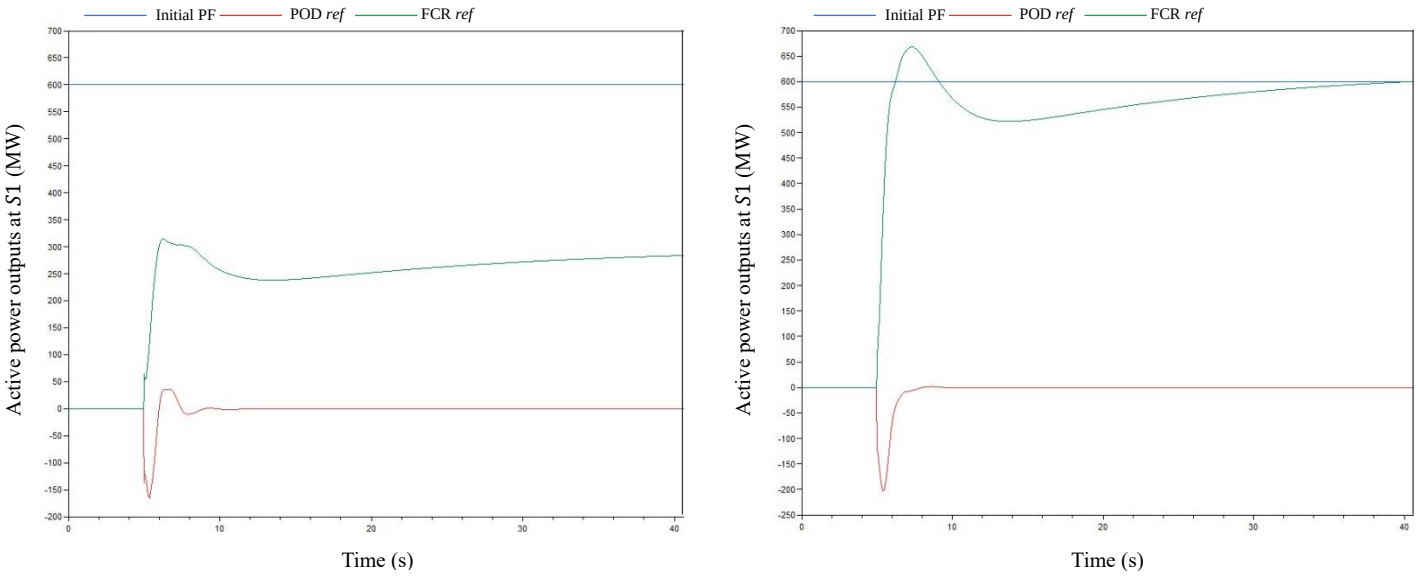

Figure 5-16: Active power references sent to the converter station $S1$ in Case 3 (left) and Case 4 (right).

The POD action awaited from $S2$ is, in this Case 4, no longer competed by FCR action at the level of converter's upper headroom limit. The POD action can therefore be fulfilled at this converter $S2$ while $S1$ takes the effort of FCR action over (see ***Figure 5-19***).

The result is a desaturation of $S2$ allowing for POD action fulfilment at the level of this converter, and additional future local action by HVDC system in Area 1.

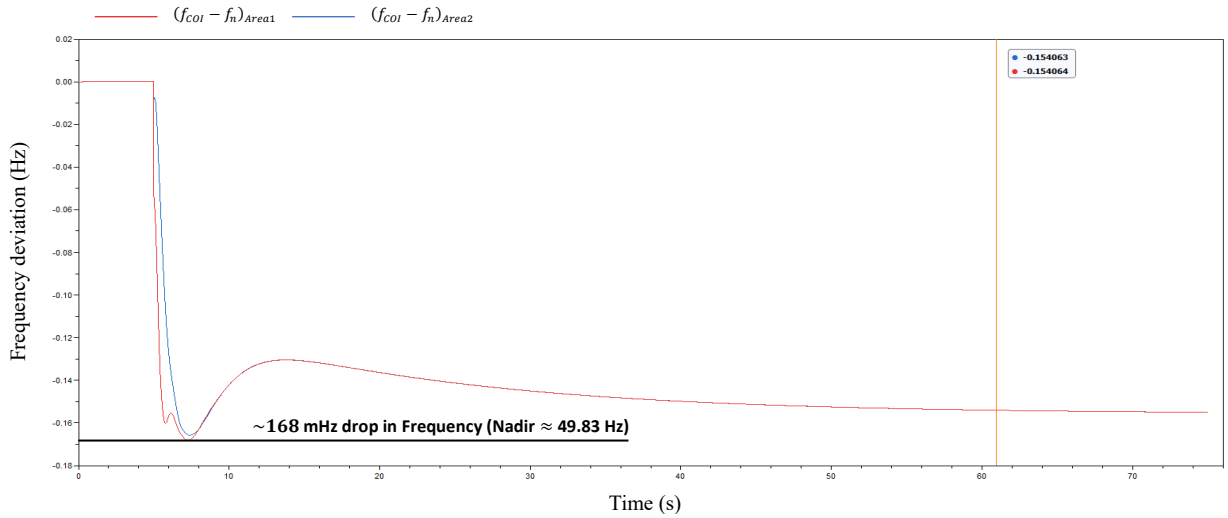

Figure 5-17: Frequency deviation from nominal value of the centre of inertia of areas 1 and 2 (measured in AC zone 1).

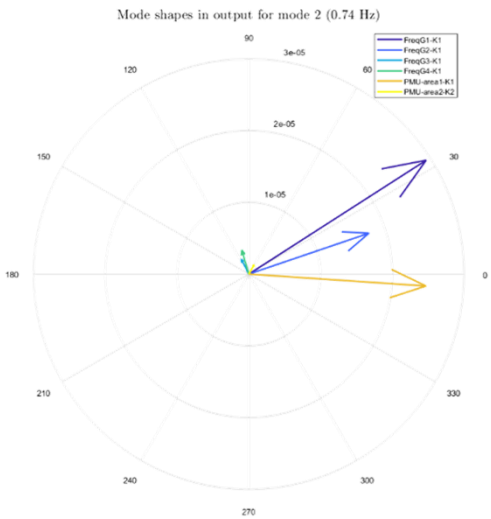

Figure 5-18: Mode shapes in output for interarea oscillation mode in AC zone 1.

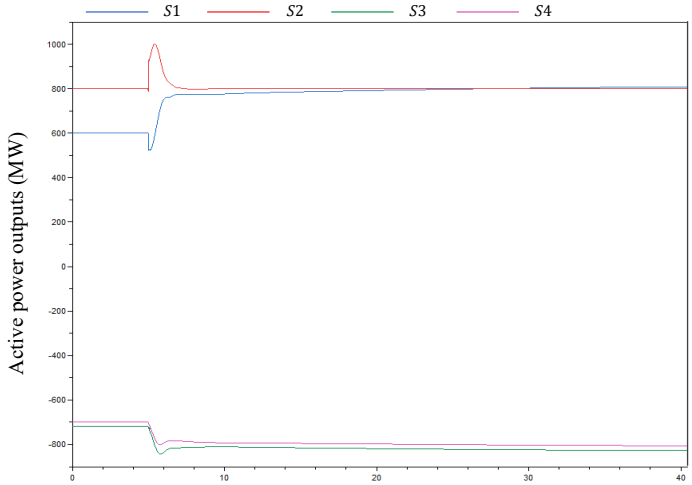

Figure 5-19: Active power outputs of the converter stations.

The following points can be concluded for this case (multiple stability aspects controlled simultaneously with active power coordination through power reference reallocation):

- Station $S2$'s output is desaturated and therefore $S2$ can now fully satisfy the POD controller's power reference output and thereby fully contribute to the damping of interarea oscillations.
- Station $S1$'s available headroom was used to enhance power oscillations damping while also significantly contributing to frequency regulation by injecting an active power equal to the sum of its own frequency controller's power reference and the reference of the frequency controller implemented at $S2$.
- The active power constraints of the power converters were not exceeded in active power references. Thus, the advantage of the Framework 3.b over Framework 3.a is the operation of power electronic converters more far from their limits and, thereby, providing a higher ability of HVDC power systems to contribute to hybrid AC/DC power system's stability enhancement.

6. Conclusion of case studies

The application of the established frameworks for stability enhancement strategies was based on a hybrid AC/DC power system where multiple stability aspects were tackled. Stability indicators showed that global power system stability was enhanced thanks to the proposed active power reallocation strategy.

III. Conclusion

In this chapter, the potential stability degradation resulting from adding an HVDC system to an existing AC system was shown. Individual stability aspects and then, combined aspects, were examined in the first sections of the chapter.

In a progressive approach, multiple stability issues emerging from the combination of multiple controllers were illustrated. These controllers are likely to coexist if an HVDC power system is expected to simultaneously propose several ancillary services.

In the final part of this chapter, a multiple stability enhancement approach was proposed based on active power reallocation. To validate this approach, several case studies were made based on a hybrid AC/DC power benchmark using multiple stability indicators (frequency Nadir, damping, DC voltage Nadir). Different frameworks of stability enhancement were compared. The necessity of active power

coordination was evaluated. In the last stability enhancement framework case study, it was proved that, by reallocating active power references sent by local controllers, it is possible to desaturate a converter. This allows it to fulfil the power exchange requested by its stability controllers. This was possible by preliminarily analysing which converter's active power reference could be reallocated to which converter.

In next chapter, the focus will be on a different global stability enhancement approach based on constrained headroom allocation.

Chapter 6 : AC/DC global stability enhancement approach based on headroom allocation

I. Introduction

1. Context

In the previous chapter, the need of a global stability enhancement approach was shown. In fact, the controllers added because of the proposed HVDC ancillary services interact together in an antagonist way. Based on active power reallocation among AC/DC converters in a hybrid AC/DC power system, the proposed approach proved that interactions between frequency and rotor angle controllers were decreased in an attempt of enhancing the system's global stability.

In the current chapter based on [101], a new AC/DC centralized controller – composed of distributed rotor angle and frequency controllers – is firstly proposed. It sends the control power references to all the converters. A new frequency controller was proposed in the flow of the chapter, which also helps enhance stability by minimizing the interactions between frequency and DC voltage controllers. Finally, another multi-stability enhancement approach is proposed. It is based on headroom allocation for each converter. As in the previous chapter, the study is led progressively on an AC/DC power system benchmark where multiple perturbation scenarios occur.

The used benchmark, perturbation scenarios and the initial AC/DC power flow are shown in the ***Figure 3-17***.

2. Organization of the chapter

In section II, the AC/DC controllers are recalled in the light of the expected HVDC functionalities. In contrast to previous chapter, this part includes the rotor angle difference controller (ADC) and a comparative study of different frequency controllers (FCR) followed by the selection of a new frequency controller. In the following section III, a multi-criteria stability study is led and in, its end, the other stability enhancement approach is mathematically formulated and validated by simulation.

II. Synthesis of selected ancillary services and proposition of new frequency controller

1. Power system dynamics

For a system composed of N synchronous machines connected to the same synchronous area, the modified swing equations **(6.1)** of the ith synchronous machine $\forall i \in \{1, .., N\}$ are:

$$\begin{aligned} \dot{\delta}_i &= \omega_i \\ M_i\dot{\omega}_i &= -D_i\omega_i + P_{m,i} - P_{e,i} \end{aligned} \quad \textbf{(6.1)}$$

where δ_i is the rotor angle, ω_i the rotor speed deviation from the speed corresponding to the nominal frequency (synchronous speed), M_i is the inertia coefficient, D_i is the damping torque inherent to the

machine, $P_{m,i}$ is the mechanical power given by the controlled turbine, $P_{e,i}$ is the electrical output power of the machine.

These equations govern the dynamics of AC power system. When AC/DC power converters interface AC and HVDC systems, the power exchange $P_{HVDC,k}$ between converter k and a synchronous zone l modifies the classical AC dynamics. The convention in this work considers power flow positive from DC to AC side (i.e., $P_{HVDC,k} > 0$ when converter extracts power from DC grid and injects it in AC grid).

Based on the AC and DC dynamics, the power references of the AC/DC converters are modified by the central controller (regulating the AC frequency, rotor angle, power oscillations) and DC voltage control. A focus on the potential supplementary controls is made in the next part.

2. Selected services: recall and design of new frequency controller

The expected HVDC functionalities [6] that this work tackles are:

- AC line emulation, called Angle Difference Control (ADC)
- Power oscillation damping (POD)
- Frequency support (FCR)

These stability enhancement strategies offered by ancillary services are valid if DC voltage is not at risk since this risk can lead to HVDC system loss, and no ancillary service could be provided anymore. If an event puts DC voltage at risk, the mentioned ancillary services should be stopped until the DC voltage stability becomes guaranteed again.

In the proposed benchmark (see ***Figure 3-17***), the following is valid:

- The initial AC active power flow is indicated in the figure.
- Converters' rated values are: $\{V_{dc} = 640 \text{ kV}; P = 1 \text{ GW}\}$.
- The converters are all operating in DC voltage droop mode with same droop gain $K_{V_{dc}} = 8$ MW/kV, such that:

$$P^*_{DC_{droop_k}}(t) = K_{V_{dc}} \cdot \left(V^k_{dc}(t) - V^k_{dc_0}(t)\right) \quad \textbf{(6.2)}$$

Also here, the models and simulations have been made using the Dymola software based on Modelica language. The works use the OpenIPSL library [102] and HVDC Library developed at SuperGrid Institute [103], [104], [105]. The initialization of the AC zones has been done through GridCal tool [106].

i. AC line emulation – Angle Difference Control (ADC)

Based on phase angles' difference at the PCCs of the AC/DC stations, the ADC sends a power reference to the converters involved in extracting power at one PCC, transfers it through a DC path and injects it at another converter embedded in the same AC synchronous zone.

The main purpose of this service is to reinforce rotor angle stability of an AC system by emulating the behavior of AC lines for power transmission. It is normally used for steady-state rotor angle enhancement: it reduces the angle difference between the PCCs which lowers the amount of power transmitted through the AC lines parallel to the DC path. This reduces the risk of AC overcurrent and system split.

As it is based on angle measurements, AC line emulation cannot be applied to two non-synchronous power systems. Besides, this service needs well-established communication between the converters used so that the same power is exchanged between the two converters.

For a couple of converters k and j connected to the same synchronous area, ADC control sends the following power references [93]:

$$\begin{aligned} P^*_{ADC\,kj}(t) &= K_{ADC,kj} \cdot \left(\theta_j(t) - \theta_k(t)\right) \\ P^*_{ADC\,jk}(t) &= -P^*_{ADC\,kj}(t) \end{aligned} \quad \textbf{(6.3)}$$

where $K_{ADC,kj} > 0$ is the gain of the ADC between converters k and j, θ_k and θ_j are the bus angles at the PCCs, and $P^*_{ADC\,kj}$ is the power reference sent to converter k due to the existing ADC control between it and converter j.

The second equation in **(6.3)** ensures that power balance is respected so that DC voltage remains stable.

A low-pass filter **(6.4)** is added to the ADC to avoid unnecessary power compensations (oscillating power compensation, quickly disappearing events, etc.). Although the main purpose of ADC is steady-state enhancement, it may contribute to rotor angle stability during transients. The drawback with higher low-pass filter time constants is that AC line may not be less emulated during quick transients since they are filtered. The s-domain transfer function of the implemented filter is shown in equation **(6.4)**) where the time constant $\tau_{ADC,kj}$ for the ADC implemented between converters k and j helps avoid emulating the power oscillations through the DC system.

$$LPF_{ADC,kj}(s) = \frac{\Delta\theta_{out}}{\Delta\theta_{in}} = \frac{1}{1 + \tau_{ADC,kj}s} \quad \textbf{(6.4)}$$

To understand the impact of the ADC, the controller was solely implemented on the study benchmark. The case study is summarized in ***Table 6-1***. The same gain and time constant are used for the ADCs of $\{S1 \leftrightarrow S2\}$ and $\{S3 \leftrightarrow S4\}$.

As shown in the ***Figure 6-1***, AC line emulation by DC path through ADC reduces the steady-state power transfer on the observed AC tie line[1] (in the proposed benchmark, the AC zone 1 can be considered to have two AC areas (left side and right side) connected through four AC tie lines. The tie-line considered to observe the power flow is mentioned in ***Figure 3-17***). Therefore, the effort of compensating for the

[1] An AC tie line is an electrical transmission line connecting two sub-zones in a synchronous zone.

loss of the AC tie line is shared between the remaining AC system and the DC system.

Table 6-1: Case study for ADC (check *Figure 3-17* to see the location of the fault).

Contingency	K_{ADC} (MW / °)	τ_{ADC} (s)
Power fault at Bus 9 in AC zone 1 ($t = 1$ s) leading to the trip ($t = 1.1$ s) of one AC tie line	1005	5

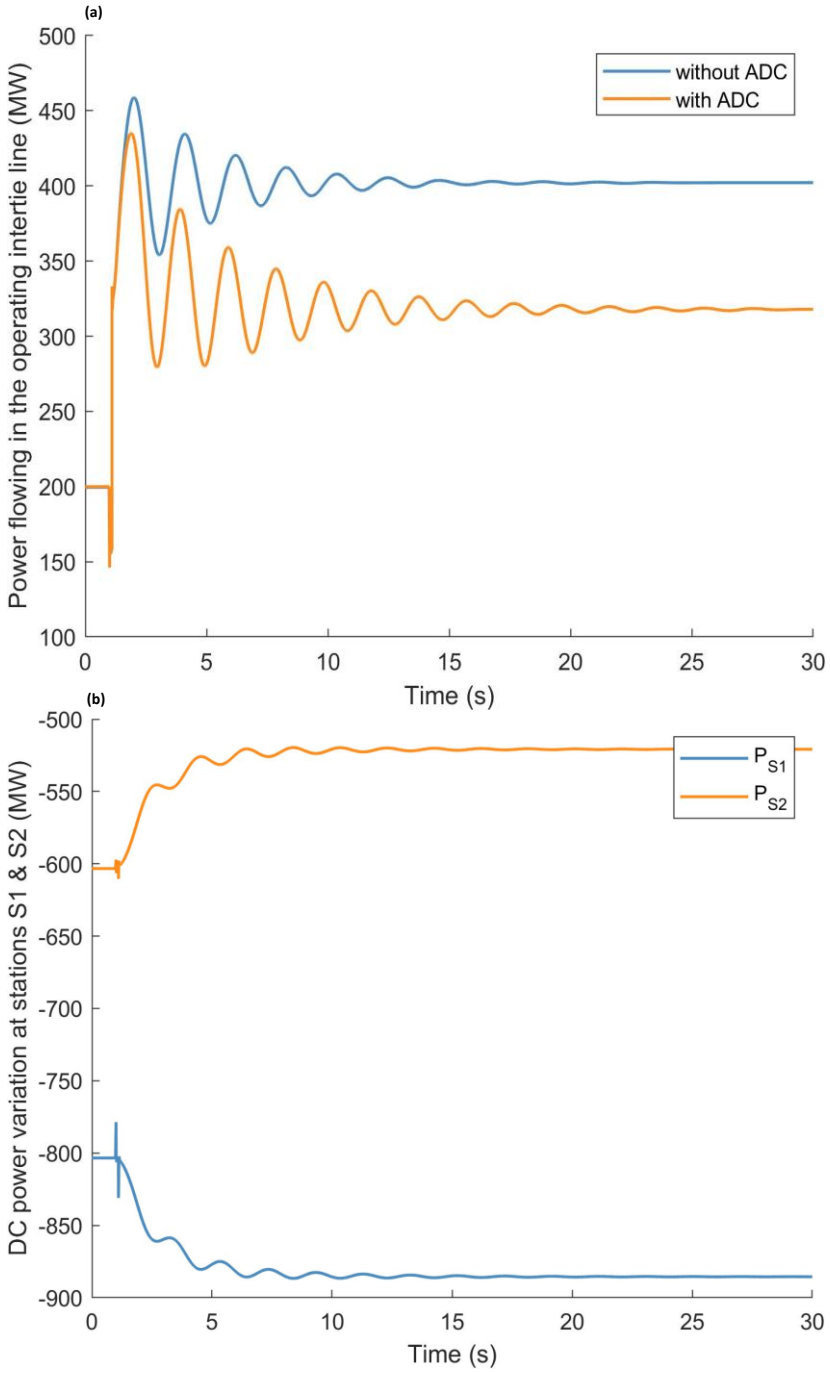

Figure 6-1: (a) Active power flowing through the observed AC tie line parallel to the lost line. Steady-state values show ~84 MW less AC power flowing thanks to line emulation by ADC.
(b) DC power flowing at station $S1$ and $S2$. The steady-state values show that ~84 MW power flows through DC path thanks to the ADC between $S1$ and $S2$.

ii. Power Oscillation Damping (POD)

When an AC synchronous area is subject to power oscillations, an embedded HVDC system can inject damping power in addition to the action of the PSSs by sending opposite power references simultaneously to suitable converters.

Particularly, interarea power oscillations – which are of electro-mechanical nature – may occur within the same synchronous zone after a disturbance reduces the balancing capability of AC interarea connections or reduces the damping. The frequency of modes of these oscillations is generally within the range of $[0.1;\ 0.7]$ Hz [60]. An eigenvalue analysis helps identify the involved interarea eigenvalues and calculate their frequency and damping ratio. Like for the previous part, this service assumes communication is established between the involved converters.

For a couple of converters k and j connected to the same synchronous area, the POD control sends the following power references:

$$\begin{aligned} P^*_{POD\,kj}(t) &= K_{POD,kj} \cdot \left(f_j(t) - f_k(t)\right) \\ P^*_{POD\,jk}(t) &= -P^*_{POD\,kj}(t) \end{aligned} \qquad \textbf{(6.5)}$$

where $K_{POD,kj} > 0$ is the gain of the POD between converters k and j, f_k and f_j are the measured frequencies at the PCCs, and $P^*_{POD\,kj}$ is the power reference sent to converter k due to the POD control between it and converter j.

To understand the impact of the POD, the controller was solely implemented on the study benchmark. The same POD gain was chosen for the couples $\{S1 \leftrightarrow S2\}$ and $\{S3 \leftrightarrow S4\}$. The case study is summarized in ***Table 6-2***.

Table 6-2: Case study for POD.

Contingency	K_{POD} (MW / Hz)
Load increase at $L10$ (300 MW or 8.3 % of total nominal power of synchronous machines in AC zone 1, at $t = 1$ s) leading to a power imbalance and increasing power flow through AC tie lines	2500

In ***Figure 6-2.a*** – the case without POD controller – power oscillations appear between $\{G1, G2\}$ and $\{G3, G4, G5\}$. At generator's level, the local frequency (input of the PSS of the generator) decreases sufficiently to saturate the local PSS (***Figure 6-2.c***) which is insufficient to fully damp the interarea oscillations.

In the case with the POD service (***Figure 6-2.b***), although the PSSs remain saturated (***Figure 6-2.c***) due to the local frequency (input of PSS) decrease, the HVDC system helps damp the oscillations by exchanging power between the right and left areas of AC zone 1 through the DC lines. This is done proportionally to the measured frequency difference at the PCCs **(6.5)**.

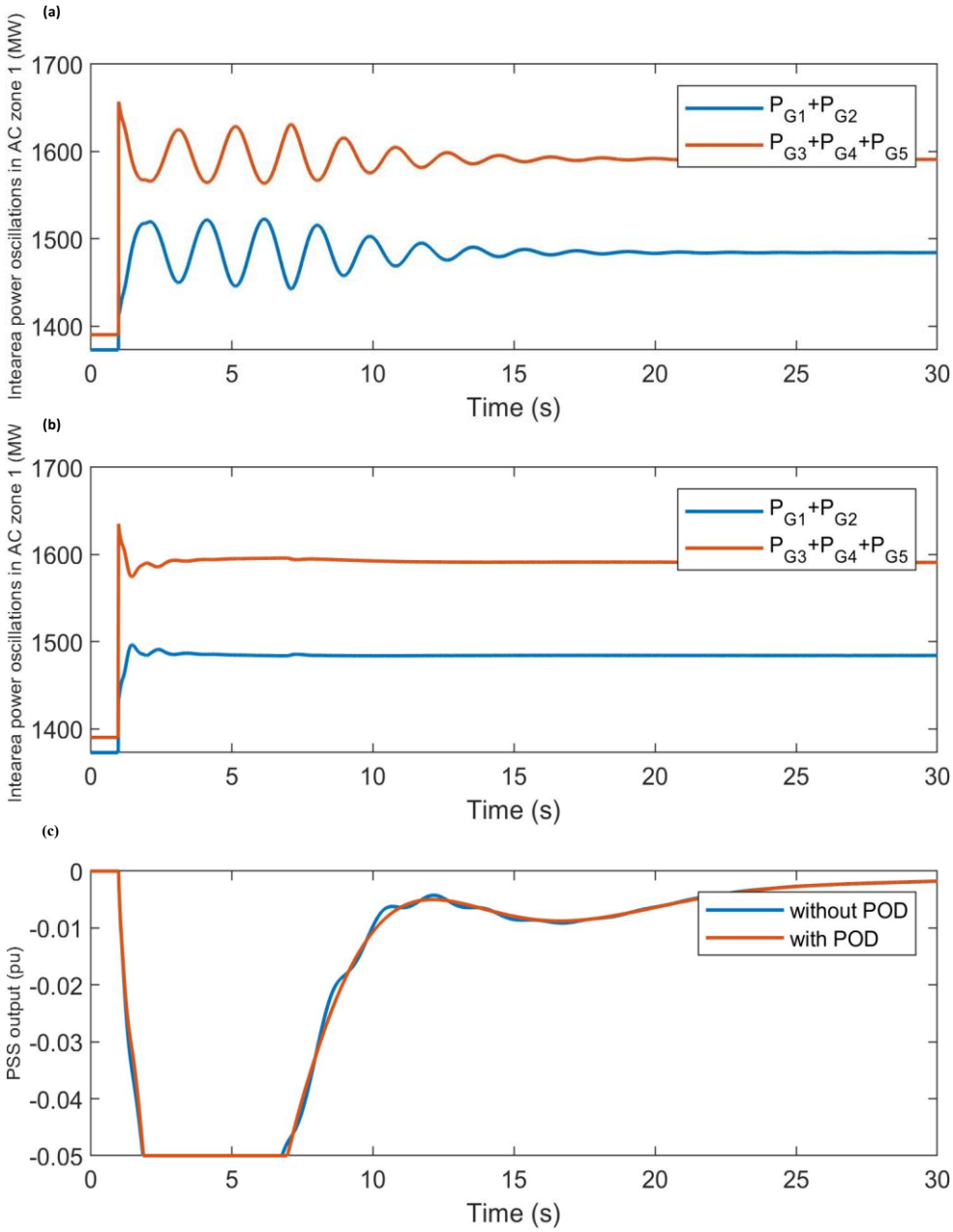

Figure 6-2: Power oscillations between left and right areas after contingency in AC zone 1 (without POD (a), with POD (b)). PSS output remains saturated right after contingency in both cases (c).

iii. Frequency Containment Reserve (FCR)

The FCR, when activated, implies that a synchronous zone shares the reserve with another synchronous zone through HVDC [107].

The advantage of FCR is to share the disturbance mitigation effort between different AC zones to increase the ability of responding to the contingency without losing frequency stability in the disturbed zone.

Solutions for frequency support between two synchronous zones are multiple [97]. In this work, two of them are compared.

a. Solution based on DC voltage droop control

Based on local frequency droop control, converters inject or extract power depending on PCC's frequency deviation from nominal value. The power exchanged between AC and DC systems based on this local control affects the voltage in the DC system which activates DC voltage droop control.

When this voltage controller is implemented in the same converter used by the frequency droop controller, interactions appear between both controllers [97], [108]. As shown in the mentioned papers, a rescaling of the frequency control parameters is needed to limit frequency variation.

However, when DC voltage control is also/only implemented in the converters connected to another synchronous zone, the following happens. The power injected/extracted in the disturbed synchronous zone – due to local frequency droop controller – by the converter connected to this zone impacts the DC voltage of the HVDC grid. In this case, the stations connected to another synchronous zone and operating in DC voltage control mode react to the voltage perturbation in HVDC grid and extract/inject power from their own synchronous zone. In this process, the power needed in the disturbed AC zone is transferred – through DC voltage droop control – from another AC zone which is considered to propose frequency support to the disturbed AC zone.

The main drawback of this method is the existing interactions between AC frequency and DC voltage at the converting station connected to the disturbed zone [8]. To limit DC voltage variation, enough power reserve should be available for DC droop control, and this may be jeopardized if a converter contributing to DC voltage control trips.

b. Solution based on distributed frequency droop control

Frequency support can alternatively be based on direct communication means between contributing stations [97] to guarantee power balance in the DC grid and therefore preserve the DC voltage from big variations.

In this solution, needed power for frequency support is calculated based on local droop controller too but the power references of this controller are directly sent to a couple of converters connected to different synchronous zones. For each couple of converters – one connected to the disturbed and the other to an undisturbed synchronous zone – the power references are sent in opposite signs: if one converter should inject power in an AC zone, the other one from the couple should extract the same amount from the distinct AC zone to which it is connected. Therefore, power balance is guaranteed within the HVDC grid and DC voltage control reserve is not required.

The FCR power references are determined from:

$$\begin{aligned} P^*_{FCR_{kj}}(t) &= K_{FCR,kj} \cdot \left(f_{k,nominal} - f_k(t)\right) - K_{FCR,jk} \cdot \left(f_{j,nominal} - f_j(t)\right) \\ P^*_{FCR_{jk}}(t) &= -P^*_{FCR_{kj}}(t) \end{aligned} \quad \textbf{(6.6)}$$

where $K_{FCR,kj} > 0$ is the frequency droop gain of the converter k with respect to converter j, $K_{FCR,jk} > 0$ is the frequency droop gain of the converter j with respect to converter k, f_k and f_j are the measured frequencies of these converters, $f_{k,nominal}$ and $f_{j,nominal}$ are the nominal frequencies of the synchronous zones to which converters k and j are connected respectively, and $P^*_{FCR\,kj}$ is the power reference sent to converter k due to the existing FCR control between it and converter j.

Frequency support can also be provided by stations connected to stored or renewable energy sources, but this is not specifically studied within the scope of this work. To determine which synchronous area should contribute to frequency support in priority in real-life operation, TSOs may be based on electricity market prices. This is not within the scope of this technical work either.

c. Comparison of the two FCR solutions

In the used benchmark, two solutions of frequency support are tested and compared (***Figure 6-3***).

To understand the impact of the FCR, the controller was solely implemented on the study benchmark. The case study is summarized in ***Table 6-3***.

Table 6-3: Case study for FCR.

Contingency	Gain of the FCR (MW / Hz)
Load increase at $L10$ (150 MW or 4.15 % of total nominal power in AC zone 1, at $t = 1$ s) leading to disequilibrium between production and consumption and heavily loaded AC tie lines.	750 (only converters connected to AC zone 1 are involved in the FCR service)

After the load increases, the frequency Nadir is the lowest in the case where no frequency support is implemented (***Figure 6-3.a***). Frequency deviation from nominal value (50 Hz) is then enhanced by adding local frequency droop control at the converters $S1$ and $S2$. However, with this control, the frequency support interacts with DC droop control and leads to a drop in DC voltage's steady state (***Figure 6-3.b***). To counteract the interaction with DC voltage control, the solution presented in section Chapter 6.II.2.iii.b was tested and the results ('Distributed FCR') show that the FCR's efficiency was increased compared to the 'Local FCR' case. The DC voltage is much less impacted by frequency support as well. In the following, this last FCR solution is used.

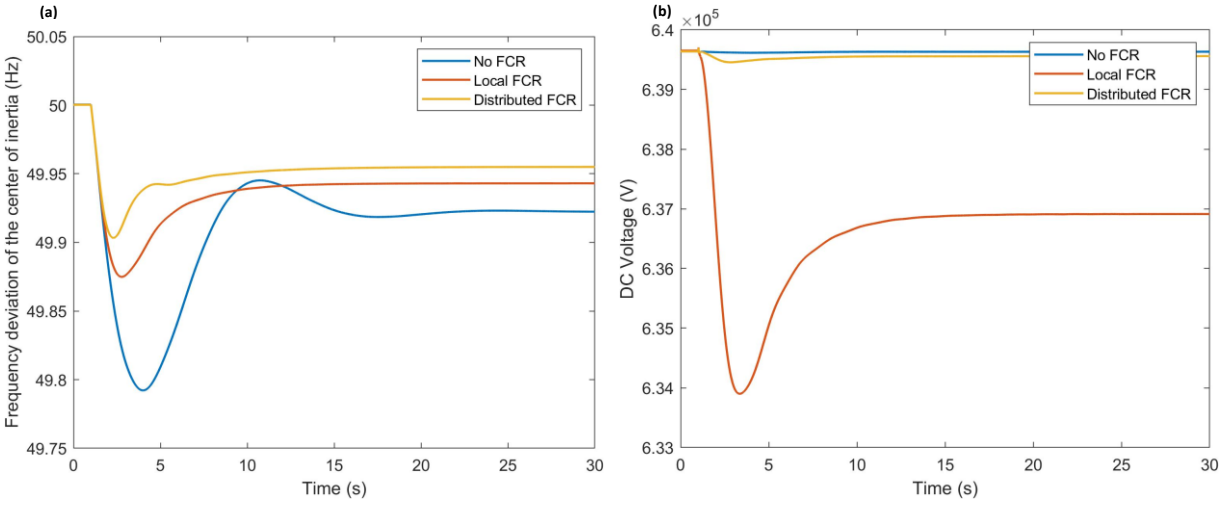

Figure 6-3: Frequency deviation to nominal frequency of the centre of inertia of disturbed AC zone 1 (a) and DC voltage variation (b) in the cases without FCR, with local droop-based FCR and distributed droop-based FCR.

III. A comparative study of control designs for multi-criteria stability enhancement

In the previous section Chapter 6.II, dedicated control structures were tested for each of the considered stability aspects individually. However, the combination of these controls is not straightforward at least due to the power constraints of the converters. In fact, it is not guaranteed that the direct combination of multiple ancillary services will result in stability enhancement. Instead, it can lead to competition between control outputs leading to antagonist effects (voltage vs frequency control) or cancellation of the control impact (POD vs FCR in case of converter's power saturation).

In most of the literature, the used approaches aim to design the control of one or two [109], [110], [111], [112] of the mentioned stability aspects. Here, a global approach is proposed to enhance the stabilities through a logical combination of the needed controllers.

Therefore, in this part, different strategies of control are evaluated. In the studies, the degrees of freedom offered by the control of MTDC system are explored. The system is, from an AC-DC perspective, constrained by the converters' power rating and their ability to inject/extract power (AC side saturation, DC lines rating, etc.). A coordination methodology to further enhance AC and DC stabilities is also proposed.

To perform the simulation studies, the perturbation scenario was chosen to solicit the control of multiple stability aspects simultaneously. A generation loss ($G4$) in right side of the AC zone 1 was the final choice since it excites interarea oscillations (POD need), increases angle differences on the boundaries of the AC intertie line (ADC need) and induces an unbalance between production and consumption (FCR need). DC voltage support is needed particularly in Case 3 (combination of different controllers without coordination) that will be shown hereby. In this work, communication between controllers is considered to be well-established in all the cases where ancillary services are implemented.

1. Ancillary services combination and case studies

The strategies to propose ancillary services by an MTDC Grid can be defined as per the targeted objectives: small-signal stability support, rotor angle support and frequency support.

The implementation of these services can be distinguished by their level of communication and their degree of coordination.

The coordination degree will be studied in section Chapter 6.III.22. Potential use cases are cited below:

- In the basic application, the HVDC system is only used for power dispatching alongside controlling the DC voltage to avoid HVDC grid from collapsing.
- Communication-free cases include controls based on local measurements like for frequency support tested in section Chapter 6.II.2.iii. A more detailed study of its interactions with DC voltage support was made in the paper [8] and its drawbacks were also shown.
- Communication-based cases make usage of WAMS either for rotor angle support [100], [113], [114] or frequency support too.

- Coordination is useful when multiple controls are implemented to propose better stability enhancement control schemes.

In the following, a comparative study is made between the stability enhancement strategies on the same comprehensive benchmark composed of two AC systems connected through a four-terminal meshed MMC-based MTDC system (***Figure 3-17***). The final aim is to define a coordination strategy between the ancillary services.

For each proposed ancillary service, the corresponding controller was tuned to individually with respect to AC and DC stability performances (oscillation damping, AC line emulation, frequency support with limited interaction with DC voltage control) for a maximal loss of 450 MW (a loss of 12.5 % of the total nominal power in the disturbed AC zone) on one side of the AC zone 1. For the considered simulation conditions, the implemented control gains are shown in the ***Table 6-4***. The ADC was designed to at least reduce by 50 % the steady state power deviation in the observed AC tie line (***Figure 6-4*** in next section Chapter 6.III.1.i). The POD was designed to damp the oscillations within 4 s after the contingency (***Figure 6-4*** in next section). The FCR was designed to deliver all a converter's nominal active power headroom (1 GW) for a frequency deviation of 0.5 Hz from the nominal value (50 Hz) constrained by the converter's remaining active power headroom.

Table 6-4: Contingency and parameters of the implemented controls for the study.

Contingency	Parameters of the ADC	Parameter of the POD	Parameter of each FCR droop	Parameter of DC voltage droop
Loss of $G4$ (450 MW or 12.5 % of total nominal power in AC zone 1, at $t = 1$ s	$K_{ADC} = 1005$ MW / ° $\tau_{ADC} = 5$ s	$K_{POD} = 2500$ MW / Hz	$K_{FCR} = 2000$ MW / Hz	$K_{V_{dc}} = 8$ MW / kV

A comparative study is made between different stability enhancement strategies. Each strategy consists of a combination of the studied controllers. The objective is to propose a coordination strategy between the multiple HVDC ancillary services to enhance global AC stability.

2. Comparative study and problem exposition

Through the case studies, the need of power coordination appears mostly when all the selected ancillary services coexist. The coordination strategy is proposed in the last case study.

Tests of stability enhancement strategies are the following:

- **Case 0** – Reference case w/o suppl. control.
- **Case 1** – w/ {POD}, w/o {ADC + FCR}: small-signal stability is only tackled.
- **Case 2** – w/ {ADC + POD}, w/o {FCR}: small-signal and rotor angle steady-state stabilities are tackled.
- **Case 3** – w/ {ADC + POD + FCR}: small-signal, rotor angle steady-state and frequency stabilities are tackled.
- **Case 4** – w/ {ADC + POD + FCR}, w/ coordination: same as Case 3 but in an enhanced way.

The selected physical quantities to compare are:

- Measured frequency deviation from nominal value (50 Hz) of each remaining machine in AC zone 1.

- Active power output of each converter.
- Active power flow at one AC tie line in AC zone 1 (line between Buses 7 and 8 in the AC zone 1). The observed tie line is mentioned in ***Figure 3-17***.
- DC voltage at converter $S2$.

i. Case 0 – Reference case w/o suppl. Control

After the contingency happens, the frequency of the remaining connected machines decreases as shown in ***Figure 6-5***. The frequency Nadir reaches 49.17 Hz while the frequency's steady-state value is 49.73 Hz. Interarea oscillations appear between $\{G1, G2\}$ and $\{G3, G5\}$. The power oscillations are of almost 150 MW in the observed AC tie line (***Figure 6-4***). The oscillations are damped after the PSSs in AC zone 1 return to their unsaturated working area (like the case shown in ***Figure 6-2.c***). In this reference case, the power outputs of the stations remain unchanged because no HVDC service is implemented.

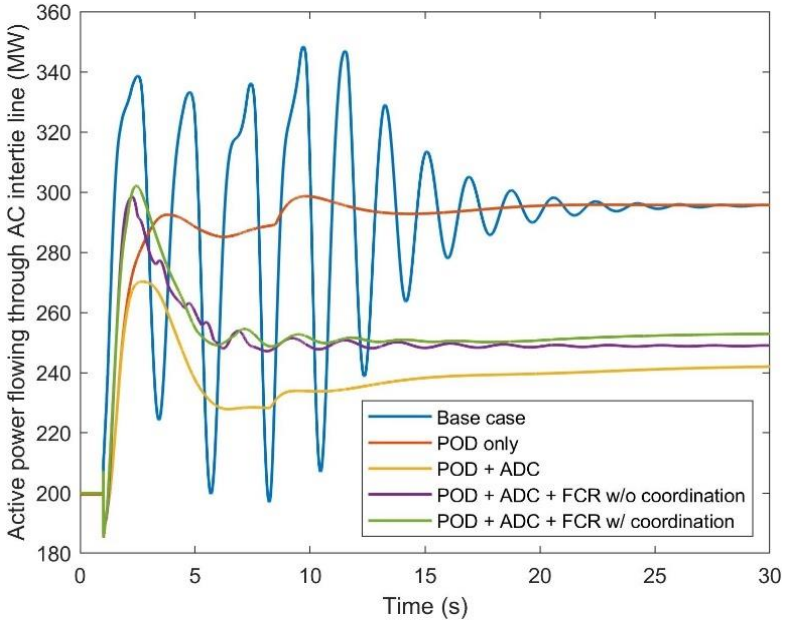

Figure 6-4: Active Power flowing through the observed AC tie line in different stability enhancement strategies.

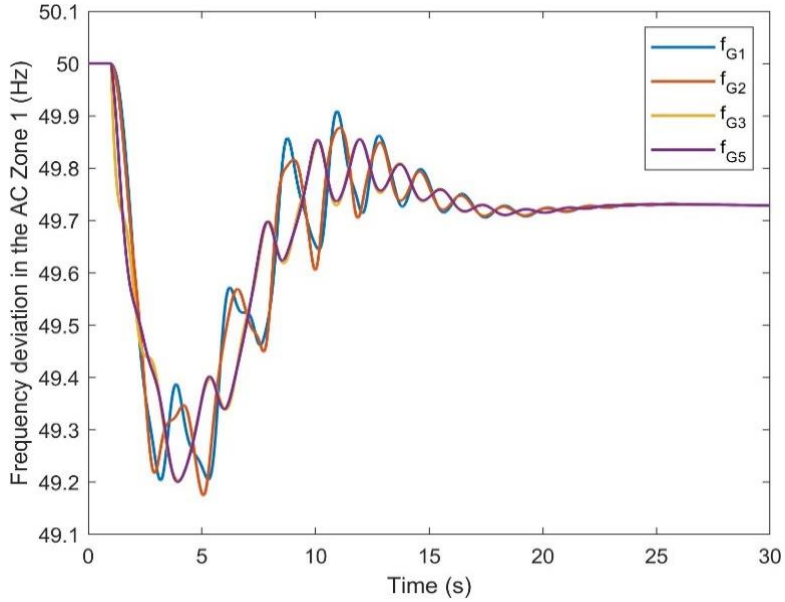

Figure 6-5: Frequency deviation from nominal value of the remaining connected generators in AC zone 1 in reference case. The group $\{G1, G2\}$ oscillates against the group $\{G3, G5\}$.

ii. Case 1 – w/ {POD}, w/o {ADC + FCR}

To efficiently damp the interarea oscillations, two POD controllers, each based on the frequency difference respectively between $S1$ and $S2$, and between $S3$ and $S4$, are added. The results in ***Figure 6-6*** and ***Figure 6-4*** show reduced oscillations amplitude and quicker damping time (4 s vs 25 s in Case 0). By design, when the interarea oscillations are totally damped, the active power outputs of the converters come back to initial values (at steady state) and therefore they are only modified during the disturbance (***Figure 6-7***). Although the small-signal stability was enhanced, the HVDC system can still propose new ancillary services to enhance frequency and rotor angle stabilities.

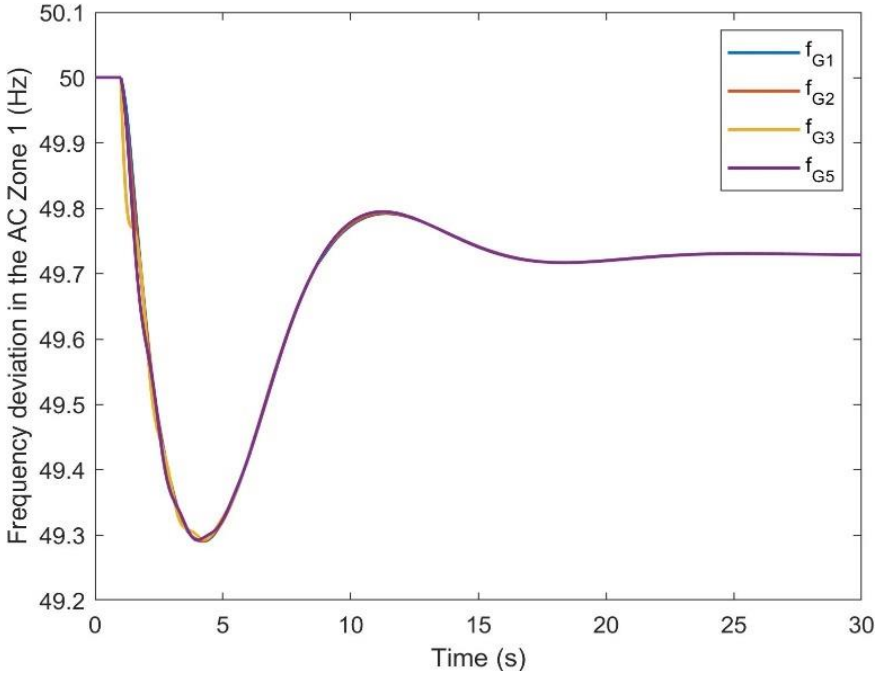

Figure 6-6: Frequency deviation from nominal value of the remaining connected generators in AC zone 1 after POD was added.

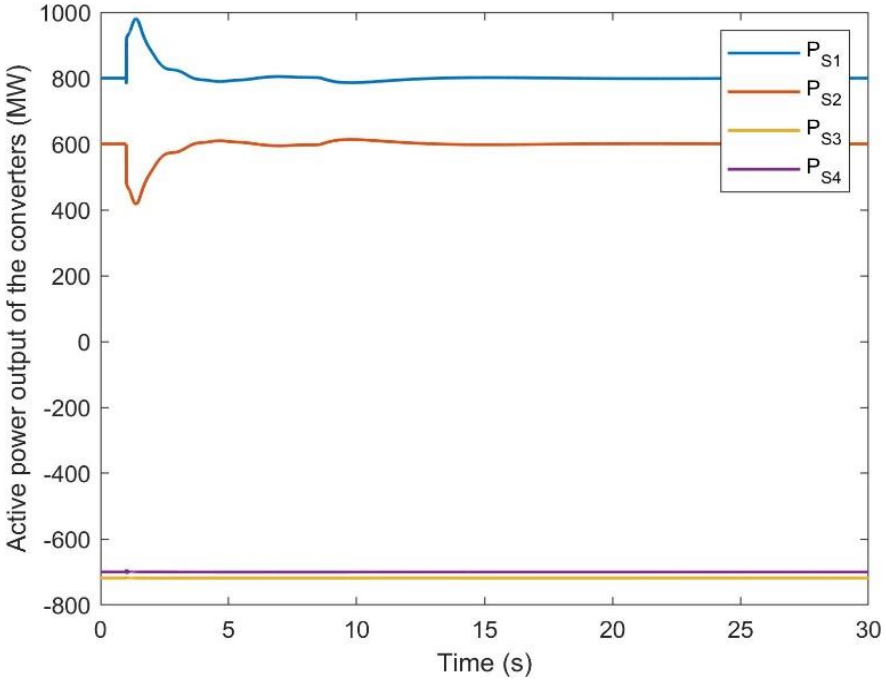

Figure 6-7: Case 1 – Active power output of the stations $S1$, $S2$, $S3$ and $S4$. In steady state, the converters' output returns to initial value after full damping of the oscillations.

iii. Case 2 – w/ {ADC + POD}, w/o {FCR}

In the previous case, the active power increase in each of the AC tie lines is relatively high (95 MW per line, 47.5 % of the initial value, ***Figure 6-4***). Consequently, in Case 2, DC system emulates AC lines thanks to the ADC that uses the measured electric angles at the PCCs.

This ADC control changes the steady-state power output of $S1$ by $+100$ MW and $S2$ for -100 MW (***Figure 6-8***). By transmitting power through the HVDC system, the AC tie lines are less loaded (42 MW per line, 21 % of the initial value, ***Figure 6-4***) and therefore less sensitive to tripping. The risk of system split in AC zone 1 is also reduced since the rotor angles difference at the boundaries of the observed tie line is decreased by the ADC. The DC voltage is almost unmodified since the same amount of active power is extracted from one area (left side) of the AC zone 1 and reinjected in the other area (right side) (***Figure 6-9***).

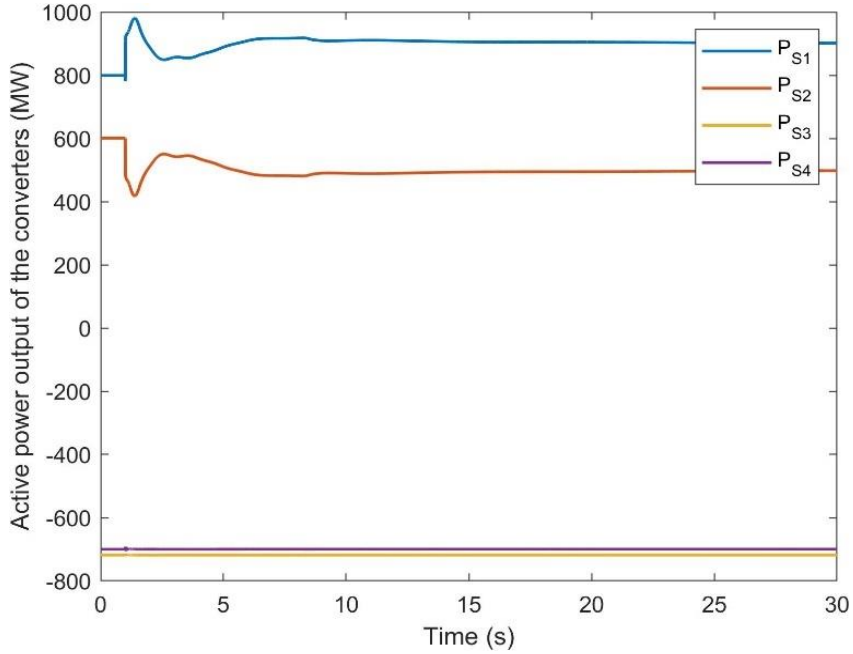

Figure 6-8: Case 2 – Active power output of the stations $S1$, $S2$, $S3$ and $S4$. In steady state, the converters' output is different from initial value since the angle difference is not zero.

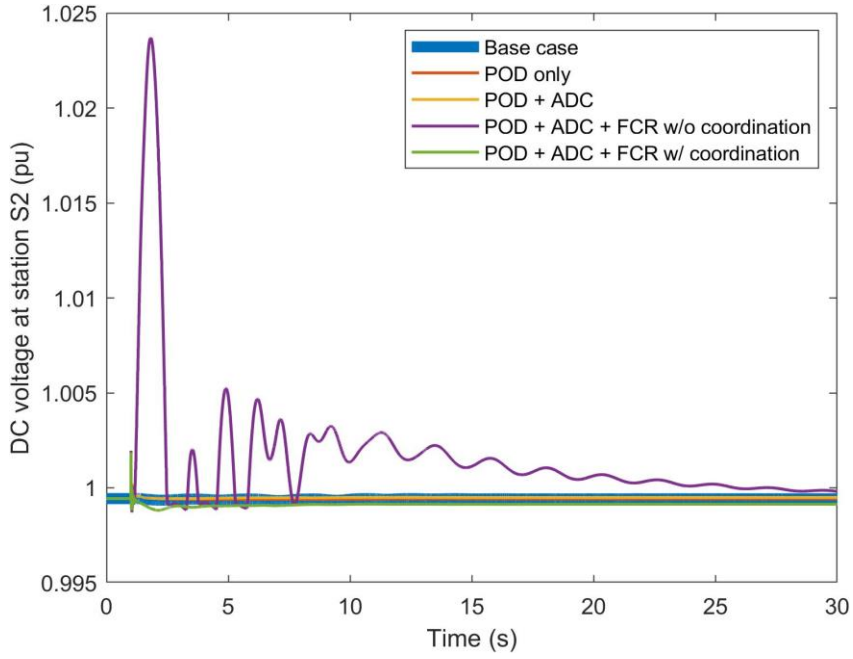

Figure 6-9: DC voltage at the DC terminal of station $S2$ in different stability enhancement strategies.

iv. Case 3 – w/ {ADC + POD + FCR}

To enhance frequency stability (in this thesis, deviation from nominal value at frequency Nadir, and steady state), FCR control layer was added to the control of MTDC system. The frequency deviations are shown in ***Figure 6-10***.

The FCR increases the frequency Nadir to $\mathbf{49.61}$ Hz which means a reduction of the deviation from the nominal frequency ($\mathbf{50}$ Hz) by $\mathbf{47}$ % compared to the value in Case 0. The steady state value of the frequency is $\mathbf{49.85}$ Hz which corresponds to an enhancement by $\mathbf{56}$ % as per the same base case.

Nevertheless, although the FCR helps desaturate the PSS more quickly, the interarea oscillations between $\{\boldsymbol{G1}, \boldsymbol{G2}\}$ and $\{\boldsymbol{G3}, \boldsymbol{G5}\}$ reappear. To explain this phenomenon, the power exchanged by the converters with AC sides are plotted in ***Figure 6-11***. During the disturbance, station $\boldsymbol{S2}$ can effectively extract the necessary amount of power at the PCC to damp the oscillations while, due to the combined action of the FCR, station $\boldsymbol{S1}$ is only able to inject limited damping power at its PCC. This is due to the limitation of the output of the converters that prevents the area of $\{\boldsymbol{G1}, \boldsymbol{G2}\}$ from receiving the needed power. Therefore, as shown in ***Figure 6-10***, oscillations are less damped – in amplitude and duration – than when small-signal stability was individually enhanced by the POD (Case 1, ***Figure 6-6***).

Moreover, with POD control, since the station $\boldsymbol{S1}$ injects in AC system less active power (due to $\boldsymbol{S1}$'s saturation) than station $\boldsymbol{S2}$ extracts from it, the DC voltage increases slightly in HVDC system ($\mathbf{2.4}$ %, ***Figure 6-9***).

In conclusion, although the POD and the FCR inject power in the same direction at $S1$, they interact in an antagonist way during disturbance due to the existing power constraints of the converter station. Their interaction also decreases the DC voltage stability. Therefore, a coordination strategy is needed at least between these two controls to limit or prevent antagonist effects from happening.

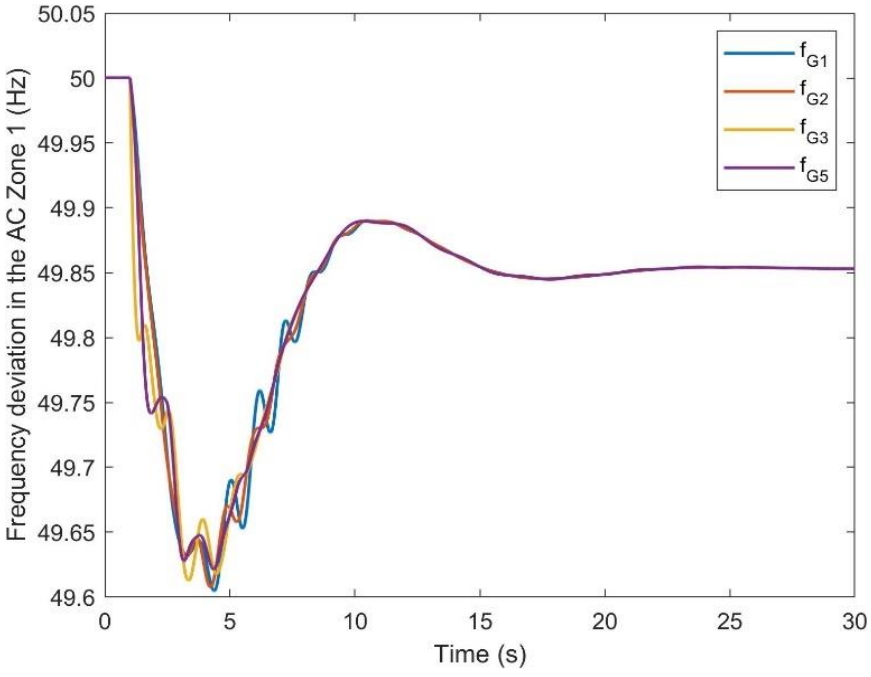

Figure 6-10: Frequency deviation from nominal value of the remaining connected generators in AC zone 1 after POD, ADC and FCR were added to the control of the MTDC.

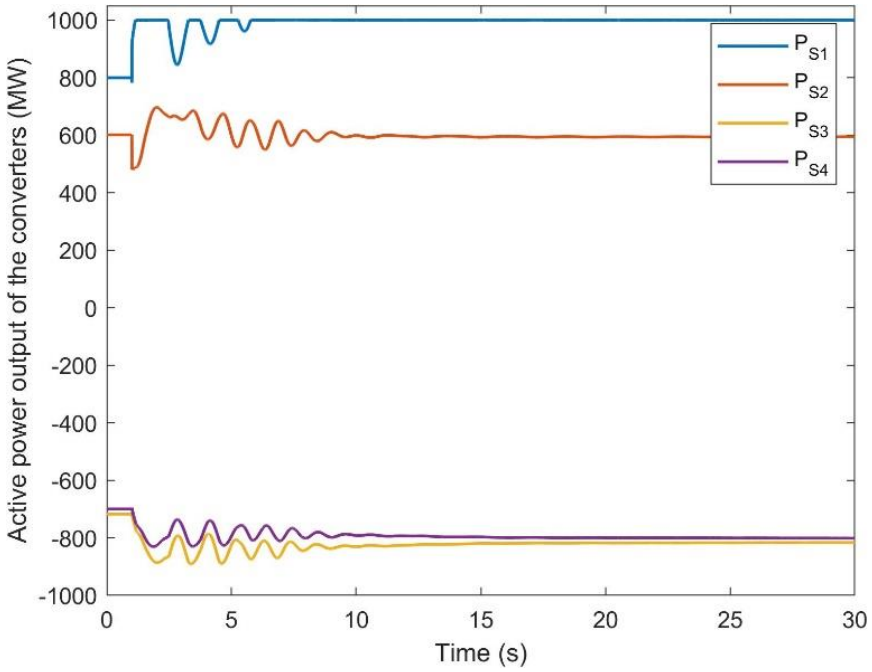

Figure 6-11: Case 3 – Active power output of the stations $S1$, $S2$, $S3$ and $S4$. Saturation appears at $S1$, which creates competition between POD (small-signal stability) and FCR (frequency stability) during the transient phase.

v. Coordination strategy and Case 4 – w/ {ADC + POD + FCR}, w/ coordination

a. Proposed coordination strategy

In the following, a conservative but secure strategy is proposed for the coordination of the different HVDC ancillary services from an AC/DC Power System perspective.

1. Headroom fragmentation and allocation

When implemented, each ancillary service sends an active power control reference to the converter which may be able to fulfil it or not depending on its remaining headroom. This means that all the services share the same remaining headroom and, if the tuning of the control parameters (gains and time constants of the filters) is not updated regularly, one or more control(s) will saturate the involved converter, leaving less or no room for other control references. This was the issue in Case 3 since control parameters were not changed during simulation.

However, regular retuning of the parameters of POD, ADC and FCR is not common since the parameters of the converters' controllers are usually calibrated depending on the operating conditions of the grid as is the case of Hydro Quebec and RTE [115], [116]. For the sake of research, the solution of parameter retuning was tested for the benchmark and the available results showed enhancement of the mentioned stabilities, but the work presented in this thesis aims to propose a solution that avoids regular proportional gain retuning.

The idea in this thesis is to propose a solution that guarantees that each control power reference is accomplished without changing the gains and time constants of the controllers too frequently. To do so, the concept of headroom fragmentation was developed. To secure the correct operation of the controllers

corresponding to the proposed ancillary services (POD, ADC and FCR in this case), the remaining headroom of the contributing converters was fragmented and allocated to different services before the occurrence of any contingency. This compartmentation within the constrained remaining headroom ensures that no controller dominates another one when the contingency happens. It consequently allows the TSO to decide on how the ancillary services will be allocated by the HVDC system for a given power flow and most credible contingency scenarios.

Practically, for each service, a controller is implemented, and pairs of converters are used to transfer the power sent by the controller's references. To conserve power balance in the MTDC system, the power reference sent to a converter k is sent the same but in opposite direction to the converter j of the pair kj of converters used for a given control. A 'virtual link kj' corresponds to a control (ADC, POD or FCR in this thesis) operating in the pair of converters kj where effort is made by converter k. The 'virtual link' is specifically created between these converters to transfer the needed power between them. The mentioned 'headroom per service' of the previous paragraph can be interpreted as virtual link saturation. Paradoxically, to enhance the global stability of an AC/DC system, each of these links should have an upper and lower limit. This prevents a given control from dominating the others so that the correct operation of all controllers is ensured.

The mathematical formulation of the previous functioning of control and the mathematical foundation of the proposed headroom allocation concept are presented in the following. For the sake of clarity, only power injection and ancillary services (no DC voltage control) are considered in the control scheme.

For a system composed of a set $\mathcal{N}$ of N AC/DC converters, the following is the active power reference sent to converter k, $\forall k \epsilon \{1, .., N\}$:

$$P^*_{conv_k} = P^0_{conv_k} + \sum_{j=1}^{N} P^*_{ADC,kj} + \sum_{j=1}^{N} P^*_{POD,kj} + \sum_{j=1}^{N} P^*_{FCR,kj} \quad \textbf{(6.7)}$$

which can be reduced to:

$$P^*_{conv_k} = P^0_{conv_k} + \sum_{j \in \mathcal{S}_k} P^*_{ADC,kj} + \sum_{j \in \mathcal{S}_k} P^*_{POD,kj} + \sum_{j \in \mathcal{A}_k} P^*_{FCR,kj} \quad \textbf{(6.8)}$$

where:

- $P^0_{conv_k}$ is the active power reference sent by power dispatch (initial power before any contingency),
- $P^*_{ADC,kj}$ is the active power reference sent to converter k by the ADC implemented between converters k and j (check equations **(6.3)** and **(6.4)**). If no ADC is implemented between these converters, the corresponding gain $K_{ADC,kj}$ is set to 0,

- $P^*_{POD,kj}$ is the active power reference sent to converter k by the POD implemented between converters k and j (check equation **(6.5)**). If no POD is implemented between these converters, the corresponding gain $K_{POD,kj}$ is set to 0,
- $P^*_{FCR,kj}$ is the active power reference sent to converter k by the FCR implemented between converters k and j (check equation **(6.6)**). If no FCR is implemented between these converters, the corresponding gain $K_{FCR,kj}$ is set to 0,
- $\mathcal{N}$ is the set of AC/DC converter index connected considered in the HVAC/HVDC system,
- $\mathcal{S}_k$ is the set of converter index connected to the same synchronous zone as converter k,
- $S_k = cardinality(\mathcal{S}_k)$ is the number of elements in $\mathcal{S}_k$. If a converter $j \epsilon \mathcal{S}_k$ does not contribute to the ADC (respectively POD), the corresponding gain $K_{ADC,kj}$ (respectively $K_{POD,kj}$) is set to 0,
- $\mathcal{A}_k$ is the set of converter index connected to a different synchronous zone from converter k,
- $A_k = cardinality(\mathcal{A}_k)$ is the number of elements in $\mathcal{A}$. If a converter $j \epsilon \mathcal{A}_k$ does not contribute to the FCR, the corresponding gain $K_{FCR,kj}$ is set to 0.

Before headroom fragmentation, the control law of the converter k was constrained as:

$$P^{min}_{conv_k} \leq P^*_{conv_k} \leq P^{max}_{conv_k} \quad \textbf{(6.9)}$$

where $P^{min}_{conv_k}$ and $P^{max}_{conv_k}$ are respectively the lower and upper rated power of converter k.

The equations **(6.8)** and **(6.9)** give:

$$P^{min}_{conv_k} - P^0_{conv_k} \leq \sum_{j \in \mathcal{S}_k} P^*_{ADC,kj} + \sum_{j \in \mathcal{S}_k} P^*_{POD,kj} + \sum_{j \in \mathcal{A}_k} P^*_{FCR,kj} \leq P^{max}_{conv_k} - P^0_{conv_k} \quad \textbf{(6.10)}$$

The headroom $[P^{min}_{conv_k} - P^0_{conv_k}\ ;\ P^{max}_{conv_k} - P^0_{conv_k}]$ is commonly shared between the different ancillary services controllers. This was the case shown in section Chapter 6.III.2.iv and the results showed degraded global stability as was explained before.

To cope with this issue, headroom fragmentation and allocation per virtual link are proposed as the following equations show. Since ADC and POD act on decoupled timescales, their headrooms can be shared as it will be shown below. Since the FCR may be active during disturbances and at steady state, its headroom is separated from that of the ADC and POD.

In the following, the power reference sent by a controller to a given pair of converters kj is noted $P^*_{virtual\ link,kj}$ where the 'virtual link' corresponds to 'ADC', 'POD' or 'FCR'. The set of virtual links is noted $\mathcal{V} = \{'ADC', 'POD', 'FCR'\}$.

The sum of all possible virtual links $v\epsilon\mathcal{V}$ corresponding to the pair kj with the converters $j\epsilon\mathcal{N}\backslash\{k\}$ is noted as $\Delta P^*_{conv_k,tot}$:

$$\Delta P^*_{conv_k,tot} = P^*_{conv_k,tot} - P^0_{conv_k} = \sum_{v\epsilon\mathcal{V}}\sum_{j=1}^{N} P^*_{v,kj} = \sum_{j\in\mathcal{S}_k} P^*_{v,kj} + \sum_{j\in\mathcal{A}_k} P^*_{v,kj} \quad \textbf{(6.11)}$$

where $P^*_{v,kj}$ corresponds to the power reference sent to station k by the virtual link v that connects it with station j.

To distinguish between power injection and extraction, two headroom zones (above and below $P^0_{conv_k}$) within the total headroom of the considered converter k are separated for fragmentation and allocation. For each virtual link v corresponding to a control ({ADC and/or POD} or FCR) implemented between the converter k and j, the headroom fragmentation is designed as the following:

- Fragmentation of the remaining headroom above $P^0_{conv_k}$:

$$\begin{cases} P^{min}_{v,kj} = 0 \leq P^*_{v,kj} \leq P^{max}_{v,kj} \\ P^{max}_{v,kj} = -P^{min}_{v,jk} \end{cases} \quad \textbf{(6.12)}$$

  where:

  - $P^*_{v,kj}$ is the power reference sent to converter k by the virtual link v corresponding to a controller ({ADC and/or POD} or FCR) implemented between converters k and j.
  - $P^{max}_{v,kj}$ and $P^{min}_{v,kj}$ are respectively the upper and lower limits (check section Chapter 6.III.2.v.a.2 for value definition) of the power flowing through the virtual link v for the pair of converters kj considered at station k.
  - $P^{min}_{v,jk}$ is the lower limit considered for the same virtual link v, kj considered at station j.

  This means that the power reference $P^*_{v,kj}$ sent to converter k through the virtual link kj is limited within the range $[0; P^{max}_{v,kj}]$ (first part of equation **(6.12)**) which must be identical but in opposite direction at the level of converter j (second part of equation **(6.12)**).

- Fragmentation of the remaining headroom below $P^0_{conv_k}$:

$$\begin{cases} P^{min}_{v,kj} \leq P^*_{v,kj} \leq 0 = P^{max}_{v,kj} \\ P^{min}_{v,kj} = -P^{max}_{v,jk} \end{cases} \quad \textbf{(6.13)}$$

  This means that the power reference $P^*_{v,kj}$ sent to converter k through the virtual link kj is limited within the range $[P^{min}_{virtual\ link,kj}; 0]$ (first part of equation **(6.13)**) which must be identical but in opposite direction at the level of converter j (second part of equation **(6.13)**).

The second part of equation **(6.12)** and equation **(6.13)** refers to the needed symmetry in the considered headrooms. Even if the converters are not identical, the following conditions should be satisfied for all pairs kj of converters to guarantee power balance in DC system: $P_{v,kj}^{max} = -P_{v,jk}^{min}$ and $P_{v,kj}^{min} = -P_{v,jk}^{max}$.

With the fragmentation (equations **(6.12)**, **(6.13)**), the following headroom is allocated per virtual link v:

$$P_{v,kj}^{min} \leq P_{v,kj}^{*} \leq P_{v,kj}^{max} \tag{6.14}$$

where $P_{v,kj}^{min} = 0$ if v operates in the headroom above $P_{conv_k}^{0}$, and $P_{v,kj}^{max} = 0$ in the opposite case.

With **(6.14)**, the sum of all headrooms (respectively above and below $P_{conv_k}^{0}$) is given by:

$$\begin{cases} \sum_{v\epsilon\mathcal{V}} \sum_{j=1}^{N} P_{v,kj}^{max} = \sum_{v\epsilon\mathcal{V}} \left(\sum_{j\in\mathcal{S}_k} P_{v,kj}^{max} + \sum_{j\in\mathcal{A}_k} P_{v,kj}^{max} \right) = \sum_{v\epsilon\mathcal{V}} \sum_{j\in\mathcal{S}_k} P_{v,kj}^{max} + \sum_{v\epsilon\mathcal{V}} \sum_{j\in\mathcal{A}_k} P_{v,kj}^{max} \\ \sum_{v\epsilon\mathcal{V}} \sum_{j=1}^{N} P_{v,kj}^{min} = \sum_{v\epsilon\mathcal{V}} \left(\sum_{j\in\mathcal{S}_k} P_{v,kj}^{min} + \sum_{j\in\mathcal{A}_k} P_{v,kj}^{min} \right) = \sum_{v\epsilon\mathcal{V}} \sum_{j\in\mathcal{S}_k} P_{v,kj}^{min} + \sum_{v\epsilon\mathcal{V}} \sum_{j\in\mathcal{A}_k} P_{v,kj}^{min} \end{cases} \tag{6.15}$$

At this stage, all virtual links are constrained by lower and upper limits. However, another condition on the sum of headrooms should be respected to avoid control interactions. While in **(6.10)** the converter's remaining headroom is shared between the power references of the controllers, the approach to avoid control interaction is to share the converter's remaining headroom between the allocated headrooms of each virtual link.

Therefore, the following must be applied $\forall k\epsilon\mathcal{N}$ using equation **(6.15)**:

$$\begin{cases} \sum_{v\epsilon\mathcal{V}} \sum_{j=1}^{N} P_{v,kj}^{max} \leq P_{conv_k}^{max} - P_{conv_k}^{0} \\ \sum_{v\epsilon\mathcal{V}} \sum_{j=1}^{N} P_{v,kj}^{min} \leq P_{conv_k}^{min} - P_{conv_k}^{0} \end{cases} \tag{6.16}$$

If converters are identical or at least allow for symmetrical remaining total headrooms before fragmentation, the inequalities in **(6.16)** become equalities.

Finally, with equations **(6.14)**, **(6.15)** and **(6.16)**, at the converter k, the sum of all possible power references of the virtual links $v\epsilon\mathcal{V}$ with the converters $j\epsilon\mathcal{N}\backslash k$ are constrained by the sums of upper and lower limits of the headrooms which are in turn limited by the total remaining headroom of k-th converter:

$$P_{conv_k}^{min} - P_{conv_k}^{0} \leq \sum_{v \epsilon \mathcal{V}} \sum_{j=1}^{N} P_{v,kj}^{min} \leq \Delta P_{conv_k,tot}^{*} \leq \sum_{v \epsilon \mathcal{V}} \sum_{j=1}^{N} P_{v,kj}^{max} \leq P_{conv_k}^{max} - P_{conv_k}^{0} \quad \textbf{(6.17)}$$

2. Coordination of headroom

The headroom fragmentation and allocation per virtual link presented in the previous paragraph requires coordination which solves the following problem: what exact values should be given for the upper and lower limits of the allocated headroom per service to enhance the global stability of the AC/DC power system compared to the Case 3 (Chapter 6.III.2.iv) with common headroom?

To solve this issue, coordination is realized following these two rules:

- The headroom of {ADC+POD} are defined before the ones of the FCR since AC system split should be avoided in priority to maintain synchronism within the same AC zone. In fact, synchronous AC zones are usually equipped with frequency primary and secondary reserves which are designed for the worst frequency contingency (e.g., loss of 3 GW generation within CE synchronous zone AC system [117]). Consequently, after designing headroom for {ADC+POD} services, if the HVDC system can still offer FCR services, the remaining headroom is used for it.

- To calculate the headroom for {ADC+POD}, a heuristic approach is adopted for a given power flow and a given worst case contingency scenario. It is explained in the following. The simulation results which show the required amount for ADC and/or POD per converter are used to implement the upper and lower limits of the virtual links as defined in section Chapter 6.III.2.v.a.1. Practically, a trade-off between the amounts of allocated headroom per controller should be found in order to simultaneously enhance the different stability aspects of the hybrid AC/DC system. In this thesis, the trade-off is found by sweeping headroom parameters in the simulation environment with headroom values around the actual power references sent by ADC, POD and FCR. An optimization-based approach could be adopted for a better trade-off.

The section Chapter 6.III.2.v.b describes how headroom fragmentation, allocation and coordination was realized for this study Case 4 using the benchmark presented in ***Figure 3-17***.

b. Case 4 – w/ {ADC + POD + FCR}, w/ coordination

In this case, the headrooms of the stations $\{S1, S2, S3, S4\}$ are represented in the ***Figure 6-12*** (bar plots).

Around initial power flow value (***Figure 6-12***), POD and ADC actions have fixed headrooms. The remaining headroom of each station is allocated for FCR. FCR exists between the "virtual links" $S1-S3$, $S1-S4$, $S2-S3$ and $S2-S4$: when one converter of a couple extracts power from an AC zone, the other injects same amount in the other synchronous AC zone of the benchmark. The FCR headroom allocation is arbitrarily chosen equal between $S1-S3$ and $S1-S4$ from one side, and $S2-S3$ and $S2-S4$ from the other side (see blue block in ***Figure 6-12***).

With the two-rules approach described in the section Chapter 6.III.2.v.a.2, for Case 4, the allocated headroom ***ranges*** (not 'headrooms') calculated for the used power flow and the previously defined contingency scenario are mentioned in **Table *6-5*** which is explained below. Since the explicit values are headroom ranges and not direct headrooms, the positive values in this table are affected to headroom ranges above the absolute zero value of the converters and negative range values are affected to headroom ranges below this absolute zero.

Table 6-5 : Coordinated headroom allocation (in solicited zone) per actual virtual link.

Station	Control	Allocated headroom range (MW)
S1	$[\mathrm{POD} + \mathrm{ADC}]_{12}$	$[0; 125]$
	$\mathrm{FCR}_{13} + \mathrm{FCR}_{14}$	$[0; 37.5] + [0; 37.5]$
S2	$[\mathrm{POD} + \mathrm{ADC}]_{21}$	$[-125; 0]$
	$\mathrm{FCR}_{23} + \mathrm{FCR}_{24}$	$[0; 137.5] + [0; 137.5]$
S3	$[\mathrm{POD} + \mathrm{ADC}]_{34}$	$[0; 125]$
	$\mathrm{FCR}_{31} + \mathrm{FCR}_{32}$	$[-37.5; 0] + [-137.5; 0]$
S4	$[\mathrm{POD} + \mathrm{ADC}]_{43}$	$[-125; 0]$
	$\mathrm{FCR}_{41} + \mathrm{FCR}_{42}$	$[-37.5; 0] + [-137.5; 0]$

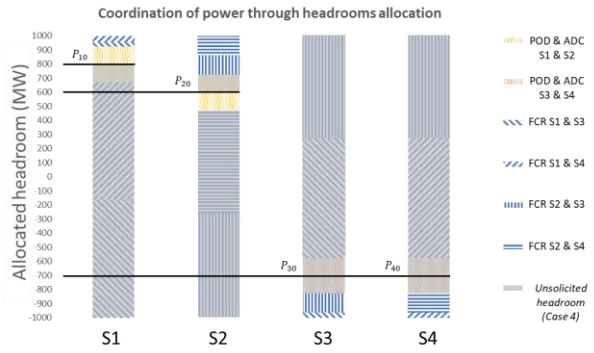

Figure 6-12: Coordinated headroom allocation between all stations and per virtual link.

The power references at S1 of POD and ADC are of $\sim$175 MW and $\sim$100 MW as per ***Figure 6-7*** and ***Figure 6-8*** respectively. ADC and POD will be combined in a single dedicated headroom since they operate at different time scales. Therefore, the maximal power reference for {ADC + POD} is of 175 MW at S1. Nevertheless, if $\pm$175 MW value is considered for headroom allocation at $S1$ of virtual link {ADC + POD} between converters $S1$ and $S2$, the remaining maximal headrooms for FCR will be 25 MW and 225 MW for $S1$ and $S2$ respectively. This amount is not sufficient for frequency stability support since the Nadir of frequency still needs to be increased. A variation of the headrooms by sweeping their values is made to reach an acceptable trade-off between rotor angle, small-signal and frequency stability. This trade-off is reached by affecting $\pm$125 MW of maximal headroom for {ADC + POD} at $S1$ and $S2$ (and $S3$ and $S4$ also) and the remaining for FCR (75 MW at $S1$, 275 MW at $S2$, $-$175 MW at $S3$ and $-$175 MW at $S4$). The approach used (parameter sweep) is heuristic since it is based on simulations (checking if stability aspects are enhanced or not consistently deteriorated with trial and error, starting with virtual link headroom values around the ones sent by the reference of each

controller) and it is not yet optimized. A better trade-off could be found, and this is a next step in the elaboration of the active power coordination strategy.

By fixing these headrooms per service, the action of each of them should theoretically be correctly realized and therefore the global stability of the AC/DC system enhanced compared to Case 3.

To verify this, the simulation results of Case 4 (with coordination) are shown in ***Figure 6-4*** (AC line power), ***Figure 6-9*** (DC voltage) and ***Figure 6-13*** (frequency deviation).

Three observations corresponding to global stability enhancement can be made:

- The frequency oscillations are totally damped after 4 s of the contingency (vs 9 s in Case 3, ***Figure 6-10***) and their amplitude is reduced (***Figure 6-10*** vs ***Figure 6-13***).
- DC voltage is also enhanced since its variation is reduced compared to Case 3 (***Figure 6-9***).
- Steady-state AC power flowing through the observed tie-line is only increased by 4 MW compared to Case 3 (***Figure 6-4***). This still is an enhancement compared to the cases without ADC.

In conclusion, through the proposed coordination strategy between multiple ancillary services, the global stability of the proposed benchmark is enhanced.

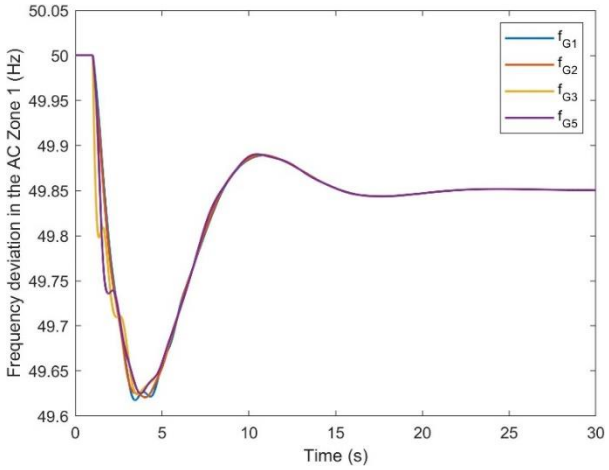

Figure 6-13: Frequency deviation from nominal value of the remaining connected generators in AC zone 1 after POD, ADC and FCR were implemented to the control of the MTDC with the proposed coordination strategy.

IV. Conclusion

This chapter focuses on the stability aspects related to rotor angle steady-state, small-signal interarea oscillations, frequency, and DC voltage. To regulate these aspects, HVDC functionalities were implemented. Respectively, AC line emulation through the regulation of angle difference measured at PCC, power oscillation damping by measuring frequency difference at PCC, frequency containment reserve deployment through distributed power references, and DC voltage droop control. These functionalities (except for DC voltage control) are called ancillary services by HVDC system since they are added to the main functionality of power dispatch affected to this system.

Each ancillary service was tested and validated individually on a proposed comprehensive benchmark power system composed of two separate AC systems (each inspired by 'Kundur' two-area system) connected through a four-terminal MTDC. The functionalities of the HVDC were solicited by different disturbances, each corresponding to a pre-established contingency scenario: AC line trip, load increase and generator trip. The implemented controllers were designed to reduce these potential interactions: POD vs ADC (by tuning the low-pass filter of the ADC) and FCR vs DC voltage droop (by implementing an FCR solution that aims to guarantee power balance in MTDC system).

To evaluate the effectiveness of the implemented controls, different indicators were proposed and used: duration and amplitude of oscillations (for small-signal stability), steady-state deviation of active power flowing through AC tie-line (for rotor angle stability), DC voltage deviation from initial value (during transient), and frequency deviation from nominal value at Nadir and steady-state.

After validation, the ancillary services were combined through different control strategies. A comparative study (using a given initial power flow and generator trip as contingency scenario) showed that the converters' intrinsic active power constraint created control interactions. These should be avoided to deploy the ancillary services more effectively, i.e., to better enhance the AC system's global stability.

A control strategy considering the multiple stability aspects problem was proposed and tested in the current work. It is based on a combination of known control loops (ADC, POD, FCR, DC voltage droop) and involves the converters' headroom fragmentation and allocation. Afterwards, the amount of headroom to allocate per ancillary service was coordinated between the mentioned controllers to further enhance AC/DC hybrid system's stability compared to the case without coordination of headroom. All this process was mathematically formulated and shown through a picture of the headroom allocation in a separate case study.

Through simulation analysis, stability indicators showed that the proposed coordination strategy enhanced global AC/DC stability. The coordination of headroom was based on a tradeoff between these indicators that the used controllers aim to enhance. The tradeoff was proposed in a heuristic approach but in the future works, an optimization-based approach can be used to find the best headroom coordination. The research focus will be based on developing this optimal approach and on enhancing stability in multiple power flow and contingency scenarios.

Chapter 7 : Optimization of the HVDC control for AC/DC stability enhancement

I. Introduction

1. Context

In the previous Chapter 5 and Chapter 6, two different approaches were presented. They are based on active power control coordination to enhance the stability of an AC/DC power system. In fact, the studies unveiled the potential interactions between the different HVDC implemented controllers that propose ancillary services for the AC systems. To tackle this issue, power coordination was proposed through active power reallocation and through headroom allocation.

In this chapter, the aim is to go further than the proposed approaches that proved the effective enhancement of the AC/DC power systems' stability aspects. The optimality of the proposed controllers was, however, not guaranteed. The objective, in this chapter, is to propose an optimization approach to better tune the parameters of the HVDC controllers in order to have a higher stability enhancement.

To clarify, the aim of the thesis was to propose a controller that tackles multiple stability aspects simultaneously to enhance the global AC/DC power system's stability using active power control of the AC/DC converters. This chapter aims to add a layer on the proposed approaches, which corresponds to the proposition of one possible control optimization approach.

The objective in this chapter is therefore to contribute to the potential optimization approaches and formulate the mathematical problem to solve if optimization was to be included in HVDC control design.

2. Organization of the chapter

The chapter is organized as follows: in section IIII, the different optimization approaches are presented and the problem is mathematically formulated. The results are then shown in this same section.

II. Optimization approach

1. Types of optimization problems

When not trivial, optimization problems require a mathematical formulation with one or multiple objectives to optimize. The aim of optimization is to minimize a defined "cost function" or "objective function" to reduce a risk, a cost, a dimension, etc. To mathematically formulate the optimization problem through a cost function, three main elements need to be defined: the objective to minimize/maximize, the decision variables and the constraints of the problem.

Before formulating the optimization problem, some elements need to be identified. They are listed in the following parts of this section.

i. Continuous or discrete [118]

Usually, a discrete optimization problem is a set of continuous optimization sub-problems, with the final aim to decide if a permutation should be applied or find an optimal graph within a given set of elements.

A continuous optimization problem aims, within a given continuous space of variables, to find a solution for a given problem using continuous optimization algorithms.

In this thesis, the objective is to optimize control parameters of a power system for a given initial power flow and a given perturbation scenario. Although it is not yet possible to formulate the optimization problem in this section, it is to note that the control parameters are considered to evolute within a continuous space of values with upper and lower limits. This characterizes the optimization problem as a continuous one.

ii. Constrained or unconstrained [119], [120], [121]

Optimization problems are either formulated with constraints on the used variables (like upper and lower headroom limits of a power converter) or without any constraint. In the former case, the mathematical expression of the optimization problem must explicitly include the constraints in the cost function as a distinct part of it. In the latter case, the object to study may have natural constraints but the cost function may not include them as so. In fact, the constraints may be included in the cost function as a penalty to the objective to optimize. The amplitude of the penalty should be relatively high when the calculation of the cost function is applied for a range of variables near the constraints or when these are violated.

Constraints may be of different natures depending on the limitation: linear range of values, non-linear range, differentiability of a function, convexity of a function, etc.

In this thesis, the problem is naturally constrained by the physical limits of the components of the power system. These constraints will be studied in detail in the section Chapter 7.II.2.

iii. Deterministic or stochastic [122], [123]

In some cases, the data of the studied object is fully and precisely known. In these cases, the optimization problem is deterministic in its nature. In other cases, like in metrology, some uncertainties exist, and these may be included in the mathematical expression of the cost function to optimize. In these cases, a stochastic optimization problem is studied.

When the mathematical model of a system can be clearly and completely defined, the optimum can be calculated through a deterministic approach. Oppositely, it may not be possible to use such an approach for black-box type problems or when influent uncertainties exist [124].

In this thesis, measurement data is considered to be fully known and precise and all the constraints are fully known as well. However, the relationship between stability KPIs (computed based on measured data) and control tuning cannot be straightforwardly defined. The optimization problem is therefore more of a black-box type problem and metaheuristics (stochastic) approaches are more adapted to it.

Examples of deterministic approaches exist in [125]. While deterministic approaches guarantee the reach of an optimum within a finite calculation time, stochastic approaches [122] guarantee this when calculation time is infinite. Therefore, for a finite computational duration, a stochastic approach gives "probably" the global optimum of a problem.

A taxonomy of various optimization techniques is available in the diagram in [126].

iv. Single or multi-objective

A multi-objective optimization problem arises when contradictory and/or incomparable objectives need to be optimized. Such a problem can be reduced to a single objective one to decrease the difficulty of solution calculation. In fact, it is possible to aggregate the various objective functions in a single one through a ponderation of a normed per unit sum of different objectives to minimize. The higher the ponderation of a term in the mentioned sum, the higher the priority of the term in the optimum calculation.

For multi-objective type optimization problems, the Pareto Front technique allows to find a curve tangent to the different 'costs' to minimize. The trade-off between the different objectives belongs therefore to this curve.

In this PhD thesis, to further enhance the multiple stability aspects of a power system, the optimal tuning of multiple controllers used simultaneously was tested. It is a multi-objective problem that was reduced to a single objective one through the sum of the different elements to minimize.

2. Mathematical formulation of the optimization problem

The previous section concludes that the problem is of type continuous, constrained, stochastic and multi-objective but reduced to a single objective problem. This will be explained further in this section.

The objective to reach in this section is a simultaneous enhancement of the multiple stability aspects considered in the thesis. To evaluate these stability aspects, the following KPIs are calculated through time-domain simulations:

- For DC voltage: voltage Nadir deviation from nominal value, called $Nadir_{V_{DC}\,max}$,
- For frequency: maximal frequency Nadir deviation from nominal value called $Nadir_{f\,max}$ and maximal frequency RoCoF called $RoCoF_{f\,max}$,
- For rotor angle: a measure of the inverse of minimal damping of interarea modes called $d_{\lambda_{interarea}\,max}$ (check next paragraph and equation **(7.1)**) and maximal $ISGA$ (Chapter 4.V.2.i) called $ISGA_{max}$.

Discussion about the damping of interarea modes KPI: to precisely calculate this KPI, the previously adopted process was the following:

- Linearize the whole AC/DC power system around an operating point (usually initial operating point),

- Perform eigenvalue analysis to calculate the real and imaginary parts of the eigenvalues of the power system,
- Perform mode shape analysis to identify the modes corresponding to interarea oscillations,
- Calculate the damping of these interarea modes.

This process gives precise values of the interarea mode's damping at any time of the simulation, but it relies on linearization. This supposes that the system is linearizable and that the linearization's errors are tolerable. In the combined stability controllers' cases shown in Chapter 6, the main issue was the power converter's saturation. This problem cannot be expressed during linearization, which may lead to a high error in interarea mode's damping value calculation. Therefore, the KPI for the damping cannot rely on eigenvalue analysis which assumes a linearization with tolerable errors. This KPI should therefore express the value of the damping without using the classical eigenvalue analysis approach. Therefore, a fitting damping indicator inspired by the ISGA indicator is defined. To characterize the damping of interarea oscillations, two quantities are selected: amplitude of oscillations and their duration. To combine these two elements in one indicator, the KPI calculates the integral of the difference between the frequency of centre of inertia of an area and the one of another area. This is done for the whole simulation time duration. This gives the following damping KPI $d_{\lambda_{interarea}}(T_{start}, T_{end})$ for a given interarea mode $\lambda_{interarea}$:

$$d_{\lambda_{interarea}}(T_{start}, T_{end}) = \int_{T_{start}}^{T_{end}} \left| \omega_{COI_{Area_1}}(t) - \omega_{COI_{Area_2}}(t) \right|^2 dt \quad \textbf{(7.1)}$$

where T_{start} and T_{end} are the starting and ending times between which the damping needs to be evaluated by the user (usually, $T_{start} = 0$ and $T_{end} = duration\ of\ simulation$), $\omega_{COI_{Area_k}}$ is the per-unit derivative of the rotor angle of the centre of inertia of an Area k calculated as $\delta_{coi_{Area_k}} = \sum_{i=1}^{N_g} \frac{M_i \delta_i(t)}{M_{tot}}$ (with N_g the number of generators in the Area k, M_i the inertia of the machine i in the Area k, $M_{tot} = \sum_{i=1}^{N_g} M_i$ and δ_i the rotor angle of the same machine i).

The decision variables used as a degree of freedom in this section of the thesis are the active power headrooms (check Chapter 6.III.2.v.a) allocated to the controls of the AC/DC power converters.

The considered constraints are power balance between production and consumption, power balance in the MTDC system, power limits of the converters, current range limits in the DC links, DC voltage range limits, frequency range limits and rotor angle difference limits.

Due to system complexity, the relationships between each stability KPI and the values of the set power headrooms cannot be formulated straightforwardly. The system where optimization problem occurs can be described as a black-box system with inputs, outputs, and state variables. The diagram in ***Figure 7-1*** illustrates this information.

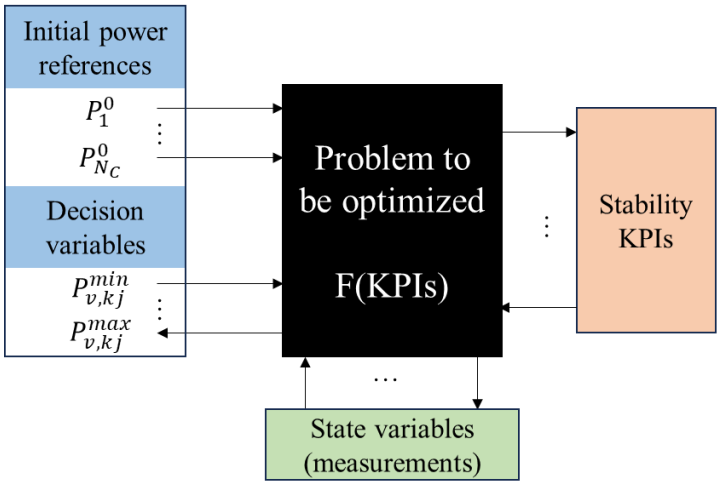

Figure 7-1: Diagram illustrating the black-box type of the optimization problem. N_C is the total number of converters. The decision variables are the same as the ones represented in equation (6.14).

In this case, the function F in the optimization problem can be expressed as follows:

$$F = \alpha_1 Nadir_{V_{DC}\,max} + \alpha_2 Nadir_{f\,max} + \alpha_3 RoCoF_{f\,max} + \alpha_4 d_{\lambda_{interarea}\,max} + \alpha_5 ISGA_{max} \quad \textbf{(7.2)}$$

The coefficients α_i in the equation **(7.2)** are the ponderations (weights) put to stability KPIs. They can vary from an optimization method to another.

The optimization problem is finally:

$$\min_{\substack{P_{v,kj}^{min}, P_{v,kj}^{max} \\ \forall\, virtual\ link\ v}} F\left(Nadir_{V_{DC}\,max}, Nadir_{f\,max}, RoCoF_{f\,max}, d_{\lambda_{interarea}\,max}, ISGA_{max}\right) \quad \textbf{(7.3)}$$

The identified constraints are the following:

$$\begin{cases} \sum_{g \in \mathcal{S}_{Gen}} P_{Gen_g} = \sum_{l \in \mathcal{S}_{Load}} P_{Load_l} \\ \sum_{c \in \mathcal{S}_{Conv}} P_{Conv_c} = 0 \\ P_{Conv_c}^{min} \le P_{Conv_c}(t) \le P_{Conv_c}^{max} \\ I_{ij}^{min} \le I_{ij}(t) \le I_{ij}^{max} \\ V_{DC_b}^{min} \le V_{DC_b}(t) \le V_{DC_b}^{max} \\ f_i^{min} \le f_i(t) \le f_i^{max} \\ \delta_{ij}^{min} \le \delta_{ij}(t) \le \delta_{ij}^{max} \end{cases} \quad \textbf{(7.4)}$$

where:

- P_{Gen_g} is the power output of generator g,
- $\mathcal{S}_{Gen}$ is the set of generators,
- P_{Load_l} is the power consumption of load l,
- $\mathcal{S}_{Load}$ is the set of loads,
- P_{Conv_c}, $P_{Conv_c}^{min}$ and $P_{Conv_c}^{max}$ are respectively the power output of converter c, its minimal and maximal power headrooms,
- $\mathcal{S}_{Conv}$ is the set of converters,
- I_{ij}, I_{ij}^{min} and I_{ij}^{max} are respectively the current flowing through the branch ij, the minimal allowable current amplitude and the maximal allowable current amplitude,
- V_{DC_b}, $V_{DC_b}^{min}$ and $V_{DC_b}^{max}$ are respectively the DC voltage at bus b, its minimal allowable amplitude and its maximal allowable amplitude,
- f_i, f_i^{min} and f_i^{max} are respectively the frequency at point of measurement i, its minimal allowable amplitude and its maximal allowable amplitude,
- δ_{ij}, δ_{ij}^{min} and δ_{ij}^{max} are respectively the rotor angle difference between buses i and j, its minimal allowable amplitude and its maximal allowable amplitude.

3. Optimization results

Since the optimization problem is of black-box type, metaheuristic methods are more adapted to solve it. Particle Swarm Optimization (PSO) method seems adapted to the problem. This method requires that the terms in the cost function be of the same order of magnitude. This can be realized through the ponderation parameters as explained before.

A metaheuristic optimization method is developed in Python software for orchestration/interface with Dymola and using Python optimization libraries. This is a supplementary contribution to the Ph.D. thesis work but, for the sake of illustrating optimization in this chapter, parameter screening was applied to the last case study shown in Chapter 6.

To visualize the benefit of optimization, a two-dimensional parameters evaluation was developed using the multi-parameter sweep feature built-in in Dymola tool.

The two swept parameters are chosen as the maximal power headrooms of {POD+ADC} (same for $\{S1, S2\}$ and $\{S3, S4\}$) and FCR (of $\{S1\}$) controllers implemented in the power system shown in ***Figure 3-17***. The other parameters kept same values as in Chapter 6.

The following KPIs were selected for the optimization function 'F' shown in **(7.3)**: maximum rotor angle difference in AC zone 1, maximum frequency deviation from nominal value in AC zone 1 and maximal damping criterion in AC zone 1 too. The weights attributed to the KPIs are equal to 1 since the KPIs show the same order of magnitude.

The obtained results are shown in the 3D plots in ***Figure 7-2***. The ranges in which the parameters vary are selected to show the optimization's purpose.

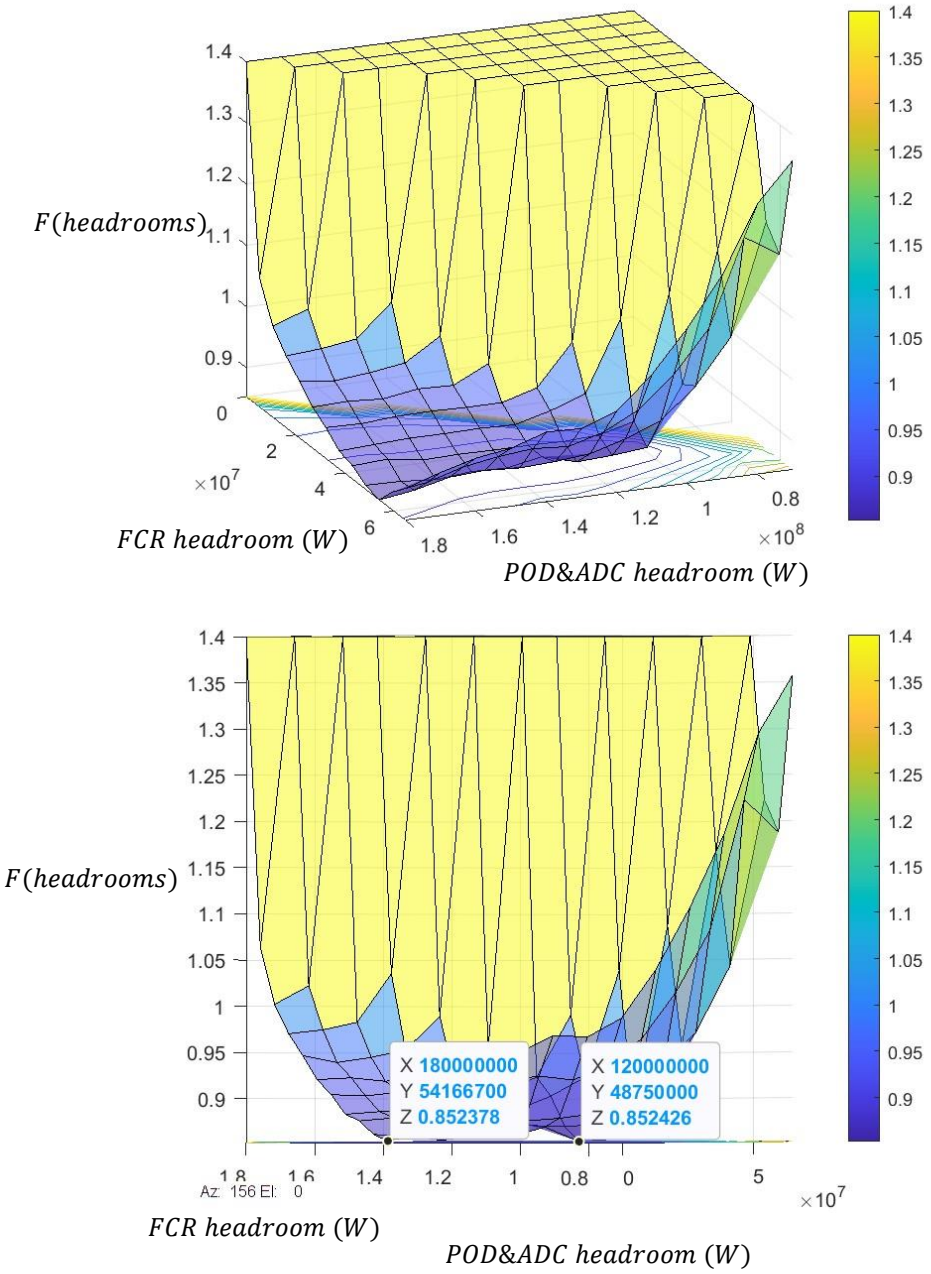

Figure 7-2: Two snapshots of the 3D plot obtained from parameter screening of the {POD+ADC} and FCR controllers' maximal power headrooms.

The following points can be observed in the plots in ***Figure 7-2*** and from the simulations themselves:

- For very low values of power headrooms (yellow diagonal in the plot), simulation shows high function F values. These values begin to decrease when the two parameters start to increase.
- For different combinations of the two parameters, local minima can be reached.
    - For values of FCR controller's maximal headroom below 50 MW, when {POD+ADC} controller's maximal headroom varies from 80 MW to 100 MW, the values of F

decrease significantly. This is because the rotor angle controllers enhance the system's stability significantly in this range of values.

- For values of FCR parameter below 50 MW, and for a fixed {POD+ADC} parameter, the cost function's values decrease with the increase of this parameter.

- Beyond the values mentioned above, the cost function starts to increase.

  - For fixed values of FCR parameter, the impact of POD and ADC becomes relatively limited even when their headroom parameter continues to increase.

  - For fixed values of {POD+ADC} parameter, the increase of FCR's parameter creates competition with rotor angle stability controllers' impact on the calculated cost function F. This increases the values of the cost function, which means that the sum of the multiple stability KPIs increases due to 'global' stability decrease.

- Finally, two optima are show in the bottom plot in ***Figure 7-2***. The first one is the global optimum obtained for the couple of parameters [180; 54.17] MW for [{POD+ADC}; FCR]. The cost function value is of 0.852378. Another minimum of 0.852426 of the cost function is reached for the couple [120; 48.75] MW. From a pure mathematical point of view, the first couple of parameters enhances the power system's multiple stability aspects the best. But from a technical-financial point of view, the second couple of parameters seems to be more interesting. In fact, the improvement in the cost function is relatively low for a relatively big change in power headroom allocation. The global optimum's tuning assumes higher POD headroom allocation, leaving less headroom for other controllers. Moreover, it assumes higher FCR headroom as well. If the FCR support is a marketed HVDC ancillary service (it is the case of frequency support provided by AC components), the higher the FCR headroom allocation, the higher may be the cost of stability enhancement services provided by the HVDC links. More generally, when putting things into perspective, the TSOs may decide to choose a local minimum of the cost function they define in stability enhancement headroom allocation approach instead of choosing a global minimum.

The financial aspect may be included in the cost function, but this goes beyond the scope of this thesis.

III. Conclusion

In this final chapter, the basis of one possible optimization approach to the stability enhancement objective was defined. The mathematical optimization problem was formulated through a sum of multiple stability KPIs. A proof of concept was also realized using parameter screening approach.

The obtained results showed an improvement of multiple stability aspects for a given set of parameters. Beyond this mathematical aspect, a technical-financial perspective is necessary to decide which optimal point of operation should be chosen by TSOs.

Chapter 8 : Conclusion and Perspectives

I. Context

In the recent years, HVDC grids have proved their interest as a solution for power transmission systems. The usage of HVDC transmission systems is expected to increase in the coming years especially with the changes occurring in the power systems. In fact, the flexibility and controllability offered by power electronics suggest that HVDC systems, and particularly MMC systems, play a major role in the future grids.

To ensure the stability and reliability of hybrid AC/DC power systems, HVDC systems may offer support services also called ancillary services. Each service may implicate one or multiple additional controllers. These controllers can particularly make changes in the active power references set to the converters. The design and implementation of these controllers requires a meticulous understanding of the potential interactions they may induce in a hybrid AC/DC power system.

II. Conclusions per chapter

- Chapter 2:

Before addressing the problematics linked to stability aspects of hybrid AC/DC power systems, a general state of the art of the HVDC links' opportunities and challenges was presented. The different HVDC architectures and types of AC/DC power converters were also discussed. Then, the definition of the different stability aspects of a power system was presented. From these aspects, three were selected for the rest of the thesis: rotor angle, frequency, and DC voltage. Finally, the literature mentioned in this chapter showed that AC and DC power systems may have linked perturbations due to the existing coupling between them.

- Chapter 3:

In this chapter, the modelling and control of the various components of the AC and DC power systems was presented. The most important ones are the generators and their internal controllers (PSS, AVR, turbine governor), the loads, the AC and DC links, and the AC/DC power converters. The control of the MMC-based power electronics was explained.

Composed by the mentioned components, power system benchmarks were built in order to perform stability studies. The complexity of the benchmarks is progressively increased as the stability studies' complexity increased. Two main types of stability assessments are possible: eigenvalue analysis and time-domain analysis.

To assess power system stabilities, Dymola software (based on MODELICA language) is used. The benchmarks are modelled in this tool and simulations' methodology and workflow are explained.

- Chapter 4:

This chapter explores the different stability aspects explained in Chapter 2 through different assessment methodologies explained in Chapter 3. The assessment approach is progressively built:

- Study of impact of adding power converters on the stability of AC power systems.
- Study of rotor angle stability aspect separately: transient, steady-state and small-signal
- Study of frequency, DC voltage and rotor angle stability aspects in a simultaneous approach.

Throughout the chapter, the grid requirements are also discussed.

After showing the potential interactions between different controllers when a perturbation occurs, decoupling strategies are proposed in this chapter. The studies showed that these strategies can work for simplistic benchmarks. However, for more complex power systems, a framework for stability assessment and enhancement is needed. Five frameworks were developed in the thesis and presented in this chapter as well. They differ by their degree of communication and their degree of active power coordination.

- Chapter 5:

In this chapter, a power system benchmark is used to tackle multiple stability aspects simultaneously. Thus, various stability controllers are implemented in the power benchmark. They are local controllers that coexist together and propose supplementary functions by the power converters.

A comparative case study is lead. It shows how, when HVDC links propose multiple ancillary services simultaneously after a given disturbance happens, interactions emerge between different controllers. These interactions impact badly some stability aspects, normally enhanced when their controller is individually implemented.

Finally, to solve the issues raised by the antagonist interactions, a stability enhancement strategy is proposed in this chapter. The approach relies on the concept of active power reallocation among the operating converters. The approach is mathematically formulated and tested numerically. Its use on the implemented controllers shows an enhancement in the multiple stability aspects combination compared to the reference case.

- Chapter 6:

In this chapter, a different stability enhancement strategy is examined. Here, the approach is based on power converter headroom constrains.

Before numerically implementing the strategy, a centralized AC/DC controller is designed. It uses wide-area measurements to enhance different stability aspects simultaneously. A new frequency controller is implemented in the central controller as well.

A power system stability analysis is made through comparative case studies. Here also, the perturbation scenario is designed and implemented such as to solicitate all the features of the centralized controller simultaneously.

The active power headroom allocation strategy was mathematically formulated and then tested on the used power benchmark. This strategy also showed an enhancement of the multi-criteria stability of the power system compared to the case without active power coordination.

- Chapter 7:

In this last chapter of the thesis, an optimization approach is proposed and tested.

The different types of optimization problems are discussed. Then, the problem to optimize in this thesis is characterized and mathematically formulated. The objective function to minimize is composed of a weighted sum of different criteria to optimize. It also considers the inherent system constrains such as power converter limits, line limits, etc.

A proof-of-concept of the optimization approach was made through a case study. The output of the study shows that, for a set of control parameters, the value of the objective function can be minimized. This means that, in addition to the control layer that deals with active power coordination, a supplementary enhancement is possible through an optimization layer.

III. General conclusion and scientific contributions

Through this PhD thesis, different power system benchmarks were studied. The studies aimed for individual as well as multiple stability criteria assessment of a power system. The assessment is based on stability KPIs that use the power system measurements.

The studies showed the risk of development of control interactions leading to antagonist impacts on the stability aspects. To tackle this issue, control decoupling strategies were proposed in the thesis. For more complex power systems, these strategies cannot be straightforwardly used. Therefore, comprehensive frameworks for stability assessment and enhancement were proposed.

Distributed as well as centralized controllers were designed to enhance AC/DC stability. Specific perturbation scenarios were developed, and specific initial conditions were tested. The realistic stability issues emerging from the perturbations were first tackled in an individual then in a wholistic approach.

To minimize the mentioned control interactions, two active power control coordination approaches are explored. The first proposed one is based on active power reallocation among converters, while the second one is based on constrained headroom allocation.

To further enhance the stability, an optimization layer is added to the AC/DC power system's control. The problem to optimize is mathematically formulated and a test on a power benchmark is made. The results validate the benefit of solving such optimization problems. They show how, in order to enhance stability further, one can maximally benefit from the degrees of freedom offered by HVDC systems.

IV. Perspectives

To go further in the Research, some perspectives of development were identified. Though the combination of other stability is interesting, this section focuses on different scientific perspectives. They are described in this section.

1. For optimization

Four main development paths exist for the optimization layer added in the thesis:

- **Optimizing the first stability enhancement approach proposed:** The optimization problem was formulated for the second stability approach (headroom allocation). However, it is interesting to evaluate the results of optimizing active power reallocation ratios (in first approach) in terms of multi-criteria stability enhancement.
- **Optimizing control parameters:** The control parameters (ADC, POD, DC voltage droop, FCR) were set as per physical stability criteria (maximal rotor angle difference, DC voltage maximal deviation, etc.). Some trial-and-error tests were performed to determine best values for these parameters. However, an optimization approach could also help give the best set of parameters for the implemented controllers.
- **Including cost model in the cost function:** The actual KPIs used in the optimization's objective function do not include a model of the cost of the application and implementation of HVDC controls. The impact of including these costs (OPEX and CAPEX) may influence a TSO's strategy of deployment of HVDC ancillary services and therefore the stability of the power systems.
- **Use of advanced optimization techniques:** The used technique in Chapter 7 is based on a screening of control parameters but other techniques are also be adapted to the problem exposed in the thesis. This is the case of metaheuristic approach-based techniques such as PSO. The work on this approach is finalized but the results will not be shown in this manuscript for the sake of publication of a scientific paper previously.

2. For validation

Two main development paths are identified:

- **Offline to real-time:** The studies are based on offline simulation approaches, adapted for planning stage (by TSOs). It is scientifically interesting to test the proposed control strategies through a real-time operating power system (of type HIL/PHIL).

- **Offline to online:** The coordination strategies proposed are valid for offline simulation. They may be definitively implemented by the TSOs according to a worst-case scenario to avoid instability. Therefore, control parameters are set according to the worst-case scenario.

However, when the perturbation does not lead to the worst-case scenario, the chosen set of parameters may not correspond the best reachable stability performances. The set of parameters may need to be changed online, according to the detected perturbation (generator trip, line trip, etc.).

Sure, TSOs prefer to have planned behaviour of power systems. TSOs also do not usually change their set of control parameters on the flow.

But, if computer processing capabilities and TSO acceptability allow for this, the situation may evolute. It becomes interesting to test coordination strategies that can change the values of control parameters according to the system KPIs measured online.

3. For control

Two main advancements may be scientifically interesting:

- **Use of Model Predictive Control (MPC):**

  For the power system stability problem studied in the thesis, the examination of an MPC-based enhancement strategy may be interesting. MPC is not really developed in the Power System community and TSOs do not fully adhere to such controllers (since they prefer classical controllers). Nevertheless, the MPC is very adapted for constrained optimization problems. It solves them by predicting the state of the power system in the following instants, which allows MPC to find the optimal set of parameters during operation of a power system.

  Replacing classical controllers by MPC-type ones is a huge change of paradigm for TSOs. Examining the impact of MPC control for Research is, however, realistic.

- **Use of Artificial Intelligence (AI):**

  In this thesis, classical control designs were implemented. The main aim was to propose coordination strategy among active power controllers and, additionally, to formulate the optimization problem to solve.

  The AI may be implemented in two different aspects:

  - Assessment: for example, classify the system's eigenvalues as critical or not, etc.
  - Enhancement: find best set of parameters based on deep learning of power system's performances.

  This also deserves dedicated effort, but AI is definitely an interesting Research field for Power Systems.

4. For contingencies

The study of Dc power fault, converter trip and the inversion of the direction of power exchanged by the AC/DC converters requires specific fault modelling methods. Since the current version of the used libraries does not allow to do such studies, it would be interesting to tackle these contingency scenario modelling.

ANNEX 1

Summary of physical stability aspects and their implications on power system stability.

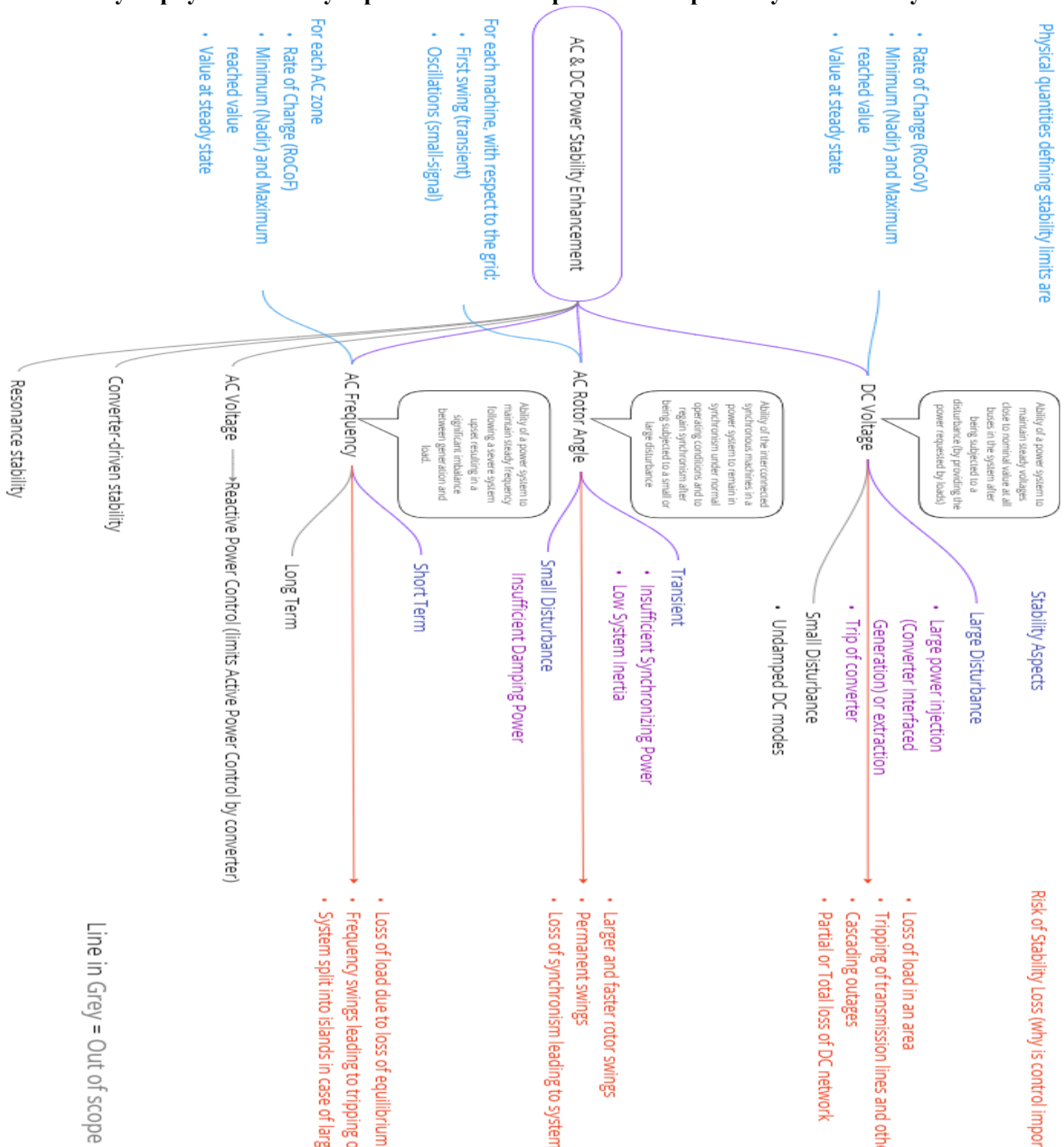

ANNEX 2

Developed Algorithm for static and dynamic active power reallocation control coordination strategy.

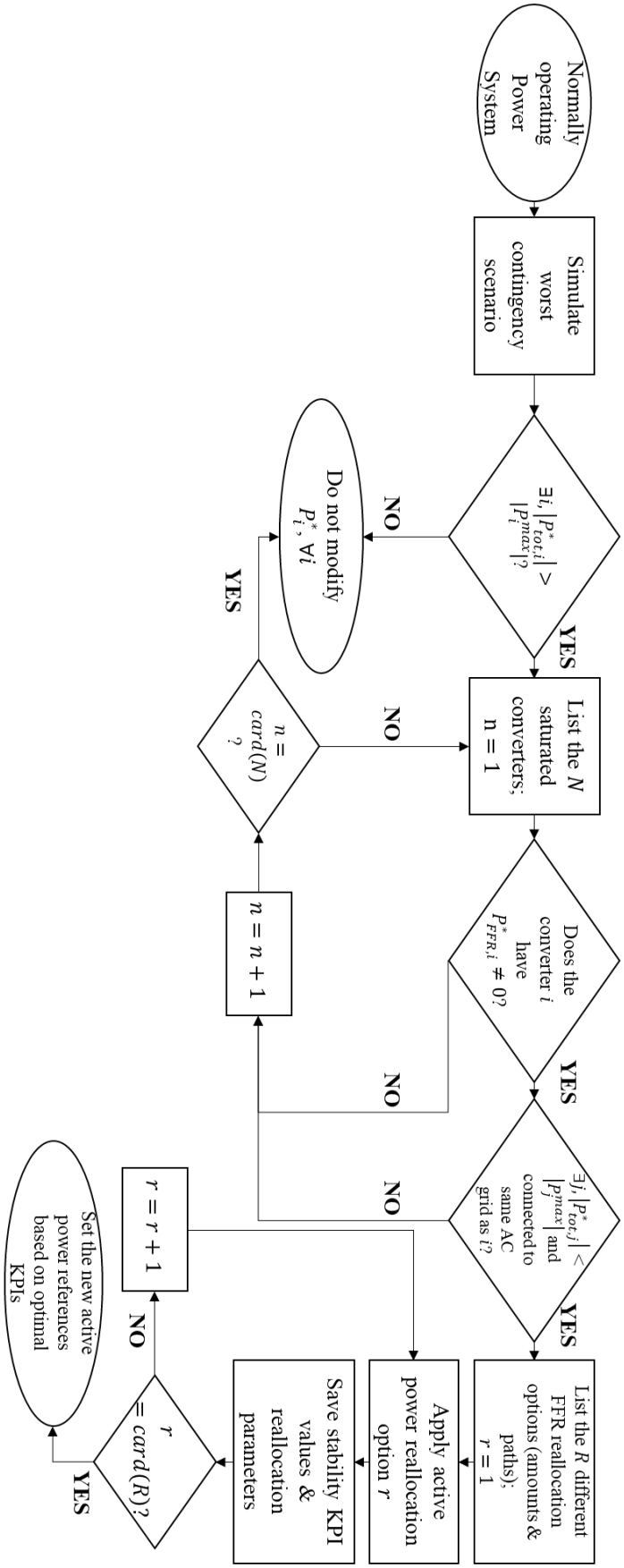

REFERENCES

[1] « Statistical Review of World Energy.pdf ». [En ligne]. Disponible sur: https://www.energyinst.org/statistical-review

[2] I. Oleinikova, « micro vs MEGA: trends influencing the development of the power system ».

[3] A. Fernández-Guillamón, « Power systems with high renewable energy sources_ A review of inertia and frequency control strategies over time », *Renew. Sustain. Energy Rev.*, 2019.

[4] W. Feng, Q. Shi, H. Cui, et F. Li, « Optimal power allocation strategy for black start in VSC-MTDC systems considering dynamic impacts », *Electr. Power Syst. Res.*, vol. 193, p. 107023, avr. 2021, doi: 10.1016/j.epsr.2021.107023.

[5] « ENTSO-E TYNDP 2022 High-Level Report – Final Version May 2023 ».

[6] « HVDC links in system operations.pdf ». ENTSOE, 2 décembre 2019. [En ligne]. Disponible sur: https://eepublicdownloads.entsoe.eu/clean-documents/SOC%20documents/20191203_HVDC%20links%20in%20system%20operations.pdf

[7] B. Silva, C. L. Moreira, L. Seca, Y. Phulpin, et J. A. Pecas Lopes, « Provision of Inertial and Primary Frequency Control Services Using Offshore Multiterminal HVDC Networks », *IEEE Trans. Sustain. Energy*, vol. 3, nº 4, p. 800-808, oct. 2012, doi: 10.1109/TSTE.2012.2199774.

[8] G. Bakhos, K. SHINODA, J. C. Gonzalez-Torres, A. Benchaib, L. Vanfretti, et S. Bacha, « Aspects of stability issues of HVAC/HVDC coupled grids ».

[9] S. Berlijn *et al.*, « ENTSO-E Research, Demonstration, and Innovation Roadmap 2020-2030 ».

[10] « Stability Management in Power Electronics Dominated Systems: A Prerequisite to the Success of the Energy Transition ». ENTSO-E, juin 2022.

[11] *HVDC Grid Systems and connected Converter Stations. Guideline and Parameter Lists for Functional Specifications. Part 1, Guidelines*. London: British Standards Institution, 2020.

[12] W. Du, F. K. Tuffner, K. P. Schneider, R. H. Lasseter, et B. Bhattarai, « Modeling of Grid-Forming and Grid-Following Inverters for Transient Stability Simulation of Large-Scale Distribution Systems ».

[13] S. Huang, W. Zuo, D. Vrabie, et R. Xu, « Modelica-based system modeling for studying control-related faults in chiller plants and boiler plants serving large office buildings », *J. Build. Eng.*, vol. 44, p. 102654, déc. 2021, doi: 10.1016/j.jobe.2021.102654.

[14] F. V. D. Linden, « General fault triggering architecture to trigger model faults in Modelica using a standardized blockset », présenté à the 10th International Modelica Conference, March 10-12, 2014, Lund, Sweden, mars 2014, p. 427-436. doi: 10.3384/ecp14096427.

[15] L. F. Normandia Lourenço *et al.*, « A Review on Multi-Terminal High Voltage Direct Current Networks for Wind Power Integration », *Energies*, vol. 15, nº 23, p. 9016, nov. 2022, doi: 10.3390/en15239016.

[16] C. Kim, V. K. Sood, G. Jang, S. Lim, et S. Lee, *HVDC Transmission: Power Conversion Applications in Power Systems*, 1re éd. Wiley, 2009. doi: 10.1002/9780470822975.

[17] A. Kalair, N. Abas, et N. Khan, « Comparative study of HVAC and HVDC transmission systems », *Renew. Sustain. Energy Rev.*, vol. 59, p. 1653-1675, juin 2016, doi: 10.1016/j.rser.2015.12.288.

[18] D. Mondal, A. Chakrabarti, et A. Sengupta, *Power system small signal stability analysis and control*, 2nd ed. London: Academic Press, 2020.

[19] F. Gonzalez-Longatt, J. L. Rueda, et M. A. M. M. Van Der Meijden, « Effects of grounding configurations on post-contingency performance of MTDC system: A 3-Terminal example », in *2015 50th International Universities Power Engineering Conference (UPEC)*, Stoke On Trent, United Kingdom: IEEE, sept. 2015, p. 1-6. doi: 10.1109/UPEC.2015.7339912.

[20] P. Rodriguez et K. Rouzbehi, « Multi-terminal DC grids: challenges and prospects », *J. Mod. Power Syst. Clean Energy*, vol. 5, nº 4, p. 515-523, juill. 2017, doi: 10.1007/s40565-017-0305-0.

[21] A. Alassi, S. Bañales, O. Ellabban, G. Adam, et C. MacIver, « HVDC Transmission: Technology Review, Market Trends and Future Outlook », *Renew. Sustain. Energy Rev.*, vol. 112, p. 530-554, sept. 2019, doi: 10.1016/j.rser.2019.04.062.

[22] H. Xiao, K. Sun, J. Pan, et Y. Liu, « Operation and control of hybrid HVDC system with LCC and full-bridge MMC connected in parallel », *IET Gener. Transm. Distrib.*, vol. 14, nº 7, p. 1344-1352, avr. 2020, doi: 10.1049/iet-gtd.2019.1336.

[23] R. R. Ahrabi, Y. W. Li, et F. Nejabatkhah, « Hybrid AC/DC Network With Parallel LCC-VSC Interlinking Converters », *IEEE Trans. Power Syst.*, vol. 36, nº 1, p. 722-731, janv. 2021, doi: 10.1109/TPWRS.2020.3020235.

[24] O. Damanik, O. C. Sakinci, G. Grdenic, et J. Beerten, « Evaluation of the use of short-circuit ratio as a system strength indicator in converter-dominated power systems », in *2022 IEEE PES Innovative Smart Grid Technologies Conference Europe (ISGT-Europe)*, Novi Sad, Serbia: IEEE, oct. 2022, p. 1-5. doi: 10.1109/ISGT-Europe54678.2022.9960381.

[25] « IEEE Guide for Planning DC Links Terminating at AC Locations Having Low Short-Circuit Capacities », IEEE. doi: 10.1109/IEEESTD.1997.85949.

[26] L. Vanfretti, W. Li, T. Bogodorova, et P. Panciatici, « Unambiguous power system dynamic modeling and simulation using modelica tools », in *2013 IEEE Power & Energy Society General Meeting*, Vancouver, BC: IEEE, 2013, p. 1-5. doi: 10.1109/PESMG.2013.6672476.

[27] O. E. Oni, I. E. Davidson, et K. N. I. Mbangula, « A review of LCC-HVDC and VSC-HVDC technologies and applications », in *2016 IEEE 16th International Conference on Environment and Electrical Engineering (EEEIC)*, Florence, Italy: IEEE, juin 2016, p. 1-7. doi: 10.1109/EEEIC.2016.7555677.

[28] A. Korompili, Q. Wu, et H. Zhao, « Review of VSC HVDC connection for offshore wind power integration », *Renew. Sustain. Energy Rev.*, vol. 59, p. 1405-1414, juin 2016, doi: 10.1016/j.rser.2016.01.064.

[29] A. Raza, X. Dianguo, S. Xunwen, L. Weixing, et B. W. Williams, « A Novel Multiterminal VSC-HVdc Transmission Topology for Offshore Wind Farms », *IEEE Trans. Ind. Appl.*, vol. 53, nº 2, p. 1316-1325, mars 2017, doi: 10.1109/TIA.2016.2628901.

[30] J. Danielsson, S. Patel, J. Pan, et R. Nuqui, « CIGRE US National Committee 2015 Grid of the Future Symposium ».

[31] M. Pinto, « ABB High Voltage Direct Current ».

[32] N. R. Watson et J. D. Watson, « An Overview of HVDC Technology », *Energies*, vol. 13, nº 17, p. 4342, août 2020, doi: 10.3390/en13174342.

[33] M. N. Sakib, S. P. Azad, et M. Kazerani, « A Critical Review of Modular Multilevel Converter Configurations and Submodule Topologies from DC Fault Blocking and Ride-Through Capabilities Viewpoints for HVDC Applications », *Energies*, vol. 15, nº 11, p. 4176, juin 2022, doi: 10.3390/en15114176.

[34] « IEC 60050 - International Electrotechnical Vocabulary - Details for IEV number 692-01-05 ». International Electrotechnical Commission, 15 décembre 2017.

[35] « IEC 60050 - International Electrotechnical Vocabulary - Details for IEV number 692-01-11 ». International Electrotechnical Commission, 15 décembre 2017.

[36] « IEC 60050 - International Electrotechnical Vocabulary - Details for IEV number 692-01-14 ». International Electrotechnical Commission, 15 décembre 2017.

[37] « CIGRE Articles Defining power system resilience ». Cigre for power system expertise, 30 septembre 2019. [En ligne]. Disponible sur: http://www.cigre.org/article/defining-power-system-resilience

[38] Mo Xuehong et Yang Wenpei, « Some superficial view on renewable energy power full and security acquisition — Based on stakeholder perspective », in *2011 International Conference on Materials for Renewable Energy & Environment*, Shanghai, China: IEEE, mai 2011, p. 30-33. doi: 10.1109/ICMREE.2011.5930758.

[39] « Definition and Classification of Power System Stability IEEE/CIGRE Joint Task Force on Stability Terms and Definitions », *IEEE Trans. Power Syst.*, vol. 19, nº 3, p. 1387-1401, août

2004, doi: 10.1109/TPWRS.2004.825981.

[40] N. Hatziargyriou *et al.*, « Definition and Classification of Power System Stability – Revisited & Extended », *IEEE Trans. Power Syst.*, vol. 36, nº 4, p. 3271-3281, juill. 2021, doi: 10.1109/TPWRS.2020.3041774.

[41] Y. Shu et Y. Tang, « Analysis and Recommendations for the Adaptability of China's Power System Security and Stability Relevant Standards », 4 décembre 2017.

[42] M. A. Hannan *et al.*, « Advanced Control Strategies of VSC Based HVDC Transmission System: Issues and Potential Recommendations », *IEEE Access*, vol. 6, p. 78352-78369, 2018, doi: 10.1109/ACCESS.2018.2885010.

[43] D. Van Hertem et M. Ghandhari, « Multi-terminal VSC HVDC for the European supergrid: Obstacles », *Renew. Sustain. Energy Rev.*, vol. 14, nº 9, p. 3156-3163, déc. 2010, doi: 10.1016/j.rser.2010.07.068.

[44] P. Rault, X. Guillaud, F. Colas, et S. Nguefeu, « Investigation on interactions between AC and DC grids », in *2013 IEEE Grenoble Conference*, Grenoble, France: IEEE, juin 2013, p. 1-6. doi: 10.1109/PTC.2013.6652229.

[45] S. Cole, J. Beerten, et R. Belmans, « Generalized Dynamic VSC MTDC Model for Power System Stability Studies », *IEEE Trans. Power Syst.*, vol. 25, nº 3, p. 1655-1662, août 2010, doi: 10.1109/TPWRS.2010.2040846.

[46] L. Zhang, L. Harnefors, et H.-P. Nee, « Interconnection of Two Very Weak AC Systems by VSC-HVDC Links Using Power-Synchronization Control », *IEEE Trans. Power Syst.*, vol. 26, nº 1, p. 344-355, févr. 2011, doi: 10.1109/TPWRS.2010.2047875.

[47] R. Eriksson, J. Beerten, M. Ghandhari, et R. Belmans, « Optimizing DC Voltage Droop Settings for AC/DC System Interactions », *IEEE Trans. Power Deliv.*, vol. 29, nº 1, p. 362-369, févr. 2014, doi: 10.1109/TPWRD.2013.2264757.

[48] Gen Li, J. Liang, C. E. Ugalde-Loo, P. Coventry, et J. Rimez, « Dynamic interactions of DC and AC grids subject to DC faults », in *2016 IEEE 8th International Power Electronics and Motion Control Conference (IPEMC-ECCE Asia)*, Hefei, China: IEEE, mai 2016, p. 2627-2633. doi: 10.1109/IPEMC.2016.7512712.

[49] A. Emhemed, G. Adam, Q. Hong, et G. Burt, « Studies of dynamic interactions in hybrid ac-dc grid under different fault conditions using real time digital simulation », in *13th IET International Conference on AC and DC Power Transmission (ACDC 2017)*, Manchester, UK: Institution of Engineering and Technology, 2017, p. 10 (5 .)-10 (5 .). doi: 10.1049/cp.2017.0010.

[50] D. Obradovic, M. Oluic, R. Eriksson, et M. Ghandhari, « Supplementary Power Control of an HVDC System and Its Impact on Electromechanical Dynamics », *IEEE Trans. Power Syst.*,

vol. 36, nº 5, p. 4599-4610, sept. 2021, doi: 10.1109/TPWRS.2021.3056763.

[51] « Review and outlook of HVDC grids as backbone of the transmission system », *CSEE J. Power Energy Syst.*, 2020, doi: 10.17775/CSEEJPES.2020.04890.

[52] A. B. Salas, « Control interactions in power systems with multiple VSC HVDC converters ».

[53] G. Grdenić, M. Delimar, et J. Beerten, « AC Grid Model Order Reduction Based on Interaction Modes Identification in Converter-Based Power Systems », *IEEE Trans. Power Syst.*, vol. 38, nº 3, p. 2388-2397, mai 2023, doi: 10.1109/TPWRS.2022.3180426.

[54] « Systems with Multiple DC Infeed ». Cigre, 2005. [En ligne]. Disponible sur: https://e-cigre.org/publication/364-systems-with-multiple-dc-infeed

[55] C. Karawita et U. D. Annakkage, « Multi-Infeed HVDC Interaction Studies Using Small-Signal Stability Assessment », *IEEE Trans. Power Deliv.*, vol. 24, nº 2, p. 910-918, avr. 2009, doi: 10.1109/TPWRD.2008.2002986.

[56] « Influence of Embedded HVDC Transmission on System Security and AC Network Performance ». Cigre, avril 2013.

[57] P. W. Sauer et M. A. Pai, « Power system dynamics and stability ».

[58] I. Report, « Excitation System Models for Power System Stability Studies », *IEEE Trans. Power Appar. Syst.*, vol. PAS-100, nº 2, p. 494-509, févr. 1981, doi: 10.1109/TPAS.1981.316906.

[59] Z. Shen, Z. Wei, G. Sun, et S. Chen, « Representing ZIP loads in convex relaxations of optimal power flow problems », *Int. J. Electr. Power Energy Syst.*, vol. 110, p. 372-385, sept. 2019, doi: 10.1016/j.ijepes.2019.03.011.

[60] P. Kundur, *Power System Stability And Control*. McGraw-Hill, Inc, 1994.

[61] E. Prieto-Araujo, A. Egea-Alvarez, S. Fekriasl, et O. Gomis-Bellmunt, « DC Voltage Droop Control Design for Multiterminal HVDC Systems Considering AC and DC Grid Dynamics », *IEEE Trans. Power Deliv.*, vol. 31, nº 2, p. 575-585, avr. 2016, doi: 10.1109/TPWRD.2015.2451531.

[62] J. Beerten, S. D'Arco, et J. A. Suul, « Frequency-dependent cable modelling for small-signal stability analysis of VSC-HVDC systems », *IET Gener. Transm. Distrib.*, vol. 10, nº 6, p. 1370-1381, avr. 2016, doi: 10.1049/iet-gtd.2015.0868.

[63] R. Pierre, « Dynamic Modeling and Control of Multi-Terminal HVDC Grids ».

[64] N. G. Hingorani et L. Gyugyi, « Understanding FACTS », 1999.

[65] N. Acharya, A. Sode-Yome, et N. Mithulananthan, « Facts about Flexible AC Transmission

Systems (FACTS) Controllers: Practical Installations and Benefits ».

[66] S. Bacha, I. Munteanu, et A. I. Bratcu, *Power Electronic Converters Modeling and Control: with Case Studies*. in Advanced Textbooks in Control and Signal Processing. London: Springer London, 2014. doi: 10.1007/978-1-4471-5478-5.

[67] A. Yazdani et R. Iravani, « A Unified Dynamic Model and Control for the Voltage-Sourced Converter Under Unbalanced Grid Conditions », *IEEE Trans. Power Deliv.*, vol. 21, nº 3, p. 1620-1629, juill. 2006, doi: 10.1109/TPWRD.2006.874641.

[68] H. A. Saad, « Modélisation et simulation d'une liaison HVDC de type VSC-MMC ».

[69] J. Freytes, L. Papangelis, H. Saad, P. Rault, T. Van Cutsem, et X. Guillaud, « On the modeling of MMC for use in large scale dynamic simulations », in *2016 Power Systems Computation Conference (PSCC)*, Genoa, Italy: IEEE, juin 2016, p. 1-7. doi: 10.1109/PSCC.2016.7540938.

[70] S. Akkari, « Control of a multi-terminal HVDC (MTDC) system and study of the interactions between the MTDC and the AC grids. ».

[71] A. Zama, S. A. Mansour, D. Frey, A. Benchaib, S. Bacha, et B. Luscan, « A comparative assessment of different balancing control algorithms for modular multilevel converter (MMC) », in *2016 18th European Conference on Power Electronics and Applications (EPE'16 ECCE Europe)*, Karlsruhe, Germany: IEEE, sept. 2016, p. 1-10. doi: 10.1109/EPE.2016.7695315.

[72] A. Zama, A. Benchaib, S. Bacha, D. Frey, et S. Silvant, « High Dynamics Control for MMC Based on Exact Discrete-Time Model With Experimental Validation », *IEEE Trans. Power Deliv.*, vol. 33, nº 1, p. 477-488, févr. 2018, doi: 10.1109/TPWRD.2017.2707343.

[73] A. Zama, S. Bacha, A. Benchaib, D. Frey, et S. Silvant, « Comparison and assessment of implementation techniques for dynamics MMC type models », in *2019 21st European Conference on Power Electronics and Applications (EPE '19 ECCE Europe)*, Genova, Italy: IEEE, sept. 2019, p. P.1-P.10. doi: 10.23919/EPE.2019.8914946.

[74] H. Golestani Far, « Damping of electromechanical oscillations in wide-area power systems such as the trans-canadian grid », McGill University, Montréal, Québec, Canada, 2010.

[75] « COMMISSION REGULATION (EU) 2017/ 1485 - of 2 August 2017 - establishing a guideline on electricity transmission system operation ».

[76] « COMMISSION REGULATION (EU) 2016/ 631 - of 14 April 2016 - establishing a network code on requirements for grid connection of generators ».

[77] « COMMISSION REGULATION (EU) 2016/ 1447 - of 26 August 2016 - establishing a network code on requirements for grid connection of high voltage direct current systems and direct current-connected power park modules ».

[78] M. Gu, L. Meegahapola, et K. L. Wong, « Review of Rotor Angle Stability in Hybrid AC/DC Power Systems », in *2018 IEEE PES Asia-Pacific Power and Energy Engineering Conference (APPEEC)*, Kota Kinabalu: IEEE, oct. 2018, p. 7-12. doi: 10.1109/APPEEC.2018.8566570.

[79] A. Benchaib, « Advanced Control of AC/DC Power Networks ».

[80] Z. Assi Obaid, L. M. Cipcigan, et M. T. Muhssin, « Power system oscillations and control: Classifications and PSSs' design methods: A review », *Renew. Sustain. Energy Rev.*, vol. 79, p. 839-849, nov. 2017, doi: 10.1016/j.rser.2017.05.103.

[81] W. Peres, « Multi-band power oscillation damping controller for power system supported by static VAR compensator », *Electr. Eng.*, vol. 101, nº 3, p. 943-967, sept. 2019, doi: 10.1007/s00202-019-00830-9.

[82] T. Bogodorova, S. A. Dorado-Rojas, et L. Vanfretti, « DeepGrid: A Deep Learning Computing System for Resilient Grid Operations », p. 151.

[83] G. N. Baltas, N. B. Lai, L. Marin, A. Tarraso, et P. Rodriguez, « Grid-Forming Power Converters Tuned Through Artificial Intelligence to Damp Subsynchronous Interactions in Electrical Grids », *IEEE Access*, vol. 8, p. 93369-93379, 2020, doi: 10.1109/ACCESS.2020.2995298.

[84] G. N. Baltas, N. B. Lai, A. Tarraso, L. Marin, F. Blaabjerg, et P. Rodriguez, « AI-Based Damping of Electromechanical Oscillations by Using Grid-Connected Converter », *Front. Energy Res.*, vol. 9, p. 598436, mars 2021, doi: 10.3389/fenrg.2021.598436.

[85] R. Preece, J. V. Milanovic, A. M. Almutairi, et O. Marjanovic, « Damping of inter-area oscillations in mixed AC/DC networks using WAMS based supplementary controller », *IEEE Trans. Power Syst.*, vol. 28, nº 2, p. 1160-1169, mai 2013, doi: 10.1109/TPWRS.2012.2207745.

[86] L. Vanfretti, S. Bengtsson, et J. O. Gjerde, « Preprocessing synchronized phasor measurement data for spectral analysis of electromechanical oscillations in the Nordic Grid: PREPROCESSING SYNCHRONIZED PHASOR MEASUREMENT DATA FOR MODE ESTIMATION », *Int. Trans. Electr. Energy Syst.*, vol. 25, nº 2, p. 348-358, févr. 2015, doi: 10.1002/etep.1847.

[87] K. W. V. To, A. K. David, et A. E. Hammad, « A robust co-ordinated control scheme for HVDC transmission with parallel AC systems », *IEEE Trans. Power Deliv.*, vol. 9, nº 3, p. 1710-1716, juill. 1994, doi: 10.1109/61.311190.

[88] O. Kotb, M. Ghandhari, R. Eriksson, R. Leelaruji, et V. K. Sood, « Stability enhancement of an interconnected AC/DC power system through VSC-MTDC operating point adjustment », *Electr. Power Syst. Res.*, vol. 151, p. 308-318, oct. 2017, doi: 10.1016/j.epsr.2017.05.026.

[89] N. T. Anh, L. Vanfretti, J. Driesen, et D. Van Hertem, « A Quantitative Method to Determine

ICT Delay Requirements for Wide-Area Power System Damping Controllers », *IEEE Trans. Power Syst.*, vol. 30, nº 4, p. 2023-2030, juill. 2015, doi: 10.1109/TPWRS.2014.2356480.

[90] J.-C. Gonzalez-Torres, G. Damm, C. Valentin, A. Benchaib, et F. Lamnabhi-Lagarrigue, « Transient stability of power systems with embedded VSC-HVDC links: stability margins analysis and control ».

[91] P. L. Francos, S. S. Verdugo, H. F. Alvarez, S. Guyomarch, et J. Loncle, « INELFE - Europe's first integrated onshore HVDC interconnection », in *2012 IEEE Power and Energy Society General Meeting*, San Diego, CA: IEEE, juill. 2012, p. 1-8. doi: 10.1109/PESGM.2012.6344799.

[92] J. Renedo, L. Sigrist, L. Rouco, et A. Garcia-Cerrada, « Impact on power system transient stability of AC-line-emulation controllers of VSC-HVDC links ». arXiv, 30 avril 2021. Consulté le: 2 août 2023. [En ligne]. Disponible sur: http://arxiv.org/abs/2104.15039

[93] J. C. Gonzalez-Torres, V. Costan, G. Damm, A. Benchaib, F. Lamnabhi-Lagarrigue, et B. Luscan, « Method for Controlling an Electrical Transmission Network », US 2022/0360089 A1, 10 novembre 2022 [En ligne]. Disponible sur: https://patents.google.com/patent/US20220360089A1/en

[94] D. Carroll et P. Krause, « Stability Analysis of a DC Power System », *IEEE Trans. Power Appar. Syst.*, vol. PAS-89, nº 6, p. 1112-1119, juill. 1970, doi: 10.1109/TPAS.1970.292701.

[95] S. D. Sudhoff, S. F. Glover, S. D. Pekarek, E. J. Zivi, D. E. Delisle, et D. Clayton, « Stability Analysis Methodologies for DC Power Distribution Systems ».

[96] K. Sharifabadi *et al.*, « TB 657: Guidelines for the preparation of "connection agreements" or "Grid Codes" for multi-terminal schemes and DC Grids. » 2016.

[97] K. Shinoda, G. Bakhos, J. C. Gonzalez-Torres, J. Dai, et A. Benchaib, « FCR Provisions by Multi-Terminal HVDC System ».

[98] K. Shinoda, J. Dai, G. Bakhos, J. C. Gonzalez-Torres, A. Benchaib, et S. Bacha, « Design consideration for frequency containment reserve provisions by a multi-terminal HVDC system », *IET Gener. Transm. Distrib.*, vol. 17, nº 18, p. 4024-4037, sept. 2023, doi: 10.1049/gtd2.12955.

[99] Y. Chompoobutrgool et L. Vanfretti, « Identification of Power System Dominant Inter-Area Oscillation Paths », *IEEE Trans. Power Syst.*, vol. 28, nº 3, p. 2798-2807, août 2013, doi: 10.1109/TPWRS.2012.2227840.

[100] K. Uhlen, L. Vanfretti, M. M. De Oliveira, V. H. Aarstrand, et J. O. Gjerde, « Wide-Area Power Oscillation Damper implementation and testing in the Norwegian transmission network », in *2012 IEEE Power and Energy Society General Meeting*, San Diego, CA: IEEE, juill. 2012, p. 1-7. doi: 10.1109/PESGM.2012.6344837.

[101] G. Bakhos *et al.*, « Hybrid AC/DC Power System Stability: An Attempt of Global Approach ». 2024. doi: 10.2139/ssrn.4704802.

[102] M. De Castro *et al.*, « Version [OpenIPSL 2.0.0] - [iTesla Power Systems Library (iPSL): A Modelica library for phasor time-domain simulations] », *SoftwareX*, vol. 21, p. 101277, févr. 2023, doi: 10.1016/j.softx.2022.101277.

[103] S. Boersma, X. Bombois, L. Vanfretti, J.-C. Gonzalez-Torres, et A. Benchaib, « Probing signal design for enhanced damping estimation in power networks », *Int. J. Electr. Power Energy Syst.*, vol. 129, p. 106640, juill. 2021, doi: 10.1016/j.ijepes.2020.106640.

[104] J. C. Gonzalez-Torres, R. Mourouvin, K. Shinoda, A. Zama, et A. Benchaib, « A simplified approach to model grid-forming controlled MMCs in power system stability studies », in *2021 IEEE PES Innovative Smart Grid Technologies Europe (ISGT Europe)*, Espoo, Finland: IEEE, oct. 2021, p. 01-06. doi: 10.1109/ISGTEurope52324.2021.9640024.

[105] R. Mourouvin, J. C. Gonzalez-Torres, J. Dai, A. Benchaib, D. Georges, et S. Bacha, « Understanding the role of VSC control strategies in the limits of power electronics integration in AC grids using modal analysis », *Electr. Power Syst. Res.*, vol. 192, p. 106930, mars 2021, doi: 10.1016/j.epsr.2020.106930.

[106] « GridCal tool for powerflow calculation ». [En ligne]. Disponible sur: https://github.com/SanPen/GridCal

[107] N. R. Chaudhuri, R. Majumder, et B. Chaudhuri, « System Frequency Support Through Multi-Terminal DC (MTDC) Grids », *IEEE Trans. Power Syst.*, vol. 28, nº 1, p. 347-356, févr. 2013, doi: 10.1109/TPWRS.2012.2196805.

[108] S. Akkari, J. Dai, M. Petit, et X. Guillaud, « Coupling between the frequency droop and the voltage droop of an AC/DC converter in an MTDC system », in *2015 IEEE Eindhoven PowerTech*, Eindhoven, Netherlands: IEEE, juin 2015, p. 1-6. doi: 10.1109/PTC.2015.7232285.

[109] L. Meegahapola, S. Bu, et M. Gu, *Hybrid AC/DC Power Grids: Stability and Control Aspects*. in Power Systems. Cham: Springer International Publishing, 2022. doi: 10.1007/978-3-031-06384-8.

[110] A. S. Kumar et B. P. Padhy, « Headroom based Frequency and DC-Voltage Control for Large Disturbances in Multi-Terminal HVDC (MTDC) Grids », in *2022 IEEE International Conference on Power Electronics, Drives and Energy Systems (PEDES)*, Jaipur, India: IEEE, déc. 2022, p. 1-6. doi: 10.1109/PEDES56012.2022.10080455.

[111] S. Akkari, M. Petit, J. Dai, et X. Guillaud, « Interaction between the Voltage-Droop and the Frequency-Droop Control for Multi-Terminal HVDC Systems ».

[112] J. Renedo, L. Rouco, A. Garcia-Cerrada, et L. Sigrist, « Coordinated control in multi-terminal

VSC-HVDC systems to improve transient stability: Impact on electromechanical-oscillation damping ». arXiv, 29 juillet 2022. Consulté le: 4 août 2023. [En ligne]. Disponible sur: http://arxiv.org/abs/2208.00083

[113] Y. Chompoobutrgool et L. Vanfretti, « Using PMU signals from dominant paths in power system wide-area damping control », *Sustain. Energy Grids Netw.*, vol. 4, p. 16-28, déc. 2015, doi: 10.1016/j.segan.2015.09.001.

[114] L. Díez-Maroto, L. Vanfretti, M. S. Almas, G. M. Jónsdóttir, et L. Rouco, « A WACS exploiting generator Excitation Boosters for power system transient stability enhancement », *Electr. Power Syst. Res.*, vol. 148, p. 245-253, juill. 2017, doi: 10.1016/j.epsr.2017.03.019.

[115] F. Guay, P.-A. Chiasson, N. Verville, S. Tremblay, et P. Askvid, « New Hydro-Québec Real-Time Simulation Interface for HVDC Commissioning Studies ».

[116] Y. Vernay, A. D. D'Aubigny, Z. Benalla, et S. Dennetière, « New HVDC LCC replica platform to improve the study and maintenance of the IFA2000 link ».

[117] P. Bertolini et M. Emilie, « Documentation Technique de Référence Article 4.1 ».

[118] M. Hladík, « Discrete and Continuous Optimization ». 17 mai 2022.

[119] R. Yadav, S. Kamble, D. S. Rao, R. Saradha, et G. U. Ansurkar, « Data Mining and Business Intelligence ».

[120] D. P. Bertsekas, « Constrained Optimization and Lagrange Multiplier Methods ». 1996.

[121] R. Fletcher, « Practical Methods of Optimization ». 1987.

[122] R. C. Bansal, « Optimization Methods for Electric Power Systems: An Overview », *Int. J. Emerg. Electr. Power Syst.*, 2005.

[123] P. E. Gill, W. Murray, et M. H. Wright, « Practical Optimization ». Academic Press, 1982.

[124] V. Fulber-Garcia, « Deterministic and Stochastic Optimization Methods ». Consulté le: 5 septembre 2023. [En ligne]. Disponible sur: https://www.baeldung.com/cs/deterministic-stochastic-optimization

[125] M.-H. Lin, J.-F. Tsai, et C.-S. Yu, « A Review of Deterministic Optimization Methods in Engineering and Management », *Math. Probl. Eng.*, vol. 2012, p. 1-15, 2012, doi: 10.1155/2012/756023.

[126] « Optimization Problem Types - NEOS Guide ». Consulté le: 5 septembre 2023. [En ligne]. Disponible sur: https://neos-guide.org/guide/types/